

# University of Southampton Research Repository

Copyright © and Moral Rights for this thesis and, where applicable, any accompanying data are retained by the author and/or other copyright owners. A copy can be downloaded for personal non-commercial research or study, without prior permission or charge. This thesis and the accompanying data cannot be reproduced or quoted extensively from without first obtaining permission in writing from the copyright holder/s. The content of the thesis and accompanying research data (where applicable) must not be changed in any way or sold commercially in any format or medium without the formal permission of the copyright holder/s.

When referring to this thesis and any accompanying data, full bibliographic details must be given, e.g.

Thesis: Author (Year of Submission) "Full thesis title", University of Southampton, name of the University Faculty or School or Department, PhD Thesis, pagination.

Data: Author (Year) Title. URI [dataset]

UNIVERSITY OF  
**Southampton**



FACULTY OF ENGINEERING & PHYSICAL SCIENCES

**Electrochemical and photocatalytic oxidation of organic pollutants  
from waste water using efficient nano-catalytic coatings prepared by  
electrodeposition**

by

**Chemical Engineer. Syed Zohaib Javaid Zaidi**  
Supervisors: **Dr. Carlos Ponce De Leon Albarran**  
**Prof. Frank Walsh**

Thesis for the degree of Doctor of Philosophy

Dec, 2018

Dedicated to my Father Engr.Syed Javaid Iqbal Zaidi, my Mother Ghazala Javaid (M.Edu.) and my sister Syeda Jawaria Javaid Zaidi (BS-CS)

## Abstract

Wastewater from the textile industry is considered to be one of the most pollutant effluents due to its toxic organic colourants content being strongly resistant to oxidation. When these substances are directly discharged into rivers and sea they persist for long periods causing environmental and aesthetic problems together with high health risks to living organisms. The main goal of this research is to study the oxidation of different textile dyes and organic pollutants, in particular reactive black-5 (RB-5) and methylene blue (MB) dyes using different nano catalytic coatings. A 3D flexible titanium felt electrode was anodized for growing TiO<sub>2</sub> nanotubes and further decorated with PbO<sub>2</sub> subsequently employed for anodic electrochemical and photochemical treatment of wastewater containing RB-5 dye.

Similarly, reticulated vitreous carbon (RVC) surfaces were decorated with a layer of PbO<sub>2</sub> and titanate nanosheets by anodic electrophoretic deposition, with subsequent structural and morphological characterization using FESEM and Raman spectroscopy. The TiNS/PbO<sub>2</sub>/RVC electrode has titanium anatase phase which was obtained by annealing at 450°C for 60 min in air. The structure revealed a well-specified, microporous structure with hydrophilic properties along the length and thickness of the RVC struts. Electrochemical and photocatalytic behaviour of the composite assisted the decolourisation of organic RB-5 dye in aqueous solution; on one hand •OH radicals were electrochemically produced via TiNS/PbO<sub>2</sub>/RVC anode composite coating and the photocatalytic decolourisation use the synergetic photocatalytic activity associated with the holes and free electron acceptors generated during UV irradiation experiments.

Another objective of this thesis is the synthesis of efficient nanotubular titanates (TiNTs) coatings over the surface of the RVC substrate to make the organic oxidation more efficient. Titanate nanotubes (TiNTs) were deposited over the surface of a 100 pores per inch (ppi) RVC by anodic electrophoresis. The photocatalytic characteristics of the coating were enhanced by annealing at 450 °C for 60 min in air. A preliminary evaluation of novel TiNT/RVC coatings demonstrated to be useful for the photocatalytic colour removal of MB dye.

In addition, a zinc metal plate was electrochemically anodised to produce ZnO nanowires. The selected operational conditions together a subsequent dip-coating process of the anodised ZnO surface in a TiO<sub>2</sub> containing solution, produced a core-shell coating. A further electrochemical deposition of PbO<sub>2</sub> over the core-shell produced a hybrid core (ZnO-TiO<sub>2</sub>)-shell (PbO<sub>2</sub>) coatings. The electrochemical and photocatalytic behaviour of the coatings were analysed by employing them to remove RB-5 dye ( $1 \times 10^{-5}$  mol dm<sup>-3</sup>).

The nano-coatings are low cost option for the oxidation of textile dyes and improved removal of RB-5 and MB dyes at a removal efficiency of  $\approx 99$  %.

## **Table of contents**

**Abstract iii**

**Table of contents .....iv**

**List of tables.....ix**

**List of figures .....xi**

**Research Thesis: Declaration of Authorship.....xvii**

**ACKNOWLEDGEMENTS.....xviii**

**List of Abbreviations .....xix**

**List of Symbols .....xxi**

**Chapter 1: Introduction..... 1**

1.1 Background and motivation..... 1

1.2 Electrochemical Advanced oxidation processes (EAOPs) ..... 2

1.3 Aims and Objectives ..... 6

1.4 Thesis Outline ..... 7

1.5 References..... 9

**Chapter 2: Literature Review ..... 12**

2.1 Electrochemical Process ..... 12

2.2 Anodic oxidation..... 13

2.3 The reaction scheme ..... 14

2.4 Oxygen evolution overpotential and categories of anodes ..... 15

2.5 Electrode Materials ..... 17

2.6 Electrochemical flow cells..... 18

2.7 Photocatalytic water treatment..... 21

2.8 Mechanism of TiO<sub>2</sub> photocatalysis..... 21

2.9 Kinetics of decolourisation of organic compounds ..... 23

2.10 Conclusions..... 24

2.11 References..... 25

**Chapter 3: Anodising of titanium felt to grow titanium dioxide nanotube  
arrays decorated with PbO<sub>2</sub>: Characterization and Application..... 30**

3.1 Introduction..... 31

3.2 Experimental Details..... 34

3.2.1 Anodizing of Titanium felt ..... 35

3.2.2	Deposition of Lead dioxide .....	36
3.2.3	Heat treatment.....	36
3.2.4	Characterisation of the coated substrate .....	36
3.2.5	Electrochemical Experiments .....	37
3.2.6	Photocatalytic Experiments .....	38
3.2.7	Ultrasonic stability of the Ti felt/nanotube/PbO <sub>2</sub> calcined substrate..	38
3.3	Results and discussion .....	39
3.3.1	Surface characterisation of TiO <sub>2</sub> nanotubes.....	39
3.3.2	Effect of operating parameters on nanotube growth.....	46
3.3.3	Decoration of nanotubes with PbO <sub>2</sub> .....	49
3.3.4	Electrochemical studies of novel coatings containing PbO <sub>2</sub> .....	55
3.3.5	Electrochemical removal and discolouration of RB-5 dye.....	59
3.3.6	Reaction kinetics for electrooxidation of RB-5 dye .....	64
3.3.7	Current efficiency and energy consumption for oxidation of Reactive Black-5.....	65
3.3.8	Photocatalytic oxidation of Reactive Black-5 .....	68
3.4	Conclusions.....	72
3.5	References.....	73
<b>Chapter 4: Decolourisation of Reactive Black-5 at an RVC substrate decorated with PbO<sub>2</sub>/ TiO<sub>2</sub> nanosheets prepared by anodic electrodeposition .....</b>		
		<b>83</b>
4.1	Introduction.....	84
4.2	Experimental Details.....	88
4.2.1	Synthesis of titanate nanosheets .....	88
4.2.2	Electrodeposition of PbO <sub>2</sub> on RVC .....	89
4.2.3	Anodic electrophoretic Deposition .....	90
4.2.4	Heat treatment.....	91
4.2.5	Characterisation of the coated substrate .....	92
4.2.6	Electrochemical Experiments .....	92

4.2.7	Photocatalytic experiments .....	93
4.2.8	Ultrasonic stability of the TiNS/ PbO <sub>2</sub> /RVC calcined substrate .....	93
4.3	Results and discussion .....	93
4.3.1	Surface characterisation of TiNS/PbO <sub>2</sub> coated RVC.....	93
4.3.2	Electrochemical studies of TiNS/PbO <sub>2</sub> /RVC novel coatings .....	99
4.3.3	Electrochemical decolourisation of RB-5 dye.....	102
4.3.4	Photocatalytic oxidation of Reactive black-5 dye .....	107
4.4	Conclusion .....	111
4.5	References.....	112
<b>Chapter 5: Photocatalytic oxidation of dye using titanate nanotubes</b>		
<b>anodically deposited on RVC by anodic electrophoretic deposition.....</b>		<b>123</b>
5.1	Introduction.....	123
5.2	Experimental details.....	128
5.2.1	Anodic electrophoretic deposition.....	128
5.2.2	Heat treatment.....	129
5.2.3	Characterization of the coated substrate .....	129
5.2.4	Photocatalytic Experiments .....	129
5.2.5	Ultrasonic stability for TiNT/RVC calcined substrate .....	131
5.3	Results and Discussion .....	131
5.3.1	Surface characterization of TiNT coated RVC.....	131
5.3.2	Photocatalytic oxidation of methylene blue .....	137
5.4	Conclusions.....	142
5.5	References.....	143
<b>Chapter 6: Grass inspired anodised ZnO-TiO<sub>2</sub> core-shell decorated by PbO<sub>2</sub></b>		
<b>for the oxidation of reactive black-5 dye .....</b>		<b>151</b>
6.1	Introduction.....	151
6.2	Experimental Details.....	153
6.2.1	Synthesis of Zn nanoforest, grass-like nanowires by anodising.....	153
6.2.2	Preparation of ZnO-TiO <sub>2</sub> core-shell nanorods structures by dip coating .....	154

6.2.3	Heat treatment.....	155
6.2.4	Anodic electrodeposition .....	155
6.2.5	Characterization of coated substrate .....	155
6.2.6	Electrochemical Experiments .....	156
6.2.7	Photocatalytic Experiments .....	156
6.2.8	Ultrasonic stability for coatings.....	157
6.3	Results and discussion .....	157
6.3.1	Surface characterization of Zn nano forest grass like nanowires .....	157
6.3.2	Mechanism of nanowire growth .....	162
6.3.3	Effect of cell potential difference on film growth .....	164
6.3.4	Effect of NaHCO <sub>3</sub> concentration on evolution of nanowires .....	165
6.3.5	ZnO/ TiO <sub>2</sub> core-shell surface characterization.....	166
6.3.6	PbO <sub>2</sub> multi core shell over the ZnO-TiO <sub>2</sub> core shell characterization .....	167
6.3.7	Electrochemical measurements on the coatings .....	171
6.3.8	Electrochemical discolouration of RB-5 dye.....	173
6.3.9	Photocatalytic discolouration of RB-5 dye.....	178
6.4	Conclusion .....	182
6.5	References.....	182
<b>Chapter 7: Conclusion and Suggestions for Future Work.....</b>		<b>189</b>
7.1	Conclusions.....	189
7.2	References.....	193
7.3	Future Work.....	193
7.3.1	DSA electrodes over Ti felt substrate for anodic oxidation of Azo dyes .....	193
7.3.2	Evaluation of new electrode materials.....	194
7.3.3	Planned Publications.....	194
<b>Appendix.....</b>		<b>Error! Bookmark not defined.</b>





## List of tables

Table 1.1	Comparison of different pollutants with range of concentration treated by using EAOPs. ....	4
Table 3.1	Effect of operating conditions on Ti felt anodization (Ti felt anode with dimensions 2 cm × 2 cm × 0.15 cm, graphite plate cathode with dimensions 1.5 cm × 6 cm × 1.2 cm, stirring = 300 rev min <sup>-1</sup> , T = 25 °C, t = 1 hour)..	46
Table 3.2	Comparison of different parameters including pseudo rate constant, % conversion and reaction time for oxidation of RB-5 dye by Ti felt, Ti felt / TiO <sub>2</sub> nanotubes and Calcined Ti felt / TiO <sub>2</sub> nanotubes /PbO <sub>2</sub> and other related values from selected literature.....	72
Table 4.1	Comparison of pseudo rate constants for oxidation of RB-5 dye by RVC, calcined TiNS(TiO <sub>2</sub> )/PbO <sub>2</sub> /RVC and PbO <sub>2</sub> /RVC and other related values from selected literature.....	104
Table 5.1	Comparison of pseudo rate constants for photocatalytic oxidation of methylene blue dye by RVC, TiNT/RVC and calcined TiNT/RVC and other related values from selected literature.....	142
Table 6.1	Morphological evolution of anodized Zn plate at different conditions for finding the optimum conditions for Zn forest grass like nanowires Image 1 a) 10 V and 6.8 × 10 <sup>-3</sup> mol dm <sup>-3</sup> , 2 a) 5 V and 6.8 × 10 <sup>-3</sup> mol dm <sup>-3</sup> , Image 3 a) 10 V and 13.6 × 10 <sup>-3</sup> mol dm <sup>-3</sup> , Image 4 a) 5 V and 13.6 × 10 <sup>-3</sup> mol dm <sup>-3</sup> , Image 5 a) 5 V and 30 × 10 <sup>-3</sup> mol dm <sup>-3</sup> Image, 6 a) 5 V and 50 × 10 <sup>-3</sup> mol dm <sup>-3</sup> , Image 7a) 5 V and 100 × 10 <sup>-3</sup> mol dm <sup>-3</sup> where images 1-7 b) are FESEM morphologies of the image represented in images 1-7 a) at higher magnification.....	161
Table 6.2	Comparison of pseudo rate constants for oxidation of RB-5 dye by using ZnO nanoflower coating ZnO-TiO <sub>2</sub> core-shell coating and hybrid core (ZnO-TiO <sub>2</sub> )-shell (PbO <sub>2</sub> ) coating by electrochemical and photocatalytic treatment.....	176
Table 7.1	<b>List of planned publications.....</b>	195



## List of figures

Figure 1.1 Categorization for electrochemical advanced oxidation processes (EAOPs)..	3
Figure 3.1 Structure of RB-5 dye where, .....	37
Figure 3.2 FESEM Images of nanotubes on the Ti felt substrate obtained by anodization: (a) Pre-treated Ti felt substrate at $300 \times$ magnification (b) TiO <sub>2</sub> nanotubes on Ti felt at 15 V, $0.1 \text{ mol dm}^{-3}$ MSA $0.5 \text{ wt. \% NH}_4\text{F}$ at $7000 \times$ magnification. The inset shows the nanotubes over Ti felt.....	40
Figure 3.3 FESEM image of (a) TiO <sub>2</sub> nanotubes on Ti felt at 20V, $1 \text{ mol dm}^{-3}$ MSA, $1 \text{ wt. \%}$ at $7000 \times$ magnification (b) TiO <sub>2</sub> nanotubes on Ti felt at 20V, $1 \text{ mol dm}^{-3}$ MSA, $1 \text{ wt. \% NH}_4\text{F}$ at $30000 \times$ magnification (c) Bendable porous Ti felt electrode after anodization.....	41
Figure 3.4 FESEM image of (a) TiO <sub>2</sub> nanotubes on Ti felt at 5 V, $1 \text{ mol dm}^{-3}$ MSA, $1 \text{ wt. \% NH}_4\text{F}$ at 13000 magnification (b) TiO <sub>2</sub> nanotubes on Ti felt at 30 V $1 \text{ mol dm}^{-3}$ MSA, $1 \text{ wt. \% NH}_4\text{F}$ at 13000 magnification.....	47
Figure 3.5 Arrangement for the synthesis of Ti felt/ TiO <sub>2</sub> nanotubes /PbO <sub>2</sub> composite.	50
Figure 3.6 FESEM Images of nanotubes decorated with PbO <sub>2</sub> on the Ti felt substrate obtained by layer by layer immersion: (a) PbO <sub>2</sub> covered TiO <sub>2</sub> nanotubes on Ti felt at a cell potential of 20 V in $1 \text{ mol dm}^{-3}$ MSA containing $1 \text{ wt. \% NH}_4\text{F}$ at $30000 \times$ magnification (b) PbO <sub>2</sub> covered TiO <sub>2</sub> nanotubes ( $t_i = 15 \text{ min}$ ) on Ti felt at 20 V in $1 \text{ mol dm}^{-3}$ MSA + $1 \text{ wt. \% NH}_4\text{F}$ at $60000 \times$ magnification.....	51
Figure 3.7 FESEM Images of nanotubes decorated with PbO <sub>2</sub> particles on the Ti felt substrate obtained by layer by layer immersion (a) TiO <sub>2</sub> nanotubes decorated with PbO <sub>2</sub> ( $t_i = 6 \text{ h}$ ) at $200 \times$ magnification (b) TiO <sub>2</sub> nanotubes decorated with spheroid like PbO <sub>2</sub> crystals( $t_i = 6 \text{ h}$ ) on Ti felt at $1500 \times$ magnification. The inset shows the uncovered nanotubes at $35000 \times$ magnification.....	52
Figure 3.8 (a) TiO <sub>2</sub> nanotubes covered PbO <sub>2</sub> ( $t_i = 12 \text{ h}$ ) on Ti felt $200 \times$ magnification (b) TiO <sub>2</sub> nanotubes covered with cauliflower like PbO <sub>2</sub> crystals ( $t_i = 12 \text{ h}$ ) on Ti felt at $1500 \times$ magnification, the inset shows the PbO <sub>2</sub> covered nanotubes at $35000 \times$ magnification. ....	53

Figure 3.9 EDX images for elemental analysis of calcined Ti felt / TiO <sub>2</sub> nanotubes /PbO <sub>2</sub> obtained by anodization and layer by layer immersion: (a) calcined Ti felt / TiO <sub>2</sub> nanotubes /PbO <sub>2</sub> at 900 magnification (b) lead interpretation (c) titanium interpretation (d) oxygen interpretation (e) Sum spectrum for elemental plot interpretation.....	54
Figure 3.10 Raman spectra of calcined and non-calcined Ti felt / TiO <sub>2</sub> nanotubes /PbO <sub>2</sub> ( <i>t<sub>i</sub></i> = 15 min) at 450 °C and calcined non-calcined Ti felt / TiO <sub>2</sub> nanotubes.	55
Figure 3.11 Polarization curve by using the coatings a) Ti felt / TiO <sub>2</sub> nanotubes /PbO <sub>2</sub> as positive electrode after annealing at 450 °C in an electrolyte containing in 0.05 mol dm <sup>-3</sup> H <sub>2</sub> SO <sub>4</sub> . b) Ti felt / TiO <sub>2</sub> nanotubes in an electrolyte containing in 0.05 mol dm <sup>-3</sup> H <sub>2</sub> SO <sub>4</sub> background electrolyte; potential scan rate of 10 mV s <sup>-1</sup> ; T = 25 °C.....	56
Figure 3.12 Electrochemical oxidation of RB-5 dye in an electrolyte having 2 × 10 <sup>-5</sup> mol dm <sup>-3</sup> R.B-5 dye in 0.5 mol dm <sup>-3</sup> Na <sub>2</sub> SO <sub>4</sub> (Experimental conditions: applied potential = 1.4 V vs. Hg/HgO pH = 3.0, T = 25 °C) by using ▲) Ti felt, ●) Ti felt / TiO <sub>2</sub> nanotubes, and ■) Ti felt / TiO <sub>2</sub> nanotubes / PbO <sub>2</sub> ....	61
Figure 3.13 Electrochemical oxidation kinetics of RB-5 dye in an electrolyte having 2 × 10 <sup>-5</sup> mol dm <sup>-3</sup> R.B-5 dye in 0.5 mol dm <sup>-3</sup> Na <sub>2</sub> SO <sub>4</sub> (Experimental conditions: applied potential = 1.4 V vs. Hg/HgO pH = 3.0, T = 25 °C) by using ▲) Ti felt, ●) Ti felt / TiO <sub>2</sub> nanotubes, and ■) Ti felt / TiO <sub>2</sub> nanotubes /PbO <sub>2</sub> .	63
Figure 3.14 Degradation pathway for the oxidation RB-5 dye.....	67
Figure 3.15 Photocatalytic oxidation of 2 × 10 <sup>-5</sup> mol dm <sup>-3</sup> RB-5 dye in 0.5 mol dm <sup>-3</sup> of sodium sulfate by ●) calcined Ti felt / TiO <sub>2</sub> nanotubes /PbO <sub>2</sub> ( <i>t<sub>i</sub></i> =15 min), ▲) uncalcined Ti felt / TiO <sub>2</sub> nanotubes Inset shows ■) oxidation kinetics by using calcined Ti felt /nanotubes /PbO <sub>2</sub> ( <i>t<sub>i</sub></i> = 15 min) ○) uncalcined Ti felt / TiO <sub>2</sub> nanotubes (Experimental conditions: UV lamp intensity = 1.5 mW cm <sup>-2</sup> , pH = 3.0, T = 25 °C).....	69
Figure 4.1 Schematic view for electroplating of PbO <sub>2</sub> , solution containing 1 mol dm <sup>-3</sup> Pb(CH <sub>3</sub> SO <sub>3</sub> ) <sub>2</sub> and 0.2 mol dm <sup>-3</sup> MSA at 2.5 A and 60°C for 30 min in a small undivided glass cell containing 100 cm <sup>3</sup> of electrolyte. ....	90
Figure 4.2 Schematic view for deposition of TiNS, suspension containing 100 cm <sup>3</sup> of TiNS exfoliated with tetrabutylammonium hydroxide (TBAOH) for 15min of electrophoretic deposition.....	91

Figure 4.3 FESEM Images of TiNS/PbO <sub>2</sub> coatings on the RVC substrate obtained by anodic electrophoresis: (a) PbO <sub>2</sub> /RVC substrate after anodic EPD with inset at 7000 magnification, (b) Layer thickness of PbO <sub>2</sub> /RVC substrate.....	94
Figure 4.4 (a) TiNS/PbO <sub>2</sub> /RVC layer showing fully covered layer of TiNS film over PbO <sub>2</sub> / RVC (b) TiNS/PbO <sub>2</sub> /RVC layer at higher magnification.....	95
Figure 4.5 (a) TiNS/ PbO <sub>2</sub> /RVC after calcination at 450 °C, (b) calcined TiNS/PbO <sub>2</sub> /RVC layer having undulated surfaces at higher magnification.....	96
Figure 4.6 EDX images for elemental analysis of TiNS/PbO <sub>2</sub> /RVC (calcined) obtained by anodic electrophoretic deposition: (a) calcined TiNS/PbO <sub>2</sub> /RVC at 900 magnification (b) titanium elemental analysis (c) carbon (RVC) elemental analysis (d) lead elemental analysis. ....	97
Figure 4.7 Raman spectra of the TiNS/PbO <sub>2</sub> /RVC obtained by anodic electrophoretic deposition a) calcined and b) non-calcined at 450 °C, where A denotes anatase, T denotes Titanate. ....	98
Figure 4.8 Polarization curve by using coating 1) (TiNS /PbO <sub>2</sub> / RVC) as anode after calcination at 450 °C in 0.5 mol dm <sup>-3</sup> Na <sub>2</sub> SO <sub>4</sub> , pH=3.0. 2) (PbO <sub>2</sub> / RVC) as anode in 0.5 mol dm <sup>-3</sup> Na <sub>2</sub> SO <sub>4</sub> , Experimental conditions: Potential sweep rate = 10 mV s <sup>-1</sup> , temperature: 25 °C.....	100
Figure 4.9 Polarization curve by using 1) TiNS /PbO <sub>2</sub> / RVC coating as anode in an electrolyte 1× 10 <sup>-5</sup> mol dm <sup>-3</sup> R.B-5 dye in 0.5 mol dm <sup>-3</sup> Na <sub>2</sub> SO <sub>4</sub> , pH=3.0. 2) (PbO <sub>2</sub> / RVC) as anode after calcination at 450 °C in an electrolyte 1× 10 <sup>-5</sup> mol dm <sup>-3</sup> , R.B-5 dye in 0.5 mol dm <sup>-3</sup> Na <sub>2</sub> SO <sub>4</sub> , pH=3.0, Experimental conditions: Potential sweep rate = 10 mV s <sup>-1</sup> , Temperature: 25 °C. ....	101
Figure 4.10 Electrochemical oxidation of RB-5 dye in a solution containing 1× 10 <sup>-5</sup> mol dm <sup>-3</sup> of RB-5 dye and 0.5 mol dm <sup>-3</sup> Na <sub>2</sub> SO <sub>4</sub> by ■) RVC, □) Photoassisted Fenton using Iron oxide on activated alumina support [49], ▲) RVC/PbO <sub>2</sub> , and ○) calcined TiNS/PbO <sub>2</sub> /RVC (Experimental conditions: applied current density = 2 mA cm <sup>-2</sup> , pH = 3.0, T = 25 °C).....	102
Figure 4.11 Electrochemical oxidation kinetics of RB-5 dye in a solution containing 1× 10 <sup>-5</sup> mol dm <sup>-3</sup> of RB-5 dye and 0.5 mol dm <sup>-3</sup> Na <sub>2</sub> SO <sub>4</sub> by ■) RVC, □) Photoassisted Fenton using Iron oxide on activated alumina support [49], ▲) RVC/PbO <sub>2</sub> , and ○) calcined TiNS/PbO <sub>2</sub> /RVC (Experimental conditions: applied current density = 2 mA cm <sup>-2</sup> , pH = 3.0, T = 25 °C). ....	106

Figure 4.12 Photocatalytic oxidation of RB-5 dye in a solution containing $1 \times 10^{-5}$ mol $\text{dm}^{-3}$ of RB-5 dye and $0.5 \text{ mol dm}^{-3}$ $\text{Na}_2\text{SO}_4$ by ▼) RVC , ●) calcined TiNS/ $\text{PbO}_2$ /RVC (Experimental conditions: UV lamp intensity = $1.5 \text{ mW cm}^{-2}$ , pH = 3.0, T = 25 °C).....	108
Figure 4.13 Photocatalytic oxidation kinetics of RB-5 dye in a solution containing $1 \times 10^{-5}$ mol $\text{dm}^{-3}$ of RB-5 dye and $0.5 \text{ mol dm}^{-3}$ $\text{Na}_2\text{SO}_4$ by ▼) RVC, ●) calcined TiNS/ $\text{PbO}_2$ /RVC (Experimental conditions: UV lamp intensity = $1.5 \text{ mW cm}^{-2}$ , pH = 3.0, T = 25 °C).....	110
Figure 5.1 Structure of Methylene blue dye where,.....	130
Figure 5.2 SEM images of TiNT coatings over the RVC substrate obtained by anodic electrophoretic deposition (a) TiNT/RVC layers at $30 \times$ magnification, (b) TiNT/RVC at $15000 \times$ magnification (c) TiNT/RVC at $17,000 \times$ magnification (d) TiNT/RVC at $18,000 \times$ magnification (e) TiNT/RVC at $20,000 \times$ magnification. ....	132
Figure 5.3 SEM images of calcined TiNT/RVC substrate obtained by anodic electrophoretic deposition (a) TiNT/RVC layers at $30 \times$ Magnification (b) TiNT/RVC inside layer 2 at $160 \times$ Magnification. ....	134
Figure 5.4 SEM images of TiNT coatings over the RVC substrate obtained by anodic electrophoretic deposition (a) TiNT/RVC (non-calcined) layer thickness (b) TiNT/RVC (calcined) layer thickness.....	135
Figure 5.5 Raman spectra of the TiNT/RVC obtained by anodic electrophoretic deposition non-calcined and calcined at $450 \text{ }^\circ\text{C}$ .....	136
Figure 5.6 Photocatalytic oxidation of $1.29 \times 10^{-6}$ mol $\text{dm}^{-3}$ methylene blue dye and $0.5 \text{ mol dm}^{-3}$ $\text{Na}_2\text{SO}_4$ illuminated by UV radiation by using ●) RVC acid treated, ▲) TiNT/RVC and ○) TiNT/RVC calcined (Experimental conditions: UV lamp intensity = $1.5 \text{ mW cm}^{-2}$ , T = 25 °C). ....	138
Figure 5.7 Photocatalytic pseudo oxidation kinetics of $1.29 \times 10^{-6}$ mol $\text{dm}^{-3}$ methylene blue dye and $0.5 \text{ mol dm}^{-3}$ $\text{Na}_2\text{SO}_4$ methylene blue dye illuminated by UV radiation by using ●) RVC acid treated, ▲) TiNT/RVC and ○) TiNT/RVC calcined (Experimental conditions: UV lamp intensity = $1.5 \text{ mW cm}^{-2}$ , T = $25 \text{ }^\circ\text{C}$ ). ....	140
Figure 6.1 FESEM (a) surface morphology (b) cross-sectional view of anodised Zn plate complete film layer over zinc surface with forest grass like structure	

	(c) more magnified image of (a), in an electrolyte containing $30 \times 10^{-3} \text{ mol dm}^{-3} \text{ NaHCO}_3$ at 5 V for 10 min. ....	158
Figure 6.2	FESEM (a) magnified surface morphology of anodized Zn plate (b) the evolution of a layered pattern with regular hexagonal wires complete film layer over zinc surface with forest grass like structure (c) surface morphologies and cross-sections demonstrating the primary development of scattered nanowires in an electrolyte containing $30 \times 10^{-3} \text{ mol dm}^{-3} \text{ NaHCO}_3$ at 5 V for 10 min. ....	158
Figure 6.3	FESEM Images of a) Anodization of Zn plate at 1V and $30 \times 10^{-3} \text{ mol dm}^{-3}$ b) magnified image of a). ....	164
Figure 6.4	FESEM Images of a) Anodising of Zn plate at 10 V b) magnified image of a). ....	165
Figure 6.5	FESEM Images of a) dip coating and calcination ( $400 \text{ }^\circ\text{C}$ ) of anodized zinc plate at optimum conditions ( $5 \text{ V}$ and $30 \times 10^{-3} \text{ mol dm}^{-3} \text{ NaHCO}_3$ at 10 min anodising time) (b) magnified image of a) with inset showing up the ZnO/TiO <sub>2</sub> core-shell, c) EDX elemental analysis of ZnO/TiO <sub>2</sub> core-shell coating d) Zn elemental analysis e) Ti elemental analysis. ....	167
Figure 6.6	FESEM images of a) electrodeposition of PbO <sub>2</sub> using ZnO/TiO <sub>2</sub> core-shell in a bath containing $80 \text{ cm}^3$ of $0.1 \text{ mol dm}^{-3}$ boric acid with $0.01 \text{ mol dm}^{-3}$ Pb(NO <sub>3</sub> ) <sub>2</sub> at a current density of $5 \text{ mA cm}^{-2}$ under galvanostatic conditions for 30 min, b) magnified image of a) with inset showing up the hybrid core (ZnO-TiO <sub>2</sub> )-shell (PbO <sub>2</sub> ), c) coating hybrid core (ZnO-TiO <sub>2</sub> )-shell (PbO <sub>2</sub> ) at 30000 magnification (d) lead elemental analysis. ....	168
Figure 6.7	Raman spectra of a) non calcined substrate after anodization of Zn plate and dip coating with titanium (IV) butoxide (ZnO-TiO <sub>2</sub> core-shell coating) and b) calcined ZnO-TiO <sub>2</sub> core-shell coating calcined at $400 \text{ }^\circ\text{C}$ . ....	170
Figure 6.8	Polarization curves by using coatings a) ZnO-TiO <sub>2</sub> core-shell coating as anode in an electrolyte containing $0.05 \text{ mol dm}^{-3} \text{ H}_2\text{SO}_4$ . b) hybrid core (ZnO-TiO <sub>2</sub> )-shell (PbO <sub>2</sub> ) coating as an anode after calcination at $400 \text{ }^\circ\text{C}$ in an electrolyte containing $0.05 \text{ mol dm}^{-3} \text{ H}_2\text{SO}_4$ , Experimental conditions: Potential sweep rate $5 \text{ mV s}^{-1}$ , temperature: $25 \text{ }^\circ\text{C}$ . ....	172
Figure 6.9	Electrochemical oxidation of $20 \text{ mg dm}^{-3}$ RB-5 dye and $0.6 \text{ mol dm}^{-3} \text{ Na}_2\text{SO}_4$ (Experimental conditions: applied potential = $1.0 \text{ V vs. Hg/HgO}$	



pH = 3.0, T = 25 °C) by using ▲) ZnO nanoflower coating, ●) ZnO-TiO<sub>2</sub> core-shell coating and ■) hybrid core (ZnO-TiO<sub>2</sub>)-shell (PbO<sub>2</sub>) coating... 175

Figure 6.10 Electrochemical oxidation kinetics of RB-5 dye of 20 mg dm<sup>-3</sup> RB-5 dye and 0.6 mol dm<sup>-3</sup> Na<sub>2</sub>SO<sub>4</sub> (Experimental conditions: applied potential = 1.0 V vs. Hg/HgO pH = 3.0, T = 25 °C) by using ▲) ZnO nanoflower coating, ●) ZnO-TiO<sub>2</sub> core-shell coating and ■) hybrid core (ZnO-TiO<sub>2</sub>)-shell (PbO<sub>2</sub>) coating. .... 177

Figure 6.11 Photocatalytic oxidation of 20 mg dm<sup>-3</sup> RB-5 dye and 0.6 mol dm<sup>-3</sup> Na<sub>2</sub>SO<sub>4</sub> (Experimental conditions: UV lamp intensity = 1.5 mW cm<sup>-2</sup>, pH = 3.0, T = 25 °C) in 0.6 mol dm<sup>-3</sup> of sodium sulphate by using ●) hybrid core (ZnO-TiO<sub>2</sub> core-shell coating )-shell (PbO<sub>2</sub>) coating, ▲) ZnO nanorods coating, and ■) ZnO-TiO<sub>2</sub> core-shell coating..... 180

Figure 6.12 Photocatalytic oxidation kinetics of 20 mg dm<sup>-3</sup> RB-5 dye and 0.6 mol dm<sup>-3</sup> Na<sub>2</sub>SO<sub>4</sub> (Experimental conditions: UV lamp intensity = 20 mW cm<sup>-2</sup>, pH = 3.0, T = 25 °C) in 0.6 mol dm<sup>-3</sup> of sodium sulphate by using ●) hybrid core (ZnO-TiO<sub>2</sub> core-shell coating)-shell (PbO<sub>2</sub>) coating, ▲) ZnO nanoflower coating and ■) ZnO-TiO<sub>2</sub> core-shell coating..... 181

### Research Thesis: Declaration of Authorship

Print name:	Syed Zohaib Javaid Zaidi
-------------	--------------------------

Title of thesis:	Electrochemical and photocatalytic oxidation of organic pollutants from waste water using efficient nano-catalytic coatings prepared by electrodeposition
------------------	---

I declare that this thesis and the work presented in it are my own and has been generated by me as the result of my own original research.

I confirm that:

1. This work was done wholly or mainly while in candidature for a research degree at this University;
2. Where any part of this thesis has previously been submitted for a degree or any other qualification at this University or any other institution, this has been clearly stated;
3. Where I have consulted the published work of others, this is always clearly attributed;
4. Where I have quoted from the work of others, the source is always given. With the exception of such quotations, this thesis is entirely my own work;
5. Where the thesis is based on work done by myself jointly with others, I have made clear exactly what was done by others and what I have contributed myself;
6. Parts of this work have been published at:  
Zaidi, S.Z.J., Harito, C., Walsh, F.C., Ponce de Leon, C., J Solid State Electrochem (2018) 22: 2889.

Signature:		Date:	27 May, 2018
------------	--	-------	--------------

## ACKNOWLEDGEMENTS

I would like to express my sincerest gratitude to my research supervisors Dr. Carlos Ponce de Leon Albarran and Prof. Frank Walsh for their overwhelming support, motivation, and outstanding scientific guidance to excel in my doctoral studies and research as well as my future professional career.

I would like to appreciate my PhD colleague and collaborator Dr. Christian Harito for his sincere ideas for my experimental design and setup and efforts during this journey of my PhD. I also acknowledge and indebted to internal examiners Dr. Dimitry Bavykin and Dr. Monica Ratoi for useful discussions and for encouraging my research work throughout my studies along with advices to present my valuable contributions in more reputed forms. The result of those encouraging comments has enabled me to publish a novel research article in journal of solid state electrochemistry.

I would like to extend my thanks to my primary supervisor Dr. Carlos Ponce de Leon Albarran who provided the necessary equipments including hardware and softwares to perform my experiments. I am also grateful to Dr. Christian Harito and Alex Keeler for their assistance in developing analytical methods using SEM and Raman spectroscopy. I am also thankful to Dr Rachel, Dr. Fernando, Dr. Horacio, Nicholas and Abdul Aziz who assisted me to acquire useful knowledge in the field of electrochemical engineering.

Special mention should be made of my beloved parents and sister for their moral support who managed my absence with courage and patience.

## List of Abbreviations

<b>Abbreviation</b>	<b>Meaning</b>
AM	Anodic material
AO	Anodic oxidation
BDD	Boron-doped diamond
CE	Counter electrode
CF	Carbon felt
CV	Cyclic voltammetry
DSA	Dimensional stable anode
EAOPs	Electrochemical Advanced oxidation processes
EDX	Energy dispersive x-ray spectroscopy
EPD	Electrophoretic deposition
ECTS	Electrochemical technologies
FESEM	Field emission scanning electron microscopy
NG	Not given
OMR	Organic matter residue
O	Oxidized species (reductant)
ORR	Oxygen reduction reaction
PTFE	Polytetrafluoroethylene
PVP	Polyvinylpyrrolidone
R	Reduced species (oxidant)
RE	Reference electrode
RVC	Reticulated Vitreous Carbon
RT	Room temperature
SCE	Saturated calomel electrode
SHE	Standard hydrogen electrode
TBAOH	Tetrabutylammonium hydroxide
TiNT	Titanate nanotubes
TiNS	Titanate nanosheets

WE	Working electrode
WAO	Wet air oxidation
UV	Ultraviolet irradiation
UV vis	Ultraviolet visible

## List of Symbols

Symbol	Meaning	Units
$A$	Electrode area	$\text{cm}^2$
$c$	Concentration of species	$\text{mol cm}^{-3}$
$d$	Interelectrode gap	cm
$I_D$	Disorder band	a.u
$I_G$	Graphitic band	a.u
$k$	Pseudo first order rate constant	$\text{min}^{-1}$
$t$	Time	s
$\lambda$	Incident light wavelength	

# Chapter 1: **Introduction**

## **1.1 Background and motivation**

Industrial wastewater possess a mixture of dissolved organic and inorganic pollutants, in combination with suspended material, and not a single process is possible for the treatment of such wastewater, instead, an integral approach with different methods is necessary. As for the treatment of wastewater contaminated with dissolved organic compounds only, biological oxidation is the most affordable process, but the presence of toxic molecules or bio-refractory agents affects this process [1]. These problems have led to the development of treatment methods such as adsorption, coagulation, flocculation, filtration, ozone, hydrogen peroxide and electrochemical advanced oxidation processes (EAOPs) which are being putting in practice, depending on the needs and type of effluent. However, all the above mentioned processes have drawbacks. For instance, when the concentrations of the organic pollutants in the discharge wastewater are high, adsorption and filtration processes are obsolete, while coagulation produce sludge and electrochemical advanced oxidation processes (EAOPs) require high investment equipment cost with overheads [1]. The subject of the present research is the anodic oxidation of organic material contained in wastewater. This method is one of the AOP technologies that has attracted the attention of research groups over the last thirty years. Electrochemical oxidation processes provides an alternative method to environmental issues in the applied chemical enterprises, since the electrons and free radicals offers a safe, efficient, controllable, cost-effective, secure, clean and pure non pollutant reagent at the point of use [2, 3].

One of the problems with the EAOP's is the use of expensive noble metals (platinum, ruthenium, and palladium) or special coatings BDD (boron doped diamond) and DSA (dimensional stable anodes), which make the process costly in particular when large volumes of water need to be treated. Therefore new and advanced low cost materials such as RVC and Ti felt substrates are the motivation for this research work. These materials were explored in combination with electrophoretic deposition of titania (nanotubes and nanosheets) and metal oxides deposited over their surfaces and used for the environmental oxidation of artificial water containing RB-5 dye. This compound is an anionic dye and can be adsorbed by the positively charged nanosheets during an anodic oxidation process.

## **1.2 Electrochemical Advanced oxidation processes (EAOPs)**

Progress in chemical and wastewater remediation has led to the evolution of techniques called electrochemical advanced oxidation processes (EAOPs). EAOPs are liquid phase treatment methods mediated by powerful reactive species like  $\bullet\text{OH}$  radicals which lead to the mineralisation of toxic dissolved organic matter [2, 4, 5]. With  $\bullet\text{OH}$  radicals as the major oxidizing agent, the oxidation of pollutants to carbon dioxide, water and inorganic compounds can occur, or the transformation of organic substances into distinctly oxidized, lower molecular weight harmless compounds.

EAOPs can be categorized into those with or without the consumption of electrical energy, as shown in figure 1.1.



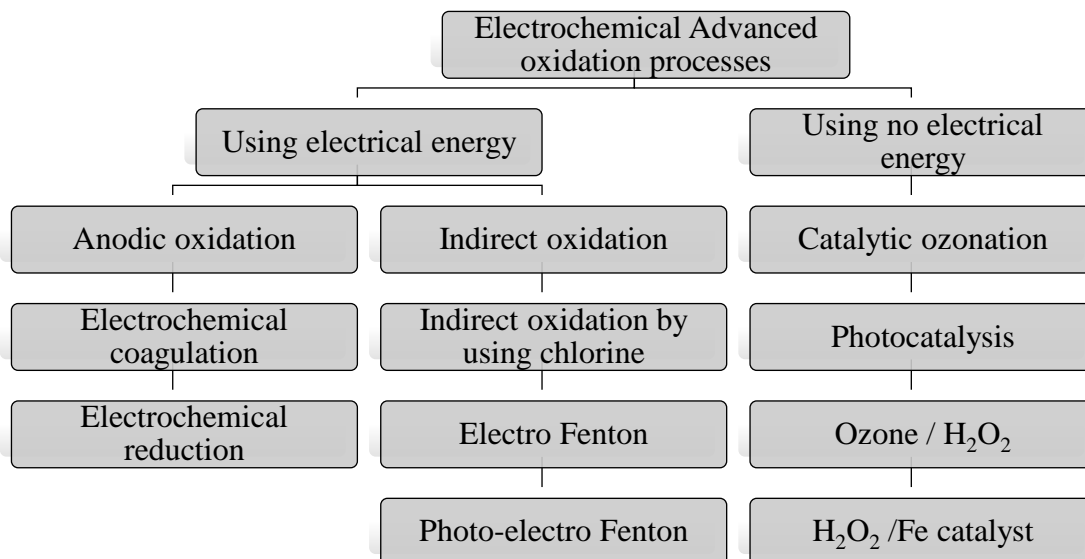


Figure 1.1 Categorization for electrochemical advanced oxidation processes (EAOPs).

Another mineralization process usually assessed as EAOP is WAO a homogenous process, where organic matter residue (OMR) is oxidized in a liquid medium with oxygen from the atmospheric air at higher temperature (250-300 °C) and pressure (1500 PSI) in the presence of  $\text{Cu}^{2+}$  ions as catalyst. Water and waste water treatment are the most important domain in the joint research effort to develop EAOP, however the purification of groundwater, soil removal, urban waste water management and conditioning of the sludge, the production of ultrapure water, and the treatment of volatile organic compounds and odour control have also been discussed in the literature [2,4,5].

During the water treatment process, many types of industrial sewage waste are discharged, these include: distillery, agrochemical waste, pulp and paper industry waste, textile dye house, oilfields and refineries and metal-plating. In addition, there are hazardous waste waters that need to be treated, such as: residues from hospitals and slaughterhouses, removal of pathogens and persistent, endocrine disrupting pharmaceutical pollutants from

the municipality wastewater, oxidation of organics such as pesticides and heavy metals such as arsenic and chromium [2].

<b>Pollutant</b>	<b>Concentration (mg dm<sup>-3</sup>)</b>	<b>Electrochemical Reactor</b>	<b>Conve rsion / %</b>	<b>EAOP method</b>	<b>Refere nce</b>
Remazol Black -B	159	Undivided reactor	99	Anodic oxidation	[6]
Pharmaceutical industry wastewater	COD = 12000	Parallel plate flow reactor	100	Anodic oxidation	[7]
Real textile wastewater	COD = 1224	Undivided reactor	75	Electro Fenton	[8]
Orange II dye	50	Undivided reactor	100	Photoelectr o Fenton	[9]
Perchloroethylene	57	Photocatalytic reactor	43	Photocataly sis	[10]
Reactive orange 16	100	Dual Compartment divided reactor	100	Photoelectr ocatalysis	[11]

Table 1.1 Comparison of different pollutants with range of concentration treated by using EAOPs.

Table 1.1 shows some examples of EAOP: industrial waste water from a textile industry containing 159mg dm<sup>-3</sup> remazol black –B dye [6] treated with BDD electrodes in a single compartment cell, resulted in a complete decolourisation with mineralization of up to 85% by applying a current density of 50 mA cm<sup>-2</sup> under acidic conditions (pH=1) in 180 min of electrolysis. Further, electrochemical degradation of wastewater (initial COD = 12000 mg dm<sup>-3</sup>) obtained from pharmaceutical industry has been studied in bench scale plant flow cell having BDD electrode as an anode [7]. Under alkaline conditions (pH=8.5) at

current density of  $179 \text{ mAcm}^{-2}$ , complete mineralization was obtained at a flowrate of  $0.56 \text{ dm}^3 \text{ min}^{-1}$  [12]. Similarly, anodic oxidation of real landfill leachate has been studied in a 3D undivided granular carbon bed electrochemical reactor. The results reported the removal of COD to 60% and mineralization of 83% in 60 min by applying a constant current of 3A [13]. Some studies revealed the superiority of one EAOP over another for example, Chou et al. found only 75% decay of wastewater containing textile dyes by using electroFenton EAOP [8] while in another study complete mineralization of dye was reported by using photo-electro Fenton method [9]. This superiority of photo-electro Fenton method, is reported due to the dual effect of hydroxyl radicals and free electron-hole pair under UV light produced during photo-electro Fenton EAOP.

Anodic oxidation is a method for partial or full mineralization of organic pollutants, it is considered to be very effective for the treatment of certain dilute wastewater with Chemical Oxygen Demand (COD) between  $30\text{-}100 \text{ g dm}^{-3}$  [14, 15]. The main benefit of anodic oxidation process is that it requires no chemicals. Only the electrical power is utilized while electrochemistry plays an environmentally feasible role, because the electron itself deemed to be a reactant that leaves no pollution and is clean at the point of use, it is a secure and active species during the process. The main advantages of the EAOP process discussed in literature are as follows [2, 3]:

1. **Versatility;** anodic oxidation is particularly adaptable and can cope with different types of organic matter and treatments, from micro-litre to tons of litres of effluents.

2. **Power requirements;** since the oxidation process occurs at room temperature in comparison to other treatment processes (like thermal incineration method), the applied voltage can be regulated and the operating conditions can be optimized to reduce electrical energy requirements.
3. **Data automation;** the parameters used in electrochemical processes are suitable for data management, process control and instrumentation.

The electrode material plays an important role for water treatment. Many electrodes like BDD, DSA and metal oxides based electrodes have been used for the degradation of organic pollutants by anodic oxidation methods. Recently, increasing trends has been seen for the use of Titanium based nanomaterials for water treatment as these materials possess high surface area with reasonable chemical resistance. Ramirez et al. for example synthesized composite containing titanate nanotubes for the anodic oxidation of methyl orange dye obtaining 98% colour removal at 0.6 A in 45 min [3]. Based on this information and other literature findings it is reasonable to suggest that anodic oxidation and Ti based nanomaterials like Ti-nanosheets can also be used for oxidation of organic pollutants.

### 1.3 Aims and Objectives

The main aim of this thesis is to synthesis several coatings embedded with nanostructured titanate (nanotubes and nanosheets) with a metal oxide, such as lead dioxide, as a precursors for producing  $\cdot\text{OH}$  free radicals during anodic oxidation. The study employs characterisation techniques such as FESEM, EDX and Raman analysis of the coatings on the low cost titanium and carbon based substrates. The investigation also include the

effect of the operating conditions on the formation of nanostructured titanate nanotubes on the titanium felt substrate. This research pursues the following objectives:

- Anodising titanium felt to grow arrays of titanium dioxide nanotubes decorated with  $\text{PbO}_2$ : Characterisation and application
- Preparation of  $\text{PbO}_2/\text{TiO}_2$  nanosheets at an RVC substrate by anodic electrophoretic deposition with subsequent use for electrochemical water treatment.
- Deposition of titanate nanotubes at an RVC substrate by anodic electrophoretic deposition with subsequent use for photocatalytic oxidation.
- Development of  $\text{ZnO}_2$  nanowire arrays on Zn metal substrate by using electrochemical anodization.
- Formation of a  $\text{ZnO-TiO}_2$  core-shell decorated by  $\text{PbO}_2$  on a Zn metal substrate with subsequent application for removal of RB-5 dye from aqueous solution.

#### **1.4 Thesis Outline**

This thesis is divided into literature review chapter 2, results and discussion and experimental details in chapters 3, 4, 5 and 6 for the objectives listed above, followed by conclusion and suggestions for future work in chapter 7. The experimental work emphasizes different approaches to synthesise titanate nanotubes on Ti felt by anodization and deposition of  $\text{PbO}_2$  characterised by SEM and Raman studies and utilized for electrochemical water treatment, discussed in chapter 3. Titanate nanosheets and  $\text{PbO}_2$

deposited by anodic electrophoretic deposition over RVC substrate and further characterized and applied for water treatment are presented in chapter 4. Titanate nanotubes anodically deposited on RVC by anodic electrophoretic deposition and further applied for photocatalytic oxidation of MB dye are shown in chapter 5. It is thought that since MB is cationic, it can be attracted by negatively charged nanotubes to improve its oxidation. Some of novel coatings involving ZnO-TiO<sub>2</sub> core-shell decorated by PbO<sub>2</sub> are synthesized and utilized for the electrochemical and photocatalytic oxidation of reactive black-5 dye in chapter 6.

## 1.5 References

1. M. Panizza, G. Cerisola. Direct and mediated anodic oxidation of organic pollutants *Chem.Rev.* 109 (2009) 6541-6569.
2. C. Comninellis, A. Kapalka, S. Malato, S.A. Parsons, L. Poulios, D. Mantzavinos. Advanced oxidation processes for water treatment: advances and trends for R&D, *J Chem Technol Biot*, 83 (2008) 769-776.
3. G. Ramírez, F.J. Recio, P. Herrasti, C. Ponce-de-León, I. Sirés, Effect of RVC porosity on the performance of PbO<sub>2</sub> composite coatings with titanate nanotubes for the electrochemical oxidation of azo dyes, *Electrochimica Acta*, 204 (2016) 9-17.
4. J.M. Poyatos, M.M Munio, M.C Almecija, JC Torres, E Hontoria, F Osorio. Advanced oxidation processes for wastewater treatment: State of the Art, *Water Air and Soil Pollution*, 205 (2010) 187-204.
5. J.J. Pignatello, E. Oliveros, A. MacKay. Advanced oxidation processes for organic contaminant destruction based on the Fenton reaction and related chemistry, *Crit.Rev.Environ.Sci.Technol.* 36 (2006) 1-84.
6. E. Tsantaki, T. Velegraki, A. Katsaounis, D. Mantzavinos, Anodic oxidation of textile dyehouse effluents on boron-doped diamond electrode. *Journal of hazardous materials*, 207 (2012) 91-96.
7. J.R. Domínguez, T. González, P.Palo, J. Sánchez-Martín, M.A.Rodrigo, C. Sáez, Electrochemical degradation of a real pharmaceutical effluent. *Water, Air, & Soil Pollution*, 223 (2012) 2685-2694.

8. W.L. Chou, M.H. Chung, Y.M Kuo, COD removal from real dyeing wastewater by electro-Fenton technology using an activated carbon fiber cathode. *Desalination*, 253 (2010) 129-134.
9. J.M. Peralta-Hernández, Y. Meas-Vong, F.J. Rodríguez, T.W. Chapman, M.I. Maldonado, L.A. Godínez, Comparison of hydrogen peroxide-based processes for treating dye-containing wastewater: decolourisation and destruction of Orange II azo dye in dilute solution. *Dyes and Pigments*, 76 (2008) 656-662.
10. D.H. Chen, X.U.E.J.U.N. Ye, K. Li, Oxidation of PCE with a UV LED photocatalytic reactor. *Chemical Engineering & Technology: Industrial Chemistry-Plant Equipment-Process Engineering-Biotechnology*, 28 (2005) 95-97.
11. P.A. Carneiro, M.E. Osugi, J.J. Sene, M.A. Anderson, M.V.B. Zanoni. Evaluation of colour removal and degradation of a reactive textile azo dye on nanoporous TiO<sub>2</sub> thin-film electrodes *Electrochim. Acta*, 49 (2004) 3807-3820
12. F.C Moreira, R.A Boaventura, E. Brillas, V.J Vilar, Electrochemical advanced oxidation processes: a review on their application to synthetic and real wastewaters. *Applied Catalysis B: Environmental*, 202 (2017) 217-261.
13. N.N.Rao, M. Rohit, G. Nitin, P.N. Parameswaran, J.K Astik, Kinetics of electrooxidation of landfill leachate in a three-dimensional carbon bed electrochemical reactor. *Chemosphere*, 76 (2009) 1206-1212.
14. R.M.Serikawa, Y. Senda, K. Sasaki. Industrial E-AOP application using boron doped diamond electrodes, *Proceedings of the 5th IWA specialist conference on oxidation technologies for water and wastewater Treatment* (2009).



15. M. Fryda, T. Matthee, S. Mulcahy, A. Hampel, L. Schafer, I. Troster. Fabrication and application of Diachem® electrodes, *Diamond and Related Materials*, 12 (2003) 1950-1956.

## Chapter 2: **Literature Review**

The electro oxidation of organics have been a subject of study from mid 1970s [1]. Within last two decades different research groups have been working to improve the anodic oxidation to contribute with new technologies [2-4] to protect water reserves. The major contributors on the theoretical and experimental aspects of electrochemical methods are groups of F.C Walsh [5-7], C.Comninellis [8-10], M. Panizza [11-13], P. Cañizares [14-16], E. Brillas [17-19] and A.M. Polcaro [20-22]. These groups have provided clear examples of electrochemical methods that follow different pathways for oxidation such as direct and indirect mechanisms that follow efficient removal of organics. This chapter will discuss the underlying principles of anodic oxidation mechanism and AOPs processes.

### **2.1 Electrochemical Process**

In an electrochemical process, direct oxidation of organic compounds dissolved in an aqueous solution can be achieved by conducting an electrolysis at positive potentials at the anode electrode. This process might also involve water discharge and the participation of the hydroxyl radical formed before oxygen evolution reaction (OER) [22].

This electrochemical reaction induces partial conversion or full mineralization of the pollutants, with the advantage of non-toxic by-products and does not require a catalyst in the solution. However, a particular disadvantage is the low current efficiency due to the secondary reactions associated with the OER during anodic oxidation, while oxidation. The current efficiency is also influenced by the electrode materials and solution

conditions (pH, temperature and conductivity). Comninellis et. al. suggested an underlying mechanism of anodic oxidation processes for water treatment highlighting the nature of the electrode material [24]. Some electrode materials have a strong influence over the conversion of pollutants (oxidation) due to their higher oxidation power producing full mineralization, while others electrodes with low oxidation power provide partial mineralization.

## **2.2 Anodic oxidation**

Anodic oxidation is a well-known direct electrochemical advanced oxidation process. This method is widely used for waste water treatment and it works on the generation of  $\bullet\text{OH}$  radical at the anode surface by water oxidation. The anodic oxidation process is usually a heterogeneous process that produce  $\bullet\text{OH}$  radicals adsorbed or chemisorbed at the anode surface, depending on the type of electrode used. Anodic oxidation process has benefits like easier operation, complete and fast conversion, and improved efficiency. One major disadvantage is the low current efficiencies which is due to the secondary reaction of oxygen evolution which causes the wastage of electric current during the process.

### 2.3 The reaction scheme

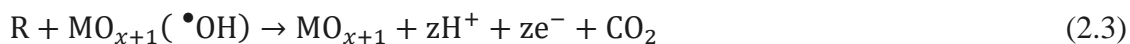
The initial step in the electrochemical water treatment is the discharge of water molecules at the electrode surface forming adsorbed  $\bullet\text{OH}$  radicals, where M denotes the electrode surface.



The electrode materials generally characterized into two classes; ‘active and non-active’ electrodes. The active anodes possess greater oxidation states over the electrode surface and these linked strongly with the adsorbed  $\bullet\text{OH}$  by further conversion, producing higher oxides as shown in the following reaction;



$\text{MO}_{x+1}/\text{MO}_x$  redox couple is often termed as chemisorbed oxygen and serves as a mediator for the removal of organics [24] which is represented by the following equations:



Where;

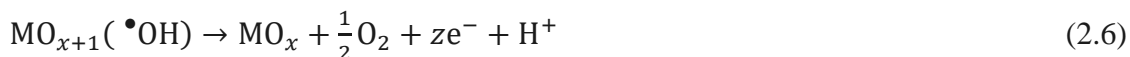
R is the concentration of organics in aqueous solution

$\text{MO}_x$  is the concentration of active sites

$z\text{e}^-$  is the number of electrons

Non-active electrodes have weak interaction with the adsorbed hydroxyl radical (physisorbed active oxygen). These hydroxyl radical favours complete oxidation of organics during the electrochemical process. Both active and non-active electrodes

produce oxygen as secondary reaction which cause energy loss with decrease in anodic efficiency. This can be represented by the following reactions:



#### 2.4 Oxygen evolution overpotential and categories of anodes

The overpotential is the difference between the actual required potential for electrolytic changes to occur during electrochemical process and the predicted value from the thermodynamics standard reduction potential. It has been reported that the active anodes have low overpotential for oxygen evolution which usually allow only partial conversion of organics into intermediates, while non-active electrodes favours complete conversion of organics into carbon dioxide, since these electrodes possess high oxygen evolution over potential. The examples of active electrodes are platinum, carbon and graphite whereas non active electrodes are lead dioxide, BDD and antimony doped tin oxide [24]. As an example the over potential values of Ti/Pt and Si/BDD for oxygen evolution are 0.3V and 1.9 V respectively. Some values of the oxidation power for different active and non-active electrodes are shown in Table 2.1. The partial oxidation is related to the active anodes and these are typically denoted as low oxidation power anodes.

Electrode	Oxidation potential (V)	Overpotential for O <sub>2</sub> evolution (V)	Adsorption enthalpy of •OH radical	Anode oxidation power	Electrode type
RuO <sub>2</sub> /TiO <sub>2</sub>	1.4-1.7	0.18	↑	↓	Active
Ti/Pt	1.7-1.9	0.3			Active
Ti/PbO <sub>2</sub>	1.8-2.0	1.5			Non-Active
Ti/SnO <sub>2</sub> -Sb <sub>2</sub> O <sub>5</sub>	1.9-2.2	1.7	↑	↓	Non-active
p-Si/BDD	2.2-2.6	1.9			Non-active

Table 2.1 Categories of electrodes on the basis of electrode power for oxygen evolution reaction [24].

The non-active anodes have greater tendency for •OH radical generation and these are considered to be ideal for waste water treatment. One of the most important non-active electrodes are the BDD with the highest anodic oxidation power. However, the main disadvantage of these electrodes is their cost and the required substrate material to deposit the boron doped diamond film. Typical substrate for the deposition of stable diamond

films are niobium, tungsten, tantalum and silicon but these remained unsuitable for commercial scale because of the higher cost of rare earth metals and poor conductivity of the silicon [26].

## 2.5 Electrode Materials

The electrodes play a critical role in the performance. In flow reactors where the electrolyte flows at certain flow velocity over the surface of the electrode, the electrodes be mechanically and chemically strong to withstand the friction of the electrolyte and the strong acid environment during oxygen reduction reaction. The reaction can create local high temperatures and at the extreme oxidizing conditions require special materials. In addition, the anodes have to operate under the oxidizing conditions. Naturally, plates and meshes of noble metals were the first choice of electrode materials during the early stages of development [24]. These electrodes are known as dimensionally stable anodes (DSA) and are a mixture of Ir, Ru, Sb, Sn and Ti oxides. DSA electrodes can withstand under strong acidic media. However, these electrodes only showed a limited conversion of the organic dye molecules during anodic oxidation process. For instance, Chen et al. employed Ti/Sb<sub>2</sub>O<sub>5</sub>-SnO<sub>2</sub> anodes for the electrochemical oxidation of Orange II dye in Na<sub>2</sub>SO<sub>4</sub> aqueous solution in an undivided cell. The COD removal was 27 % at constant current density of 20 mA cm<sup>2</sup> with current efficiency of 16%. Similarly, Pt electrodes have been tested for the removal of different dyes and showed the ability of decolourize dyes. Lopez et al. reported colour removal of 90% using Ti/Pt anode in a batch reactor under basic conditions by applying a current density of 40 mA cm<sup>2</sup> in 1h of electrolysis [28]. Some carbonaceous electrodes have been employed for the anodic removal of

organic dyes. Graphite has been reported effective for the decolourisation of Indigo dyes under neutral conditions. By applying cell voltage of 5V, the decolourisation efficiency of 98% was achieved with the energy consumption of 92 kWh m<sup>3</sup> [29]. BDD electrodes are reported as a new class of electrode material with corrosion resistance, improved oxidation power, high oxygen evolution overpotential, inert to acidic conditions. These electrodes are classed as non-active electrodes which offered the advantage of complete mineralization of dyes at high efficiency. Ti/BDD electrodes have been found effective for the demineralization of Acid orange 7 dye at a current density of 20 mAcm<sup>-2</sup> with an overall mineralization of 92% [27].

## **2.6 Electrochemical flow cells**

Different kind of flow systems have been tested for the electrochemical flow studies of the treatment of dyestuff. Single compartment two electrodes cell has been utilized and is shown in fig.2.1.



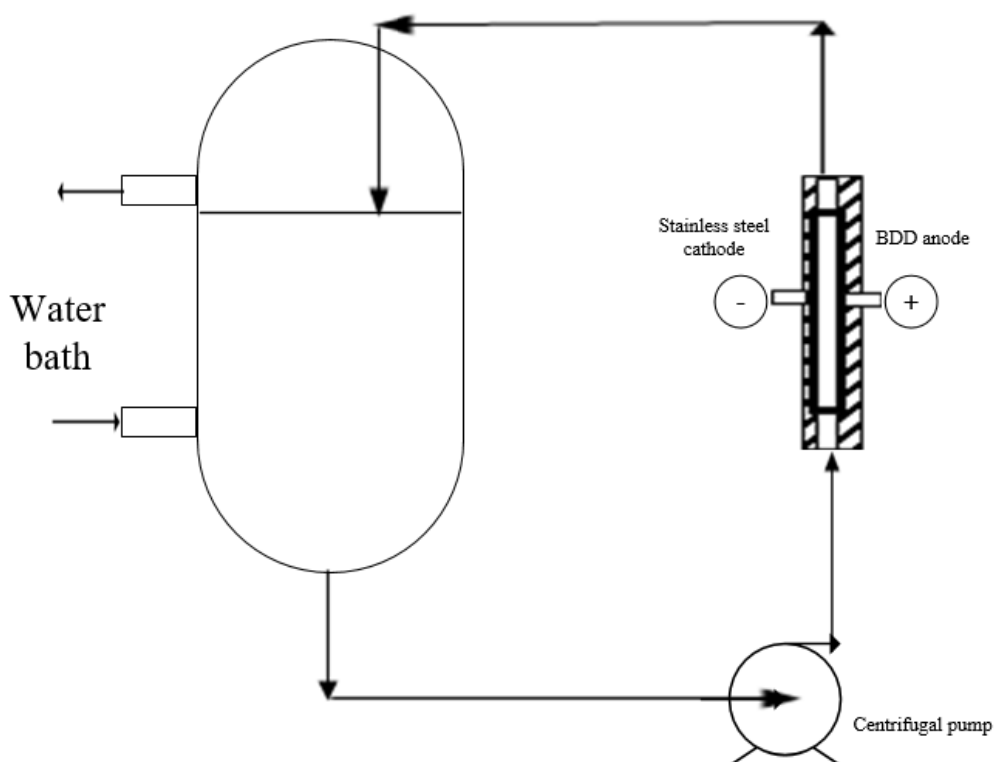


Figure 2.1 2 electrodes single compartment electrochemical flow reactor [30].

In this 2 electrode cell the electrochemical degradation studies of acid yellow dye in aqueous solution was studied. BDD was used as an anode while stainless steel was used as cathode. The geometrical area of both electrodes was  $50 \text{ cm}^2$ . The electrolyte was circulated in an electrochemical flow cell by using centrifugal pump. By applying constant current of 1000 mA, the decolourisation of 99 % was achieved in 2.5 h of electrolysis at a flow rate of  $300 \text{ dm}^3\text{h}^{-1}$  [30].

In another work carried out at University of Southampton, Ponce de León *et al.* described the operation of a filter press electrochemical divided cell (fig 2.2) in alkaline media [31]. This device consisted of four polymer rectangular section chambers provided with flow channels and separated by a Nafion<sup>®</sup> 115 proton exchange membrane. Silicone rubber

gaskets were used to seal the cell components. The positive and negative electrodes were placed in their corresponding half-cells with a membrane-electrode gap of 19 mm.

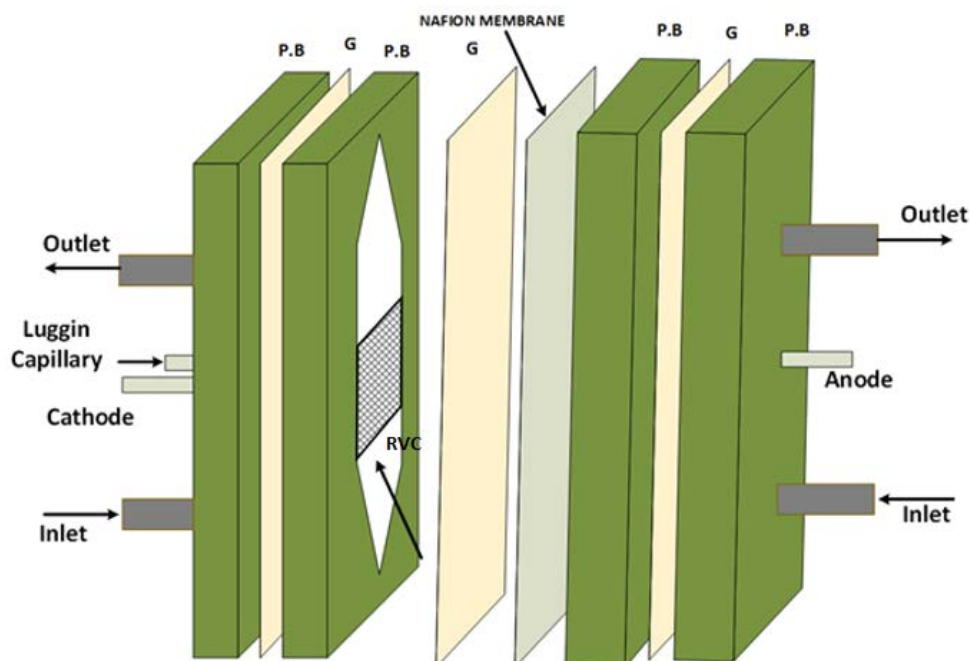


Figure 2.2 Parallel plate electrochemical flow reactor where P.B (polymer block), G (gasket), RVC (reticulated vitreous carbon) [31].

The RVC cathode (60ppi) dimensions were 50 mm × 50 mm × 12 mm, with the projected area of 25cm<sup>2</sup> while the anode was a lead plate of 50 mm × 50 mm. It was found that the RVC yielded the best performance with a current efficiency up to 94%. Low potential values at the cathode were beneficial for the ORR. Under optimal conditions, the cell showed a current efficiency of 99.4% with hydrogen peroxide concentration of 10 × 10<sup>-3</sup> mol dm<sup>-3</sup>. Different grades of RVC were used as the cathode and promoted the ORR in the negative half-cell. The hydrogen peroxide generation combined with Fe<sup>2+</sup> ions achieved the highest removal rate for the 60 ppi RVC cathode.

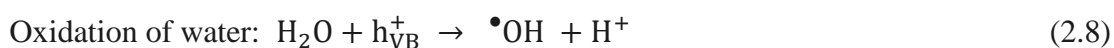
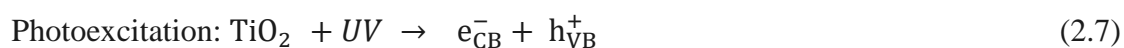
## 2.7 Photocatalytic water treatment

Another well-known water treatment process is the photocatalytic method which utilize semiconductor photocatalyst like Ti-oxide, Zn oxide and Fe oxide. Photocatalytic water treatment is based on the in situ production of reactive species such as  $\bullet\text{OH}$ ,  $\text{O}_3$ ,  $\text{H}_2\text{O}_2$  and  $\text{O}_2\bullet^-$ . These radicals are transitory phase species which attack the organic compounds and lead to their mineralization. Titanium oxide catalyst has received an increasing attention from various research groups around the world. Compared to other semiconductor photocatalyst,  $\text{TiO}_2$  offers thermal stability, chemical resistance and high mechanical strength [32]. Ti based photocatalysis were first reported by Fujishima and Honda. They investigated the oxidation of reducing species like  $\text{I}^-$ ,  $\text{Br}^-$ ,  $\text{Cl}^-$  in a photo-electrochemical cell having single crystal of  $\text{TiO}_2$  as an electrode and unfolded pioneering  $\text{TiO}_2$  based catalyst [33].

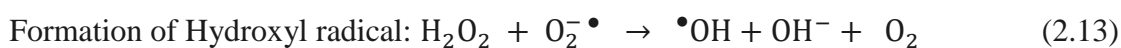
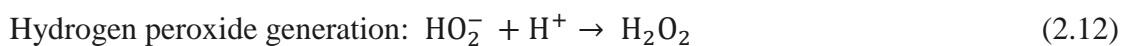
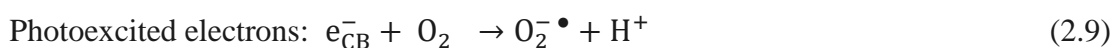
## 2.8 Mechanism of $\text{TiO}_2$ photocatalysis

The mechanism of  $\text{TiO}_2$  for photocatalytic water treatment has been extensively reported in the literature [32-35]. It has been widely accepted that photocatalyst  $\text{TiO}_2$  initiates a series of both reductive and oxidative reactions on its surface. This is promoted by the presence of lone electron pair in the outer orbital. The band gap of  $\text{TiO}_2$  photocatalyst for anatase phase is 3.2 eV while for rutile phase is about 3 eV. When UV light having photon energy greater than or equal to the band gap of the photocatalyst, the lone electron pair is photocatalytically excited to the conduction band. The wavelength of UV light illuminated over the substrate should be below 400 nm. This phenomenon creates an

electron hole pair as photoexcitation generates an empty valance band. The series of photocatalytic reaction producing electron hole pair and free radicals are given in equations (2.7-2.12) below:



As indicated in equation (2.7), the illumination of TiO<sub>2</sub> by UV irradiation excites an electron from the valance band to the conductive band with the generation of holes at the valance band. The oxidation of water is initiated by these positive holes pairs, forming short lived and powerful oxidizing agents  $\bullet\text{OH}$  radicals, as indicated in equation (2.8), which are capable to degrade and mineralize the organic matter to carbon dioxide, water and low molecular weight compounds of low toxicity [34-36].



Equations (2.9), (2.10) and (2.11) indicate the formation of oxidative radicals formed by the reaction of valence band electrons with superoxide such as  $O_2^{\bullet-}$  and hydroperoxyradical. Equations (2.12) and (2.13) involve the production of hydrogen peroxide and subsequent formation of hydroxyl radicals,  $\bullet OH$  [35].

## 2.9 Kinetics of decolourisation of organic compounds

The decolourisation kinetics of organic dyes usually follows the Langmuir-Hinshelwood scheme;

$$r = -\frac{d[c]}{dt} = k [c] \quad (2.14)$$

Where  $r$  denotes the rate of oxidation,  $c$  the initial concentration of the reactant,  $t$  the reaction time and  $k$  is the rate reaction constant.

By rearranging;

$$\frac{d[c]}{[c]} = -k dt \quad (2.15)$$

Integrating both sides;

$$\int_{[c]_0}^{[c]} \frac{d[c]}{[c]} = -\int_{t_0}^t k dt \quad (2.16)$$

Upon integration;

$$\ln[c] - \ln[c]_0 = -kt \quad (2.17)$$

Rearranging

$$\ln[c] = \ln[c]_0 - kt \quad (2.18)$$

$$\ln[c] = -kt + \ln[c]_0 \quad (2.19)$$

$$\ln\left(\frac{[c]}{[c]_0}\right) = -k t \quad (2.20)$$

where,  $c$  is the concentration at time  $t$  and  $c_0$  is the initial concentration  $k$  is the pseudo first order rate constant.

It should be noted that the rate law for the decolourisation kinetics of organic dyes is a mathematical relationship between the reaction rate and the concentration of the organic dyes in solution as indicated by equation 2.14. Rate laws are usually expressed as a differential rate law i.e. by relating the change in dye concentration as a function of time, in comparison to initial concentration. The rate of reaction depends on the concentration of the dye while the rate constant ( $k$ ) is proportionality constant between the dye concentration and the rate of reaction. The exponential value of the concentration indicates the order of the reaction [34].

## 2.10 Conclusions

This chapter provide an overview of the water treatment technologies for the removal of organic dyes with a specific significance on electrochemical anodic oxidation and photocatalytic treatment. A detailed analysis of the anodic oxidation method with reaction scheme was analysed with special emphasis on the categories of different electrodes e.g. active and non-active electrodes. Active and non-active electrodes explanation exhibited that oxidation power is an important aspect to define the categories of these electrodes. It

has been concluded from this discussion that active anodes like Pt, RuO<sub>2</sub> permit only partial conversion of organics while non-active electrodes like PbO<sub>2</sub>, BDD and SnO<sub>2</sub> have the potential for complete mineralization of the organic materials. This chapter also analysed the importance of photocatalytic water treatment with a brief discussion about different photocatalyst with particular emphasis on TiO<sub>2</sub> as a photocatalyst. The mechanism of the TiO<sub>2</sub> photocatalysis has also been presented. Finally an explanatory discussion about kinetics of decolourisation of organic dyes has also been derived using Langmuir-Hinshelwood equation.

## 2.11 References

- [1] A Dabrowski, J Mieluch, A Sadkowski, J Wild, P Zoltowski. Pilot Scale Studies on Purification of Phenol Waste-Waters by Electrochemical Method, *Przemysl Chemiczny*, 54 (1975) 653-655.
- [2] C. Comninellis, C. Pulgarin. Anodic oxidation of phenol for waste water treatment, *J Appl Electrochem.* 21, (1991) 703-708.
- [3] M. Panizza, B. Cristina, G. Cerisola. Electrochemical treatment of wastewater containing polyaromatic organic pollutants, *Water Res.* 34, (2000) 2601-2605.
- [4] F. L.Souza, , C. Saéz, M. RV Lanza, P. Cañizares, M. A. Rodrigo. Removal of pesticide 2, 4-D by conductive-diamond photoelectrochemical oxidation, *Appl. Catal B: Environ.* 180 (2016) 733-739.
- [5] G.W. Reade, A.H. Nahle, P. Bond, J.M. Friedrich, F.C. Walsh, Removal of cupric ions from acidic sulfate solution using reticulated vitreous carbon rotating cylinder electrodes, *J. Chem. Technol. Biotechnol.* 79 (2004) 935-945.

- [6] F. J. Recio, P.Herrasti, I. Sirés, A.N Kulak, D.V Bavykin, C. Ponce-de-León, F.C. Walsh, The preparation of PbO<sub>2</sub> coatings on reticulated vitreous carbon for the electro-oxidation of organic pollutants. *Electrochim. Acta.* 56 (2011) 5158-5165.
- [7] S. Bebelis, K. Bouzek, A. Cornell, M.G.S Ferreira, G.H Kelsall, F. Lapicque, & F.CWalsh, Highlights during the development of electrochemical engineering. *Chem. Eng. Res. Des.* 91, (2003) 1998-2020.
- [8] A Kapalka, G Foti, C Comninellis. Kinetic modelling of the electrochemical mineralization of organic pollutants for wastewater treatment, *J. Appl. Electrochem.*, 38 (2008) 7-16.
- [9] I. Duo, C. Levy-Clement, A. Fujishima, C Comninellis. Electron transfer kinetics on boron-doped diamond Part I: Influence of anodic treatment, *J.Appl.Electrochem.* 34 (2004) 935-943.
- [10] O Simond, V Schaller, C Comninellis. Theoretical model for the anodic oxidation of organics on metal oxide electrodes, *Electrochim.Acta*, 42 (1997) 2009-2012.
- [11] M Panizza, A Kapalka, C Comninellis. Oxidation of organic pollutants on BDD anodes using modulated current electrolysis, *Electrochim.Acta*, 53 (2008) 2289-2295.
- [12] M Panizza, G Cerisola. Influence of anode material on the electrochemical oxidation of 2-naphthol - Part 1. Cyclic voltammetry and potential step experiments, *Electrochim.Acta*, 48 (2003) 3491-3497.
- [13] M Panizza, P.A Michaud, G Cerisola, C Comninellis Anodic oxidation of 2naphthol at boron-doped diamond electrodes, *J Electroanal Chem*, 507 (2001) 206-214.
- [14] P Canizares, J Garcia-Gomez, J Lobato, MA Rodrigo. Modelling of wastewater electro-oxidation processes part I. General description and application to inactive electrodes, *Ind Eng Chem Res*, 43 (2004) 1915-1922.
- [15] P Canizares, J Garcia-Gomez, J Lobato, MA Rodrigo. Modeling of wastewater electro-oxidation processes part II. Application to active electrodes, *Ind Eng Chem Res*, 43 (2004) 1923-1931.

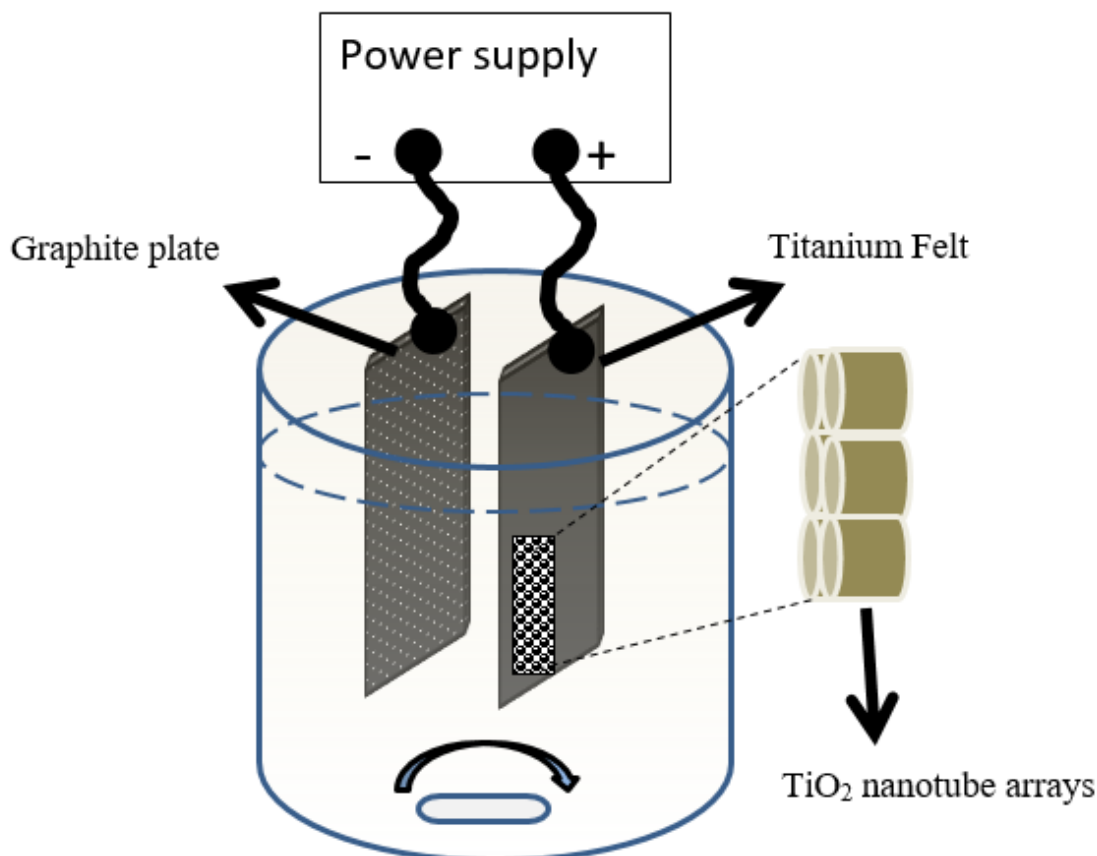


- [16] P Canizares, J Garcia-Gomez, C Saez, MA Rodrigo. Electrochemical oxidation of several chlorophenols on diamond electrodes - Part I. Reaction mechanism, *J.Appl.Electrochem.* 33 (2003) 917-927.
- [17] E Brillas, I Sires, M.A Oturan. Electro-Fenton Process and Related Electrochemical Technologies Based on Fenton's Reaction Chemistry, *Chem.Rev.* 109 (2009) 6570-6631.
- [18] Martínez-Huitle, C. A., & Brillas, E. Decontamination of wastewaters containing synthetic organic dyes by electrochemical methods: a general review. *Appl. Catal. B: Environ.* 87 (2009) 105-145.
- [19] Sirés, I., & Brillas, E. Oxidation of water pollution caused by pharmaceutical residues based on electrochemical separation and oxidation technologies: a review. *Environ. Int.* 40 (2012) 212-229.
- [20] A.M Polcaro, A Vacca, M Mascia, S Palmas, JR Ruiz. Electrochemical treatment of waters with BDD anodes: kinetics of the reactions involving chlorides, *J.Appl.Electrochem.* 39 (2009) 2083-2092.
- [21] A.M Polcaro, M Mascia, S Palmas, A Vacca. Electrochemical oxidation of phenolic and other organic compounds at boron doped diamond electrodes for wastewater treatment: Effect of mass transfer, *Ann.Chim.*, 93 (2003) 967-976.
- [22] A.M Polcaro, M Mascia, S Palmas, A Vacca. Kinetic study on the removal of organic pollutants by an electrochemical oxidation process, *Ind Eng Chem Res*, 41 (2002) 2874-2881.
- [23] C Comninellis, A Kapalka, S Malato, S.A Parsons, L Poulios, D Mantzavinos. Advanced oxidation processes for water treatment: advances and trends for R&D, *J Chem Technol Biot*, 83 (2008) 769-776.
- [24] C.Comninellis. Electrocatalysis in the Electrochemical Conversion /Combustion of Organic Pollutants for Waste Water Treatment, *Electrochim.Acta.* 39 (1994) 1857-1862.
- [25] M.Panizza, G. Cerisola, Application of diamond electrodes to electrochemical processes, *Electrochim. Acta.* 51 (2005) 191-199.

- [26] M Panizza Importance of Electrode Material in the Electrochemical Treatment of Wastewater Containing Organic Polutants, in: Comninellis C, Chen GH (Eds.), *Electrochemistry for the Environment*, 1st ed., Springer Science, LLC, (2010) 25-54.
- [27] X. Chen, G. Chen, P.L Yue, Anodic oxidation of dyes at novel Ti/B-diamond electrodes. *Chem. Eng. Sci.* 58 (2003) 995-1001.
- [28] V. López-Grimau, M.C.Gutierrez,, Decolourisation of simulated reactive dyebath effluents by electrochemical oxidation assisted by UV light. *Chemosphere*, 62 (2006) 106-112.
- [29] C.Cameselle, M.Pazos, M.A Sanroman, Selection of an electrolyte to enhance the electrochemical decolourisation of indigo. Optimisation and scale-up. *Chemosphere*, 60 (2005) 1080-1086.
- [30] J. Rodriguez, M.A. Rodrigo, M. Panizza, G. Cerisola, Electrochemical oxidation of Acid Yellow 1 using diamond anode. *J.Appl.Electrochem.* 39 (2009) 2285.
- [31] C. Ponce De Leon, D. Pletcher, Removal of formaldehyde from aqueous solutions via oxygen reduction using a reticulated vitreous carbon cathode cell. *J. Appl. Electrochem.* 25 (1995) 307-314.
- [32] S. Malato, P. Fernández-Ibáñez, M.I Maldonado, J.Blanco, W.Gernjak, Decontamination and disinfection of water by solar photocatalysis: recent overview and trends. *Catal Today*. 147 (2009) 1-59.
- [33] A. Fujishima, T. Inoue, K. Honda, Competitive photoelectrochemical oxidation of reducing agents at the titanium dioxide photoanode. *J. Am. Chem. Soc.* 101 (1979) 5582-5588.
- [34] U. Gaya, I. Aque, A.H Abdullah, Heterogeneous photocatalytic oxidation of organic contaminants over titanium dioxide: a review of fundamentals, progress and problems. *J. Photochem. Photobiol.* 9 (2008). 1-12.

- [35] Fujishima, A., Rao, T. N., & Tryk, D. A. Titanium dioxide photocatalysis. *Journal of photochemistry and photobiology C: Photochemistry reviews*, 1 (2000) 1-21.
- [36] M.B. Muneer, D. Qamar, M. Tariq, M.A. Faisal, Photocatalysed reaction of few selected organic systems in presence of titanium dioxide. *Appl. Catal., A*, 289 (2005) 224-230.

Chapter 3: **Anodising of titanium felt to grow titanium dioxide nanotube arrays decorated with PbO<sub>2</sub>: Characterization and Application**



This chapter will study TiO<sub>2</sub> nanotube arrays formed on bendable, 3D fibrous network of titanium felt (Ti felt) substrate, using anodization at room temperature (25 °C) in a fluoride and MSA based solution. In addition, PbO<sub>2</sub> will be deposited over the nanotubes by immersion in a solution containing Pb (NO<sub>3</sub>)<sub>2</sub> and (NH<sub>4</sub>)<sub>2</sub>S<sub>2</sub>O<sub>8</sub> during a certain time ( $t_i$ ). The Ti felt/ TiO<sub>2</sub> nanotube and the Ti felt/ TiO<sub>2</sub> nanotube/PbO<sub>2</sub> composites were

characterised using field emission scanning electron microscopy (FESEM), energy dispersive X-ray (EDX) and Raman spectroscopy. It was revealed that PbO<sub>2</sub> deposited over the nanotubes was well-dispersed after 6 hours immersion, resembling cauliflower-like clusters on the top of the TiO<sub>2</sub> nanotube anodized on felt substrate. The coatings exhibited well defined morphology with anatase phase of TiO<sub>2</sub>. The electrochemical and photochemical performance of novel coatings were recorded in aqueous solutions at pH = 3 containing  $2 \times 10^{-5}$  mol dm<sup>-3</sup> reactive black 5 (RB-5) azo dye. The electrochemical properties relate with the generation of •OH free radical over the Ti felt/ TiO<sub>2</sub> nanotube /PbO<sub>2</sub> substrate while photocatalytic characteristics were related to the synergistic photocatalytic effect imparted by the photo-induced holes and free electron acceptors formed at high pH solutions. Discolouration of RB-5 dye achieved 99% (measured at 597 nm visible absorption wavelength) after 60 min of electrochemical anodic oxidation using Ti felt/ TiO<sub>2</sub> nanotube /PbO<sub>2</sub> as anode. The calcination of coating Ti felt/ TiO<sub>2</sub> nanotube /PbO<sub>2</sub> coating at 450 °C for 60 min in air transformed the titania nanotubes into anatase phase, which showed 97% of RB-5 dye discolouration in 30 min during photocatalytic oxidation.

### 3.1 Introduction

In recent years, the oxidation of organic matter residue (OMR) by anodic oxidation treatment, has received attention as a way to purify and clean wastewater. New materials are needed in order to improve the process efficiency and develop effective coatings, which remain stable during the electrochemical wastewater oxidation treatment, at low cost [1]. Most of the research has centred on materials that are effective for the generation

of photo-induced active oxidising species on illumination with UV light and at the same time poses high conductivity and electrochemical characteristics like electro-activity regarding for anodic oxidation. A single material cannot exhibit the above mentioned properties. However, a composite of two or more materials with the two characteristics mentioned above, might accomplish this goal. These composite coatings for environmental oxidation are formed by anodization and deposition of photocatalytic active materials over conductive substrates that also provide electrocatalytic characteristics.

The use of titanium as a substrate is useful because of its hardness, good conductivity and chemical stability [2, 3]. However, titanium generates oxide layer ( $\text{TiO}_2$ ) over the surface which ultimately alters many properties including charge propagation and the ability to attach precipitates on its surface. Under certain conditions,  $\text{TiO}_2$  may acts as a photocatalyst [4-6], gas sensor [7] or an electrode for dye-sensitized solar cells (DSCs) [8, 9]. In addition to the above properties, titanium can serve as a suitable material for deposition of non-active metal oxide like  $\text{PbO}_2$ . Without  $\text{PbO}_2$ ,  $\text{TiO}_2$  as an electrode is inadequate due to its poor electrocatalytic activity as an anode for electro oxidation of organic compounds. By modifying the properties of  $\text{TiO}_2$ , the oxide can acquire more mechanical strength, stability and unreactive characteristics to certain chemicals and increase charge propagation through the  $\text{TiO}_2$  layer. Over the past two decades, the improvement of  $\text{TiO}_2$  catalytic properties has been pursued by depositing active and unreactive metal oxides, e.g. as reported for  $\text{TiO}_2/\text{RuO}_2$  composite system [10, 11, 12]. In this work, the composite of  $\text{TiO}_2/\text{PbO}_2$  was manufactured on porous 3D electrode (titanium felt) for anodic oxidation of reactive black 5 (RB-5) dye.

Anodic oxidation is an electrochemical process widely utilized for water treatment which generates physisorbed  $\bullet\text{OH}$  radicals during water discharge at the anode electrode coating by the reaction indicated in equation 2.1[13]:

$\text{PbO}_2$  deposited over titanium dioxide nanoparticles ( $\text{TiO}_2$ ) is able to generate these radicals and it is a low cost material that can be used for the environmental oxidation of wastewater. The Ti based nanoparticles are well known for the photochemical and electrochemical treatment of wastewater [14, 15]. Contemporary research work shows that the synthesis of  $\text{PbO}_2$  and Sb-doped  $\text{SnO}_2$  decorated  $\text{TiO}_2$  nanotube arrays on flat titanium sheet proved useful for the entire mineralization (about 99%) of Reactive black-194 by applying constant current at a density of  $150 \text{ mA cm}^{-2}$  [16].

Lead dioxide properties are very well known due to its use in lead acid battery and its current applications in environmental water treatment can take advantage of the knowledge already acquired. It exhibits greater overpotential for oxygen evolution reaction at  $1.9 \text{ V vs. SHE}$  [17], enabling an effective production of  $\bullet\text{OH}$  free radicals which are effective powerful oxidants of organic dyes. The  $\text{PbO}_2$  electrodes [18-22] exhibit enough mechanical resistance for different applications which involve anodic oxidation for water treatment and lead acid batteries.  $\text{PbO}_2$  modified  $\text{TiO}_2$  has been reported on a Ti plate [23, 24, 25, 26]. The  $\text{TiO}_2$ , as a layer between titanium and  $\text{PbO}_2$ , improved the photochemical properties of the substrate, while  $\text{PbO}_2$  enhanced the electrocatalytic nature of the electrode [25, 26].

Since early 2000s,  $\text{TiO}_2$  nanotubes arrays have been grown by anodizing of titanium plates with focus on a planar surface, in aqueous hydrofluoric acid (HF), fluoride containing non-aqueous solution such as glycerol, ethylene glycol, diethylene glycol [27,

28, 29]. Herein, methanesulphonic acid (MSA) was used as an electrolyte which is a versatile, and environmental friendly electrolyte (decomposed into sulphate and carbon dioxide) with good electrolytic conductivity [30]. Anodising was performed on a compressed 3D fibrous network of titanium felt (Ti felt), which is capable of being bent or flexed without breaking. Such complex 3D structure provides more relevant base material to manufacture TiO<sub>2</sub> nanotubes arrays with high integrity and adherence to the substrate surface. On the other hand, 3D porous structure of titanium felt has more surface area than planar structure providing more catalytic sites on the anode. The main challenge is to find out the suitable electrolyte and the applied anodic potential for the anodization of nanotubes. The TiO<sub>2</sub> nanotubes can be used to realize photocatalytic activity [31] or to provide an active support for the deposition of electroactive species, such as PbO<sub>2</sub> [32]. PbO<sub>2</sub> is particularly attractive for electrochemical water treatment [33] having a conductivity of  $2.5 \times 10^3 \Omega^{-1}\text{cm}^{-1}$  [34].

In this work, Ti-felt was anodized in aqueous methanesulfonic acid (MSA) and ammonium fluoride electrolyte under controlled operating conditions for the growth of TiO<sub>2</sub> nanotubes and further decorated with PbO<sub>2</sub> by hydrothermal treatment to produce a coating with combined photo and electrochemical characteristics. The results provide important information related to anodization of Ti felt with MSA, and interfacial surface deposition of PbO<sub>2</sub> layers.

### **3.2 Experimental Details**

Reagent grade 70% methanesulphonic acid (MSA) in aqueous solution, ammonium fluoride, ammoniumpersulfate, 99 % oxalic acid, polyvinylpyrrolidone (PVP) (MW = 55000) and RB-5 dye were obtained from Sigma Aldrich, while lead nitrate, Pb(NO<sub>3</sub>)<sub>2</sub>,



sodium hydroxide, sulphuric acid, sodium hydroxide, ethanol (98 %) sodium sulphate, acetone were received from Fischer sci. and employed as obtained.

### 3.2.1 Anodizing of Titanium felt

The Ti felt (NV Bekaert SA, Belgium) was pre-treated in a 10 wt. % oxalic acid aqueous solution at 80 °C for 20 min. The Ti felt was washed with ethanol and then dried overnight at 90 °C in air.

The anodizing experiments were carried out in an undivided glass cell (volume 100 cm<sup>3</sup>) mounted with water circulation jacket attached to a Grant water thermostat model LT D6G. The Ti felt anode with dimensions 2 cm × 2 cm × 0.15 cm was connected via a stainless steel alligator clip to a direct current power supply. A pure carbon plate of 1.5 cm × 6 cm × 1.2 cm dimensions was used as cathode with 1 cm of inter-electrode gap from the anode. The electrolyte was magnetically stirred at 300 rev min<sup>-1</sup> with a 0.06 cm diameter, 0.25 cm long PTFE-coated, cylindrical stirrer (Fischer scientific) to ensure constant concentration of the electrolyte i.e. efficient mass transport conditions across the Ti felt layers. The titanium felt was anodized in different ranges of MSA concentrations from 0.1 mol dm<sup>-3</sup> to 5 mol dm<sup>-3</sup> and ammonium fluoride 0.5 or 1 wt. % in aqueous solution. The constant potential applied between cathode and anode ranged from 5 to 30 V for 1 hour to know the optimum conditions of anodization by using 300 W Aim-TTi model EX752M power supply. The experiments were carried out at 25 °C. The anodized samples are cleaned thoroughly by washing with D.I water and allowed to dry overnight.

### 3.2.2 Deposition of Lead dioxide

The PbO<sub>2</sub> was deposited by hydrothermal process in the presence of PVP as a structure directing agent [36]. First, 0.015 mol dm<sup>-3</sup> Pb(NO<sub>3</sub>)<sub>2</sub> and 1 mol dm<sup>-3</sup> NaOH were mixed at room temperature (25 °C) and 0.1 g of PVP was added to 75 cm<sup>3</sup> of the above mixture and allowed to stir overnight until complete dissolution. Further, 3 cm<sup>3</sup> of 1.5 mol dm<sup>-3</sup> (NH<sub>4</sub>)<sub>2</sub>S<sub>2</sub>O<sub>8</sub> as oxidizing agent was dissolved in the resultant solution for 30 min. Ti felt/ TiO<sub>2</sub> nanotubes 3 different samples were immersed in the solution for 15 min, 6 h and 12 h, taken out and heated at 60 °C for 3 h in air. The resultant samples were cooled down over night. Immersion time of Ti felt in the lead oxide solution denoted as *t<sub>i</sub>*. Finally, a PbO<sub>2</sub> layer was achieved on the substrate as a result of the immersion.

### 3.2.3 Heat treatment

The resulting Ti felt/ TiO<sub>2</sub> nanotubes /PbO<sub>2</sub> composite samples were annealed at 450 °C for 1 hour in air using electric furnace to transform the phase of the nanostructures from titanium phase to anatase phase. The calcined samples were later used for photocatalytic experiments.

### 3.2.4 Characterisation of the coated substrate

A field emission scanning electron microscope (FESEM) was used to characterize the all samples obtained from anodization. A high resolution FESEM JEOL 6500F at an accelerating voltage of 20 kV was used while imaging was carried out at a working distance of 10 mm. Raman spectroscopy confocal microscope (Renishaw, RM 2000) was used to obtain Raman spectra employing light source of 632.8 nm wavelength with 10 % laser intensity. The exposure time was about 30 seconds.

### 3.2.5 Electrochemical Experiments

The electrochemical experiments were accomplished by employing computer assisted potentiostat/galvanostat model number PGSTAT302 N from Autolab supplied by Eco Chemie, Netherlands controlled by a Nova 1.11 software. The as synthesized coatings (Ti felt/ TiO<sub>2</sub> nanotubes /PbO<sub>2</sub>, Ti felt/ TiO<sub>2</sub> nanotubes and pre-treated Ti felt) were cleaned by using ultra-pure water and dried by flushing nitrogen gas. The coatings were used as anodes for electrochemical discolouration of RB-5 dye. A 100 cm<sup>3</sup> electrolyte having  $2 \times 10^{-5}$  mol dm<sup>-3</sup> of reactive black 5 dye (shown in figure 3.1) in 0.5 mol dm<sup>-3</sup> of sodium sulfate as a background electrolyte was electrolysed at constant potential of 1.4 V vs. Hg/HgO at pH 3 by addition of H<sub>2</sub>SO<sub>4</sub> and measured by using waterproof Hanna pH meter model HI 98129 and 22.5 °C.

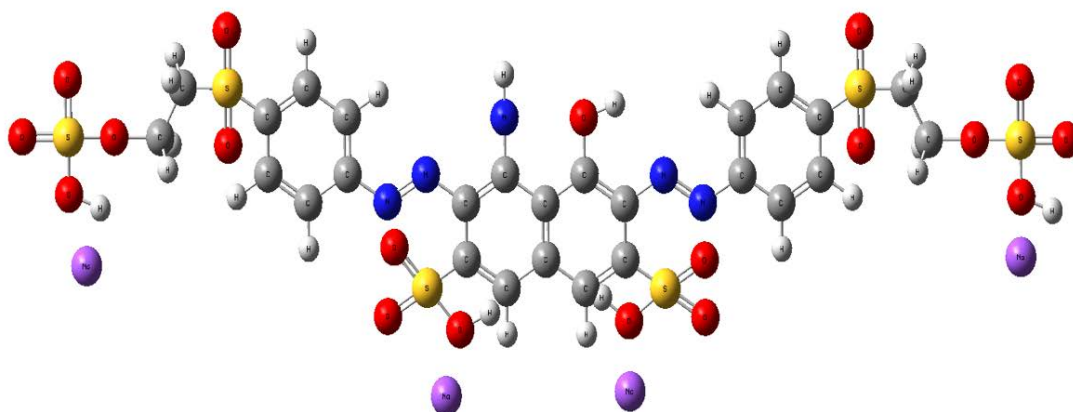
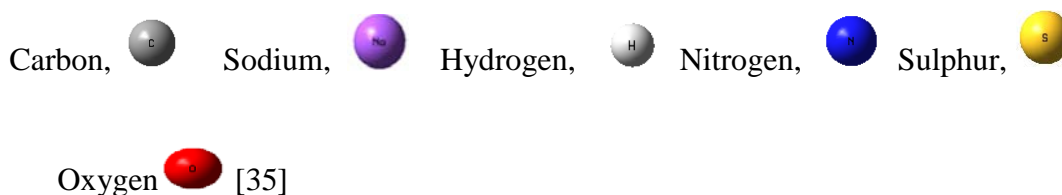


Figure 3.1 Structure of RB-5 dye where,



Molecular Formula; C<sub>26</sub>H<sub>21</sub>N<sub>5</sub>Na<sub>4</sub>O<sub>19</sub>S<sub>6</sub>, Molecular weight = 991.78 g mol<sup>-1</sup>.

The pH of the electrolyte was stable throughout the electrolysis at the constant potential. A platinum mesh (1.5 cm × 1.5 cm) and a mercury oxide (Hg/HgO, (NaOH sat.)) used as a counter and reference electrodes respectively.

### 3.2.6 Photocatalytic Experiments

The treatment of RB-5 dye contained in the above mentioned electrolyte was performed by photocatalytic experiments under UV irradiation. The 300 W Ceralux model 300 BUV 10 F xenon UV lamp with intensity of  $1.5\text{mWcm}^{-2}$ . The calcined Ti felt/ TiO<sub>2</sub> nanotubes /PbO<sub>2</sub> (0.719 g) sample was added in 10 cm<sup>3</sup> solution of  $2 \times 10^{-5}$  mol dm<sup>-3</sup> RB-5 dye in 0.5 mol dm<sup>-3</sup> of sodium sulfate at pH = 3 (by addition of H<sub>2</sub>SO<sub>4</sub> and measured by using waterproof Hanna pH meter model HI 98129). The solution was kept under the unilluminated environment for 90 min to check maximum adsorption of the dye by the electrodes calcined Ti felt/ TiO<sub>2</sub> nanotubes /PbO<sub>2</sub> and no significant adsorption was seen after measuring a solution in a Hitachi U3010 UV-Vis spectrophotometer at 597 nm wavelength. The RB-5 dye solution was exposed to the UV irradiation at pH = 3 and each sample was collected after 5 min of UV exposure. The absorbance of the RB-5 dye in an electrolyte was calculated in a UV-Vis spectrophotometer model number U3010 procured from Hitachi at a wavelength of 597 nm. A linear calibration curve obtained from plot between the absorbance vs. wavelengths at varying concentrations of RB-5 dye fulfilling the Beer-Lambert law was employed to evaluate the concentration of RB-5 dye from the solution.

### 3.2.7 Ultrasonic stability of the Ti felt/nanotube/PbO<sub>2</sub> calcined substrate

The stability of the calcined Ti felt/ TiO<sub>2</sub> nanotubes /PbO<sub>2</sub> was assessed by means of sonication in an ultrasonic bath having a transducer, with perpendicular vibration to the

bottom side of the reactor. The calcined Ti felt/ TiO<sub>2</sub> nanotubes /PbO<sub>2</sub> coating was sonicated for 3 min in 1mol dm<sup>-3</sup> of acetone and for 2 min in D.I water. The coating exhibited strong attachment with the base substrate Ti felt after sonication.

### **3.3 Results and discussion**

#### **3.3.1 Surface characterisation of TiO<sub>2</sub> nanotubes**

The morphological and surface analysis of the Ti felt was observed by SEM. Figure 3.2a shows Ti felt which was previously treated with oxalic acid at 80 °C for 20 min. SEM images of pre-treated Ti felt and hierarchal nanotubes over anodized Ti felt (Fig. 3.2b) reveal that the nanotubes have a hexagonal pattern and their surface is smooth and accordingly reported in literature by Lu et. al (with diameter of 80-90nm) [37-38]. The average diameter of the nanotubes arranged vertically, is 50 nm.

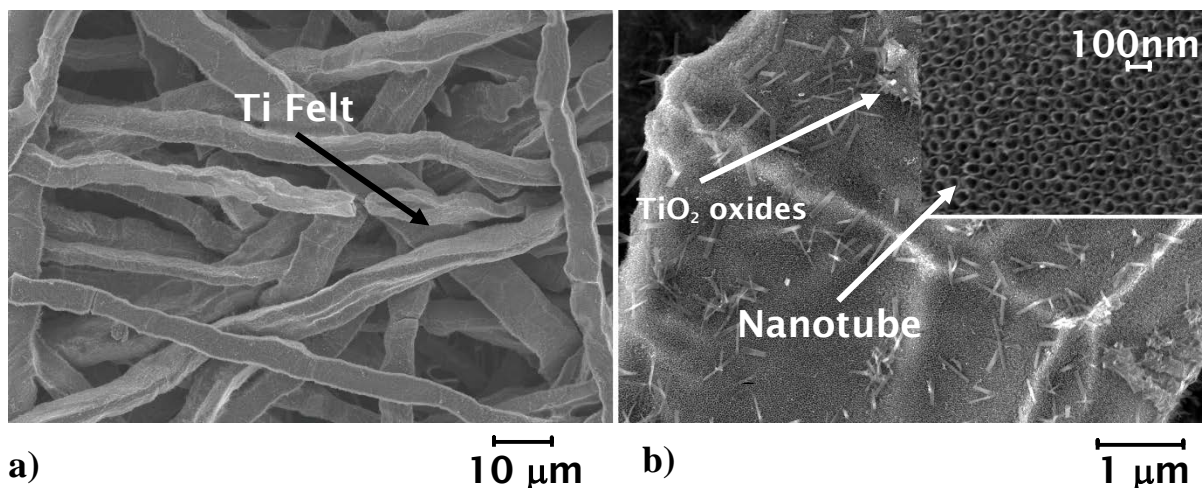
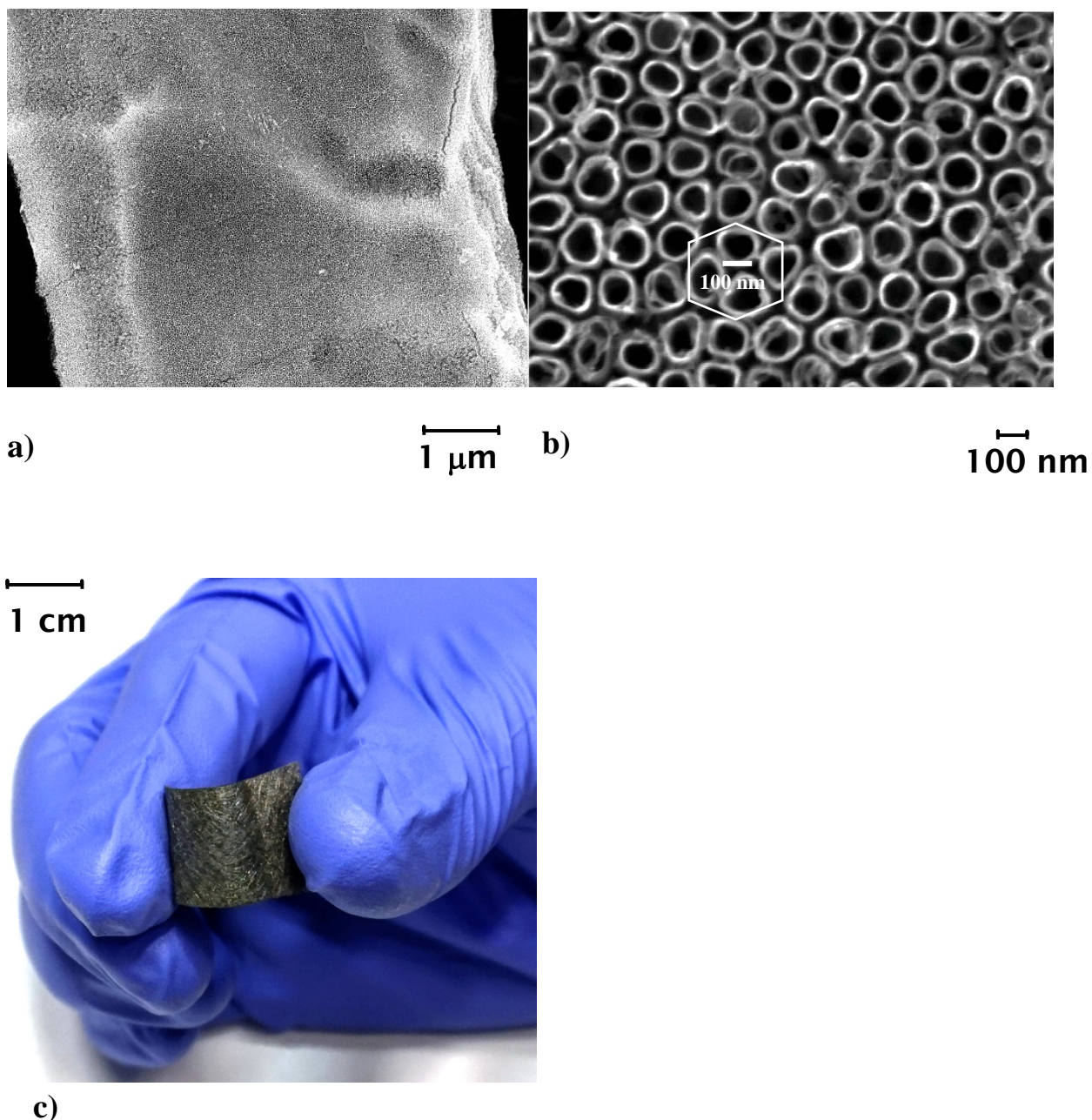


Figure 3.2 FESEM Images of nanotubes on the Ti felt substrate obtained by anodization:

- (a) Pre-treated Ti felt substrate at  $300 \times$  magnification (b)  $\text{TiO}_2$  nanotubes on Ti felt at 15 V,  $0.1 \text{ mol dm}^{-3}$  MSA 0.5 wt. %  $\text{NH}_4\text{F}$  at  $7000 \times$  magnification. The inset shows the nanotubes over Ti felt.

The small diameter of the  $\text{TiO}_2$  nanotubes at the top surface over Ti felt makes possible to decorate with metal oxide like  $\text{PbO}_2$ . This can be observed in the SEM images (Fig.3.2 b). The images also showed the agglomerates of Ti oxides at some parts of Ti-felt. The anodized titanium felt at 20 V cell voltage appeared as a dark blue colour. This may be due to the oxidation of titanium felt which turns into powdered titanium dioxide particles during the anodization process [39]. The surface of anodized felt contain uniform films. The formation of ordered nanotubes is due to the presence of fluoride ions as reported in literature [39, 40]. The fluoride ion can be used in the form of sodium fluoride, ammonium fluoride or hydrofluoric acid.



**c)**  
 Figure 3.3 FESEM image of (a)  $\text{TiO}_2$  nanotubes on Ti felt at 20V,  $1 \text{ mol dm}^{-3}$  MSA, 1 wt. % at  $7000 \times$  magnification (b)  $\text{TiO}_2$  nanotubes on Ti felt at 20V,  $1 \text{ mol dm}^{-3}$  MSA, 1 wt. %  $\text{NH}_4\text{F}$  at  $30000 \times$  magnification (c) Bendable porous Ti felt electrode after anodization.

Titanium felt was anodized in methanesulphonic acid at a range of concentrations from  $0.1 \text{ mol dm}^{-3}$  to  $5.0 \text{ mol dm}^{-3}$ . Figure 3.3 a) reveals a FESEM picture of titanium dioxide

nanotubes synthesized at 20 V in 1 mol dm<sup>-3</sup> MSA and 1 wt. % NH<sub>4</sub>F. The micrograph reveals that the nanotubes had an average diameter of approximately 100 nm and the distance between the nanotubes is in the range of 10-50 nm. The Figure 3.3 b) shows the hexagonal pattern of nanotubes. Figure 3.3 c) showed the compressed 3D fibrous network of titanium metal, felt (Ti felt), which is rigid while capable of being bent or flexed without breaking.

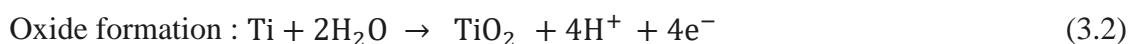
The anodization scheme involves metal oxide formation as a first step as shown by the following reaction [29];



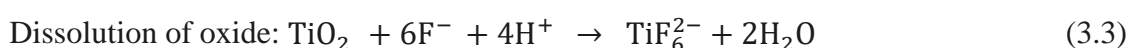
M is metal surface used as an anode

z is stoichiometric number

The electrochemical formation of the oxide layer in case of Ti felt substrate has the following mechanism:



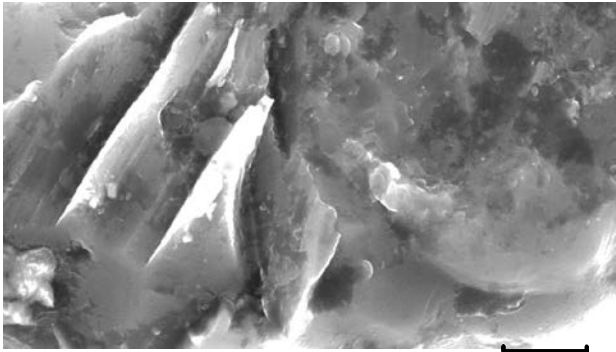
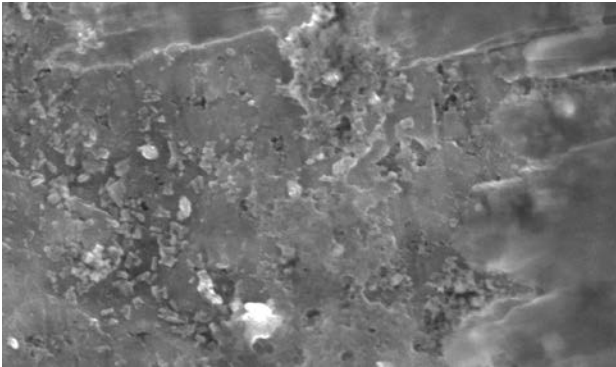
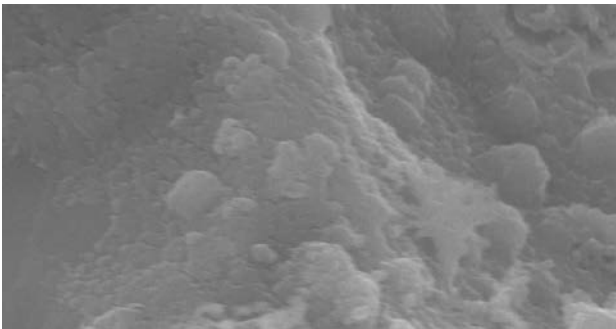
And chemical reaction with fluoride [42, 43]:

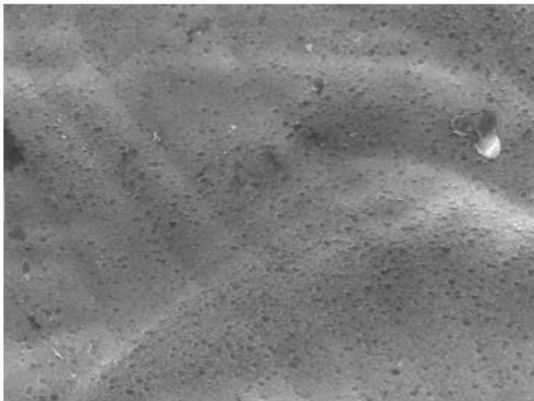
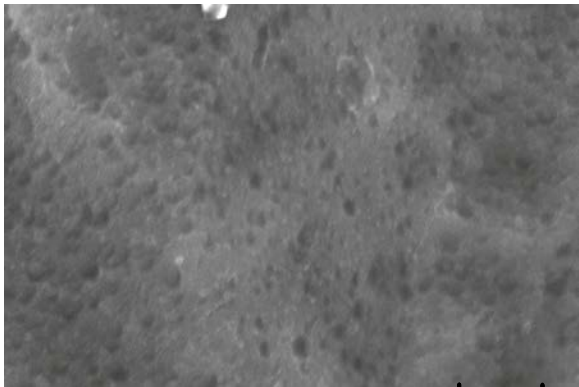
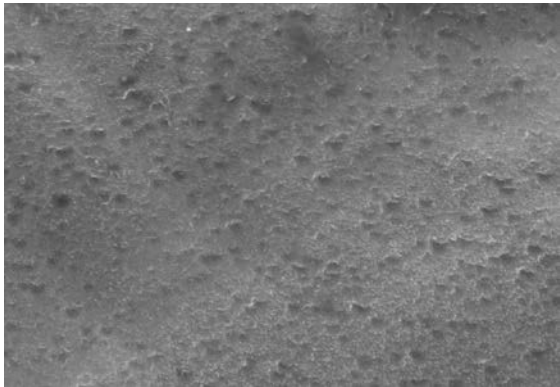




Initially, the anodization forms a dense layer of  $\text{TiO}_2$  on the Ti felt substrate. In the presence of ammonium fluoride, the  $\text{TiO}_2$  film over the Ti felt can be dissolved into an anionic, fluorotitanate complex as depicted from equation 3.3. This dissolution of the oxide surface occurs randomly and produces dispersed pores across the substrate. The pores at the top constitute links with substrate due to the structural configuration of Ti felt. This continually improves the sequence of pores over the top surface producing uniform pores in every direction of the substrate leading to orderly distribution of nanotubes arrays with defined structure. The oxide layer dissolves at the mouth of the pore and oxide formation held at the bottom of the pores [45].

Ordered arrangement and growth of nanotubes is influenced by the pre-treatment method for cleaning the Ti felt. The hexagonal structure depends upon anodization conditions, such as the potential and, the composition of the electrolyte. The use of an untreated Ti felt substrate causes irregularities with disordered structures. Initially, anodising formed a solid agglomerated layer of  $\text{TiO}_2$  on the titanium felt. This compact layer depends upon factors including acid concentration, fluoride intake and applied potential as concluded in literature [43].

Volts	Concentration of $\text{NH}_4\text{F}$ and MSA	FESEM image
1 V	0.5wt. % $\text{NH}_4\text{F}$ $0.1 \text{ mol dm}^{-3}$	 <b>Image a)</b> <span style="float: right;"><b>1 μm</b></span>
5 V	0.3wt. % $\text{NH}_4\text{F}$ $0.1 \text{ mol dm}^{-3}$	 <b>Image b)</b> <span style="float: right;"><b>100nm</b></span>
10 V	0.02wt. % $\text{NH}_4\text{F}$ $0.1 \text{ mol dm}^{-3}$	 <b>Image c)</b> <span style="float: right;"><b>1 μm</b></span>

Volts	Concentration of $\text{NH}_4\text{F}$ and MSA	FESEM image
10 V	0.5 wt. % $\text{NH}_4\text{F}$ $0.1 \text{ mol dm}^{-3}$	 <p><b>Image d)</b> <math>1 \mu\text{m}</math></p>
20 V	0.5 wt. % $\text{NH}_4\text{F}$ $0.1 \text{ mol dm}^{-3}$	 <p><b>Image e)</b> <math>1 \mu\text{m}</math></p>
25 V	1 wt. % $\text{NH}_4\text{F}$ $1 \text{ mol dm}^{-3}$	 <p><math>1 \mu\text{m}</math></p>

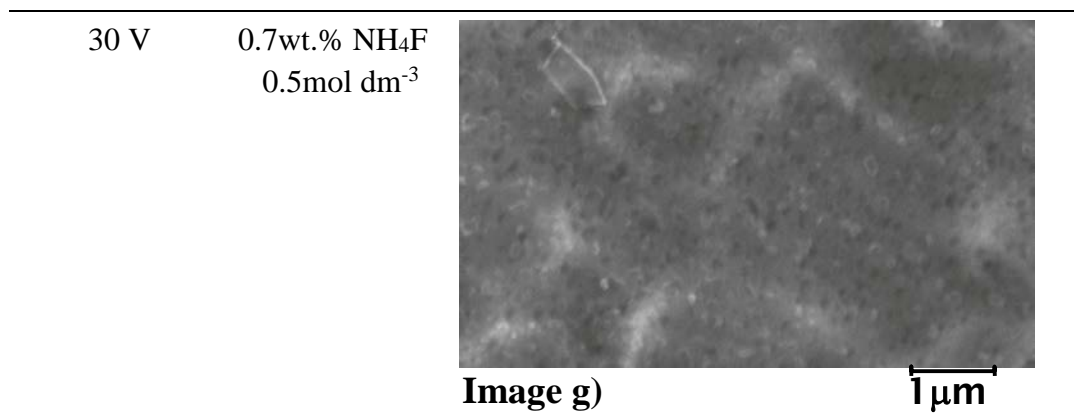


Table 3.1 Effect of operating conditions on Ti felt anodization (Ti felt anode with dimensions 2 cm × 2 cm × 0.15 cm, graphite plate cathode with dimensions 1.5 cm × 6 cm × 1.2 cm, stirring = 300 rev min<sup>-1</sup>, T = 25 °C, t = 1 hour).

### 3.3.2 Effect of operating parameters on nanotube growth

#### 3.3.2.1 Effect of fluoride concentration on nanotube formation

Seven different compositions containing different concentration of ammonium fluoride were investigated. The concentration of ammonium fluoride was 0.02, 0.1, 0.3, 0.5, 0.7 or 1.0 wt. % fluoride ion in 0.1 mol dm<sup>-3</sup> methanesulphonic acid. A cell potential of 20 V difference was applied by means of power supply while the solution was at room temperature (25 °C) and the anodisation time was 1.0 h. The magnetic stirrer was used at a rotation speed of 300 rev min<sup>-1</sup>.

Figure 3.3 a) and b) show the substrate morphology of anodized Ti felt with ordered TiO<sub>2</sub> nanotubes at a fluoride ion concentration of 1.0 wt. %. The nanotubes had an inner diameter of approximately 100 nm with a wall thickness of 20 nm and a hexagonal grid spacing.

At low fluoride concentrations of 0.02-0.03 wt. % there is no formation of nanotubes. Table 3.1 Image f) depicts the morphology of the anodized Ti felt at a fluoride

concentration of 0.02 wt. % fluoride ion which shows just oxide layer on the surface. At 0.3 wt. % of fluoride ion, there is still has some oxide layer on the surface as shown in Table 3.1 Image g). The reason could be that the concentration of fluoride ions was too low to dissolve the oxide layer present on the substrate. The oxide dissolution to hexafluorotitanium is limited in comparison to the oxide formation on the substrate.

The above findings showed that ordered and well defined  $\text{TiO}_2$  nanotubes were formed at fluoride concentration of 1.0 wt. %. The formation of hexafluorotitanium anion in the solution depends upon the fluoride ion which further promotes the dissolution of Ti oxide layer, as depicted in reaction (3.3). At low concentration fluoride ions are unable to dissolve oxide layer at the pore mouth and no nanotubes formed. However if the concentration of fluoride ions is too high, more hexafluorotitanium anion is form in the solution leading to the excessive dissolution of the oxide layer at the pore mouth ending up towards the destruction of nanotube arrays [42, 43, 45].

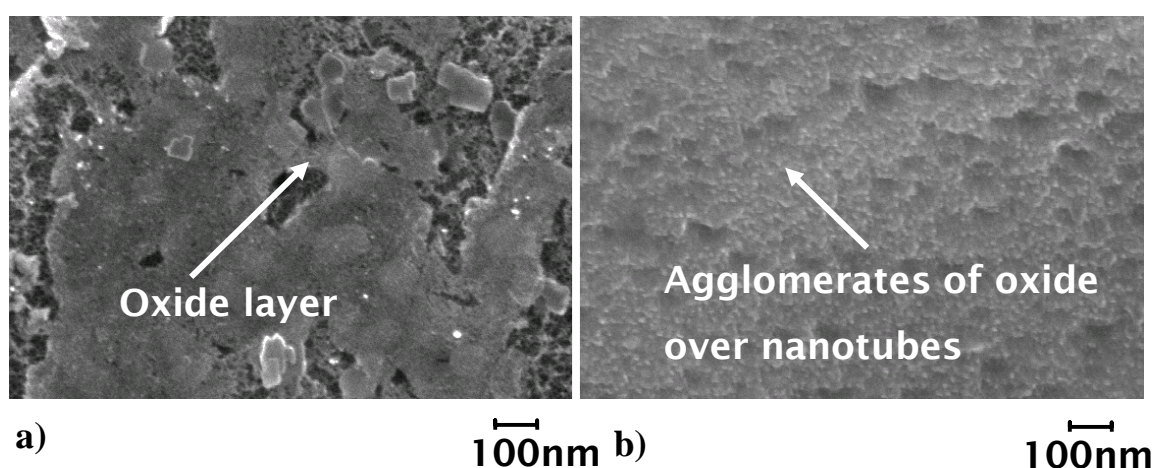


Figure 3.4 FESEM image of (a)  $\text{TiO}_2$  nanotubes on Ti felt at 5 V,  $1 \text{ mol dm}^{-3}$  MSA, 1 wt. %  $\text{NH}_4\text{F}$  at 13000 magnification (b)  $\text{TiO}_2$  nanotubes on Ti felt at 30 V  $1 \text{ mol dm}^{-3}$  MSA, 1 wt. %  $\text{NH}_4\text{F}$  at 13000 magnification.

### 3.3.2.2 Effect of methanesulphonic acid concentration on nanotubes formation

Three different concentrations of methanesulphonic acid were studied, namely 0.1, 0.5 and 1 mol dm<sup>-3</sup> at a fluoride concentration of 1.0 wt. %. Other operating conditions involve constant stirring at 300 rev min<sup>-1</sup>, temperature 25 °C anodizing time 1 hour.

Titanium dioxide nanotubes were formed in all concentration of MSA. The nanotubes have residual oxide precipitates at the top surface when MSA was 0.1 mol dm<sup>-3</sup>, as shown in figure 3.1b. The average diameter of nanotube was 50 nm with a wall thickness of 10 nm. An organized nanotubes growth was seen at higher concentrations of MSA (1 mol dm<sup>-3</sup>) as shown in figure 3.3 a). However, on increasing the concentration of MSA, the nanotubes look clean and more confined with no traces of surface oxide. The dimensions of nanotubes were 100 nm with a wall thickness of 20 nm. This is in agreement with the previous investigations, which demonstrated that the pH of the electrolyte influences the rate of oxide formation at the bottom of the pore and the rate of oxide dissolution at the mouth of the pore [40, 49].

At higher acidic concentration at 1 mol dm<sup>-3</sup>, there is much easier formation of hexafluorotitanium anion which ultimately increase the dissolution of oxide layer. Consequently, more ordered nanotubes form on the Ti felt substrate.

### 3.3.2.3 Effect of applied potential on nanotube growth

Seven different cell voltages were applied i.e. 1, 5, 10, 15, 20, 25 and 30 V in an electrolyte 1 wt. % of fluoride ion with 1 mol dm<sup>-3</sup> MSA. While other parameters were similar to that used in the section 3.2.1 i.e. (solution was at room temperature (25 °C) and

the anodisation time was 1.0 h and magnetic stirrer was used at a rotation speed of 300 rev min<sup>-1</sup>).

Figure 3.3 b) shows that an applied cell potential of 20 V produced well defined and ordered TiO<sub>2</sub> nanotubes. At a lower cell voltage, the tubes became less stable while more compact oxide layer was seen at lower voltages (1-10V). There is little or no electrochemical etching of the oxide layer at lower applied potentials. For instance, no nanotubes were seen at 1-10 V as can be seen from figure 3.4 a). At 15 V some nanotubes were observed with wall thickness of 10 nm with some oxides as shown in figure 3.2 b). By increasing potential to 20 V the wall thickness increased to about 20 nm as depicted in figure 3.3 b). It can be concluded that by anodising at this applied potential the oxide dissolution at the pore mouth decreased due to higher electrochemical etching of oxide layer over the Ti felt. At applied potential of 30 V, gas evolution was seen on both electrodes which ultimately enhanced the rate of oxide formation at the pore bottom and its dissolution at the pore mouth which generated agglomerates of oxides on nanotubes as can be seen in figure 3.4 b).

### **3.3.3 Decoration of nanotubes with PbO<sub>2</sub>**

The nanotubular arrangement of TiO<sub>2</sub> nanotubes is hydrophilic. Therefore, these structures are able to absorb the content of an aqueous phase on immersion into a solution. This wetting characteristics enable deposition of the nanotubes with electrolyte in the presence of PVP as a structure directing agent [36].

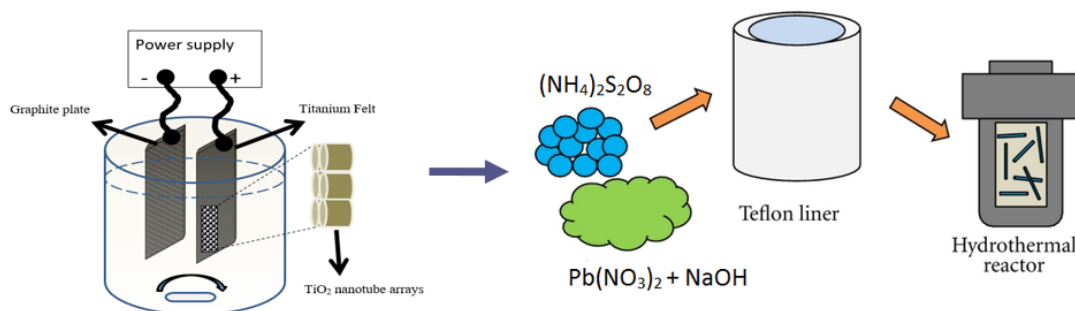
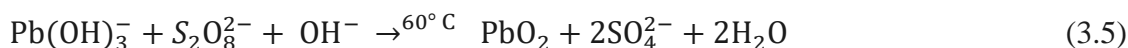


Figure 3.5 Arrangement for the synthesis of Ti felt/  $\text{TiO}_2$  nanotubes / $\text{PbO}_2$  composite.

Figure 3.5 shows the stepwise arrangement for the synthesis of the composite electrodes where  $\text{TiO}_2$  nanotubes were obtained via anodization and further deposited with  $\text{PbO}_2$ . The nanotubular arrangement at Ti felt substrate was immersed in a solution containing lead nitrate and ammonium sulphate. The lead ions are adsorbed over the surface of  $\text{TiO}_2$  nanotubes and converted to  $\text{PbO}_2$  after heat treatment and accumulated over the surface of the Ti-felt on via following reactions



In reaction 3.4, lead nitrate was converted to  $\text{Pb}(\text{OH})_3^-$  and further it was oxidized by ammonium persulphate to lead dioxide as depicted in equation 3.5 at a temperature of  $60^\circ\text{C}$ . The deposition of  $\text{PbO}_2$  on the nanotubular arrangement on Ti felt was proved by Raman and FESEM studies. Figure 3.6 a-b) reveals SEM images for a deposited lead dioxide over Ti felt during 15 min of immersion on the  $\text{TiO}_2$  nanotubes, which shows partial deposition of  $\text{PbO}_2$  on nanotubes. Some of the uncovered nanotubes can still be seen as immersion time is lower. The deposition of  $\text{PbO}_2$  over the nanotube arrays can be



increased by tuning the immersion time. In this case the immersion time was increased to 6 h and 12 h. Figure 3.7 and Figure 3.8 represent the SEM images of these immersion time for deposited  $\text{PbO}_2$ .

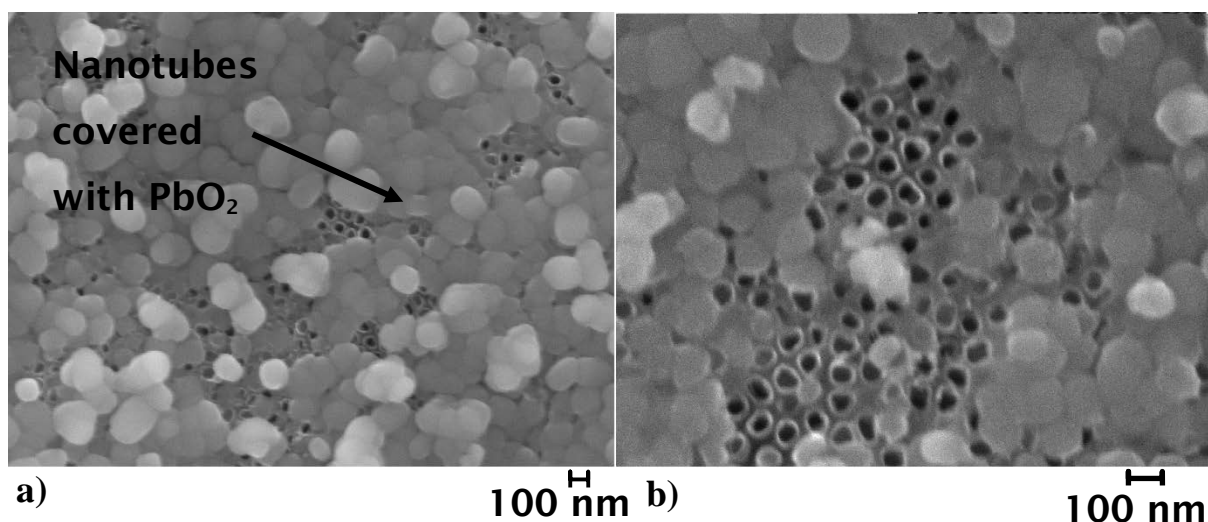


Figure 3.6 FESEM Images of nanotubes decorated with  $\text{PbO}_2$  on the Ti felt substrate obtained by layer by layer immersion: (a)  $\text{PbO}_2$  covered  $\text{TiO}_2$  nanotubes on Ti felt at a cell potential of 20 V in  $1 \text{ mol dm}^{-3}$  MSA containing 1 wt. %  $\text{NH}_4\text{F}$  at  $30000 \times$  magnification (b)  $\text{PbO}_2$  covered  $\text{TiO}_2$  nanotubes ( $t_i = 15 \text{ min}$ ) on Ti felt at 20 V in  $1 \text{ mol dm}^{-3}$  MSA + 1 wt. %  $\text{NH}_4\text{F}$  at  $60000 \times$  magnification.

FESEM images reveals a large amount of  $\text{PbO}_2$  on the surface of the nanotube layers as immersion time increases. In the first 15 min immersion,  $\text{PbO}_2$  deposited over the surface of the  $\text{TiO}_2$  nanotubes, without modifying the nanotubular arrangement. At  $t_i = 6 \text{ h}$ , the amount of  $\text{PbO}_2$  produced inside overflows and spills outside the nanotubular structures and develop  $\text{PbO}_2$  which after flashing with nitrogen acquire a shape of spheroid like crystalline structure. At  $t_i = 12 \text{ h}$ ,  $\text{PbO}_2$  homogenously covered the  $\text{TiO}_2$  nanotubes

surfaces and form a cauliflower shape like structure. The equilibrium absorption of lead oxide precursor have been achieved at 12 hours immersion by  $\text{TiO}_2$ , which is a known adsorbent of lead ions as reported in literature [50, 51]. The decoration of nanotubes with  $\text{PbO}_2$  on the nanotubular arrays over Ti felt substrate expected to increase the electrochemical properties of the coating.

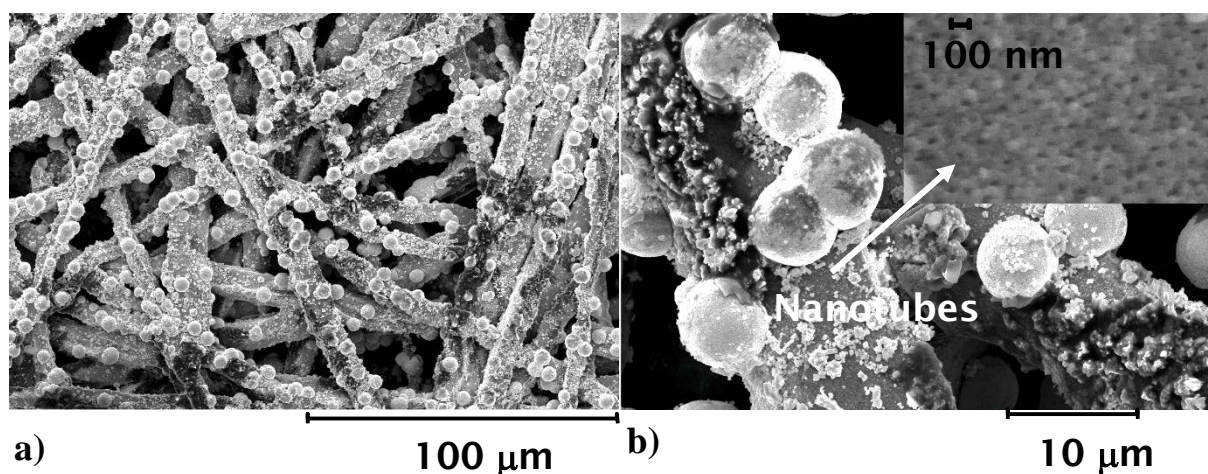


Figure 3.7 FESEM Images of nanotubes decorated with  $\text{PbO}_2$  particles on the Ti felt substrate obtained by layer by layer immersion (a)  $\text{TiO}_2$  nanotubes decorated with  $\text{PbO}_2$  ( $t_i = 6$  h) at 200 magnification (b)  $\text{TiO}_2$  nanotubes decorated with spheroid like  $\text{PbO}_2$  crystals ( $t_i = 6$  h) on Ti felt at  $1500 \times$  magnification. The inset shows the uncovered nanotubes at  $35000 \times$  magnification.

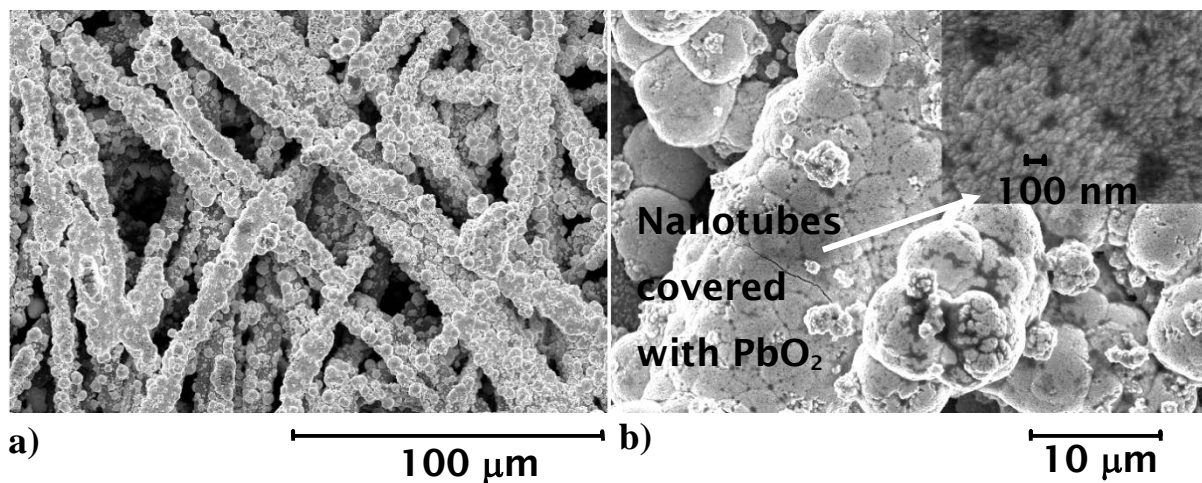


Figure 3.8 (a)  $\text{TiO}_2$  nanotubes covered  $\text{PbO}_2$  ( $t_i = 12$  h) on Ti felt  $200 \times$  magnification (b)  $\text{TiO}_2$  nanotubes covered with cauliflower like  $\text{PbO}_2$  crystals ( $t_i = 12$  h) on Ti felt at  $1500 \times$  magnification, the inset shows the  $\text{PbO}_2$  covered nanotubes at  $35000 \times$  magnification.

EDX elemental analysis was revealed in figure 3.9 for this novel coating. It showed that as obtained coating contain lead in abundance with titanium and oxygen. This shows that  $\text{PbO}_2$  adhered uniformly over the Ti felt strands.

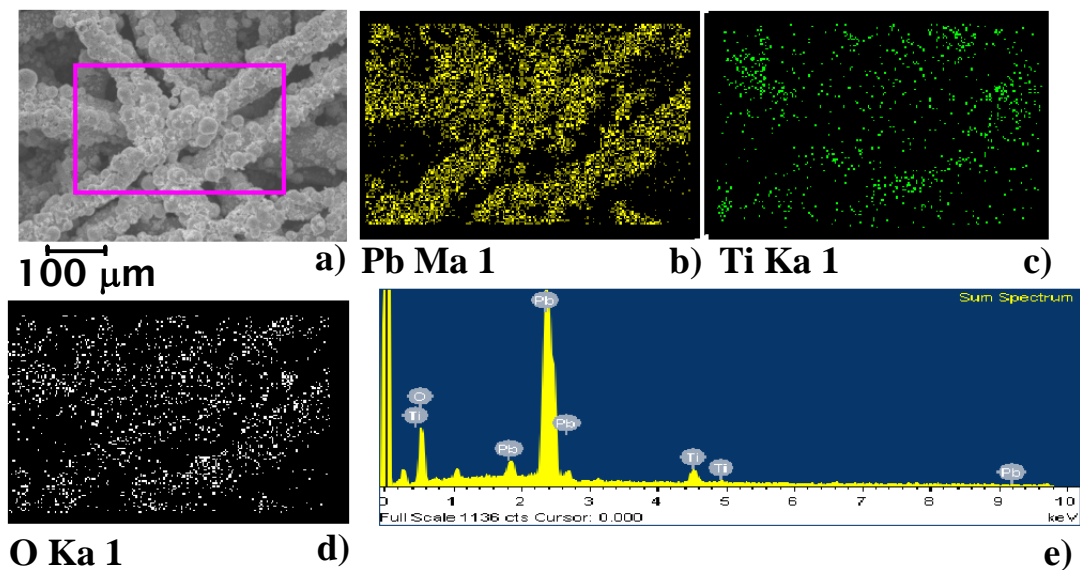


Figure 3.9 EDX images for elemental analysis of calcined Ti felt /  $\text{TiO}_2$  nanotubes /  $\text{PbO}_2$  obtained by anodization and layer by layer immersion: (a) calcined Ti felt /  $\text{TiO}_2$  nanotubes /  $\text{PbO}_2$  at 900 magnification (b) lead interpretation (c) titanium interpretation (d) oxygen interpretation (e) Sum spectrum for elemental plot interpretation.

The Raman spectroscopy revealed the structural properties of the coatings related to the presence of  $\alpha\text{-PbO}_2$  and formation of anatase phase after annealing as shown in figure 3.10. The distinct peaks observed at  $428$ ,  $285$  and  $152\text{ cm}^{-1}$  which exhibit the presence of  $\alpha\text{-PbO}_2$  at calcined and non-calcined Ti felt /  $\text{TiO}_2$  nanotubes /  $\text{PbO}_2$  [52]. The effect of annealing transform the substrate from nanotubes amorphous phase to anatase phase which was indicated by the appearance of peaks observed at  $517$ ,  $319$  and  $177\text{ cm}^{-1}$  as demonstrated in the literature [53].

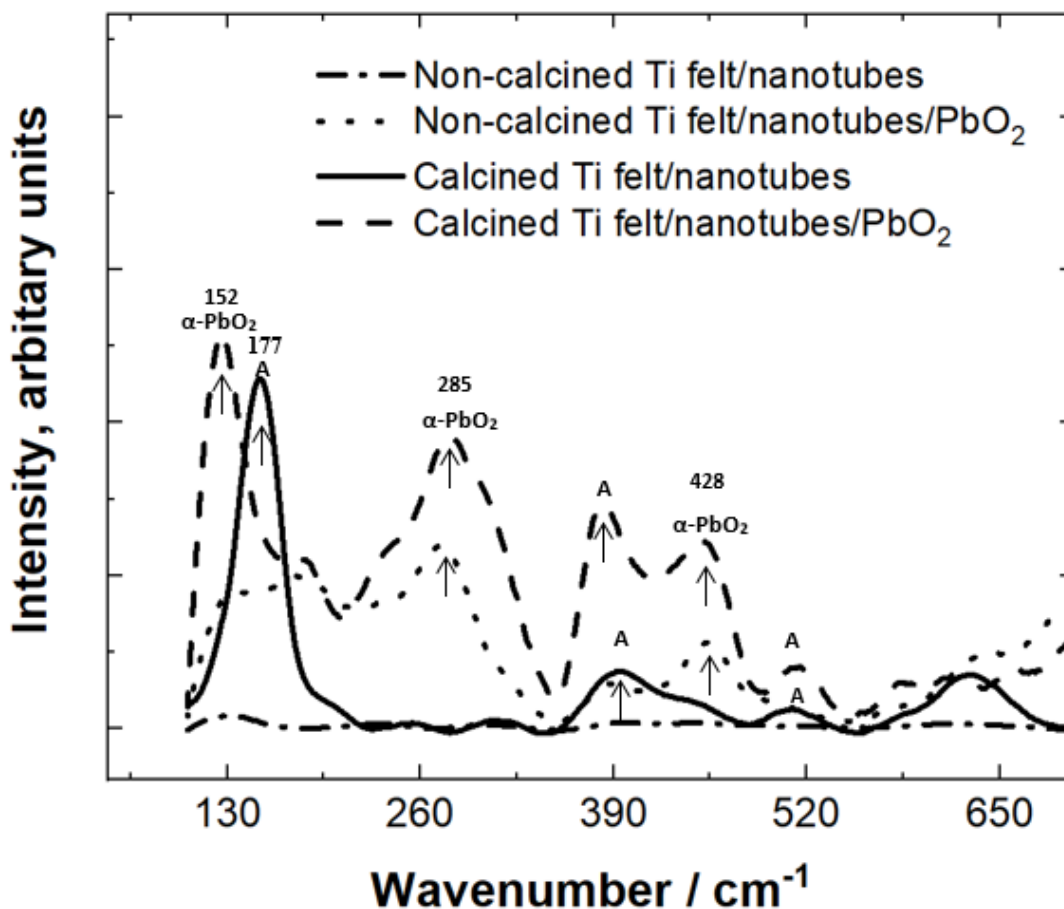


Figure 3.10 Raman spectra of calcined and non-calcined Ti felt / TiO<sub>2</sub> nanotubes /PbO<sub>2</sub> ( $t_i = 15$  min) at 450 °C and calcined non-calcined Ti felt / TiO<sub>2</sub> nanotubes.

### 3.3.4 Electrochemical studies of novel coatings containing PbO<sub>2</sub>

These nanotubes coated with PbO<sub>2</sub> nanoparticles on Ti felt substrate observed in Figure 3.8 a), are likely to be utilized as an electrode for an electrochemical anodic oxidation of RB-5 dye. Therefore, to examine the electrochemical characteristics of Ti felt/ TiO<sub>2</sub> nanotubes and Ti felt/ TiO<sub>2</sub> nanotubes /PbO<sub>2</sub> electrodes towards RB-5 dye, linear scan voltammetric studies were used. The main goal of these studies is to detect the electrocatalytic performance towards oxidation of organic molecules and to know the

limiting current at which oxygen evolution started. Figure 3.11 represented the linear scan voltammograms from - 0.4V to 1.4V vs. Hg/HgO NaOH (sat.) at a sweep rate of 10 mV s<sup>-1</sup>, in 0.05 mol dm<sup>-3</sup> H<sub>2</sub>SO<sub>4</sub> in the working and counter electrode compartment. The scan towards positive potential depicts steep rise in the anodic current corresponding to the oxygen evolution reaction.

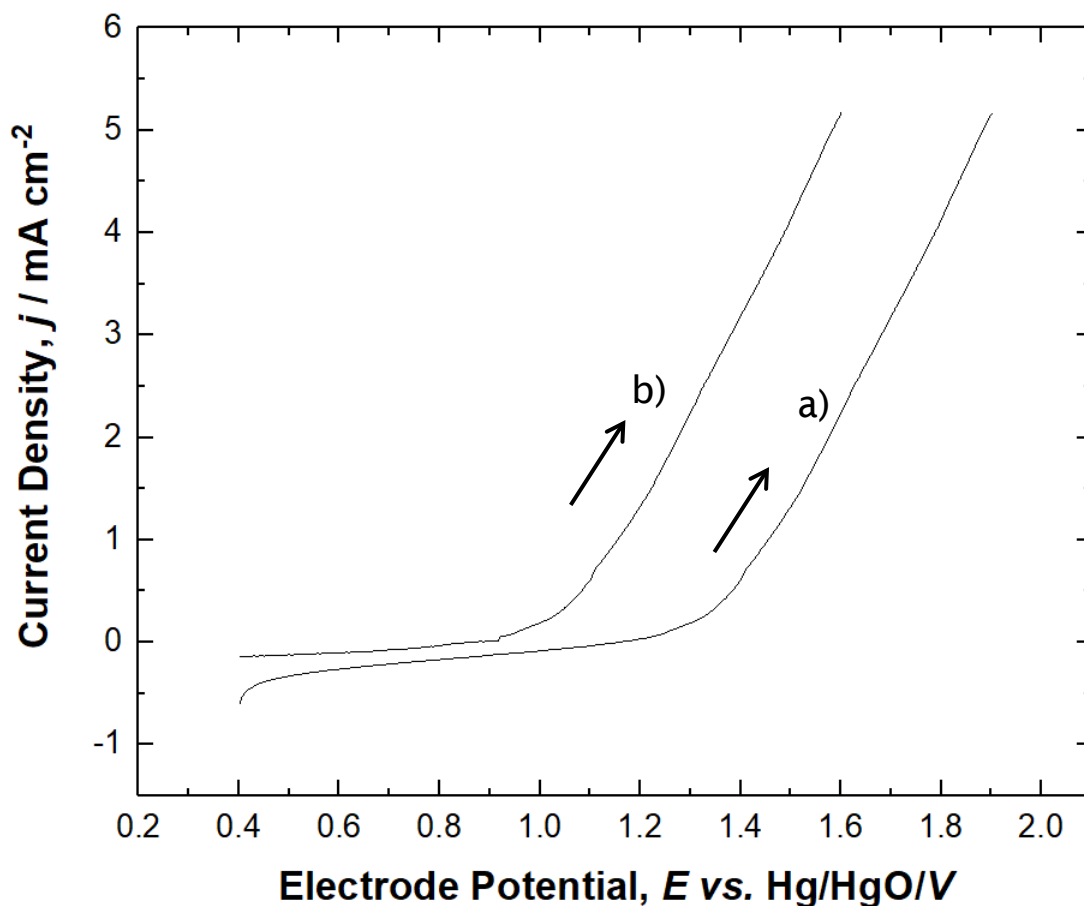


Figure 3.11 Polarization curve by using the coatings a) Ti felt / TiO<sub>2</sub> nanotubes /PbO<sub>2</sub> as positive electrode after annealing at 450 °C in an electrolyte containing in 0.05 mol dm<sup>-3</sup> H<sub>2</sub>SO<sub>4</sub>. b) Ti felt / TiO<sub>2</sub> nanotubes in an electrolyte containing in 0.05 mol dm<sup>-3</sup> H<sub>2</sub>SO<sub>4</sub> background electrolyte; potential scan rate of 10 mV s<sup>-1</sup>; T = 25 °C.

According to figure 3.11, the overpotential of electrodes utilized in this work towards the oxygen evolution reaction is in the following order: Ti felt / TiO<sub>2</sub> nanotubes /PbO<sub>2</sub> > Ti felt / TiO<sub>2</sub> nanotubes. The free radical ( $\bullet$ OH) generated during electrochemical water discharge reaction is the result of an intermediate reaction that takes place just before the oxygen evolution reaction. Oxygen evolution started at higher potential (1.5 V vs. Hg/HgO) by using Ti felt / TiO<sub>2</sub> nanotubes /PbO<sub>2</sub> which shows the positive improvement of the substrate by the addition of PbO<sub>2</sub>. This represents the better capability of the substrate anodized with TiO<sub>2</sub> nanotubes and decorated with PbO<sub>2</sub> on pre-treated Ti felt. It was reported that TiO<sub>2</sub> has been utilised as a base substrate for RuO<sub>2</sub> and IrO<sub>2</sub> anodes, where water discharge fosters  $\bullet$ OH free radical at the RuO<sub>2</sub> and IrO<sub>2</sub> anodes [1]. At the TiO<sub>2</sub> layer, the  $\bullet$ OH free radical can be produced via two routes:

- i) Photocatalytic in the presence of UV light
- ii) Electrocatalytic of Nb- or Ta-doped TiO<sub>2</sub> anode is employed [44].

The improvement contributed due to the existence of TiO<sub>2</sub> nanotubes on the substrate can be associated to the adsorption of positively charged RB-5 dye molecules to the negatively charged TiO<sub>2</sub> nanotubes and subsequent oxidation of RB-5 dye by the free radical generated at non-active PbO<sub>2</sub> present over nanotubes supported by Ti felt surface. It was explained that carbon based substrate like carbon foam coated with PbO<sub>2</sub> generates ( $\bullet$ OH) hydroxyl radical due to water discharge reaction [52].

It is well known that oxygen evolution reaction (OER) is an undesirable reaction during electro-oxidation activity. The water discharge is the first step during the course of intermediate reactions which ultimately generate mediated hydroxyl radicals ( $\bullet$ OH) in

Eq. (2.1), at the anode surface during oxygen evolution reaction. The nature of electrode also plays a significant role on the impact of hydroxyl radicals over the positive electrode surface during anodic oxidation. Two kinds of electrode materials can be categorized for electrochemical oxidation: "active" and non-active electrode materials [56]. Active electrodes are strongly influenced by hydroxyl radicals [56]. The active anodes lead to the oxygen evolution reaction at lower potentials due to the generation of higher oxides [56, 57]. Pt is one of the active anode with high adsorption enthalpies which was extensively studied due to its attractive nature towards hydroxyl radicals. Hydroxyl radical is responsible for the oxidation of electroactive species for non-active electrodes.

The decorated  $\text{PbO}_2$  over titanate nanotubes is a non-active electrode and there is a weak interaction of hydroxyl radicals. The anodic oxidation over a non-active anode ( $\text{PbO}_2$ ) is then known as ( $\bullet\text{OH}$ ) mediated oxidative oxidation of the dye. The interaction between the organic dye molecules with the physisorbed radical is intensified due to the applied potential on the anodic surface of Ti felt /  $\text{TiO}_2$  nanotubes /  $\text{PbO}_2$  and also by the greater surface area of Ti felt covered with anodized nanotubes which adsorb the dye molecule enhancing the oxidation process and hence  $\bullet\text{OH}$  radicals have tendency to react with the organic dye in the electrolyte [13] and degrade it. Tifelt/  $\text{TiO}_2$  nanotubes /  $\text{PbO}_2$  and Tifelt/  $\text{TiO}_2$  nanotubes were examined for electrocatalytic activity by using linear scan voltammetric studies. A solution containing  $0.05 \text{ mol dm}^{-3} \text{ H}_2\text{SO}_4$  was used as an electrolyte to study the oxygen evolution potential of both electrodes. The potential difference (1.5 V vs. Hg/HgO) in Figure 3.11 at which oxygen evolution reaction takes place is influenced by electrode material and formation of mediated  $\bullet\text{OH}$  radical due to water discharge. In case of Ti felt/  $\text{TiO}_2$  nanotubes /  $\text{PbO}_2$  oxygen evolution started at



potential (1.5 V) vs. Hg/HgO (0.6 mol dm<sup>-3</sup> NaOH) at a scan rate of 10 mV s<sup>-1</sup>. This corresponds to the maximum potential difference after the electrochemical reactions takes place at the anode surface as primary reactions with post-secondary oxygen evolution reaction in comparison to other electrodes used in this study. However for Ti felt/ TiO<sub>2</sub> nanotubes showed minimum potential for oxygen evolution reaction which corresponds its electro activity for oxygen evolution reaction while in case of Ti felt/ TiO<sub>2</sub> nanotubes /PbO<sub>2</sub> seems to be poor electroactive catalyst for the oxygen evolution reaction. Ti felt/ TiO<sub>2</sub> nanotubes showed oxygen evolution > 1.0 V vs. Hg/HgO. Tifelt/ TiO<sub>2</sub> nanotubes /PbO<sub>2</sub> acquire electroactive catalytic properties for the electrochemical oxidation of RB-5 dye before 1.5 V vs. Hg/HgO, as this has been presented in the previous reports that mediated •OH radicals acts as an oxidizing species produced due to water discharge and negligible adsorption of these active mediators over the non-active anode [59, 60].

### 3.3.5 Electrochemical removal and discolouration of RB-5 dye

The oxidation was studied by electrolysis of the electrolyte containing RB-5 dye using the coating described above as anode with an applied constant potential of 1.4 V vs. Hg/HgO. The volume of the electrolyte was 100 cm<sup>3</sup> containing 2 × 10<sup>-5</sup> mol dm<sup>-3</sup> of RB-5 dye and 0.5 mol dm<sup>-3</sup> of Na<sub>2</sub>SO<sub>4</sub> by adjusting pH = 3 using H<sub>2</sub>SO<sub>4</sub>. The working electrode was (Ti felt/ TiO<sub>2</sub> nanotubes /PbO<sub>2</sub>, Ti felt/ TiO<sub>2</sub> nanotubes or Ti felt) while the counter and reference electrodes were platinum and Hg/HgO, respectively. A UV-vis spectra was used to measure the concentration of RB-5 dye in samples taken during constant potential electrolysis of the electrolyte at regular intervals of time, used the maximum absorbance band for RB-5 dye in the visible region ( $\lambda_{\text{max}} = 597$  nm). The calcined Ti felt/ TiO<sub>2</sub> nanotubes /PbO<sub>2</sub> as working electrode caused the intensity of visible

band continuously decreased during 60 min of electrolysis. There was no evidence of new bands in the absorbance data, denoting prompt transformation of the dye structure during the electrochemical treatment which may associate the formation of other complex dye structures that could be oxidised into elementary low molecular weight species such as  $\text{CO}_2$  and  $\text{H}_2\text{O}$  [61]. Other different aliphatic and aromatic hydrocarbons may arise due to the oxidation of RB-5 dye, this results from the displacement of functional (chromophore group) present in azo dyes and ultimately removal of these groups to carbon dioxide and organic acids (carboxylic acid) [62, 63, 64]. The normalized concentration of the dye vs. time for during the electrolysis studies using Ti felt/  $\text{TiO}_2$  nanotubes / $\text{PbO}_2$ , Ti felt/  $\text{TiO}_2$  nanotubes and Ti felt as anodes are represented in Figure 3.12. A pseudo- first order reaction kinetics related to the dye oxidation that fits the equation 2.20 reported in section 2.9, is assumed.

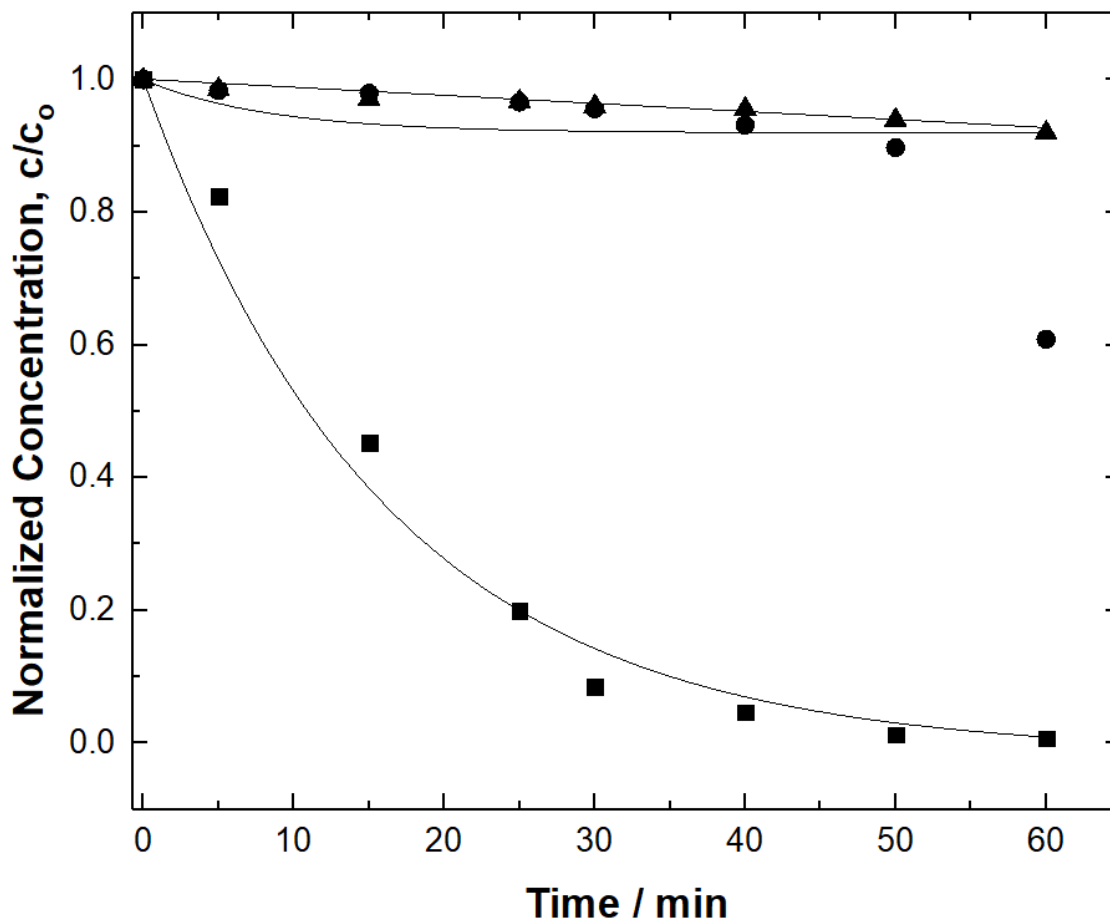
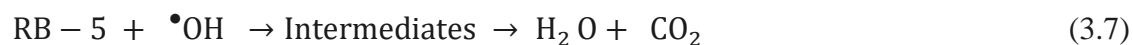


Figure 3.12 Electrochemical oxidation of RB-5 dye in an electrolyte having  $2 \times 10^{-5}$  mol dm<sup>-3</sup> R.B-5 dye in 0.5 mol dm<sup>-3</sup> Na<sub>2</sub>SO<sub>4</sub> (Experimental conditions: applied potential = 1.4 V vs. Hg/HgO pH = 3.0, T = 25 °C) by using (▲) Ti felt, (●) Ti felt / TiO<sub>2</sub> nanotubes, and (■) Ti felt / TiO<sub>2</sub> nanotubes / PbO<sub>2</sub>.

The different values of normalized concentration and pseudo first order removal kinetics constants are influenced by the electroactive nature of the different substrates used. The different performance arises due to the tendency of Ti felt/ TiO<sub>2</sub> nanotubes /PbO<sub>2</sub> to transform mediated •OH radicals into dioxygen species or may be directly attack the azo dye as represented in equations (3.6) and (3.7).



The generation of hydroxyl radicals over the active surface electrode i.e. Pt plays a critical role but it also promotes the oxygen evolution reaction rapidly, resulting in the consumption of free radical which ultimately affects the rate of organic removal [65]. Figure 3.12 showed the anodic oxidation of RB-5 dye comparing 3 electrodes i.e. Ti felt/TiO<sub>2</sub> nanotubes /PbO<sub>2</sub>, Ti felt / TiO<sub>2</sub> nanotubes and Ti felt. The plots show that calcined Ti felt/ TiO<sub>2</sub> nanotubes /PbO<sub>2</sub> produces about 99% colour removal with a kinetic pseudo rate constant value of  $k = -0.0875 \text{ min}^{-1}$  calculated from the linear pseudo first order oxidation shown in Figure 3.13, when applying constant potential value of 1.4 V vs. Hg/HgO.

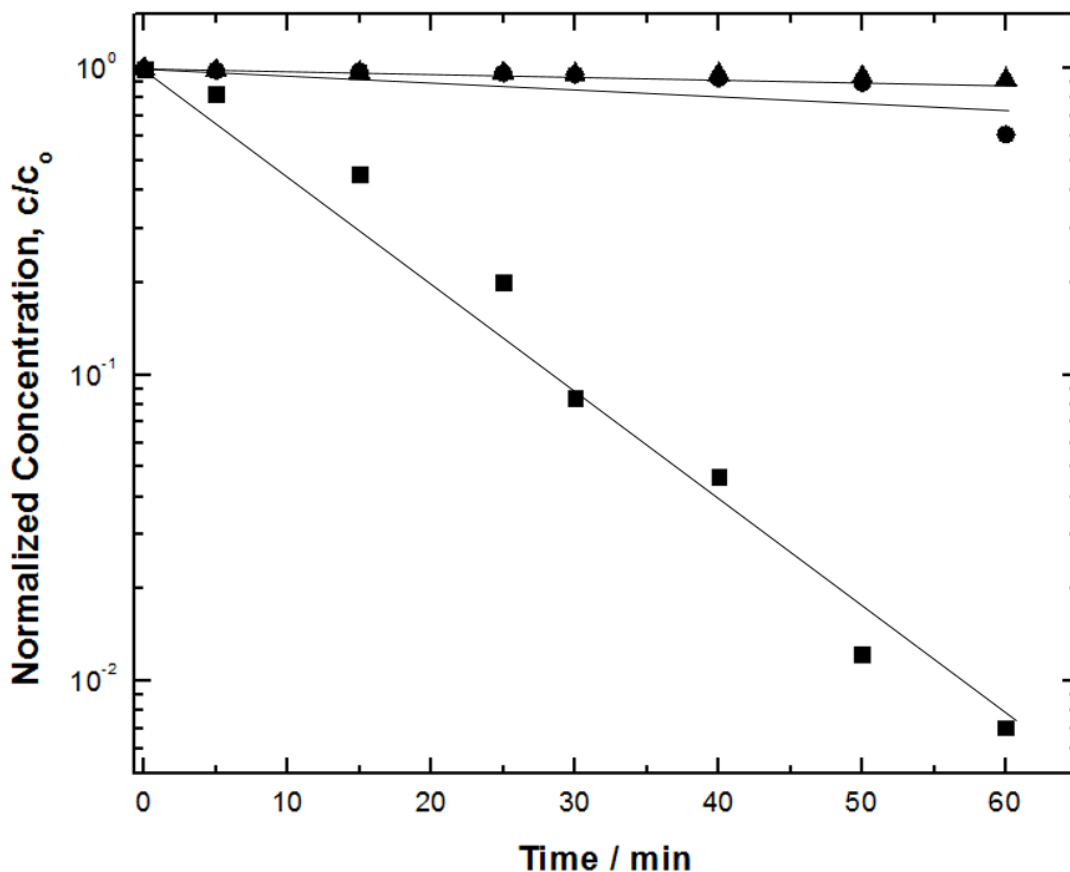


Figure 3.13 Electrochemical oxidation kinetics of RB-5 dye in an electrolyte having  $2 \times 10^{-5} \text{ mol dm}^{-3}$  R.B-5 dye in  $0.5 \text{ mol dm}^{-3}$   $\text{Na}_2\text{SO}_4$  (Experimental conditions: applied potential = 1.4 V vs. Hg/HgO pH = 3.0, T = 25 °C) by using ▲) Ti felt, ●) Ti felt /  $\text{TiO}_2$  nanotubes, and ■) Ti felt /  $\text{TiO}_2$  nanotubes /  $\text{PbO}_2$ .

The high colour removal efficiency, of 99% can be explained as water discharge and produces  $\bullet\text{OH}$  free radicals mediators which ultimately leads to the colour removal. Ti felt /  $\text{TiO}_2$  nanotubes caused almost negligible colour removal (10%) during the first 50 min of electrolysis but increased to 40% at 60 min which might be due to the adsorption of dye on the nanotubes with pseudo rate constant  $k = -0.0058 \text{ min}^{-1}$ . However, lower

oxidation results for Ti felt alone were observed, with discolouration of dye of about 7% after 60 min which is quite low while comparing results with calcined Ti felt / TiO<sub>2</sub> nanotubes /PbO<sub>2</sub> of about 99% oxidation in 60 min, this suggest that the application of positive potential might give rise to the oxidation of Ti felt and perhaps passivation. However for Ti felt / TiO<sub>2</sub> nanotubes /PbO<sub>2</sub> the non-active nature of PbO<sub>2</sub> assisted the production of •OH radical as described in equation (2.1) and nanotubes may promote the platform to adsorb the dye molecules inside the tubes on the Ti felt substrate.

### 3.3.6 Reaction kinetics for electrooxidation of RB-5 dye

Figure 3.12 represented normalized concentration profile of RB-5 dye against time during the electrolysis at 1.4 V vs. Hg/HgO, pH = 3.0 at different electrodes. The log of the normalized concentration decay vs. time is shown in figure 3.13. A linear relationship suggest that electrooxidation of reactive black 5 dye denotes a pseudo first order reaction kinetics for Ti felt / TiO<sub>2</sub> nanotubes /PbO<sub>2</sub> substrate. This showed steady removal of RB-5 dye with rate of discolouration during electrochemical reaction time. Table.3.2 shows the comparison of different technologies for the removal of RB-5 dye. Kusvuran et.al. investigated the mineralization of RB-5 dye by using the electro Fenton reaction by applying -0.55 V vs. SCE. At the operating conditions in the performed experiments of the above studies, the mineralization was only 40% with an oxidation pseudo rate constant of 0.019 min<sup>-1</sup> [66]. The Fenton process was studied for the removal of RB-5 dye, using FeSO<sub>4</sub> which showed the removal of 99 % colouration under optimum conditions in nearly 4 hours with rate constant of 0.0363 min<sup>-1</sup> [67]. Pseudo rate constant results of RB-5 dye removal found to be the fastest by using Ti felt / TiO<sub>2</sub> nanotubes /PbO<sub>2</sub> substrate in

about 60 min at constant potential 1.4 V vs. Hg/HgO. The calculated pseudo rate constant at this constant potential is  $0.0875 \text{ min}^{-1}$  which is higher if compared with those listed in table 3.2. The lowest pseudo rate constant was obtained using Ti felt which was about  $0.0012 \text{ min}^{-1}$ . This seems to be 10 times lower in comparison to the anodic oxidation of RB-5 dye by using Ti felt / TiO<sub>2</sub> nanotubes /PbO<sub>2</sub> substrate. Actually, •OH free radical produced for non-active electrode played a leading role for the oxidation of RB-5 dye. The pseudo rate constant for Ti felt / TiO<sub>2</sub> nanotubes was found to be  $0.0058 \text{ min}^{-1}$  quite lower as no electrochemical oxidation took place and which may be due to dye molecules adsorbed over the surface site of positively charged nanotubes [68].

### 3.3.7 Current efficiency and energy consumption for oxidation of Reactive Black-5

Total Organic Carbon (TOC) studies were carried out before and after the electrolysis of the solution containing RB-5 dye using calcined Ti felt / TiO<sub>2</sub> nanotubes /PbO<sub>2</sub>. This data was then used to calculate the current efficiency and power consumption.

The current efficiency (CE) values for the electrochemical process are calculated by using following relation [69];

$$CE = \frac{2.67[\text{TOC}_0 - \text{TOC}_f] FV}{8 \int_0^t I dt} \times 100 \quad (3.8)$$

Where 2.67 is the reported conversion factor of COD (Chemical Oxygen Demand) to TOC, (TOC<sub>0</sub>) and (TOC<sub>f</sub>) related to the TOC (g dm<sup>-3</sup>) values at initial and final time of electrolysis respectively, *F* is the Faraday constant (96,500 C mol<sup>-1</sup>), *V* is the volume of the solution (dm<sup>-3</sup>), 8 is the factor for oxygen equivalent mass (g eq<sup>-1</sup>),  $\int_0^t I dt$  the overall

charge passed during the electrochemical reaction and  $t$  is the overall time interval (s) of electrolysis process.

In this work, for 1h electrolysis operation, the TOC decrease from an initial value of 21.96 mg dm<sup>-3</sup> to 14.521 mg dm<sup>-3</sup> which was about 7.439 mg dm<sup>-3</sup> h with TOC removal efficiency of 33%. The current efficiency was calculated from equation 3.9 and found to be 10%. Steter et.al. studied the oxidation of amaranth dye and found that CE values decreased when they applied current density for the electrolysis process in the range of 10 to 50 mAcm<sup>-2</sup>. At the end of 90 min of electrolysis, the CE of 17 % was achieved at optimum conditions [69]. Lower CE values are attributed to the secondary reactions like oxygen evolution and intermediate species transformation during the oxidation of the organic dyes.

The proposed route is associated with the breaking of aromatic heterocyclic chain (azo bond) of reactive black 5 producing transitory intermediates. The intermediates further converted into benzene amino sulphonic acid in the presence of •OH radical by removing R = (CH<sub>2</sub>)<sub>2</sub>OSO<sub>3</sub>Na. The addition of •OH radical to amino benzene sulphonic acid results in the generation of phenol molecule by removing NH<sub>2</sub> group. Finally, reactive black 5 dye transformed into aliphatic acidic compounds, water and carbon dioxide as shown in figure 3.14.



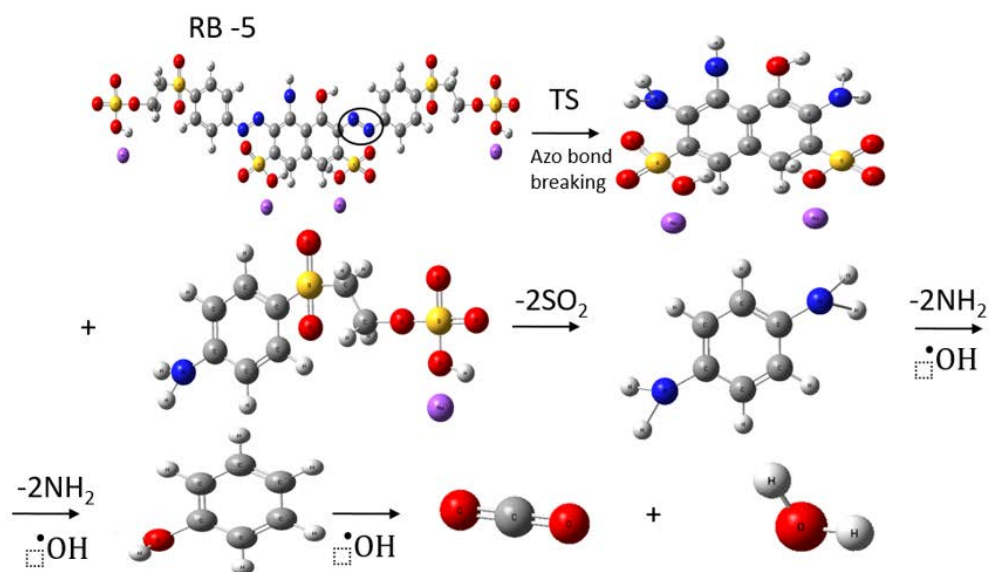








Figure 3.14 Degradation pathway for the oxidation RB-5 dye

where, Carbon  Sodium,  Hydrogen,  Nitrogen,  Sulphur,   
 Oxygen  [35].

The energy consumption,  $EC$ , ( $\text{kWh kg}^{-1}$ ) was calculated from following equation [70];

$$EC = \frac{E I_o \Delta t}{100 (\text{TOC}_0 - \text{TOC}_f) V} \quad (3.9)$$

where  $E$  (V) is the applied potential,  $I_o$  (A) is the current passed during electrochemical reaction,  $\Delta t$  (h) the electrolysis time,  $(\text{TOC}_0)$  and  $(\text{TOC}_f)$  related to the TOC ( $\text{kg dm}^{-3}$ ) values at initial and final time of electrolysis respectively and  $V$  ( $\text{dm}^3$ ) corresponds the electrolyte volume.

The energy consumption was calculated to be  $1149 \text{ kWh kg}^{-1}$  by using calcined Ti felt /  $\text{TiO}_2$  nanotubes /  $\text{PbO}_2$  for the oxidation of  $2 \times 10^{-5} \text{ mol dm}^{-3}$  of RB-5 dye. Current efficiency and energy consumption results obtained in this study are found to be comparable with the literature. Vasconcelos et.al. reported extremely higher energy consumption, using RVC electrode at a constant potential of  $-0.4 \text{ V vs. Ag/AgCl}$ . Under optimum conditions the reported EC was  $3471 \text{ kWh kg}^{-1}$  [70].

### **3.3.8 Photocatalytic oxidation of Reactive Black-5**

The Raman studies revealed anatase phase for calcined Ti felt/  $\text{TiO}_2$  nanotubes /  $\text{PbO}_2$  substrate ( $t_i = 15 \text{ min}$ ) (see figure 3.10). The activity of the anatase phase caused the photocatalytic behaviour of the coatings towards the photocatalytic oxidation of RB-5 dye in  $\text{Na}_2\text{SO}_4$  solution at pH 3.

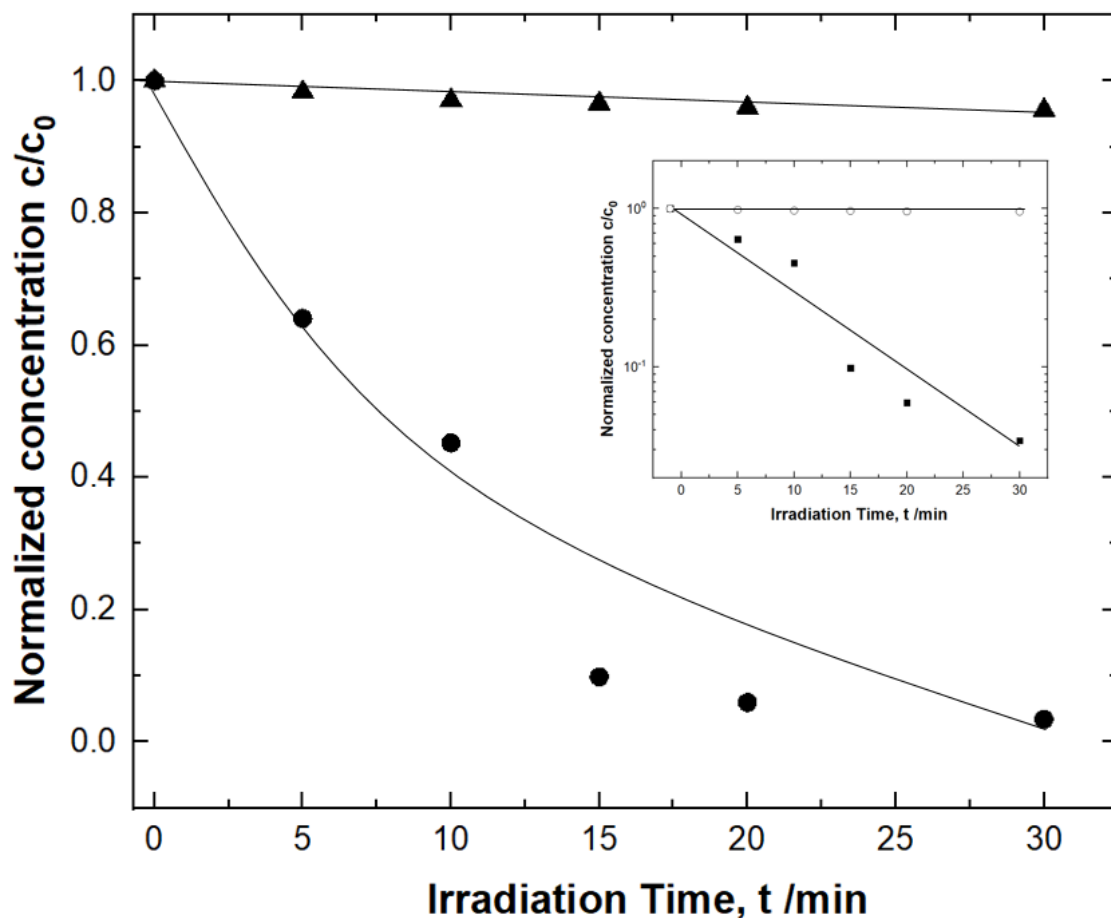


Figure 3.15 Photocatalytic oxidation of  $2 \times 10^{-5} \text{ mol dm}^{-3}$  RB-5 dye in  $0.5 \text{ mol dm}^{-3}$  of sodium sulfate by ●) calcined TiO<sub>2</sub> / TiO<sub>2</sub> nanotubes /PbO<sub>2</sub> ( $t_i = 15 \text{ min}$ ), ▲) uncalcined TiO<sub>2</sub> / TiO<sub>2</sub> nanotubes. Inset shows ■) oxidation kinetics by using calcined TiO<sub>2</sub> /nanotubes /PbO<sub>2</sub> ( $t_i = 15 \text{ min}$ ) ○) uncalcined TiO<sub>2</sub> / TiO<sub>2</sub> nanotubes (Experimental conditions: UV lamp intensity =  $1.5 \text{ mW cm}^{-2}$ , pH = 3.0, T = 25 °C).

Figure 3.15 shows decay of RB-5 dye due to the photocatalytic mechanism displayed by the coating under acidic environment at pH = 3 (by addition of H<sub>2</sub>SO<sub>4</sub>). The protonation of TiO<sub>2</sub> (anatase) on the coating [71, 72] due to the UV radiation creates holes and electrons over the surface [73, 74]; as shown in equation (3.10), the TiO<sub>2</sub> which was present over the coating reacts with H<sup>+</sup> ions to become positively charged, resulting in the

attraction of negatively charged RB-5 dye molecules, following discolouration of RB-5 dye [68]:



The illumination of the coating (anatase) in the solution of water with RB-5 dye produce electrons ( $e^-$ ) and holes ( $h^+$ ) in the conduction and valance bands of the coating respectively, as represented by equation (2.7). The oxidative nature of holes promote the direct or indirect oxidation of dye. The production of  $\bullet\text{OH}$  free radicals by the reaction between the water molecules and valance band holes as depicted in equation (2.8) leads to the oxidation of RB-5 dye. Similarly, oxidizing radicals  $\text{O}_2^{\bullet-}$  can be generated by the reaction between electron and electron acceptor like  $\text{O}_2$  [72, 73]. Overall, the photocatalytic activity is ultimately influenced by the holes and radicals produced over the anatase phase of the coating as represented in equation (2.9) to (2.13). The time dependent normalized concentration of RB-5 dye by using calcined Ti felt/ $\text{TiO}_2$  nanotubes / $\text{PbO}_2$  for photocatalytic oxidation (20 min) is shown in figure 3.15. The data shown in the inset of figure 3.15 indicates a pseudo-first order reaction kinetics for the discolouration of reactive black-5 dye on the calcined Ti felt/  $\text{TiO}_2$  nanotubes / $\text{PbO}_2$  coating according to equation 2.20.

A pseudo first order rate constant  $k$  for photochemical oxidation was found to be  $0.1244 \text{ min}^{-1}$ . Jafari et.al. studied the *Candida tropicalis* (JKS2) – $\text{TiO}_2$  as a photocatalyst for the treatment of RB-5 dye, the colour removal of 90% was achieved with oxidation pseudo rate constant of  $0.038 \text{ min}^{-1}$  [75]. The improved results by using calcined Ti felt/  $\text{TiO}_2$  nanotubes / $\text{PbO}_2$  coating could be due to heat treatment (calcination) of the coating which converts nanotubes to the individual crystal phase known as anatase which makes these

coatings photocatalytic active when exposed to UV irradiation which ultimately leads to the 97% colour removal of dye in 30 min. The pseudo first order rate constant was found to be  $0.1244 \text{ min}^{-1}$  which seems to be faster than the electrochemical oxidation of the dye. This behaviour is imparted with the generation of free electron hole pair which may directly attacks the dye or by indirectly producing hydroxyl radical to decompose the dye quicker than electrochemical oxidation. The photocatalytic behaviour of the calcined Ti felt/  $\text{TiO}_2$  nanotubes / $\text{PbO}_2$  ( $t_i = 15 \text{ min}$ ) is attributed to the photo-induced holes and indirect oxidation by the free radicals produced [73].

Method	Optimum conditions	$-k / \text{min}^{-1}$	Conversion / %	Time	Reference
Electro Fenton	$\text{Fe}(\text{NH}_4)(\text{SO}_4)_2 \cdot 6\text{H}_2\text{O}/\text{RB-5 dye}$ $= 3 \text{ mol}/\text{dm}^{-3}$ , pH = 3, Applied potential = $-0.55\text{V vs. SCE}$ , $30^\circ\text{C}$	0.019	40	30 min	[73]
Fenton	$100 \text{ mg dm}^{-3} \text{FeSO}_4$ , $400 \text{ mg dm}^{-3}$ $\text{H}_2\text{O}_2$ , $40^\circ\text{C}$ , pH = 3	0.0363	99	4 h	[74]
Photoassisted Fenton	5g/L iron oxide $\text{dm}^{-3} \text{FeSO}_4$ , $29.4 \times 10^{-3} \text{ mol dm}^{-3}$ $\text{H}_2\text{O}_2$ , pH = 7, UVA= 15W	0.0434	70	480 min	[76]
Anodic oxidation	Ti felt, $E = 1.4 \text{ V vs. Hg}/\text{HgO}$ pH = 3, T = $25^\circ\text{C}$	0.0012	7	60 mins	This study
Anodic oxidation	Ti felt / $\text{TiO}_2$ nanotubes, $E = 1.4 \text{ V}$ vs. $\text{Hg}/\text{HgO}$ , pH = 3, T = $25^\circ\text{C}$	0.0058	36	60 mins	This study
Anodic oxidation	Calcined Ti felt / $\text{TiO}_2$ nanotubes / $\text{PbO}_2$ ( $t_i = 12 \text{ h}$ ) $E = 1.4 \text{ V vs.}$ $\text{Hg}/\text{HgO}$ , pH = 3, T = $25^\circ\text{C}$	0.0875	99	60 mins	This study

Method	Optimum conditions	$-k / \text{min}^{-1}$	Conversion / %	Time	Reference
Photocatalysis	Calcined Ti felt / TiO <sub>2</sub> nanotubes /PbO <sub>2</sub> ( $t_i = 15$ min) pH = 3, T = 25 °C, UV intensity = 20 mW cm <sup>-2</sup>	0.1244	97	30 min	Photochemical rate in this study

Table 3.2 Comparison of different parameters including pseudo rate constant, % conversion and reaction time for oxidation of RB-5 dye by Ti felt, Ti felt / TiO<sub>2</sub> nanotubes and Calcined Ti felt / TiO<sub>2</sub> nanotubes /PbO<sub>2</sub> and other related values from selected literature.

### 3.4 Conclusions

In conclusion, TiO<sub>2</sub> nanotubes can be formed on the top surface of Ti felt with nanotubular arrangements using MSA (1 mol dm<sup>-3</sup>) containing ammonium fluoride about 1.0 wt-% by anodization. The nanotubes can be formed at an applied cell potential of 10 V for small nanotubes (diameter  $\approx$ 50 nm) and 20 V for large nanotubes (diameter  $\approx$ 100 nm). The PbO<sub>2</sub> can be deposited on the nanotubes by immersion of anodized Ti felt in a solution containing Pb(NO<sub>3</sub>)<sub>2</sub> and structure directing agent polyvinylpyrrolidone (PVP). The immersion time ( $t_i$ ) plays an important role for the deposition of PbO<sub>2</sub> over nanotubular structures further application of these coatings showed that Ti felt/ TiO<sub>2</sub> nanotubes /PbO<sub>2</sub> exhibits the electrochemical dye discolouration of about 99 % in 60 min at more positive potential (1.5 V vs. Hg/HgO). This electrochemical performance of coating is imparted with the presence of PbO<sub>2</sub>. Further the samples produced by 15 min immersion time of Ti felt/ TiO<sub>2</sub> nanotubes /PbO<sub>2</sub> and after calcination were effective for the photochemical discolouration of the RB-5 dye (97 %). This photochemical activity

may be imparted due to the generation of photo induced-holes, oxidative radicals evolved from reaction of electrons in conduction band and electron acceptors( $O_2^- \cdot$ ). The results revealed a favourable approach in decorating metal oxide structures on  $TiO_2$  nanotubes over bendable porous Ti-felt substrate, for utilization in environmental oxidation of wastewater.

### 3.5 References

- [1] M. Farhad, D. Changiz, Addition of  $IrO_2$  to  $RuO_2+TiO_2$  coated anodes and its effect on electrochemical performance of anodes in acid media. Progress in Natural Science: Materials International. 24 (2014) 134-141.
- [2] B.C.Lozano, C. Comninellis, A. Battisti, Electrochemical properties of Ti /  $SnO_2-Sb_2O_5$  electrodes prepared by the spray pyrolysis technique, J. Appl. Electrochem. 26 (1996) 683-688.
- [3] M.S.Neumann, Aspects of photocatalysis on semiconductors: photoelectrocatalysis, Chimia. 61 (2007) 806-809.
- [4] C.Lee, H.Choi, C. Lee, H.Kim, Photocatalytic properties of nano-structured  $TiO_2$  plasma sprayed coating, Surf. Coat. Technol. 173 (2003) 192-200.
- [5] B.Guo, Z.Liu, L.Hong, H.Jiang, Sol gel derived photocatalytic porous  $TiO_2$  thin films, Surf. Coat. Technol. 198 (2005) 24-29.
- [6] Y.Chen, E.Stathatos, D.D.Dionysiou, Microstructure characterization and photocatalytic activity of mesoporous  $TiO_2$  films with ultrafine anatase nanocrystallites, Surf. Coat. Technol. 202 (2008) 1944-1950.
- [7] I.D.Kim, A.Rothschild, D.J. Yang, H.L.Tuller, Macroporous  $TiO_2$  thin film gas sensors obtained using colloidal templates, Sens Actuators B Chem. 130 (2008) 9-13.

- [8] J.Y.Kim, S.H.Kim, H.H.Lee, K. Lee, W.Ma, X. Gong, A.J.Heeger, New Architecture for high-efficiency polymer photovoltaic cells using solution-based titanium oxide as an optical spacer, *Adv. Mater.* 18 (2006) 572-576.
- [9] A.Mills, G.Hill, S.Bhopal, I.P. Parkin, S.A.O'Neill, Thick titanium dioxide films for semiconductor photocatalysis, *J. Photochem. Photobiol. A.* 160 (2003) 185-194.
- [10] W.A.Gerrard, B.C.H Steele, Microstructural investigations on mixed RuO<sub>2</sub>-TiO<sub>2</sub> coatings, *J. Appl. Electrochem.* 8 (1978) 417-425.
- [11] Guo, Y. G., Hu, J. S., & Wan, L. J. Nanostructured materials for electrochemical energy conversion and storage devices. *Adv. Mater.* 20(2008) 2878-2887.
- [12] S.Z.Chu, K.Wada, S.Inoue, S.I.Hishita, K. Kurashima, Fabrication and Structural Characteristics of Ordered TiO<sub>2</sub>- Ru (- RuO<sub>2</sub>) Nanorods in Porous Anodic Alumina Films on ITO/Glass Substrate, *J. Phys. Chem. B.* 107 (2003) 10180-10184.
- [13] D. C de Moura, M. A Quiroz,., D. R da Silva,., R., Salazar, C.A. Martínez-Huitle, Electrochemical oxidation of Acid Blue 113 dye using TiO<sub>2</sub>-nanotubes decorated with PbO<sub>2</sub> as anode, *Environmental Nanotechnology, Monitoring & Management.* 5 (2016) 13-20.
- [14] M.Cerro-Lopez, Y. Meas-Vong, M.A.Méndez-Rojas, C.A.Martínez-Huitle, C.A., M.A.Quiroz, Formation and growth of PbO<sub>2</sub> inside TiO<sub>2</sub> nanotubes for environmental applications. *Appl. Catal. B: Environ.* 144 (2014) 174-181.
- [15] B.N.L. Biyoghe, M. P. Ibondou, X.Gu, M.Xu, S.Lu, Z.Qiu, S.M.Mbadinga, Efficiently Synthetic TiO<sub>2</sub> Nano-sheets for PCE, TCE, and TCA Oxidations in Aqueous Phase Under VUV Irradiation, *Water, Air, & Soil Pollution.* 225 (2014) 1951-1958.
- [16] H.An, H.Cui, W.Zhang, J. Zhai, Y.Qian, X. Xie, Q.Li, Fabrication and electrochemical treatment application of a microstructured TiO<sub>2</sub>-NTs/Sb-



SnO<sub>2</sub>/PbO<sub>2</sub> anode in the oxidation of C.I. Reactive Blue 194 (RB194). *Chem. Eng. J.* 209 (2012) 86–93.

- [17] M.Panizza, G.Cerisola, Direct and mediated anodic oxidation of organic pollutants, *Chem. Rev.* 109 (2009) 6541-6569.
- [18] H.S.Awad, N.A.Galwa, Electrochemical oxidation of Acid Blue and Basic Brown dyes on Pb/PbO<sub>2</sub> electrode in the presence of different conductive electrolyte and effect of various operating factors. *Chemosphere*, 61 (2005) 1327-1335.
- [19] M.A.Quiroz, S.Reyna, C.A.Martinez-Huitle, S.Ferro, A.De Battisti, Electrocatalytic oxidation of p-nitrophenol from aqueous solutions at Pb/PbO<sub>2</sub> anodes, *Appl. Catal. B.* 59 (2005) 259-266.
- [20] H.Karami, A.Yaghoobi, A.Ramazani, Sodium sulfate effects on the electrochemical behaviors of nanostructured lead dioxide and commercial positive plates of lead-acid batteries, *Int. J. Electrochem. Sci.* 5 (2010) 1046-1059.
- [21] C.A.Martínez-Huitle, A.De Battisti, S.Ferro, S.Reyna, M.Cerro-López, M.A Quiro,(2008). Removal of the pesticide methamidophos from aqueous solutions by electrooxidation using Pb/PbO<sub>2</sub>, Ti/SnO<sub>2</sub>, and Si/BDD electrodes, *Environ. Sci Technol.* 42 (2008) 6929-6935.
- [22] J.González-García, J Iniesta, E.Expósito, V. García-García, V.Montiel, A.Aldaz, Early stages of lead dioxide electrodeposition on rough titanium, *Thin solid films.* 352 (1999) 49-56.
- [23] C.Comninellis, Electrocatalysis in the electrochemical conversion/combustion of organic pollutants for waste water treatment, *Electrochim. Acta.* 39 (1994) 1857-1862.
- [24] D.Devilliers, E.Mahé, Modified titanium electrodes: Application to Ti/TiO<sub>2</sub>/PbO<sub>2</sub> dimensionally stable anodes, *Electrochim. Acta.* 55 (2010) 8207-8214.

- [25] J.Li, L. Zheng, L.Li, G. Shi, Y. Xian, L.Jin, (2006). Photoelectro-Synergistic Catalysis at Ti/TiO<sub>2</sub>/PbO<sub>2</sub> Electrode and Its Application on Determination of Chemical Oxygen Demand. *Electroanalysis*. 18 (2006) 2251-2256.
- [26] L. Vidal, C.E. Domini, A. Canals, Main parameters and assays involved with the organic pollution of water. *Handbook of Water Analysis*, 459 (2013) 472-477.
- [27] L.V.Taveira, J.M. Macak, H. Tsuchiya, L.F.P.Dick, P.Schmuki, Initiation and growth of self-organized TiO<sub>2</sub> nanotubes anodically formed in NH<sub>4</sub>F/(NH<sub>4</sub>)<sub>2</sub>SO<sub>4</sub> electrolytes, *J. Electrochem. Soc.* 152 (2005), B405-B410.
- [28] J.M.Macak, P.J. Barczuk, H.Tsuchiya, M.Z.Nowakowska, A.Ghicov, M.Chojak, P.Schmuki, Self-organized nanotubular TiO<sub>2</sub> matrix as support for dispersed Pt/Ru nanoparticles: enhancement of the electrocatalytic oxidation of methanol. *Electrochem. Comm.* 7 (2005) 1417-1422.
- [29] R.Polumi, S.Berger, P.Schmuki, TiO<sub>2</sub> nanotubes: synthesis and applications. *Ang.Chemie. Int. Ed.* 50 (2011) 2904-2939.
- [30] H. F. Zhuang, C.J.Lin, Y. K Lai, L.Sun, J. Li, Some critical structure factors of titanium oxide nanotube array in its photocatalytic activity, *Environ. Sci. Technol* 41 (2007) 4735-4740.
- [31] H.Yaghoubi, N.Taghavinia, E. K. Alamdari, Self cleaning TiO<sub>2</sub> coating on polycarbonate: surface treatment, photocatalytic and nanomechanical properties. *Surf. Coat. Technol.* 204 (2010) 1562-1568.
- [32] G. Zhao, Y. Zhang, Y.Lei, B.Lv, J.Gao, Y.Zhang, D.Li, Fabrication and electrochemical treatment application of a novel lead dioxide anode with superhydrophobic surfaces, high oxygen evolution potential, and oxidation capability, *Environ. Sci. Technol.* 44 (2010) 1754-1759.
- [33] J.P.Carr, N.A.Hampson, The lead dioxide electrode, *Chem. Rev.* 72 (1972) 679-702.

- [34] U.B.Thomas, The Electrical Conductivity of Lead Dioxide, *Journal of The Electrochemical Society*. 94 (1948) 42-49.
- [35] M.J. Frisch, G.W. Trucks, H.B. Schlegel, G.E. Scuseria, M.A. Robb, J.R. Cheeseman, G. Scalmani, V. Barone, B. Mennucci, G.A. Petersson, H. Nakatsuji, *Gaussian 09*, p. 6492. Gaussian, Inc., Wallingford (2009).
- [36] S. Ghasemi, H. Karami, H. Khanezar, Hydrothermal synthesis of lead dioxide/multiwall carbon nanotube nanocomposite and its application in removal of some organic water pollutants. *Journal of Materials Science* 49 (2014) 1014-1024.
- [37] Bavykin, D. V., & Walsh, F. C.. Titanate and titania nanotubes: synthesis, properties and applications, (RSC Nanoscience and Nanotechnology) Royal Society of Chemistry, Cambridge (2010).
- [38] C.T.J. Low, F.C. Walsh, The stability of an acidic tin methanesulfonate electrolyte in the presence of a hydroquinone antioxidant, *Electrochim. Acta*. 53 (2008) 5280-5286.
- [39] G.K. Mor, O.K. Varghese, M. Paulose, N. Mukherjee, C.A. Grimes, Fabrication of tapered, conical-shaped titania nanotubes. *J Mater Res*, 18 (2003) 2588-2593.
- [40] J. M. Macak, H. Tsuchiya, A. Ghicov, K. Yasuda, R. Hahn, S. Bauer, P. Schmuki, TiO<sub>2</sub> nanotubes: self-organized electrochemical formation, properties and applications, *Curr. Opin. Solid State Mater Sci*. 11 (2007) 3-18.
- [41] L. Burgio, J.H.C. Robin, F. Steven, Raman spectroscopy as a means for the identification of plattnerite (PbO<sub>2</sub>), of lead pigments and of their oxidation products, *Analyst*. 126 (2001) 222-227.
- [42] J. Kunze, A. Seyeux, P. Schmuki (2008). Anodic TiO<sub>2</sub> layer conversion: fluoride-Induced rutile formation at room temperature, *Electrochem. Solid-State Lett*. 11 (2008) K11-K13.
- [43] K. Yasuda, J. M. Macak, S. Berger, A. Ghicov, P. Schmuki, Mechanistic aspects of the self-organization process for oxide nanotube formation on valve metals, *J. Electrochem. Soc* 154 (2007) C472-C478.
- [44] J.M. Kesselman, O. Weres, N.S. Lewis, M.R. Hoffmann Electrochemical production of hydroxyl radical at polycrystalline Nb-doped TiO<sub>2</sub> electrodes and

estimation of the partitioning between hydroxyl radical and direct hole oxidation pathways, *J. Phys. Chem. B.* 101 (1997) 2637.

- [45] X.Xiao, R.Liu, Synthesis and bioactivity of highly ordered TiO<sub>2</sub> nanotube arrays, *Appl. Surf. Sci.* 255 (2008) 365-367.
- [46] K.Lee, D. Kim, P. Roy, I.Paramasivam, B.I.Birajdar, E. Spiecker, P. Schmuki, Anodic formation of thick anatase TiO<sub>2</sub> meso sponge layers for high-efficiency photocatalysis, *J. Am. Chem. Soc.* 132 (2010) 1478-1479.
- [47] A.Ghicov, B.Schmidt, J.Kunze, P.Schmuki, Photoresponse in the visible range from Cr doped TiO<sub>2</sub> nanotubes. *Chem. Phys. Lett.* 433 (2007) 323-326.
- [48] L. Sun, S. Zhang, X. W. Sun and X. He, Effect of electric field strength on the length of anodized titania nanotube arrays, *J. Electroanal. Chem.* 637 (2009) 6-12.
- [49] G. K. Mor, O. K. Varghese, M. Paulose, K. Shankar and C.A. Grimes. A review on highly ordered, vertically oriented TiO<sub>2</sub> nanotube arrays: fabrication, material properties, and solar energy applications. *Sol. Energ. Mat. Sol. Cells*, 90 (2006) 2011-2075.
- [50] M. Bonato, K.V. Ragnarsdottir, G.C. Allen, Removal of uranium (VI), lead (II) at the surface of TiO<sub>2</sub> nanotubes studied by X-ray photoelectron spectroscopy, *Water Air Soil Pollut.* 223 (2012) 3845–3857.
- [51] X. Zhao, Q. Jia, N. Song, W. Zhou, Y. Li, Adsorption of Pb (II) from an aqueous solution by titanium dioxide/carbon nanotube nanocomposites: kinetics, thermodynamics, and isotherms, *J. Chem. Eng. Data* 55 (2010) 4428–4433.
- [52] A. El Goresy, M. Chen, P. Gillet, L. Dubrovinsky, G. Graup, R. Ahuja, R., 2001. A natural shock-induced dense polymorph of rutile with  $\alpha$ -PbO<sub>2</sub> structure in the

- suevite from the Ries crater in Germany. *Earth and Planetary Science Letters*, 192 (2001) 485-495.
- [53] S.J. Kim, Y.U. Yun, H.J. Oh, S.H. Hong, C.A. Roberts, K. Routray, I.E. Wachs, Characterization of hydrothermally prepared titanate nanotube powders by ambient and in situ raman spectroscopy, *J. Phys. Chem Lett.* 1 (2010) 130-135.
- [54] J.M. Kesselman, O. Weres, N.S. Lewis, M.R. Hoffmann Electrochemical production of hydroxyl radical at polycrystalline Nb-doped TiO<sub>2</sub> electrodes and estimation of the partitioning between hydroxyl radical and direct hole oxidation pathways, *J. Phys. Chem. B.* 101 (1997) 2637-2641.
- [55] F.J. Recio, P. Herrasti, I. Sirés, A.N Kulak, D.V Bavykin, C. Ponce-de-León, F.C Walsh, The preparation of PbO<sub>2</sub> coatings on reticulated vitreous carbon for the electro-oxidation of organic pollutants, *Electrochim. Acta.* 56 (2011) 5158-5156
- [56] C. A. Martínez-Huitle, C. A. Martínez-Huitle, E. Brillas, Decontamination of wastewaters containing synthetic organic dyes by electrochemical methods: A general review, *Appl. Catal.B.* 87 (2009) 105-145.
- [57] I. Sirés, E. Brillas, M.A. Oturan, M.A. Rodrigo, M. Panizza, Electrochemical advanced oxidation processes: today and tomorrow. A review, *Environ. Sci.Pollut. Res.* 21 (2014) 8336–8367.
- [58] M. Panizza, G. Cerisola, Electrocatalytic materials for the electrochemical oxidation of synthetic dyes, *Appl. Catal. B: Environ.* 75 (2007) 95–101.
- [59] A.J.D. Santos, D.K.D.S. Xavier, D.R.D. Silva, M.A. Quiroz, C.A. Martínez-Huitle, Use of combined electrochemical approaches for mineralization and detection of hydroquinone using PbO<sub>2</sub> Electrodes, *J. Mex. Chem. Soc.* 58 (2014) 356-361.

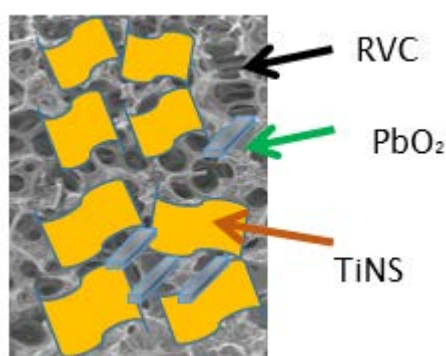
- [60] C. A. Martínez-Huitle, S. Ferro, Electrochemical oxidation of organic pollutants for the wastewater treatment: direct and indirect processes, *Chem.Soc. Rev.* 35 (2006) 1324–1340.
- [61] S.G. Segura, E.V.D. Santos, C.A. Martínez-Huitle, Role of  $sp_3/sp_2$  ratio on the electrocatalytic properties of boron-doped diamond electrodes: amini review, *Electrochem. Commun.* 59 (2015) 52–55.
- [62] A.M.S. Solano, J.H.B. Rocha, N.S. Fernandes, D.R. Silva, C.A. Martínez-Huitle, Direct and indirect electrochemical oxidation process for decolourisation treatment of synthetic wastewaters containing dye, *Oxid.Commun.* 34 (2011) 218–229.
- [63] Z. He, C. Huang, Q. Wang, Z. Jiang, J. Chen, S. Song, Preparation of a praseodymium modified Ti/SnO<sub>2</sub>-Sb/PbO<sub>2</sub> electrode and its application in the anodic oxidation of the azo dye acid black 194, *Int. J. Electrochem. Sci.* 6 (2011) 4341–4354.
- [64] G.R. Oliveira, N.S. Fernandes, J.V. Melo, D.R. Silva, C. Urgeghe, C.A. Martínez-Huitle, Electrocatalytic properties of Ti-supported Pt for decolourizing and removing dye from synthetic textile wastewaters, *Chem. Eng. J.* 168 (2011) 208–214.
- [65] E. Brillas, C.A. Martínez-Huitle, Decontamination of wastewaters containing synthetic organic dyes by electrochemical methods. An updated review. *Appl.Catal. B*, 167 (2015) 603–643.
- [66] E. Kusvuran, S. Irmak, H.I. Yavuz, A. Samil, O. Erbatur, Comparison of the treatment methods efficiency for decolourisation and mineralization of reactive black 5 azo dye, *J. Hazard. Mater. B* 119 (2005) 109–116.
- [67] S. Meriç, D. Kaptan, T. Ölmez, Colour and COD removal from wastewater containing reactive black 5 using Fenton's oxidation process, *Chemosphere* 54 (2004) 435–441.

- [68] Y. Shen, W. Wang, K. Xiao, Synthesis of three-dimensional carbon felt supported TiO<sub>2</sub> monoliths for photocatalytic oxidation of methyl orange, *J Environ. Chem. Eng.* 4 (2016) 1259-1266.
- [69] J.R. Steter, W.R. Barros, M.R. Lanza, A.J. Motheo, Electrochemical and sonoelectrochemical processes applied to amaranth dye oxidation, *Chemosphere.* 117(2014) 200-207.
- [70] V.M. Vasconcelos, C. Ponce-de-León, J.L. Nava, M.R. Lanza, Electrochemical oxidation of RB-5 dye by anodic oxidation, electro-Fenton and by combining anodic oxidation–electro-Fenton in a filter-press flow cell, *J Electroanal Chem.* 765 (2016) 179-187.
- [71] C.J. Lin, Y. Zhang, L. Wang, Y. Zhang, D. Wang, M. Yang, C. Li, Fabrication of open-ended high aspect-ratio anodic TiO<sub>2</sub> nanotube films for photocatalytic and photoelectrocatalytic applications, *Chem. Commun.* 45 (2008) 6031-6033.
- [72] Y. Jiang, W.N. Wang, P. Biswas, J.D. Fortner, Facile aerosol synthesis and characterization of ternary crumpled graphene - TiO<sub>2</sub> - magnetite nanocomposites for advanced water treatment, *ACS Appl. Mater. Interfaces* 6 (2014) 11766–11774.
- [73] I. Ilisz, Z. Laszlo, A. Dombi, Investigation of the photodecomposition of phenol in near-UV-irradiated aqueous TiO<sub>2</sub> suspensions. I: effect of charge-trapping species on the oxidation kinetics, *Appl. Catal. A* 180 (1999) 25–33.
- [74] S. Doni, M. Handajani, E. Kardena, S. Notodarmojo, Photocatalytic oxidation of textile wastewater containing reactive black 5 azo dye by using immobilized TiO<sub>2</sub> nanofiber-nanoparticle composite catalyst on glass plates. *Journal of JSCE*, 1 (2014) 69-76.
- [75] N. Jafari, R.K. Kermanshahi, M.R. Soudi, S.R. Mahvi, S. Gharavi, Oxidation of a textile reactive azo dye by a combined biological-photocatalytic process: *Candida tropicalis* Jks2-TiO<sub>2</sub>/UV. *Iran. J. Environ. Health Sci. Eng.* 9 (2012) 1-7.

- [76] C.L. Hsueh, Y.H. Huang, C.C.Wang, C.Y.Chen, Photoassisted fenton oxidation of nonbiodegradable azo-dye (Reactive Black 5) over a novel supported iron oxide catalyst at neutral pH, *J. Mol. Catal. A* 245 (2005) 78–86.



## Chapter 4: Decolourisation of Reactive Black-5 at an RVC substrate decorated with PbO<sub>2</sub>/ TiO<sub>2</sub> nanosheets prepared by anodic electrodeposition



In this chapter reticulated vitreous carbon (RVC) surfaces were deposited with a composite consisted of PbO<sub>2</sub> and TiNS, using TiNS/PbO<sub>2</sub>/RVC anodic electrophoretic deposition. The structure and morphological properties of the composite were analysed by FESEM and Raman spectroscopy. The composite coating having an anatase structural phase and revealed a well-defined, microporous structure with hydrophilic nature along the length and thickness of the RVC strands. Electrochemical and photocatalytic behaviour of the composite improved organic RB-5 dye oxidation as a pollutant in wastewater. The electrochemical decolourisation associated with the synthesis of hydroxyl free radicals at the TiNS/PbO<sub>2</sub>/RVC composite however, photocatalytic decolourisation was driven by the synergetic photocatalytic effect imparted by the photoinduced holes and the free electron acceptors. The photocatalytic properties of the TiNS/PbO<sub>2</sub> coating were achieved by calcination at 450 °C for 60 min in air which

converted the titanate phase to anatase and modified its surface area. This enabled 98 % decolourisation of the RB-5 dye solution (measured by visible absorption at 597 nm) in a time of 60 min.

#### **4.1 Introduction**

The anodic oxidation of organic compounds contained in wastewater has attracted great interest due to its ability to purify and clean effluents in a rapid and controlled manner. The methodology has demonstrated high efficiency, especially in research works for pollutant decolourisation and chemical oxygen demand (COD) that utilize boron doped diamond (BDD) electrodes in filter press flow cells [1, 2]. In many cases, however, the application of BDD is limited to laboratory scale since BDD electrodes are expensive and considerable effort is required to set up a treatment plant. Therefore, there is a need to develop cost effective coatings, which operate in a similar fashion to BDD, and remain stable in a filter press flow cell during the mineralization, decolourisation and removal of organic compounds. Over the last decade, TiO<sub>2</sub> based materials and coatings have been adopted as photocatalytic materials with the aid of ultraviolet (UV) light to degrade organic compounds. The increasing interest in electrochemical methods [2] such as electro-Fenton [3], anodic oxidation [4], electrocoagulation [5], solar photoelectro-Fenton [6] and photoassisted electrochemical methods [2] have attracted the attention of researchers in the field of water treatment as efficient, cost effective and environmental friendly technologies.

Anodic oxidation has been reported to be effective for partial and complete mineralization with colour removal of organic compounds by using mixed metal oxides

of Ru, Ti, Sb, Sn or Ir and PbO<sub>2</sub> [7]. Anodic oxidation is widely employed and recognized as much easier in comparison to other electrochemical technologies such as electrochemical reduction (e.g. direct electrochemical reduction of Amaranth azo dye) [2]. Anodic oxidation produces physisorbed hydroxyl radicals ( $\bullet\text{OH}$ ) that discharge over the anode surface (M) during the electrolysis of water as depicted in equation 2.1. The species M ( $\bullet\text{OH}$ ) react with organic material until mineralization and produce low molecular weight organic compounds [4]. Metal oxide electrodes material play an important role during the anodic oxidation reaction since both chemical reactivity and ability to electrogenerate M ( $\bullet\text{OH}$ ) are related to the characteristics of the electrode. Different anode materials have been investigated to observe the stability and efficiency in batch as well as flow studies [8, 9, 10, 11]. The anode materials should be selected on their high over potential for the oxygen evolution reaction (OER) as well as for their large surface area. On BDD electrodes for example, (OER) occurs at *ca.* + 2.3 V *vs.* SCE and it is more suitable for the production of M( $\bullet\text{OH}$ ) species than other materials [12, 13, 14].

Titanate nanotubes coating have recently emerged as an attractive alternative for wastewater oxidation due to their stability at high temperature, ease of preparation, low price and relatively high oxygen evolution potential of 1.8 V *vs.* SCE in 0.1 M Na<sub>2</sub>SO<sub>4</sub> solution. For example, titanate nanotubes/Sb-doped SnO<sub>2</sub> electrodes showed complete mineralization and decolourisation during the anodic oxidation of benzoic acid at 20 mA cm<sup>-2</sup> [15]. Other nanomaterials such as nano PbO<sub>2</sub>/TiO<sub>2</sub> and TiO<sub>2</sub> nanosheets have been used for decolourisation and demineralization of methyl orange and chloroethene [16, 17]. Recent research has shown that the preparation of PbO<sub>2</sub> anodes decorated with TiO<sub>2</sub> nanotubes was found effective for the complete mineralization and decolourisation of reactive blue-194 at a current density of 150 mA cm<sup>-2</sup> [18]. A modified Ti/SnO<sub>2</sub>-

Sb/PbO<sub>2</sub> electrode has also been utilized for the removal of the azo dye acid black-194 at a current density of 30 mA cm<sup>-2</sup> [19].

Other approaches, proposed to replace expensive metals, such as platinum [20], involve the formation of PbO<sub>2</sub> inside the TiO<sub>2</sub> nanotubes formed on a titanium substrate [21], which show high catalytic activity and large surface areas for electrooxidation. PbO<sub>2</sub> acts as a conductive bridge during the anodic oxidation [22] demonstrating their suitability as electrodes for wastewater treatment [23, 24].

PbO<sub>2</sub> coatings on RVC or a carbon-polymer substrate obtained by electrodeposition in methanesulfonic acid electrolytes have been found effective for electrochemical water treatment [25]. The inclusion of titanate nanotube (TiNT) films has been claimed to be 100 % efficient for the mineralization and removal of benzoic acid from wastewater [15]. The anatase phase of titanate nanotubes (TiNT) provides active surface area of 20 m<sup>2</sup> g<sup>-1</sup>, larger than the traditional Degussa P25 TiO<sub>2</sub> particles that have a 7 m<sup>2</sup> g<sup>-1</sup> surface area and are 20 % more efficient for the photo decolourisation of rhodamine-B dye [26]. The potential advantage of using a substrate with defined regular structure such as RVC provides efficient mass transport of the effluent over the surface, which ultimately provide efficient oxidation [27]. RVC possesses a honeycomb structure [28] and has been employed for the electro Fenton oxidation of azo dyes [1].

Polypyrrole/anthraquinone disulphonate composite film modified graphite cathodes were used for the oxidation of azo dyes and achieved up to 80 % mineralization by electroFenton [29]. RVC was also employed to produce hydrogen peroxide to form the Fenton reagent and oxidase formic acid [30] and for removing metal ions [31, 32]. RVC substrate coated with TiNT produced inexpensive novel electrodes for advanced

processes, such as anodic oxidation and photocatalytic oxidation. In another example, TiO<sub>2</sub> nanotubular arrays and titanium based electrodes have showed considerable electrocatalytic behaviour of organic compounds like ascorbic acid, glucose, dopamine and alcohols [33, 34]. The use of lower cost carbonaceous alternatives, such as carbon foam PbO<sub>2</sub> composite coatings with titanate nanotubes, is worth study due to their morphology and porosity, which increase the stability of TiNT during anodic oxidation [35].

The inclusion of photocatalytically active titanium dioxide produces electron-hole pairs, as depicted in reaction (2.7), under UV light. The adsorbed photons over the titanium dioxide nanoparticulate photocatalyst are initiated at an energy greater than 3.2 eV, which corresponds to the energy necessary to excite an electron from the valance to the conductive band with the formation of positive hole at the valance band [36]. This creates electron-hole pairs, and the active electrons can form superoxide ions ( $O_2^- \bullet$ ) and peroxide radicals by reacting with O<sub>2</sub> as shown in reactions (2.10) and (2.11) [37] [38]. Similarly, reaction (2.12) involves production of hydrogen peroxide while reactions (2.13) represent the formation of  $\bullet$ OH radicals. The oxidation of a water molecule forms the short lived and powerful oxidant  $\bullet$ OH radical (redox potential = 2.7 V vs. SCE) [40]. This oxidant is capable of decolourisation and mineralizing organic matter residue to lower molecular weight compounds and ultimately to carbon dioxide and water [41].

The aim of this study is to investigate the electrochemical and photochemical performance of TiNS/PbO<sub>2</sub> coating on RVC for the decolouration of reactive black-5 (RB-5) dye and characterize the structural and morphological properties of the coatings.

The decolouration of this dye is important due to its widely commercial usage in the leather, wool, polymer, rubber and silk industries.

## 4.2 Experimental Details

Reagent grade 50 % Pb (II) methanesulfonate ( $\text{Pb}(\text{CH}_3\text{SO}_3)_2$ ), 70 % Methanesulfonic acid (MSA), tetrabutylammonium hydroxide (TBAOH), cesium carbonate ( $\text{Cs}_2\text{CO}_3$ ), Degussa  $\text{TiO}_2$  (P25), and reactive black-5 (RB-5) dye were purchased from Sigma Aldrich, while hydrochloric acid, sulphuric acid, sodium hydroxide, sodium sulphate and acetone obtained from Fischer scientific and used as received.

### 4.2.1 Synthesis of titanate nanosheets

A single-layer of titanate nanosheets (TiNS) was developed using an adapted methodology from Sasaki *et.al* [42]. TiNS were prepared by the solid reaction between the  $\text{Cs}_2\text{CO}_3$  and P25 at molar ratio 1:5.3 and 800 °C for 90 min. Once cool down the resultant mixture was crush into finely grounded powder using an Agate hand mortar. The powder was reheated at 800 °C for two cycles of 20 hrs each, after each interval of high temperature treatment the resulting mixture was cooled overnight and ground to fine powder. The resulting white powder was lepidocrocite-like cesium titanate,  $\text{Cs}_{0.7}\text{Ti}_{1.82}\square_{0.175}\text{O}_4$  where  $\square$  represents a vacancy [43].

Ion exchange method was used to produce smectite-like acid titanate from a mixture that contained 2 g of lepidocrocite-like cesium titanate and 80  $\text{cm}^3$  of 1  $\text{mol dm}^{-3}$  HCl. The solution was stirred with a magnetic follower over 4 days at 700 rpm. The solution was replaced with a fresh acid solution every day to maintain the amount of  $\text{H}^+$  ions at 1  $\text{mol dm}^{-3}$  for acid leaching of  $\text{Cs}^+$  ions. The remaining solution was vacuum filtered by

employing a nylon membrane and ultimately cleaned with distilled water until the conductivity reached around  $10 \mu\text{S cm}^{-1}$ . The resulting smectite-like acid titanate was recovered and used to produce exfoliated single layer titanate nanosheets. This was achieved by stirring 0.4 g of smectite-like acid titanate with  $100 \text{ cm}^3$  of aqueous solution of  $0.0165 \text{ mol dm}^{-3}$  tetrabutylammonium hydroxide (TBAOH) at 200 rpm at room temperature ( $25 \text{ }^\circ\text{C}$ ) for 2 weeks. This process replaced the protons ( $\text{H}^+$ ) present in the titanate nanosheets with bulky molecule ( $\text{TBA}^+$ ) ions. The exfoliated nanosheets were obtained as a suspension in an aqueous solution [44].

#### **4.2.2 Electrodeposition of $\text{PbO}_2$ on RVC**

A piece of RVC substrate from ERG materials of 100 pores per linear inch (ppi, porosity grade of RVC) of  $2 \text{ cm} \times 2 \text{ cm} \times 0.15 \text{ cm}$  dimensions was treated with 70 % nitric acid (Fisher scientific) at  $110 \text{ }^\circ\text{C}$  for 1 hour and thoroughly rinsed and left in deionized water overnight, then dried at  $90 \text{ }^\circ\text{C}$  overnight. A Cu wire was glued with Leit-C, Agar scientific to the RVC to provide electrical connection. The RVC electrode was placed in an undivided electrochemical glass cell fitted with a water jacket connected to a water thermostat, Grant LT D6G model (Figure 4.1) and was surrounded by a cylindrical mesh of stainless steel to provide uniform potential distribution. The cell was filled with an electrolyte solution containing  $1 \text{ mol dm}^{-3}$   $\text{Pb}(\text{CH}_3\text{SO}_3)_2$  and  $0.2 \text{ mol dm}^{-3}$  MSA  $100 \text{ cm}^3$  in aqueous solution. The electrodeposition of  $\text{PbO}_2$  on the RVC anode was carried out at 2.5 A at  $60 \text{ }^\circ\text{C}$  for 30 min with a constant stirring of electrolyte at 700 rpm with a 0.25 cm long PTFE-coated magnetic stirrer [44][ 45].

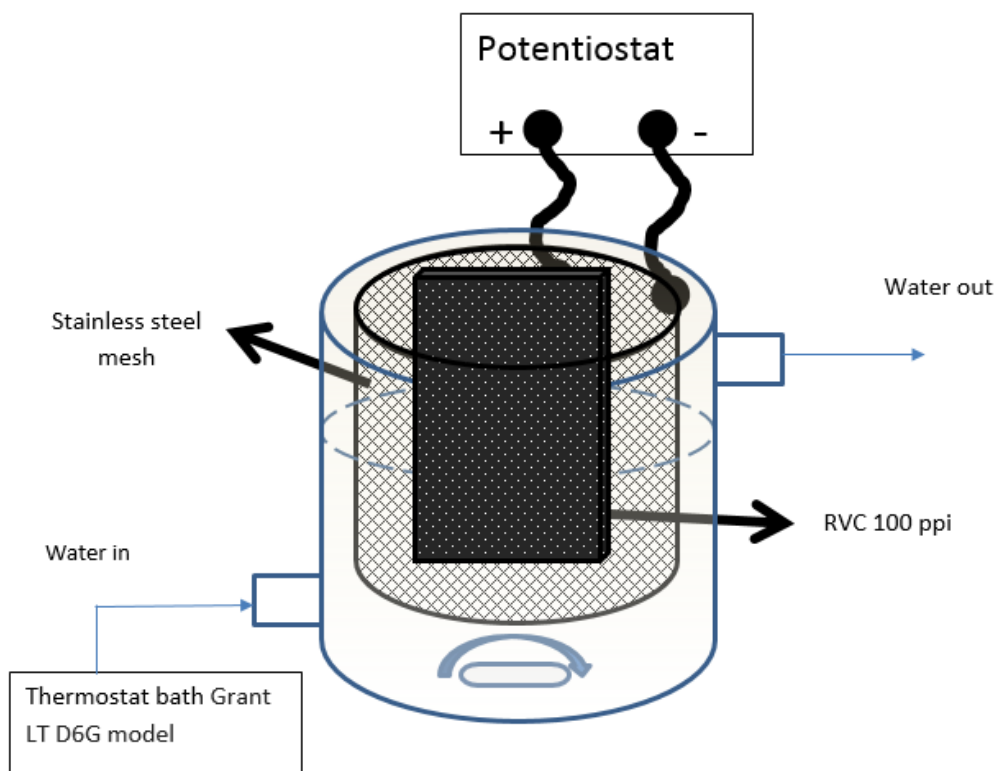


Figure 4.1 Schematic view for electroplating of  $\text{PbO}_2$ , solution containing  $1 \text{ mol dm}^{-3}$   $\text{Pb}(\text{CH}_3\text{SO}_3)_2$  and  $0.2 \text{ mol dm}^{-3}$  MSA at  $2.5 \text{ A}$  and  $60^\circ\text{C}$  for  $30 \text{ min}$  in a small undivided glass cell containing  $100 \text{ cm}^3$  of electrolyte.

### 4.2.3 Anodic electrophoretic Deposition

The RVC substrate coated with  $\text{PbO}_2$  was used as an anode for the electrophoretic deposition of TiNS from a solution containing exfoliated TiNS ( $0.4\text{g}$ ) with TBAOH. The cathode was graphite plate of  $1.5 \text{ cm} \times 6 \text{ cm} \times 1.2 \text{ cm}$  dimensions in a parallel plate configuration with an inter electrode gap,  $d$ , of  $1 \text{ cm}$ . A cell potential difference of  $15 \text{ V}$



was applied between the electrodes which created a potential gradient of  $15 \text{ V cm}^{-1}$  (the current was noted in the range of  $(0.002\text{-}0.003\text{A})$ ) by using 300 W Aim-TTi model EX752M power supply for a 10 min. The electrolyte ( $100 \text{ cm}^3$  aqueous solution containing exfoliated TiNS ( $0.4\text{g}$ ) with TBAOH ( $0.0165 \text{ mol dm}^3$ )) was vigorously stirred at 700 rpm with a magnetic stirrer as shown in figure 4.2.

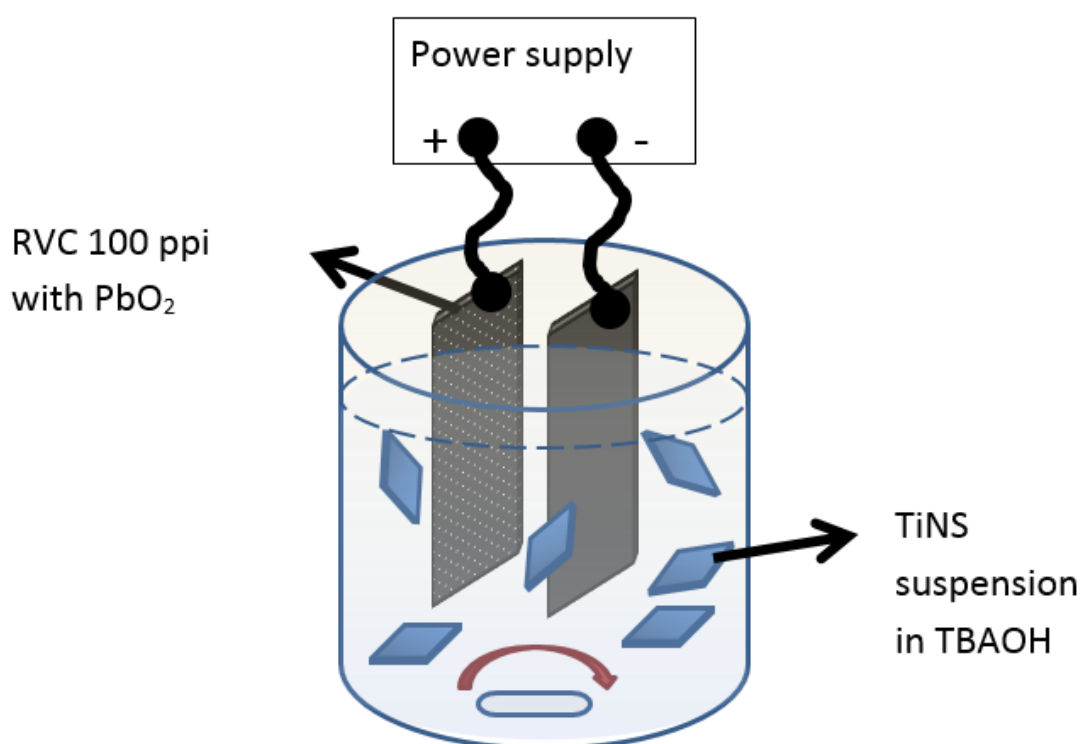


Figure 4.2 Schematic view for deposition of TiNS, suspension containing  $100 \text{ cm}^3$  of TiNS exfoliated with tetrabutylammonium hydroxide (TBAOH) for 15min of electrophoretic deposition.

#### 4.2.4 Heat treatment

The TiNS/PbO<sub>2</sub>/RVC samples obtained from electrophoretic deposition were calcined at  $450 \text{ }^\circ\text{C}$  for 1 hour. The sections of RVC that were not coated with TiNS/PbO<sub>2</sub> film due to

the fact that they were outside the electrolyte, disintegrated at such a high temperature whereas those coated with the film resisted the calcination process. The TiNS film calcined after the heat treatment exhibited uniform coating over the RVC substrate.

#### **4.2.5 Characterisation of the coated substrate**

The surface morphology of the TiNS/PbO<sub>2</sub>/RVC samples were characterized by field emission scanning electron microscope (FESEM), using a JEOL 6500F at an accelerating voltage of 20 kV. Raman spectra were obtained using a confocal microscope (Renishaw, RM 2000) fitted with a light source of 632.8 nm wavelength to measure the peaks for the presence of deposited species. The exposure time was 30 seconds with a 10 % intensity of laser radiation.

#### **4.2.6 Electrochemical Experiments**

The electrochemical experiments were performed by means of a computer aided PGSTAT302 N potentiostat/galvanostat from Autolab (EcoChemie, Netherlands) by using Nova 1.11 software. The obtained coatings including calcined TiNS/PbO<sub>2</sub>/RVC, PbO<sub>2</sub>/RVC and acid treated RVC were washed with ultra-pure water and dried. Each electrode was used to electrolyze a solution of 100 cm<sup>3</sup> containing  $1 \times 10^{-5}$  mol dm<sup>-3</sup> of RB-5 dye in 0.5 mol dm<sup>-3</sup> of sodium sulphate at pH = 3 and 25 °C at 2 mA cm<sup>-2</sup>. The electrolyte was stirred and maintained a stable pH throughout the electrochemical studies. Platinum mesh and Hg/HgO (NaOH sat.) were used as a counter and reference electrodes respectively.

#### 4.2.7 Photocatalytic experiments

The calcined TiNS/PbO<sub>2</sub>/RVC sample was cut into circular patterns of 4 mm diameter and 2 mm thickness (0.919 g) and was fitted in a glass tube holder which was immersed in a 10 cm<sup>3</sup> solution containing  $1 \times 10^{-5}$  mol dm<sup>-3</sup> of RB-5 dye in 0.5 mol dm<sup>-3</sup> of sodium sulphate at pH 3. The 300 W Ceralux model 300 BUV 10 F xenon UV lamp with intensity of 1.5mWcm<sup>-2</sup>. Prior to the photocatalytic experiments, the solution with tube holder was kept in the dark for 30 mins in order to achieve maximum adsorption of RB-5 dye on the calcined TiNS/PbO<sub>2</sub>/RVC, This ensured that the decolourisation measurements in solution were due to the UV irradiation and not to the adsorption of the dye on the composite . Following this, the UV irradiation was provided every 1 min to the solution. The absorbance of the RB-5 in solution was measured in a Hitachi U3010 UV-vis spectrophotometer at a wavelength of 597 nm. A calibration curve was used to evaluate the concentration of RB-5 dye in the solution.

#### 4.2.8 Ultrasonic stability of the TiNS/ PbO<sub>2</sub>/RVC calcined substrate

The stability of the calcined TiNS/PbO<sub>2</sub>/RVC was evaluated by sonication in an ultrasonic bath equipped with a transducer, which vibrates perpendicularly to the bottom of the reactor. The calcined coating was sonicated for 3 min in 1 mol dm<sup>-3</sup> acetone.

### 4.3 Results and discussion

#### 4.3.1 Surface characterisation of TiNS/PbO<sub>2</sub> coated RVC

Figure 4.3(a) shows PbO<sub>2</sub> layer coated over the strut of the 100 ppi RVC after electrodeposition at 2.5 A, whereas, Figure 4.3(b) shows the micrograph image of the PbO<sub>2</sub> agglomerates covering the surface of RVC at larger magnification.

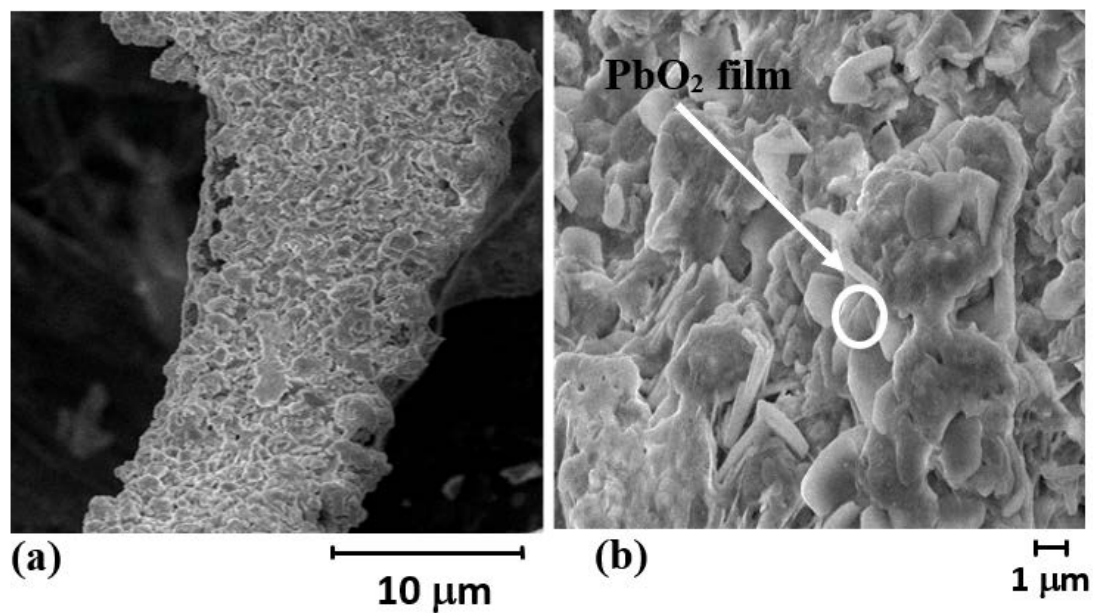


Figure 4.3 FESEM Images of TiNS/PbO<sub>2</sub> coatings on the RVC substrate obtained by anodic electrophoresis: (a) PbO<sub>2</sub>/RVC substrate after anodic EPD with inset at 7000 magnification, (b) Layer thickness of PbO<sub>2</sub>/RVC substrate.

TiNS films were anodically deposited on the PbO<sub>2</sub>/RVC surface by electrophoretic deposition as seen in Figure 4.4 (a), which provides more uniform morphology than the PbO<sub>2</sub>/RVC film. The more magnified SEM image as seen in Figure 4.4 (b) revealed the presence of smooth and elongated strands of TiNS on the top of the PbO<sub>2</sub>/RVC. The TiNS/PbO<sub>2</sub>/RVC coating covers the typical tetrahedron structure of the RVC (100 ppi) substrate.

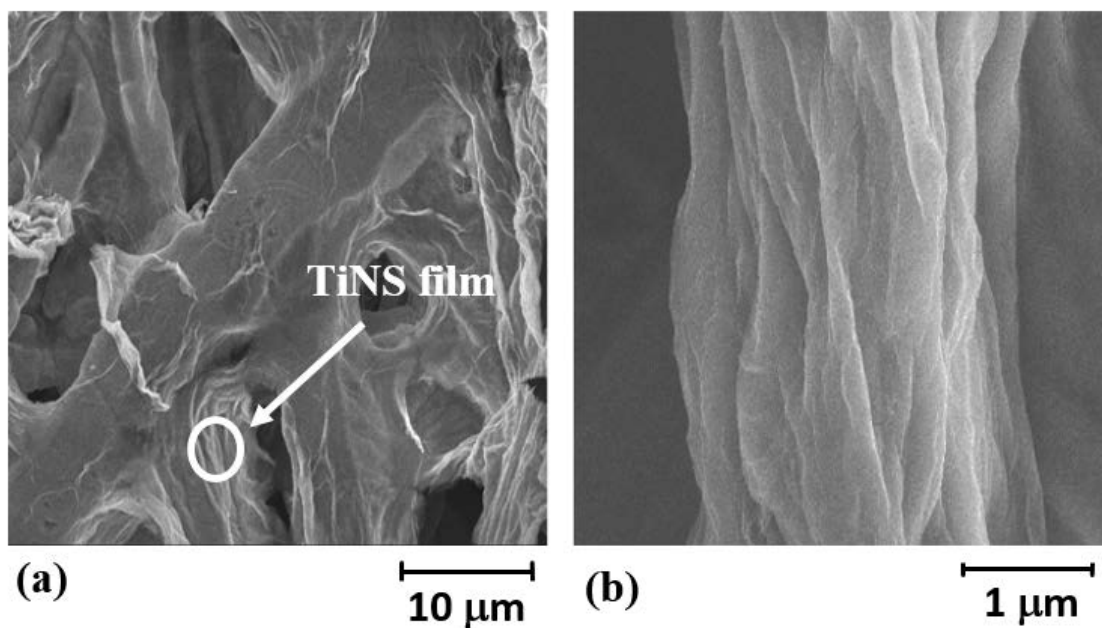


Figure 4.4 (a) TiNS/PbO<sub>2</sub>/RVC layer showing fully covered layer of TiNS film over PbO<sub>2</sub>/RVC (b) TiNS/PbO<sub>2</sub>/RVC layer at higher magnification.

After calcination at 450°C the TiNS/PbO<sub>2</sub>/RVC coatings, engulfed the surface of RVC as shown in Figure 4.5 (a) which appeared to be stable a stable composite even after calcination. The high temperature of the calcination creates surface defects over the TiNS/PbO<sub>2</sub>/RVC coatings. The image also shows that the nanosheets are still attached to the PbO<sub>2</sub>/RVC coating even after the calcination at 450 °C.

Figure 4.5 (b) is an image obtained for similar coating which denotes a rough surface with ridges and valleys on the TiNS/PbO<sub>2</sub>/RVC coating after the transformation of the TiNS from the titanate to the anatase phase, which imparts the photocatalytic active nature to the film and can be used to degrade reactive black-5 dye.

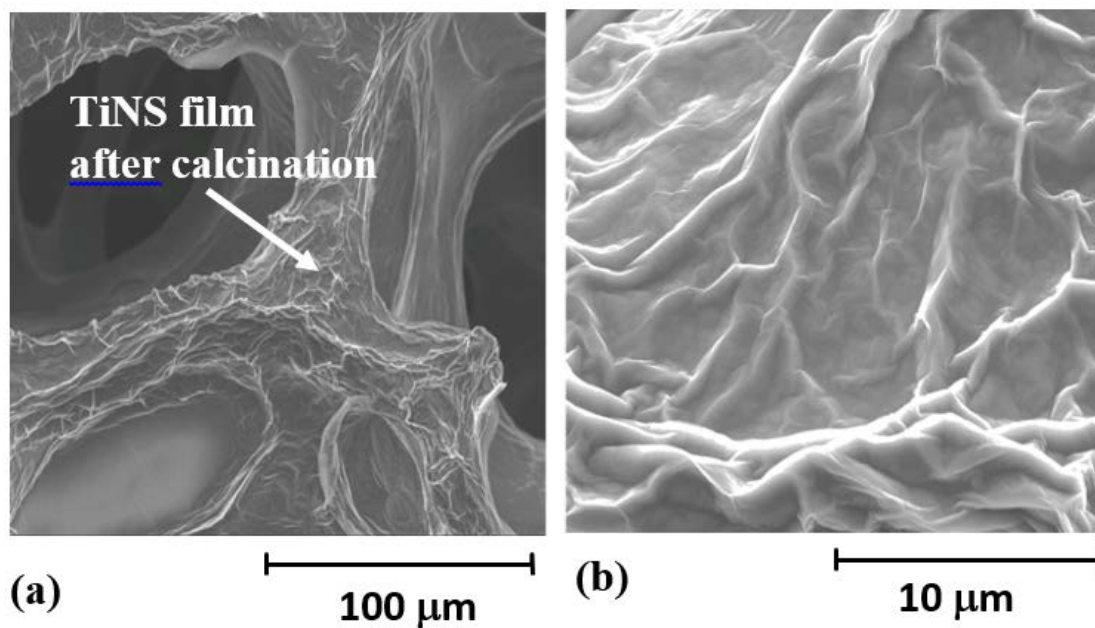


Figure 4.5 (a) TiNS/ PbO<sub>2</sub>/RVC after calcination at 450 °C, (b) calcined TiNS/PbO<sub>2</sub>/RVC layer having undulated surfaces at higher magnification.

The uncoated RVC used to connect with power supply during electrodeposition was oxidized at high temperature while the carbon on the coated areas remained intact. This suggests that the TiNS/PbO<sub>2</sub> coating preserve the mechanical integrity of the RVC structure.

The elemental analysis of the coating was determined by EDX from the micrograph shown in Figure 4.6 (a). It confirmed that the TiNS/PbO<sub>2</sub>/RVC coating contained, titanium, lead, carbon and oxygen elements.

Figures 4.6 (b) – (e) show the elemental maps of titanium (b), carbon (c) and lead (e), respectively, revealing particles uniformly distributed over the substrate.

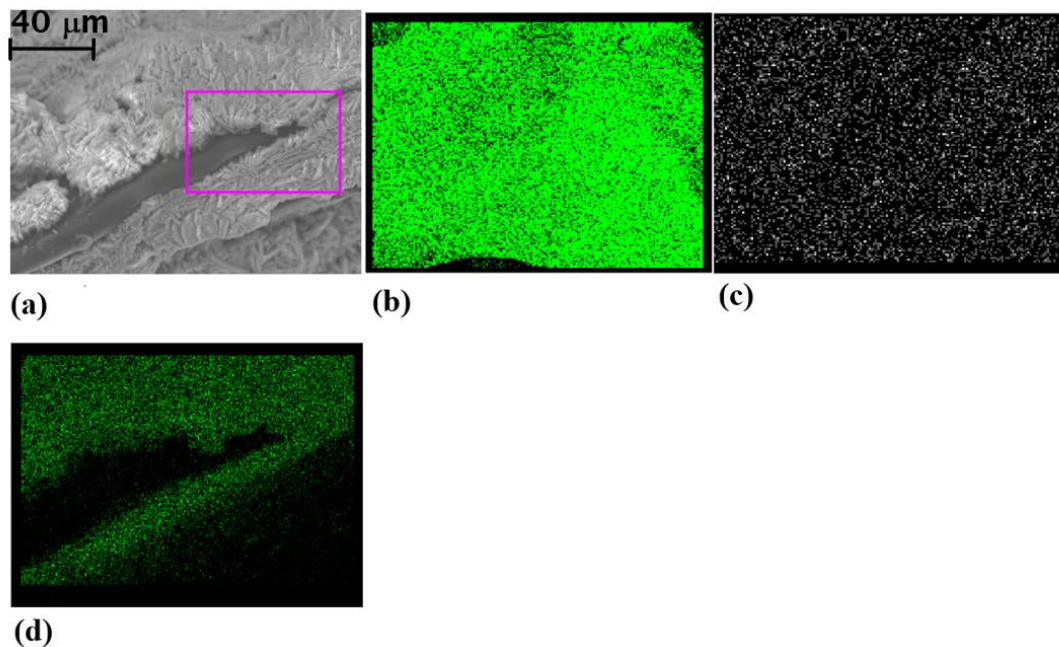


Figure 4.6 EDX images for elemental analysis of TiNS/PbO<sub>2</sub>/RVC (calcined) obtained by anodic electrophoretic deposition: (a) calcined TiNS/PbO<sub>2</sub>/RVC at 900 magnification (b) titanium elemental analysis (c) carbon (RVC) elemental analysis (d) lead elemental analysis.

The structural characteristics related to the transformation of the TiNS after the heat treatment were seen by Raman spectroscopy as shown in Figure 4.7.

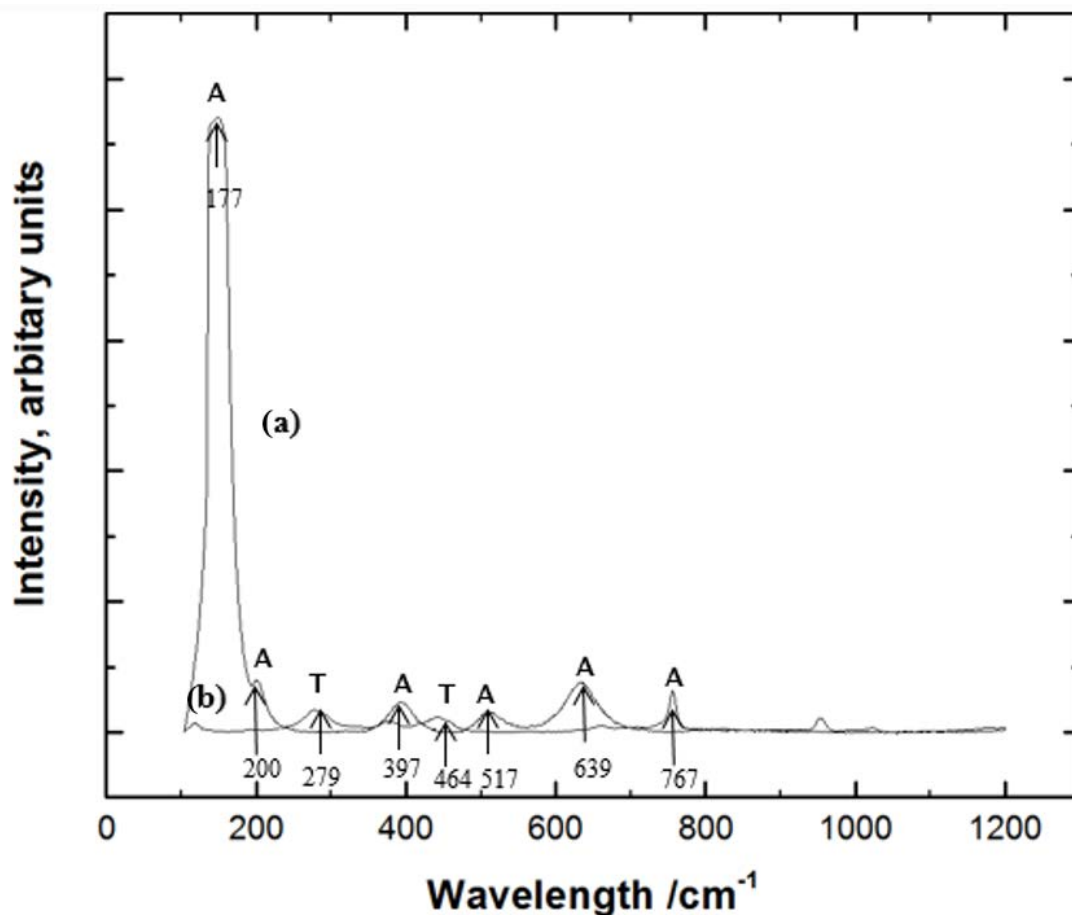


Figure 4.7 Raman spectra of the TiNS/PbO<sub>2</sub>/RVC obtained by anodic electrophoretic deposition a) calcined and b) non-calcined at 450 °C, where A denotes anatase, T denotes Titanate.

The peaks seen at 177, 200, 397, 517 639 and 767 cm<sup>-1</sup> in the curve (a) indicate that heat treatment converted the film from titanate to anatase phase which have been previously reported in the literature [46] [47] [48]. No peak for PbO<sub>2</sub>, observed this may be due to the fact that layer is covered with TiNS. The peaks observed at 279 and 464 cm<sup>-1</sup> in curve (b) are related with titanate phase for the non-calcined coatings, which are disappeared after calcination in curve a.



### 4.3.2 Electrochemical studies of TiNS/PbO<sub>2</sub>/RVC coatings

The oxygen evolution (OER) is an unwanted reaction during the direct electrochemical anodic oxidation of organic compounds. The first step is the formation of hydroxyl radical from the water oxidation at the anode substrate as indicated by equation (2.1). The following steps depend upon the nature of electrode substrate. Two types of substrates can be classified for direct anodic oxidation: “active” and “non-active” electrodes [4]. In active anodes, strong interaction of the hydroxyl radicals over electrodes takes place due to oxides generation [2] which leads to the oxygen evolution reaction [4]. Platinum is as an active anode, as it is capable of attracting hydroxyl radicals over its surface, due to its greater adsorption enthalpy. In the case of non- active electrodes like PbO<sub>2</sub>, there is weak interaction of the electrodes with hydroxyl radicals which are more prone to react in the electrolyte and oxidize organic compounds dissolved in solution [8].

Cyclic voltammetry studies using calcined TiNS/PbO<sub>2</sub>/RVC and PbO<sub>2</sub>/RVC electrodes in 0.5 mol dm<sup>-3</sup> Na<sub>2</sub>SO<sub>4</sub> at a scan rate of 10 mV s<sup>-1</sup> are shown in Figure 4.8. The electrode potential at which the OER starts to be significant (> 1 mA cm<sup>-2</sup>) on the calcined TiNS/PbO<sub>2</sub>/RVC, (curve 1) was 2.2 V vs. Hg/HgO whereas in the case of PbO<sub>2</sub>/RVC, curve 2, the oxygen evolution started at > 1.8 V vs. Hg/HgO. The higher overpotential for the oxygen evolution reaction observed in calcined TiNS/PbO<sub>2</sub>/RVC suggests that this coating can potentially be a better catalyst for the production of hydroxyl radicals.

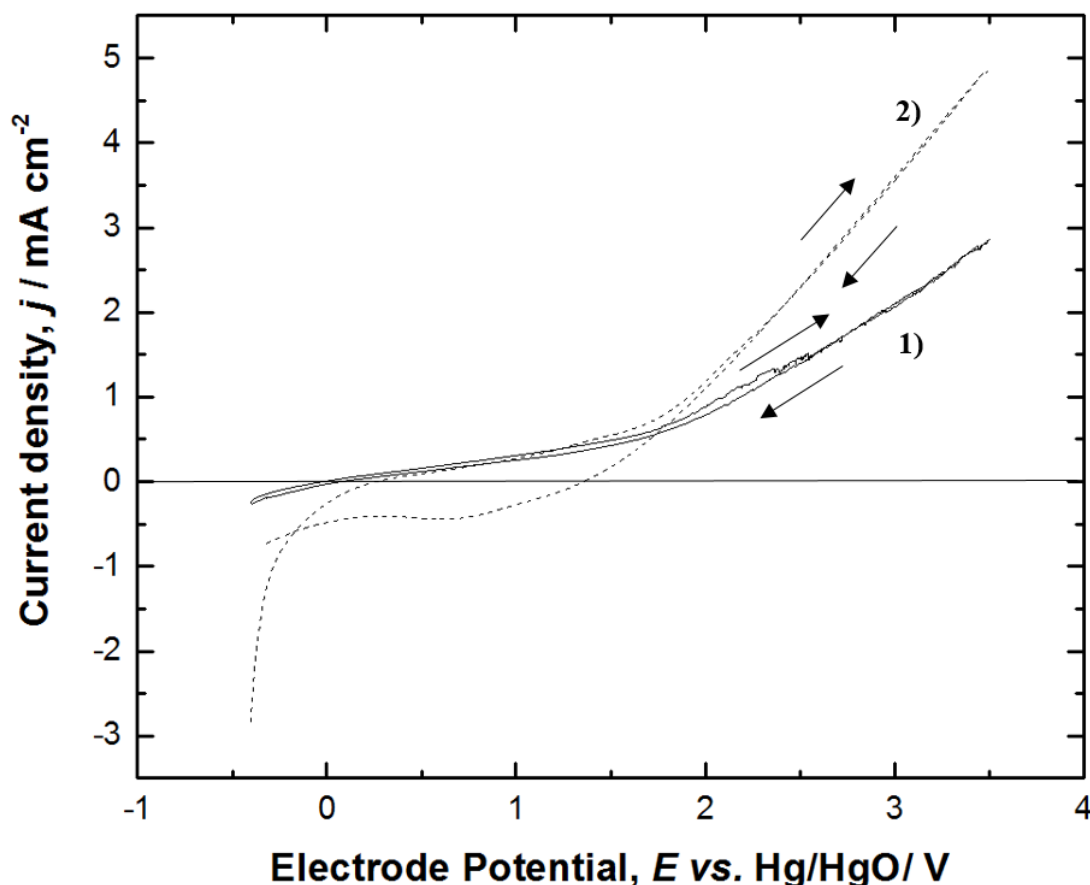


Figure 4.8 Polarization curve by using coating 1) (TiNS /PbO<sub>2</sub> / RVC) as anode after calcination at 450 °C in 0.5 mol dm<sup>-3</sup> Na<sub>2</sub>SO<sub>4</sub>, pH=3.0. 2) (PbO<sub>2</sub> / RVC) as anode in 0.5 mol dm<sup>-3</sup> Na<sub>2</sub>SO<sub>4</sub>, Experimental conditions: Potential sweep rate = 10 mV s<sup>-1</sup>, temperature: 25 °C.

When  $1 \times 10^{-5}$  mol dm<sup>-3</sup> of RB-5 dye was added to the solution of 0.5 mol dm<sup>-3</sup> Na<sub>2</sub>SO<sub>4</sub>, the oxidation process on the calcined TiNS/ PbO<sub>2</sub>/RVC started earlier at around 0.5 V vs. Hg/HgO but the current was around 1mA cm<sup>-2</sup> at 1.4 V vs. Hg/HgO. This suggest that the oxidation of the dye on this catalyst started before the OER as can be seen in Figure 4.9 (curve a). In the case of PbO<sub>2</sub>/RVC electrode (curve b), no significant oxidation of the dye was observed in comparison to curve a at 0.5 V vs. Hg/HgO and the current density

observed is higher than the calcined TiNS/PbO<sub>2</sub>/RVC after 2.5 V vs. Hg/HgO. This might be due to the fact that by increasing the potential, the formation of the hydroxyl radical competes with the direct oxidation of the dye. [10, 44].

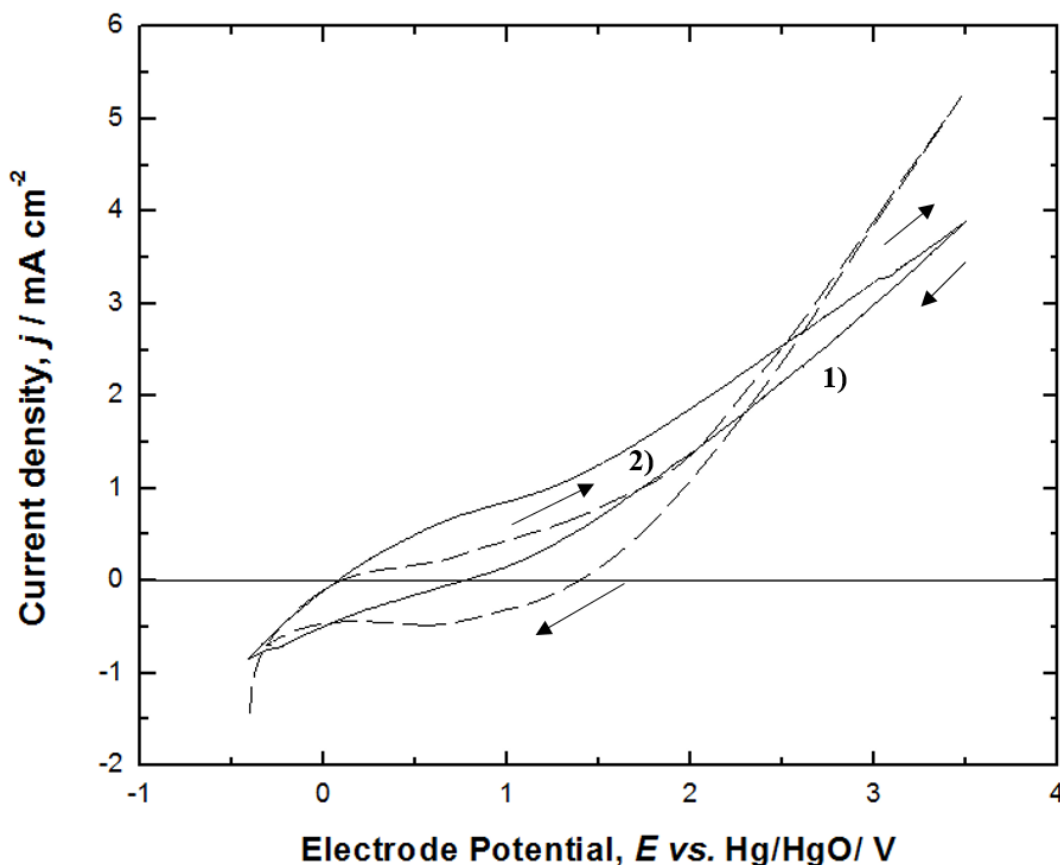


Figure 4.9 Polarization curve by using 1) TiNS /PbO<sub>2</sub> / RVC coating as anode in an electrolyte  $1 \times 10^{-5} \text{ mol dm}^{-3}$  R.B-5 dye in  $0.5 \text{ mol dm}^{-3}$  Na<sub>2</sub>SO<sub>4</sub>, pH=3.0. 2) (PbO<sub>2</sub> / RVC) as anode after calcination at 450 °C in an electrolyte  $1 \times 10^{-5} \text{ mol dm}^{-3}$ , R.B-5 dye in  $0.5 \text{ mol dm}^{-3}$  Na<sub>2</sub>SO<sub>4</sub>, pH=3.0, Experimental conditions: Potential sweep rate =  $10 \text{ mV s}^{-1}$ , Temperature: 25 °C.

### 4.3.3 Electrochemical decolourisation of RB-5 dye

Electrolysis of RB-5 dye at  $1 \times 10^{-5}$  mol dm<sup>-3</sup> concentration in 80 cm<sup>3</sup> of electrolyte containing 0.5 mol dm<sup>-3</sup> Na<sub>2</sub>SO<sub>4</sub> at pH = 3 was carried out at a current density of 2 mA cm<sup>-2</sup> in order to investigate the oxidation kinetics, colour removal on different coatings.

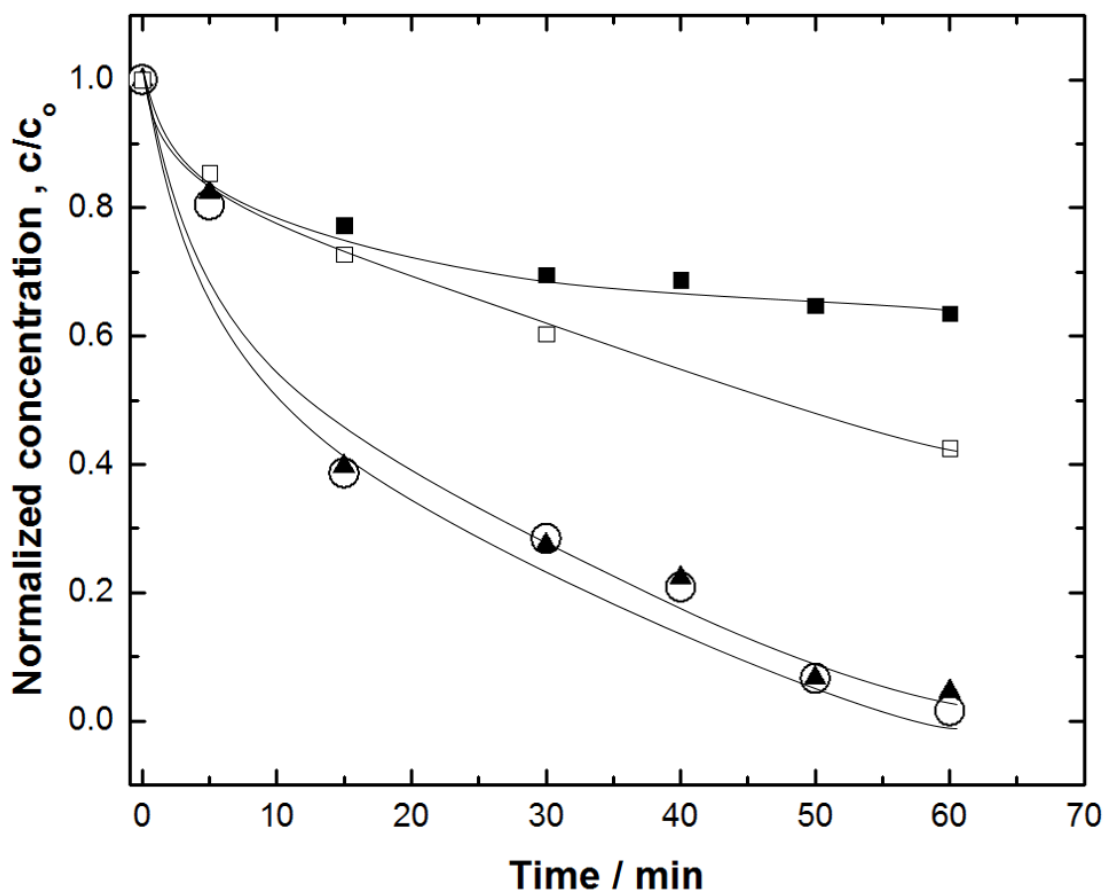


Figure 4.10 Electrochemical oxidation of RB-5 dye in a solution containing  $1 \times 10^{-5}$  mol dm<sup>-3</sup> of RB-5 dye and 0.5 mol dm<sup>-3</sup> Na<sub>2</sub>SO<sub>4</sub> by (■) RVC, (□) Photoassisted Fenton using Iron oxide on activated alumina support [49], (▲) RVC/PbO<sub>2</sub>, and (○) calcined TiNS/PbO<sub>2</sub>/RVC (Experimental conditions: applied current density = 2 mA cm<sup>-2</sup>, pH = 3.0, T = 25 °C).

The electrolyte consisted of 80 cm<sup>3</sup> of solution containing 1 × 10<sup>-5</sup> mol dm<sup>-3</sup> of RB-5 dye and 0.5 mol dm<sup>-3</sup> Na<sub>2</sub>SO<sub>4</sub> at pH 3 (adjusted by H<sub>2</sub>SO<sub>4</sub>). UV-vis spectra was used to follow the colour removal of RB-5 dye which shows a maximum absorption band in the visible light region at  $\lambda_{\text{max}} = 597$  nm. The oxidation of the azo dye complex molecule lead to low molecular weight intermediates such as aliphatic and aromatic organic molecules [4]. The formation of these compounds is due to the displacement of the chromophore functional group and followed by the oxidation of the organics to carbon dioxide and organic acids (carboxylic acids) [19-21].

The time dependent profiles of the normalized concentration  $c/c_0$ , for the electrochemical decolourisation of the dye using RVC, PbO<sub>2</sub>/RVC and calcined TiNS/PbO<sub>2</sub>/RVC anode electrodes are shown in Figure 4.10. The data of the concentration decay for the decolourisation of RB-5 dye on different electrodes can be fitted into the logarithmic relationship derived from equation 2.20. The fitting suggest a pseudo- first order reaction kinetics for the decolourisation. The comparison of pseudo rate constant ( $k$ ) is presented in Table 4.1.

<b>Substrate</b>	<b>-k / min<sup>-1</sup></b>	<b>% Decolourisation</b>	<b>Time / min</b>	<b>Reference</b>
RVC by using anodic oxidation	0.0064	36	60	This study
PbO <sub>2</sub> /RVC by using anodic oxidation	0.050	97	60	This study
Calcined TiNS(TiO <sub>2</sub> )/PbO <sub>2</sub> /RVC by using anodic oxidation	0.060	98	60	This study
Calcined TiNS(TiO <sub>2</sub> )/PbO <sub>2</sub> /RVC	0.383	85	5	Photocatalytic rate

Substrate	$-k / \text{min}^{-1}$	% Decolourisation	Time / min	Reference
by using photocatalytic decolourisation				in this study
TiO <sub>2</sub> (P25) by using photocatalytic oxidation	0.038	≈90	60	[55]
TiO <sub>2</sub> nanofiber-nanoparticle composite by using photocatalytic oxidation	0.039	94.4	60	[53]
TiO <sub>2</sub> nanofiber composite by using photocatalytic oxidation	0.026	75.5	60	[56]
Photoassisted Fenton by using iron oxide on activated alumina support	N.G	70	480	[49]
TiO <sub>2</sub> -P25 by using photocatalytic oxidation	N.G	98	150	[57]
UV/H <sub>2</sub> O <sub>2</sub> by using Iron salt	N.G	99.3	180	[58]

Table 4.1 Comparison of pseudo rate constants for oxidation of RB-5 dye by RVC, calcined TiNS (TiO<sub>2</sub>)/PbO<sub>2</sub>/RVC and PbO<sub>2</sub>/RVC and other related values from selected literature.

It can be seen that the pseudo first order rate constant decolourisation kinetics obtained using different anodes and from the data from the literature depends upon the nature of the electrocatalytic activity of the coating [40]. The anode electrodes are able to decolorize the solution to < 99 % except for RVC electrode. This may be due to the tendency of PbO<sub>2</sub>/RVC and calcined TiNS/PbO<sub>2</sub>/RVC anodes to generate the hydroxyl

radicals produced from water discharge reaction and employ them to oxidize the organic dye as shown in equation (3.8). The generation of hydroxyl radicals for the decolourisation of dyes over active electrodes plays an important part however, they are also part of the mechanism to generate oxygen. If the oxygen evolution reaction (OER) is favoured the decolourisation of organics will be compromised [5]. In order to avoid this competition, the electrodes with large overpotential for oxygen evolution like TiNS /PbO<sub>2</sub>/RVC and PbO<sub>2</sub>/RVC are preferred. As can be seen in figure 4.10, the RB-5 removal results are similar as both electrodes are non-active. The logarithm of the normalized concentration of RB-5 decay vs. time when a current density of 2 mA cm<sup>-2</sup> was applied on the anodes is shown in Figure 4.11. The comparison of these electrodes shows that using TiNS /PbO<sub>2</sub>/RVC, removes 98 % of the colour with linear pseudo first order decolourisation and pseudo rate constant  $k = - 0.060 \text{ min}^{-1}$ .

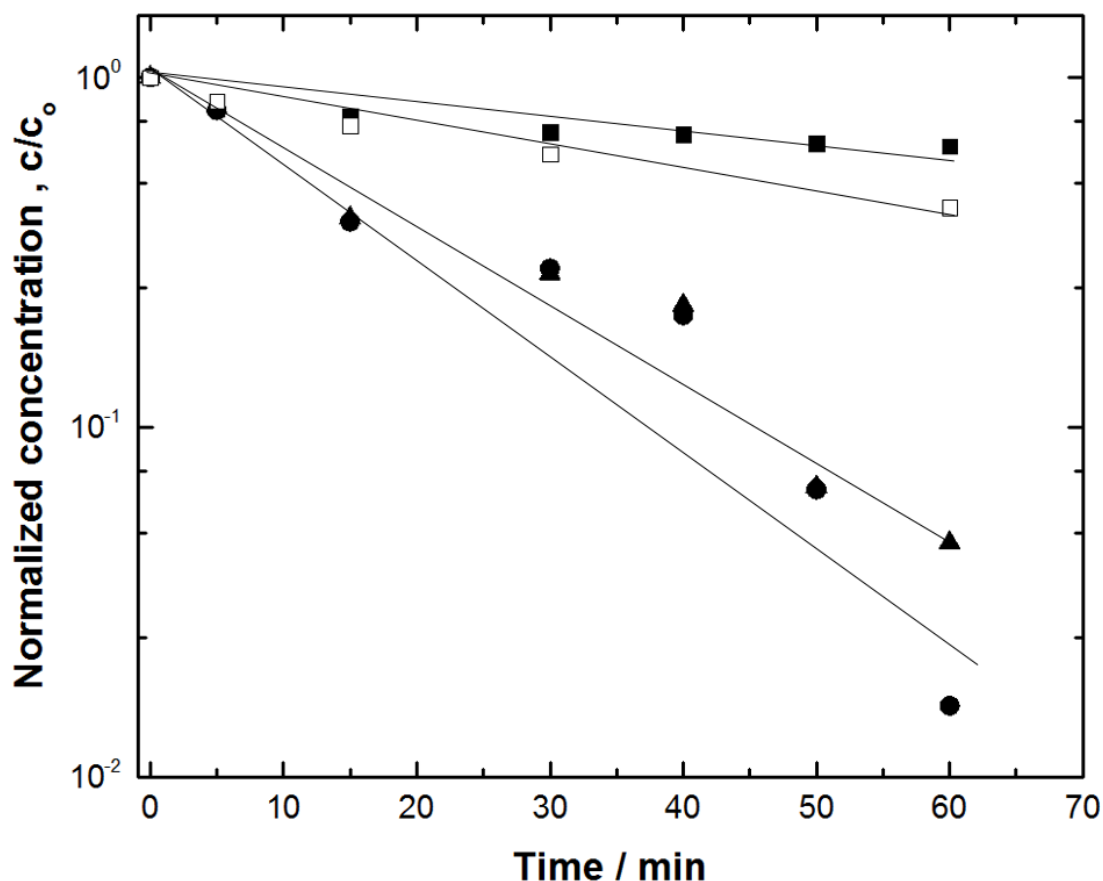


Figure 4.11 Electrochemical oxidation kinetics of RB-5 dye in a solution containing  $1 \times 10^{-5} \text{ mol dm}^{-3}$  of RB-5 dye and  $0.5 \text{ mol dm}^{-3} \text{ Na}_2\text{SO}_4$  by ■) RVC, □) Photoassisted Fenton using Iron oxide on activated alumina support [49], ▲) RVC/PbO<sub>2</sub>, and ○) calcined TiNS/PbO<sub>2</sub>/RVC (Experimental conditions: applied current density =  $2 \text{ mA cm}^{-2}$ , pH = 3.0, T = 25 °C).

Colour removal is also substantial when using PbO<sub>2</sub>/RVC electrode as shown by the normalized concentration data in Figure 4.11 which is around 98 %. This behaviour is due to the production of Pb (•OH) as explained in equation (3.1) [41]. Negligible decolourisation results were obtained in case of RVC alone; which were about 36 % colour removal after 60 min which is lower compared to the previously mentioned electrodes. Some reported works showed only 70 % conversion of RB-5 dye by using



photo assisted Fenton, which is about 28 % lower than the values reported here [49]. This revealed that the  $\bullet\text{OH}$  radical is weakly adsorbed over the surface of non-active electrode ( $\text{PbO}_2$ ) [8] and ultimately favours the production of  $\bullet\text{OH}$  radical as indicated in equation (3.7) and also subsequent adsorption of the dye molecules over the active sites provided by positively charged TiNS under acidic conditions over the  $\text{PbO}_2/\text{RVC}$  substrate.

#### **4.3.4 Photocatalytic oxidation of Reactive black-5 dye**

In order to evaluate the photocatalytic activity of the anatase phase of the calcined TiNS ( $\text{TiO}_2$ )/ $\text{PbO}_2$ /RVC coating characterized by Raman studies (Figure 4.7), photocatalytic studies of the decolourisation of RB -5 dye in  $\text{Na}_2\text{SO}_4$  and  $\text{pH} = 3$  were carried out. The coating showed noticeable photocatalytic activity towards decolourisation of RB-5 dye.

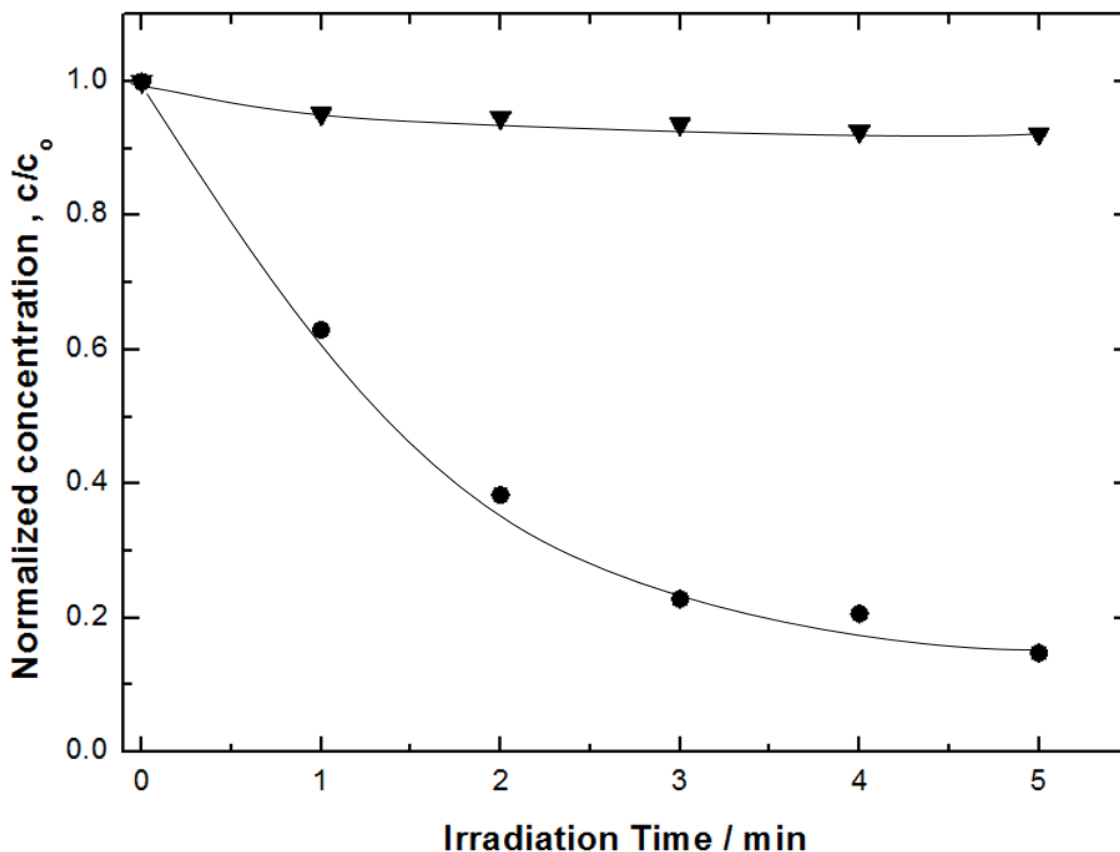


Figure 4.12 Photocatalytic oxidation of RB-5 dye in a solution containing  $1 \times 10^{-5}$  mol  $\text{dm}^{-3}$  of RB-5 dye and  $0.5 \text{ mol dm}^{-3}$   $\text{Na}_2\text{SO}_4$  by ▼) RVC , ●) calcined TiNS/PbO<sub>2</sub>/RVC (Experimental conditions: UV lamp intensity =  $1.5 \text{ mW cm}^{-2}$ , pH = 3.0, T = 25 °C).

The activity of the coating depends on factors like protonation of TiO<sub>2</sub> nanosheets in acidic media [50], the generation of holes and electrons over the nanosheets surface in the presence of UV-irradiation [51] [52]. In acidic solutions, the TiO<sub>2</sub> nanosheets become positively charged as indicated by equation (3.10), and attract the negatively charged RB-5 dye [53]. Under UV-light there is the formation of electrons ( $e^-$ ) in the conduction band and holes ( $h^+$ ) in the valence band of the TiO<sub>2</sub> nanosheets anatase as seen in equation (2.7). The photo induced holes possess oxidative properties which can attack the dye

molecule directly leading to its decolourisation, or indirectly forming hydroxyl radicals by promoting the reaction between the hydroxyl anions and water as shown by equation (2.8). The hydroxyl radicals reacts with the organic matter. However, the electrons can also react with an electron acceptor like  $O_2$  to produce oxidizing radicals  $O_2^- \cdot$  as shown by equation (2.9) [53]. Overall the holes and radicals are responsible for the photocatalytic activity and decolourisation of RB-5 dye as indicated by equations (2.9), (2.10),(2.11),(2.12) and (2.13) producing  $\cdot OH$  radical which ultimately decompose the dye as shown in equation (3.8). In this case,  $PbO_2$  dominates the base of the conduction band of TiNS (anatase  $TiO_2$ ) while the valance band belongs to the TiNS (anatase  $TiO_2$ ) nanoparticle states [54]. The formation of the new band gap will intensify the electron hole pair transfer upon photoexcitation.

The photocatalytic decolourisation is shown in Figure 4.12, and indicates that the RB-5 dye follows a pseudo- first order reaction kinetics on the calcined TiNS/ $PbO_2$ /RVC coating as revealed in Figure 4.13.

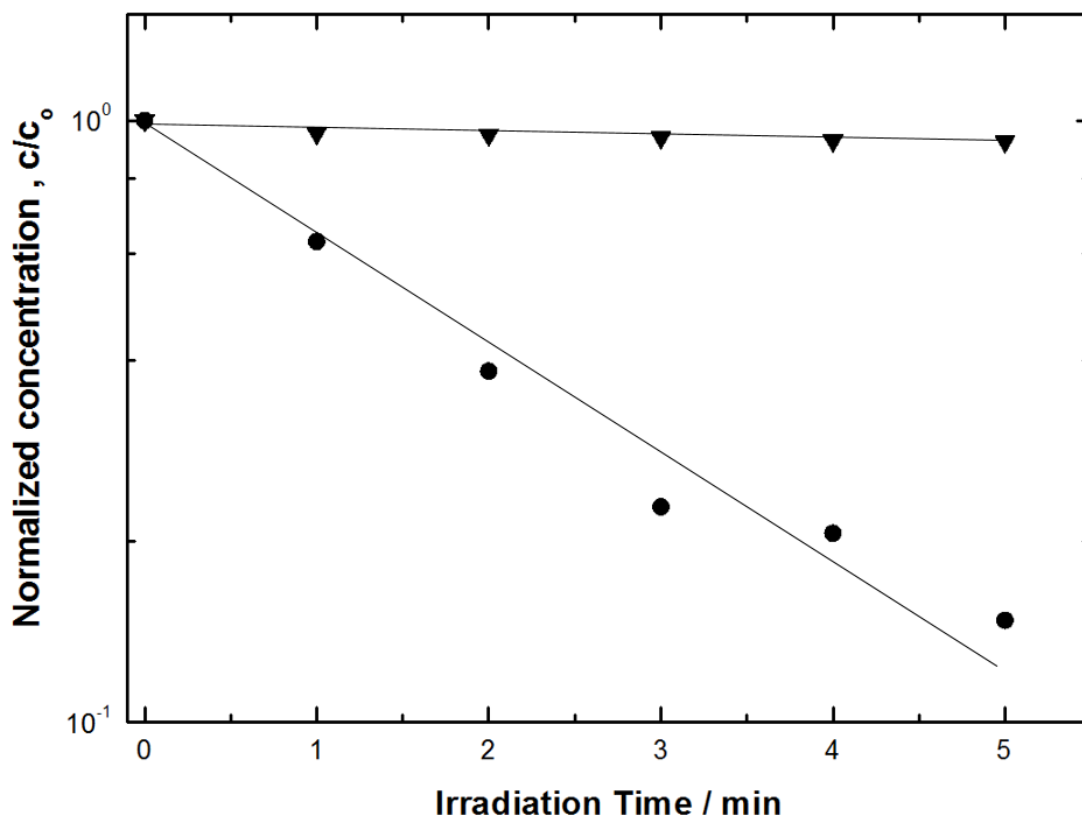


Figure 4.13 Photocatalytic oxidation kinetics of RB-5 dye in a solution containing  $1 \times 10^{-5} \text{ mol dm}^{-3}$  of RB-5 dye and  $0.5 \text{ mol dm}^{-3} \text{ Na}_2\text{SO}_4$  by  $\blacktriangledown$ ) RVC,  $\bullet$ ) calcined  $\text{TiNS/PbO}_2/\text{RVC}$  (Experimental conditions: UV lamp intensity =  $1.5 \text{ mW cm}^{-2}$ , pH = 3.0, T =  $25 \text{ }^\circ\text{C}$ ).

The comparison of the pseudo rate constant  $k$  calculated using equation (2.20) for the photocatalytic decolourisation ( $-0.383 \text{ min}^{-1}$ ) with the pseudo rate constant obtained from the electrochemical decolourisation ( $-0.060 \text{ min}^{-1}$ ) reveals that the photocatalytic activity is higher by 84 %. The annealing converts TiNS to the single crystal anatase phase which improves the photocatalytic activity when irradiated with UV light. The calcined  $\text{TiNS/PbO}_2/\text{RVC}$  decolourised reactive black-5 solution in 15 min. The improved photocatalytic activity of a coating i.e.  $\text{TiNS/PbO}_2/\text{RVC}$  is due to the formation of holes

and radicals by the incident UV light and ultimately participates in the photocatalytic decolourisation of the dye. In a recent study it was reported that Ti/Pt/PbO<sub>2</sub> electrodes did not exhibit photocatalytic activity for the degradation of DR-80 dye. This behaviour was associated with the limited or no dispersion of UV irradiation by PbO<sub>2</sub> particles in the solution and therefore these electrodes are not found effective for photocatalytic activity [59].

#### 4.4 Conclusion

In this chapter, lead dioxide was electrodeposited on RVC and the resulting coating was decorated with TiNS prepared via anodic electrophoretic deposition followed by calcination.

The main findings are:

- Compared with RVC alone and PbO<sub>2</sub>/RVC electrodes, the calcined TiNS /PbO<sub>2</sub>/RVC coatings was able to decolourate RB-5 dye from wastewater more effectively.
- The calcined TiNS/PbO<sub>2</sub>/RVC was also found effective for the photocatalytic decolourisation of the dye.
- The nature of electrode plays an important part in the decolourisation and colour removal of organic chromophore dye. The hydroxyl free radical generated on the electrode surface provides an efficient and clean method for the decolourisation of RB-5 dye. Using calcined TiNS/PbO<sub>2</sub>/RVC electrodes by applying a current density of 2 mAcm<sup>-2</sup>, a first order decolourisation rate kinetics has been determined with higher rate of reaction in comparison with some reported values in the literature.

- Raman results indicated the transformation of the titanate phase of TiNS/PbO<sub>2</sub>/RVC to the anatase structure after calcination at 450 °C.
- The anatase phase imparted with the coating also found effective in photocatalytic studies and removal results revealed a first order kinetics decolourisation of RB-5 dye in acidic conditions.
- The photocatalytic effect resulted from three mechanisms which involve photo induce holes in valance band, the protonation of TiNS in acidic solutions and the formation of oxidative radicals evolved from the reaction between the electrons from the conduction band and the electron acceptor (<sup>•</sup>O<sub>2</sub>) due to these factors the photocatalytic activity of the coating seems to be faster than the electrochemical colour removal.

This study will open a promising approach for the development of metal oxide structures decorated with TiO<sub>2</sub> nanosheets over inexpensive carbon based substrate, for their applications in wastewater treatment. TiNS coating on RVC also improved thermal resistance of RVC. Therefore, these coatings could potentially serve the purpose of decontamination of wastewater by using cheaper and flow-through electrodes such as RVC with the combination of PbO<sub>2</sub> and TiNS, as a promising coating.

#### 4.5 References

- [1] VM Vasconcelos, C. Ponce-de-León J.LNava M.R Lanza Electrochemical oxidation of RB-5 dye by anodic oxidation, electro-Fenton and by combining anodic oxidation–electro-Fenton in a filter-press flow cell. *J Electroanal Chem.* 765 (2016) 179-187.

- [2] C.A Martínez-Huitle, E. Brillas Decontamination of wastewaters containing synthetic organic dyes by electrochemical methods: a general review. *Appl Catal B*. 87 (2009) 105-145.
- [3] R. Salazar, M.S Ureta-Zañartu Mineralization of triadimefon fungicide in water by electro-Fenton and photo electro-Fenton. *Water Air Soil Pollut*. 223 (2012) 4199-4207.
- [4] C.A Martínez-Huitle, S. Ferro Electrochemical oxidation of organic pollutants for the wastewater treatment: direct and indirect processes. *Chem Soc Rev*. 35 (2006) 1324-1340.
- [5] M.A Sandoval, J.L Nava, O. Coreño, G. Carreño, L.A Arias, D. Méndez, Sulfate ions removal from an aqueous solution modelled on an abandoned mine by electrocoagulation process with recirculation. *Int J Electrochem Sci*. 12 (2017) 1318-1330.
- [6] R. Salazar , S. Garcia-Segura, M.S Ureta-Zañartu, E. Brillas, Oxidation of disperse azo dyes from waters by solar photoelectro-Fenton. *Electrochim Acta*. 56 (2011) 6371-6379.
- [7] E. Brillas, C.A. Martínez-Huitle Decontamination of wastewaters containing synthetic organic dyes by electrochemical methods. An updated review. *Appl Catal B*. 166 (2015) 603-643.
- [8] D.C De Moura, M.A Quiroz, D.R Da Silva, R. Salazar, C.A. Martínez-Huitle, Electrochemical oxidation of Acid Blue 113 dye using TiO<sub>2</sub>-nanotubes decorated

with  $\text{PbO}_2$  as anode. *Environmental Nanotechnology, Monitoring & Management*. 5 (2016) 13-20.

- [9] M. Zhou, J. He, Oxidation of cationic red X-GRL by electrochemical oxidation on modified  $\text{PbO}_2$  electrode. *J Hazard Mater*. 153 (2008) 357-363.
- [10] E.V Dos Santos, C. Sáez, C.A Martínez-Huitle, P. Cañizares, M.A Rodrigo, The role of particle size on the conductive diamond electrochemical oxidation of soil-washing effluent polluted with atrazine. *Electrochem Commun*. 55 (2015) 26-29.
- [11] A. Cano, P. Cañizares, C. Barrera, C. Sáez, M.A Rodrigo, Use of low current densities in electrolyses with conductive-diamond electrochemical—oxidation to disinfect treated wastewaters for reuse. *Electrochem Commun*. 13 (2011) 1268-1270.
- [12] M. Panizza, G. Cerisola Electrochemical materials for the electrochemical oxidation of synthetic dyes. *Appl Catal B: Environ*. 75 (2007) 95-101.
- [13] D.M De Araújo, C. Sáez, C.A Martínez-Huitle, P. Cañizares, M.A Rodrigo, Influence of mediated processes on the removal of Rhodamine with conductive-diamond electrochemical oxidation. *Appl Catal B: Environ*. 166 (2015) 454-459.
- [14] S. Garcia-Segura S, E.V Dos Santos C.A Martínez-Huitle, Role of  $\text{sp}_3/\text{sp}_2$  ratio on the electrocatalytic properties of boron-doped diamond electrodes: a mini review. *Electrochem Commun*. 59 (2015) 52-55.
- [15] G. Zhao, X. Cui, M. Liu, P. Li , Y. Zhang, T. Cao, H. Li, Y. Lei, L. Liu, D. Li, Electrochemical discolouration of refractory pollutant using a novel



- microstructured TiO<sub>2</sub> nanotubes/Sb-doped SnO<sub>2</sub> electrode. *Environ Sci Technol.* 43 (2008) 1480-1486.
- [16] M. Xu, Z. Wang, F. Wang, P. Hong, C. Wang, X. Ouyang, C. Zhu C, Y. Wei, Y. Hun, W. Fang, Fabrication of cerium doped Ti/nanoTiO<sub>2</sub>/PbO<sub>2</sub> electrode with improved electrocatalytic activity and its application in organic oxidation. *Electrochim Acta* 201 (2016) 240-250.
- [17] B.N.L Biyoghe, M.P Ibondou, X. Gu, M. Xu, S. Lu, Z. Qiu, S.M Mbadinga, Efficiently synthetic TiO<sub>2</sub> Nano-sheets for PCE, TCE, and TCA oxidations in aqueous phase under VUV irradiation. *Water Air Soil Pollut* 225 (2014)1951.
- [18] H. An, H. Cui, W. Zhang, J. Zhai, Y. Qian, X. Xie, Q. Li, Fabrication and electrochemical treatment application of a microstructured TiO<sub>2</sub>-NTs/Sb-SnO<sub>2</sub>/PbO<sub>2</sub> anode in the oxidation of C.I. Reactive Blue 194 (RB194). *Chem Eng J.* 209 (2012) 86-93.
- [19] Z. He, C. Huang, Q. Wang, Z. Jiang, J. Chen, S. Song, Preparation of apraseodymium modified Ti/SnO<sub>2</sub>-Sb/PbO<sub>2</sub> electrode and its application in the anodic discoloration of the azo dye acid black 194. *Int J Electrochem Sci* 6 (2011) 4341.
- [20] G.R Oliveira, N.S Fernandes, J.V Melo, D.R Silva, C. Urgeghe, C.A. Martínez-Huitle, Electrocatalytic properties of Ti-supported Pt for decolourizing and removing dye from synthetic textile wastewaters. *Chem Eng J.* 168 (2011) 208-214.

- [21] M. Cerro-Lopez, Y. Meas-Vong, M.A Méndez-Rojas, C.A Martínez-Huitle, Quiroz MA, Formation and growth of PbO<sub>2</sub> inside TiO<sub>2</sub> nanotubes for environmental applications. *Appl Catal B*. 100 (2014) 174-181.
- [22] D.A Frey, H.E Weaver, NMR Measurements of the Knight Shift in Conducting PbO<sub>2</sub>, *J Electrochem Soc*. 107 (1960) 930-932.
- [23] A.J.D Santos, DKDS Xavier, DRD Silva, M.A Quiroz, C.A Martínez-Huitle, Use of combined electrochemical approaches for mineralization and detection of hydroquinone using PbO<sub>2</sub> Electrodes. *J Mex Chem Soc*. 58 (2014) 356-361.
- [24] C.A Martínez-Huitle, M. Panizza, Application of PbO<sub>2</sub> anodes for wastewater treatment, *Advances in Chemistry Research: Applied Electrochemistry*. Nova Science Publishers Inc, New York (2010).
- [25] C.T.J Low, D. Pletcher, F.C Walsh, The electrodeposition of highly reflective lead dioxide coatings. *Electrochem Comm* 11 (2009) 1301-1304.
- [26] R. Savitha, R. Raghunathan, R. Chetty, Rutile nanotubes by electrochemical anodization. *RSC Adv*. 6 (2016) 74510-74514.
- [27] J. Friedrich, C. Ponce-de-León, G. Reade, F.C Walsh Reticulated vitreous carbon as an electrode material. *J Electroanal Chem*. 561 (2004) 203-217.
- [28] A. Czerwiński, R.Z Obrębowski, S. Siwek, H. Paleska, I.Chotkowski M. Łukaszewski RVC as new carbon material for batteries. *J Appl Electrochem*. 39 (2009)559-567.

- [29] G. Zhang, F. Yang, M. Gao, X. Fang, L. Liu, Electro-Fenton discolouration of azo dye using polypyrrole/anthraquinonedisulphonate composite film modified graphite cathode in acidic aqueous solutions. *Electrochim Acta*. 53 (2008) 5155-5161.
- [30] C. Ponce-de-León, D. Pletcher, (1995) Removal of formaldehyde from aqueous solutions via oxygen reduction using a reticulated vitreous carbon cathode cell. *J Appl Electrochem*. 25 (1995) 307-314.
- [31] F. Rodriguez-Valadez, C. Ortiz-Éxiga, J.G Ibanez, A. Alatorre-Ordaz, S.Gutierrez-Granados, Electro-reduction of Cr (VI) to Cr (III) on reticulated vitreous carbon electrodes in a parallel-plate reactor with recirculation. *Environ Sci Technol* 39 (2005) 1875-1879.
- [32] G.W Reade, A.H Nahle, P. Bond, J.M Friedrich, F.C Walsh, Removal of cupric ions from acidic sulfate solution using reticulated vitreous carbon rotating cylinder electrodes. *J Chem Technol Biotechnol*. 79 (2004) 935-945.
- [33] M. Hossein, M.M Momeni Preparation and characterization of TiO<sub>2</sub> nanotubular arrays for electro-oxidation of organic compounds: effect of immobilization of the noble metal particles. *Int J Mod Phys*. 5 (2012) 41-48.
- [34] O. Simond, C. Comninellis, Anodic oxidation of organics on Ti/IrO<sub>2</sub> anodes using Nafion® as electrolyte. *Electrochim Acta* 42 (1997) 2013-2018.
- [35] G. Ramírez, F.J Recio, P. Herrasti, C. Ponce-de-León, I. Sirés, Effect of RVC porosity on the performance of PbO<sub>2</sub> composite coatings with titanate nanotubes for the electrochemical oxidation of azo dyes. *Electrochim Acta*. 204 (2016) 9-17.

- [36] C.D Jaeger, A.J Bard, Spin Trapping and Electron Spin Resonance Detection of Radical Intermediates in the Photodecomposition of Water at TiO<sub>2</sub> Particulate Systems. *J Phys Chem.* 83 (1979) 3146-3152.
- [37] C. Naccache, P. Meriaudeau, M. Che, Identification of oxygen species adsorbed on reduced titanium dioxide. *Trans Faraday Soc.* 67 (1971) 506-512.
- [38] S. Fukuzawa, K.M Sancier, T. Kwan, Photoadsorption and photodesorption of oxygen on titanium dioxide. *J Catal.* 11 (1968) 364-369.
- [39] Y. Wang, R. Shi, J. Lin, Y. Zhu, Significant photocatalytic enhancement in methylene blue discolouration of TiO<sub>2</sub> photocatalyst via graphene-like carbon in situ hybridization. *Appl Catal B.* 100 (2010)179-183.
- [40] D. Lawless, N. Serpone, D. Meisel, Role of •OH radicals and trapped holes in photocatalysis. A pulse radiolysis study. *J Phys Chem.* 95 (1991) 5166-5170.
- [41] M.B Muneer, D. Qamar, M. Tariq, M.A Faisal, Photocatalysed reaction of few selected organic systems in presence of titanium dioxide. *Appl Catal A.* 289 (2005) 224-230.
- [42] T. Sasaki, M. Watanabe, Osmotic swelling to exfoliation exceptionally high degrees of hydration of a layered titanate, *J Am Chem Soc.* 120 (1998) 4682-4689.
- [43] I.E Grey, C. Li, I.C Madsen, J.A Watts The stability and structure of Cs<sub>x</sub> [Ti<sub>2-x<sub>4</sub></sub>□<sub>x<sub>4</sub></sub>]O<sub>4</sub>, 0.61<x<0.65, *J.Solid State Chem.* 66 (1987) 7-19.
- [44] C. Harito, D.V Bavykin, M.E Light, F.C Walsh, Titanate nanotubes and nanosheets as a mechanical reinforcement of water-soluble polyamic acid: Experimental and theoretical studies, *Compos B Eng.* 124 (2017) 54-63.

- [45] F.J Recio, P. Herrasti I. Sirés, A.N Kulak, D.V Bavykin, C. Ponce-de-León, F.C Walsh, The preparation of PbO<sub>2</sub> coatings on reticulated vitreous carbon for the electro-oxidation of organic pollutants. *Electrochim Acta*. 56 (2011) 5158-51652.
- [46] S.J Kim, Y.U Yun, HJ Oh, S.H Hong, C.A Roberts, K. Routray, I.E Wachs, Characterization of hydrothermally prepared titanate nanotube powders by ambient and in situ Raman spectroscopy. *J Phys Chem Lett*. 1 (2010) 130-135.
- [47] Y.V Kolen'ko, A.K Kirill, I.G Anton, V.G Alexei, F. Johannes, I.L Oleg, R.C Bulat, V.T Gustaaf, Y. Masahiro Hydrothermal synthesis and characterization of nanorods of various titanates and titanium dioxide. *J Phys. Chem. B*. 110 (2006) 4030-4038.
- [48] E. Horváth, Á. Kukovecz, Z. Kónya, I. Kiricsi, Hydrothermal conversion of self-assembled titanate nanotubes into nanowires in a revolving autoclave. *Chem mater*. 19 (2007) 927-931.
- [49] C.L Hsueh, Y.H Huang, C.C Wang, C.Y Chen, Photoassisted Fenton discolouration of nonbiodegradable azo-dye (reactive black 5) over a novel supported iron oxide catalyst at neutral pH. *J Mol Catal A*. 245 (2005) 78-86.
- [50] N.M Mahmoodia, M. Arami, N.Y Limaee, N.S Tabrizi, Decolourisation and aromatic ring discolouration kinetics of direct red 80 by UV oxidation in the presence of hydrogen peroxide utilizing TiO<sub>2</sub> as a photocatalyst. *Chem Eng J*. 112 (2005) 191-196.

- [51] Y. Jiang, W.N Wang, P. Biswas, J.D, Facile aerosol synthesis and characterization of ternary crumpled graphene - TiO<sub>2</sub> - magnetite nanocomposites for advanced water treatment. *ACS Appl Mater Interfaces*. 6 (2014) 11766-11774.
- [52] I. Ilisz, Z. Laszlo, A. Dombi, Investigation of the photodecomposition of phenol in near-UV-irradiated aqueous TiO<sub>2</sub> suspensions. I: effect of charge-trapping species on the discolouration kinetics, *Appl Catal A*. 180 (1999) 25-33.
- [53] D. Sugiyana, M. Handajani, E. Kardena, S. Notodarmojo, Photocatalytic oxidation of textile wastewater containing reactive black 5 azo dye by using immobilized TiO<sub>2</sub> nanofiber-nanoparticle composite catalyst on glass plates. *Journal of JSCE* 2. (2014) 69-76.
- [54] A. Iwaszuk, M. Nolan, Lead oxide-modified TiO<sub>2</sub> photocatalyst: tuning light absorption and charge carrier separation by lead oxidation state. *Catal Sci Technol*. 3 (2013) 2000-2008.
- [55] N. Jafari, R. Kasra-Kermanshahi, M.R Soudi, A.H Mahvi, S. Gharavi, Oxidation of a textile reactive azo dye by a combined biological-photocatalytic process: *Candida tropicalis* Jks2 -TiO<sub>2</sub>/Uv. *Iranian J Environ Health Sci Eng*. 9 (2012) 33.
- [56] S. Notodarmojo, D. Sugiyana, M. Handajani, E. Kardena, A. Larasati Synthesis of TiO<sub>2</sub> nanofiber-nanoparticle composite catalyst and its photocatalytic decolourisation performance of reactive black 5 dye from aqueous solution. *J. Eng. Technol. Sci*. 49 (2017) 340-356.

- [57] M. Muruganandham, N. Sobana, M. Swaminathan, Solar assisted photocatalytic and photochemical oxidation of Reactive Black 5. *J hazardous mater.* 137 (2006) 1371-1376.
- [58] M.S Lucas, J.A Peres, Decolourisation of the azo dye reactive black 5 by Fenton and photo-Fenton oxidation, *Dyes Pigm.* 71 (2006) 235-244.
- [59] J. Florêncio, M.J Pacheco, A. Lopes, L. Ciríaco, Application of Ti/Pt/ $\beta$ -PbO<sub>2</sub> Anodes in the Degradation of DR80 Azo Dye. *Portugaliae Electrochimica Acta.* 31 (2013) 257-264.





## Chapter 5: **Photocatalytic oxidation of dye using titanate nanotubes anodically deposited on RVC by anodic electrophoretic deposition**

Titanate nanotube (TiNT) were deposited over the surface of 100 pores per inch (ppi) reticulated vitreous carbon (RVC) by anodic electrophoresis at a potential of 15 V in a two electrode cell, from an ethanol/water suspension containing 0.25 g of TiNT and 0.2 mol dm<sup>-3</sup> of tetrabutylammonium hydroxide (TBAOH) surfactant. The TiNT/RVC coating structural morphology was analysed by field emission scanning electron microscopy (FESEM), revealing a homogenous and uniform layer of TiNT of *ca.* 30 μm thickness. The photocatalytic properties of the coating were enhanced by calcination at 450 °C for 60 min in air. The electrode material was used as a photocatalyst for the discolouration of organic methylene blue dye in water. The 97 % volumetric porosity of the RVC substrate provided a large surface area for deposition TiNT enabling 33 % higher discolouration rate compared to RVC alone and achieving a percentage of 91 % using calcined TiNT/RVC substrate.

### **5.1 Introduction**

Water demand has increased drastically for industrial, commercial and domestic activities during the last decade. These activities ultimately could lead towards a water scare in different regions of the world [1]. In order to prevent low water supply, efficient and economical effluent water treatment technologies, that can be readily scaled-up, are vital for continuing the development of the communities. These technologies allow the removal of toxic organics (dyes, pesticides, pharmaceuticals) and dissolved metallic ions from waste water [2]. There are many technologies available for organic matter residue

(OMR) oxidation and metal ion removal: these include physical [3], electrochemical [4], biological [5] and their combinations [6].

Water treatment technologies have been successfully employed for the oxidation of dyes [7, 8], pesticides and pharmaceuticals [9]. Among such OMR, azo dyes are of particular importance as they are intensively used in the textile, leather and paper industries. The colour and odour of azo dyes are strong and pose serious environmental and health issues for living communities [10]. Several methods have been employed to degrade azo dyes such as anodic oxidation, electro Fenton combined with anodic oxidation [11], photo Fenton [12], adsorption over a novel graphite intercalation material known as Nyex® 1000 [13] and coagulation using refined laterite soil [14]. However, these processes have many disadvantages, which include complexity of scale-up and sometimes expensive electrodes materials. The selection of low cost, long life electrode materials, which can achieve the complete mineralization of organics, is challenging, since many investigations have utilised expensive boron doped diamond (BDD) and dimensional stable anodes DSA coated materials. The development of simple and efficient electrochemical technologies is important in the realisation of efficient OMR oxidation issues on the industrial scale.

Photocatalytic oxidation of OMR using titanium dioxide has been reported as an effective process due to its high efficiency, low cost and lower toxicity [15]. Considerable research has been conducted onto TiO<sub>2</sub> nanoparticles as a photocatalyst for the oxidation of OMR such as phenol with oxidation efficiency of 51% [16] and RB-5 dye with removal efficiency of up to 95% [17]. Titanium dioxide has a band gap of 3.0-3.2 eV and has been synthesized by thermo-hydrolysis process in acidic conditions and has provided

substantial results with reported conversion of 95% for the photocatalytic oxidation of 4-methoxybenzyl alcohol [18].

Similarly, nanotubes derived from  $\text{TiO}_2$  are of particular interest because they have the same photocatalytic activity as titanium dioxide but can provide greater surface area and under UV light they lead to the oxidation of OMR [19]. The self-ordered titanium dioxide nanotubes produced by anodization of Ti foil, provide the ability to conduct photocurrent with greater efficiency due to their larger surface area and structure [20]. The  $\text{TiO}_2$  nanotubes attached to the titanium foil substrate, enhance the movement of the photo-illuminated electrons that benefit the photocatalytic oxidation process of 4-chlorophenol as the organic oxidation increased under acidic conditions ( $\text{pH} = 3.25$ ) and activated the  $\text{TiO}_2$  nanotubes photocatalyst. It has been reported that 95 % of 4-chlorophenol was efficiently degraded in a highly acidic ( $\text{H}_2\text{SO}_4$ ) medium [21, 22].

Nanoparticulate titanium dioxide (Degussa P25) has been electrophoretically deposited on a fluoride-doped tin oxide substrate to create dye-sensitized solar cells, followed by post thermal treatment at  $450^\circ\text{C}$  to improve the stability of the coating [23]. In the nanoparticulate titanium dioxide photocatalyst, photons adsorbed at energy greater than 3.2 eV, which corresponds to the energy to excite an electron to the conductive band, promote the formation of positive hole at the valance band as shown in equation (2.7) in section 2.8. The oxidation of water is initiated by means of positive hole pairs at the valance band, forming short lived and powerful oxidizing agent  $\bullet\text{OH}$  radicals as indicated in equation (2.8) [24], which are capable to degrade and mineralize the organic matter residue to carbon dioxide and water [25]. Further, equations (2.9), (2.10) and (2.11) indicates the formation of oxidative radicals formed by the reaction of valance band

electrons with the superoxide such as  $O_2^{\bullet-}$ . Equations (2.12) and (2.13) involve the production of hydrogen peroxide and subsequent formation of hydroxyl radicals,  $\bullet OH$  [25].

Since more advanced films are required for an effective and larger surface area for photocatalytic oxidation, it is proposed that TiNTs are deposited by anodic electrophoretic deposition (EPD) over the substrate. In previous studies the preparation of high purity nanotubes revealed that TiNT have multi layered structure [26] and electrodeposited polypyrrole coated TiNT composite shows an increase in hardness structure of 53 % as compared to the polypyrrole film only [27].

Another study, reports that TiNTs are suitable coatings for the photooxidation of rhodamine-B dye due to their large surface area, and found to be 20 % more efficient than the traditional Degussa P25  $TiO_2$  particles [28]. The selection of the substrate to deposit the TiNT should aim to high space-time and space-velocity which can be achieved by a substrate with a defined morphology and efficient mass transport of the effluent over its surface which ultimately provide efficient oxidation. RVC is a good candidate because of its honeycombed structure with high corrosion resistance under certain circumstances, thermal and electrical conductivities and lower thermal expansion [29]. The void volume (97%) and surface area ( $65\text{cm}^2\text{ cm}^{-3}$ ) of RVC are high with low resistance to fluid flow in a closed loop reactors and filter press flow cells [29] and has already been employed for the electro Fenton oxidation of azo dyes [11]. Other materials such as boron doped diamond (BDD) electrodes and perforated dimensional stable anodes (DSA) metal mesh are commercially available but are substantially more expensive than RVC and carbon felt. The use of lower cost carbonaceous alternatives like carbon foam and felt is worth

highlighting due to their high morphology and porosity [30]. Another low cost material incorporated into the TiNT is  $\text{PbO}_2$ . There are very few studies of the anodic deposition of TiNT over the  $\text{PbO}_2/\text{RVC}$  substrate with subsequent electrochemical oxidation of azo dyes. Some reports showed decolourisation of methyl orange to 98 % by using composite coatings containing RVC (45 ppi)/ $\text{PbO}_2/\text{TiNT}$  anodes [30].  $\text{TiO}_2$  influencing the electrodeposition of  $\text{PbO}_2$  and improved the formation of  $\text{PbO}_2$  layer due to the extra nucleation surfaces produced by  $\text{Ti-O}^\bullet$  radicals formed due to reaction between the  $\text{TiO}_2$  and  $^\bullet\text{OH}$  radical [31]. RVC is employed to produce hydrogen peroxide by the reduction of oxygen and produce the Fenton reactant which is used to oxidase formic acid [32]. RVC is also used for removing metal ions such as Cr (VI) [34] and Zn(II) in a parallel plate reactor with flow recirculation [33] and the removal of copper and nickel ions however, hydrogen evolution is a secondary unwanted reaction [34, 35]. The proposed methodology for the deposition of TiNT over the RVC substrate produces an inexpensive novel coating that can be used for advanced processes, such as anodic oxidation, as  $\text{TiO}_2$  nanotubular arrays and titanium based electrodes have been successfully utilized for the anodic oxidation of organic compounds [36]. Similarly, carbon based modified graphite cathodes were used in previous studies for the advanced oxidation processes to degrade azo dyes and achieved a mineralization of up to 80 % [37].

In this work, the focus is on the anodic electrophoretic deposition of TiNT on RVC substrate that are subsequently used for the photocatalytic oxidation of RB-5 dye contained in alkaline electrolytes. The deposition of TiNT was favoured by the porosity and morphology of RVC. SEM imaging was used to study the morphology of the deposited, while the oxidation kinetics of methylene blue dye during the photocatalysis was evaluated.

## 5.2 Experimental details

Tetrabutylammonium hydroxide (TBAOH), acetone and methylene blue dye reagent grade were purchased from Sigma Aldrich, while ethanol 99.86 % (v/v) was obtained from Fischer Scientific and used as received. TiNT preparation included an alkaline hydrothermal treatment of TiO<sub>2</sub> in NaOH, in which 9 g TiO<sub>2</sub> was added in a solution containing 10 mol dm<sup>-3</sup> NaOH (300 cm<sup>3</sup>) was stirred at 700 rpm. After dissolution, the solution was treated in an autoclave for about 22 h at a temperature of 140 °C. The obtained white powder containing titanates was washed with deionised water until a pH 7 was achieved and finally washed with 0.1 mol dm<sup>-3</sup> H<sub>2</sub>SO<sub>4</sub> on a glass filter for 30 min following by a wash with deionised water until pH 7. The resultant sample was vacuum dried at 80 °C [38].

### 5.2.1 Anodic electrophoretic deposition

The RVC substrate was immersed in 70 % nitric acid (Fisher Scientific) at 110 °C for 1 hour followed by thoroughly rinse and left in deionized water for 12 h and then dried at 90 °C overnight in an oven. The anodic electrophoretic deposition was carried out using a solution prepared as follows: a mixture that contained 0.25 g of TiNT and 25 cm<sup>3</sup> of 0.2 mol dm<sup>-3</sup> TBAOH was stirred continuously over 2 days at 700 rpm. The resulted TBAOH-coated TiNT were separated by vacuum filtration and 0.1 g of was transferred to a solution containing 60 cm<sup>3</sup> of ethanol (99.86 % v/v) and stirred with PTFE magnetic stirrer for 2 weeks at 300 rpm. The solution was immediately used for EPD in a 60 cm<sup>3</sup> cell that contained a 100 ppi RVC (1.5 cm × 2 cm × 0.13 cm) anode and a graphite cathode (1.5 cm × 6 cm × 1.2 cm). The interelectrode gap, *d*, was 1 cm and the applied cell potential difference was 15 V (the current was in the range of 0.001-0.003 A). The RVC was

connected using stainless steel alligator clip through pure copper plate in order to ensure electrical conductivity within the circuit.

### **5.2.2 Heat treatment**

Following the EPD process, the TiNT/RVC samples were calcined at 450 °C for 2 hours in air. RVC without TiNT coatings disintegrated at such a high temperature whereas the presence of the TiNT film prevented its oxidation. The TiNT exhibited a more uniform coating over the RVC substrate which has been shown in SEM images in results and discussion.

### **5.2.3 Characterization of the coated substrate**

The TiNT/RVC samples were characterized by field emission scanning electron microscope (SEM), using a JEOL 6500F at an accelerating voltage of 20 kV to observe the surface morphology. Raman spectroscopy confocal microscope (Renishaw, RM 2000) using a light source of 632.8 nm wavelength was used to obtain the spectra. The exposure time was 30 seconds with a 10 % intensity of laser radiation.

### **5.2.4 Photocatalytic Experiments**

The oxidation of  $10 \times 10^{-5} \text{ mol dm}^{-3}$  methylene blue (MB) dye in  $0.5 \text{ mol dm}^{-3} \text{ Na}_2\text{SO}_4$  under 300 W Ceralux model 300 BUV 10 F xenon UV lamp with intensity of  $1.5 \text{ mWcm}^{-2}$  was carried out using 0.001 g of TiNT/RVC and TiNT/RVC calcined cut into circular patterns of 4 mm diameter and 2 mm thickness. The samples were immersed in  $10 \text{ cm}^3$  deionized water containing MB in order to attain the equilibrium conditions for dye adsorption as a separate experiments. Prior to the photocatalytic experiments, the solution

was kept in the dark for 90 min to allow the adsorption of the dye on TiNT/RVC calcined to determine the final adsorption ability of the composite coating.

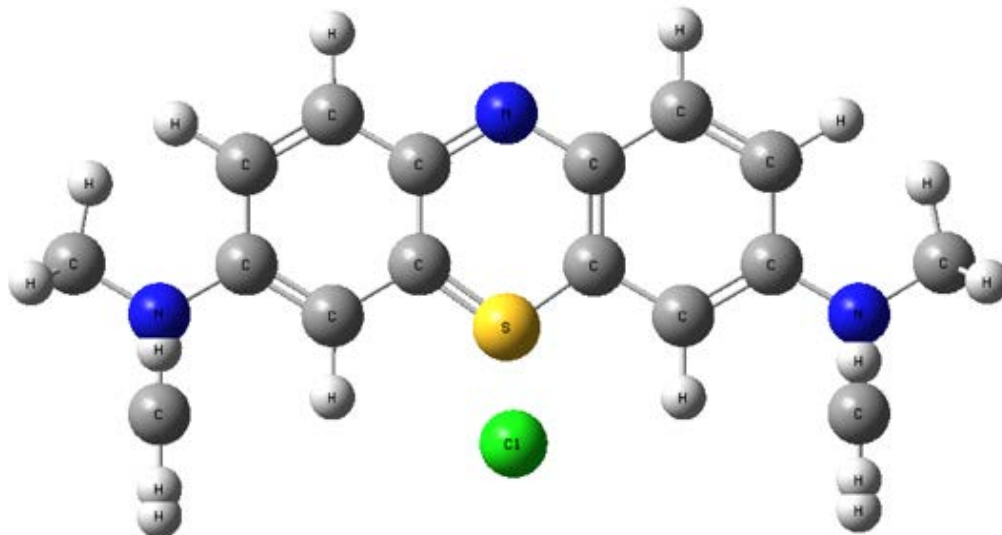
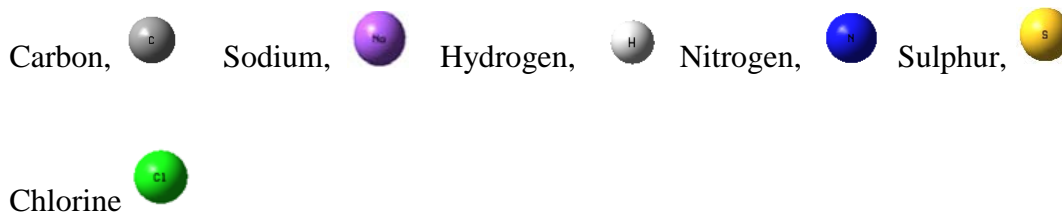


Figure 5.1 Structure of Methylene blue dye where,



Molecular formula;  $C_{16}H_{18}ClN_3S$ , Molecular weight =  $319.58 \text{ g mol}^{-1}$ .

The concentration of the dye was evaluated by UV vis spectra and was  $1.29 \times 10^{-6} \text{ mol dm}^{-3}$  after adsorption. The UV irradiation was provided every 5 min to each solution and the absorbance was measured at a Hitachi U3010 UV-Vis spectrophotometer at a wavelength of 667 nm. A linear calibration curve was used to calculate the concentration of MB. Figure 5.1 shows the typical structure of MB dye.



### **5.2.5 Ultrasonic stability for TiNT/RVC calcined substrate**

The stability of the calcined TiNT/RVC substrate was evaluated by sonication in an ultrasonic bath. The calcined substrate was sonicated for 1 minute in 1 mol dm<sup>-3</sup> acetone and physically no change in the coating was observed by naked eye.

## **5.3 Results and Discussion**

### **5.3.1 Surface characterization of TiNT coated RVC**

Detailed image of the morphology of TiNT coated RVC structures is shown in Figure 5.2 (a-e). Figure 5.2(a) shows the characteristic rigid honeycomb structure of the RVC coated with TiNT (non-calcined) with a uniform layer covering the front strands on the surface of the substrate. The strands of the RVC that are further deep into the RVC structure are also uniformly coated but the back surface behind the front of the strands might receive less amount of TiNT. Figure 5.2 (b) shows agglomerated electrodeposited TiNT over front strand of RVC and found completely covered.

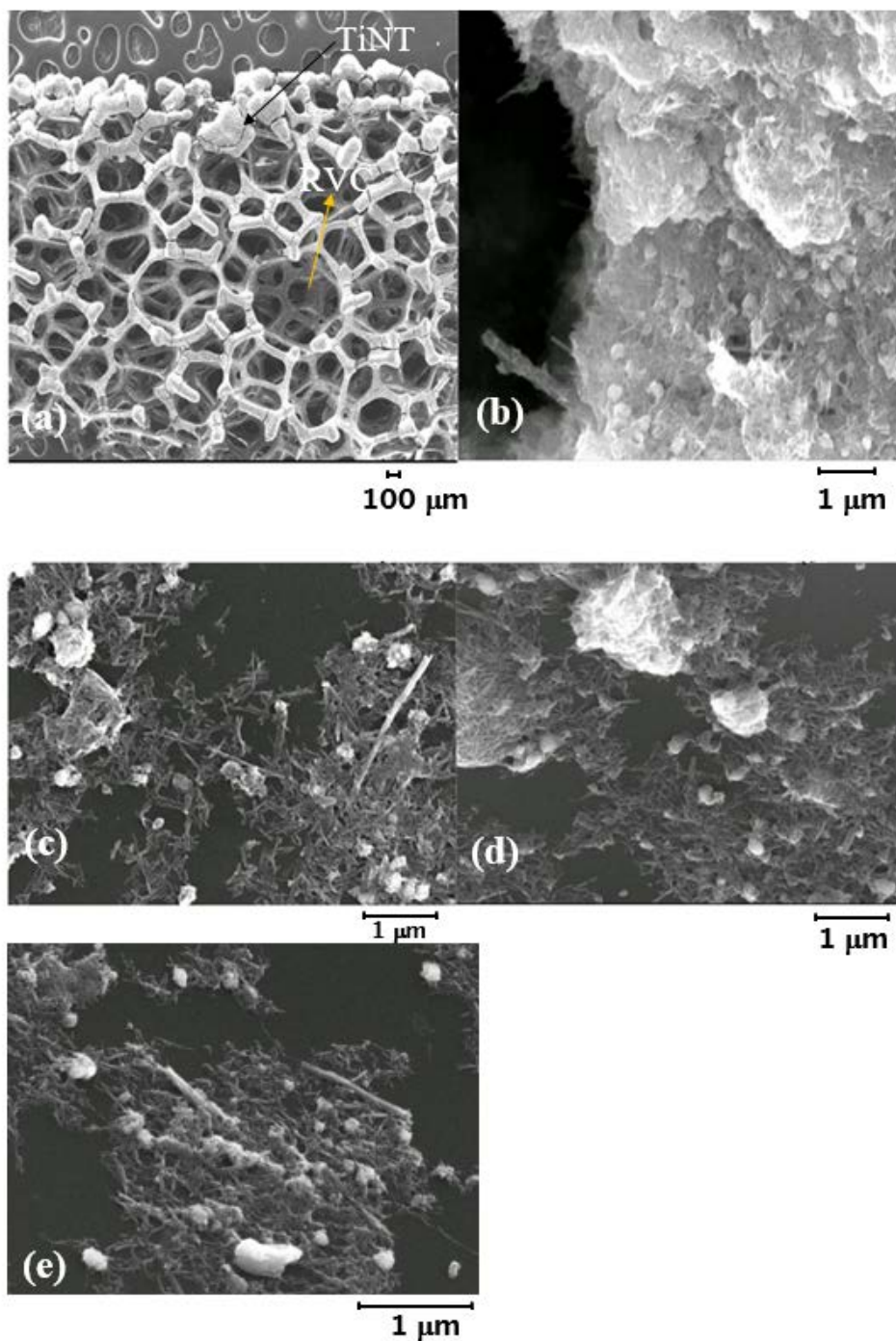


Figure 5.2 SEM images of TiNT coatings over the RVC substrate obtained by anodic electrophoretic deposition (a) TiNT/RVC layers at  $30 \times$  magnification, (b) TiNT/RVC at  $15000 \times$  magnification (c) TiNT/RVC at  $17,000 \times$  magnification (d) TiNT/RVC at  $18,000 \times$  magnification (e) TiNT/RVC at  $20,000 \times$  magnification.

Figure 5.2 (c) shows a deeper inside of the RVC structure (20,000 magnification), where TiNT agglomerates, of around 100 nm, are scatter on the RVC surface. Figures 5.2 (d) and 5.2 (e) show deeper layers inside the RVC that contain fewer TiNT covering the RVC surface. The porosity of RVC helps to improve the amount of deposited of TiNT and obtain uniform and homogenous coating over the its surface substrate however deep inside the RVC the coating is less uniform due to the fact that the strand in the front physically obstruct those at the inside. The sharp boundaries of agglomerates is an evidence of the presence of TiNT with regular structures of 30  $\mu\text{m}$  in length. The images of TiNT over RVC resembles with studies from literature where TiNT were synthesized by using layer by layer immersion technique and hydrothermal synthesis method using  $\text{TiO}_2$  (P25) [40] [41]. Due to reasonable bulk thermal conductivity of RVC (0.033 - 0.050  $\text{W m}^{-1} \text{ }^\circ\text{C}$ ) [42], the deposited TiNT coatings are consistent and stable against high temperature calcination treatment.

Figure 5.3 (a-b) show images of the RVC coated substrates after 1 hour calcination at 450  $^\circ\text{C}$  that converts the TiNT from the titanate to the anatase phase, which is photocatalytically active for the oxidation of methylene blue dye. Figure 5.3 a is a general overview of the TiNT coated RVC after calcination while Figure 5.3 b shows the layer of TiNT in more detail. The delaminated part appeared due to heat treatment as thermal expansion coefficient tends to reduce the compact nature of RVC. Despite the delamination, the figure shows that the layer of TiNT is uniform over the strands at the front of the RVC structure and they remained strongly attached to the surface even after the heat treatment. The uncoated areas of RVC oxidase at high temperatures and the carbon disintegrates whereas the coated areas remained intact due to the protection of the

mechanical integrity of the RVC structure provided by the TiNT coating. Surface defects also appeared over the substrate, which happened due to the nitric acid heat treatment producing breathing mode for disorder band over RVC surface and finally assists the attachment of TiNT coatings over the RVC surface due to the presence of functional groups. Due to these surface changes in RVC after heat treatment, the nanotubes strongly connected with the substrate even after the calcination at 450°C.

It can be possible to improve the porosity of the RVC surface by nitric acid treatment and forming more carboxylic group [41], which in turn enhances the amount of electrodeposited TiNT over the RVC substrate.

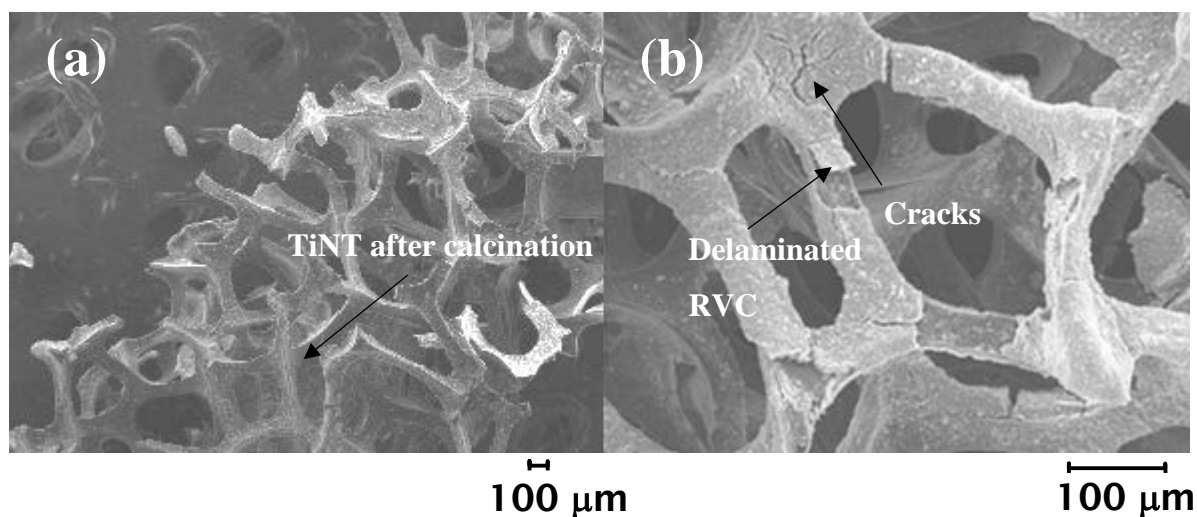


Figure 5.3 SEM images of calcined TiNT/RVC substrate obtained by anodic electrophoretic deposition (a) TiNT/RVC layers at 30 × Magnification (b) TiNT/RVC inside layer 2 at 160 × Magnification.

Figure 5.4 a shows a closer detail of an RVC strand coated with TiNT before the calcination. The cross-sectional view of the modified RVC surface allows to calculate the

thickness of TiNT, which appeared to be *ca.* 30  $\mu\text{m}$ . The film thickness is uniform due to the use of the surfactant TBAOH which improves the wettability and reduce the surface tension, increases the electron transfer and the electrical conductivity of the electrolyte [42].

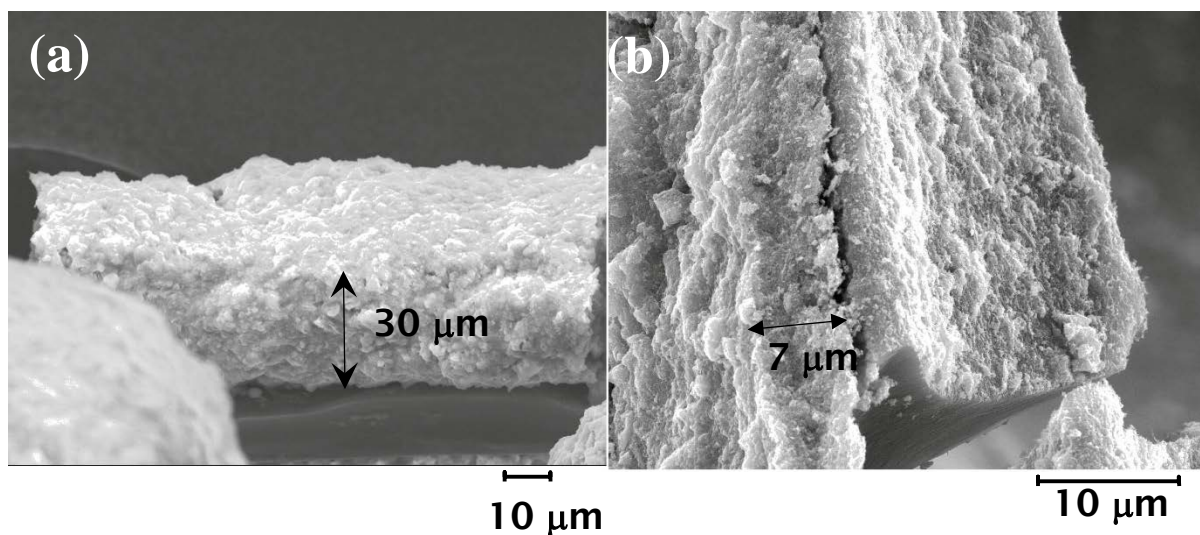


Figure 5.4 SEM images of TiNT coatings over the RVC substrate obtained by anodic electrophoretic deposition (a) TiNT/RVC (non-calcined) layer thickness (b) TiNT/RVC (calcined) layer thickness.

Figure 5.4 b shows a view of the calcined coating on the RVC with a thickness layer of approximately *ca.* 7  $\mu\text{m}$ . The TiNT seems to have a compact layer even after calcination.

Raman spectroscopy was used to observe the phase changes associated with TiNT deposition over RVC substrate and the effects of calcination over the substrate. The Raman spectra of TiNT/RVC substrate before and after calcination are presented in Figure 5.5. The spectrum that corresponds to the non-calcined TiNT/RVC shows a large

peak at  $145\text{ cm}^{-1}$  and smaller peaks at  $278$  and  $447\text{ cm}^{-1}$ , the former correspond to the presence of the titanate phase of TiNT.

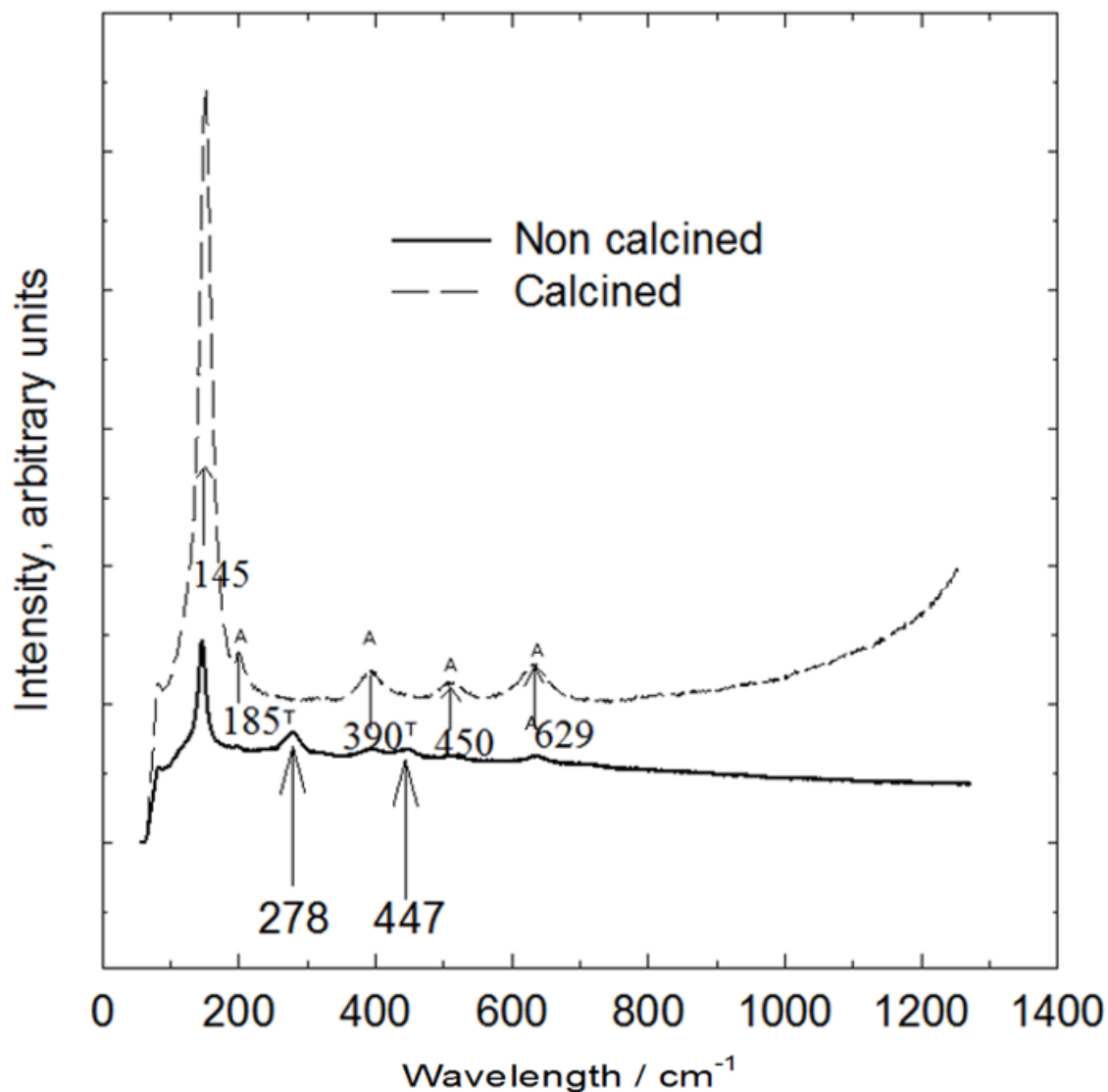


Figure 5.5 Raman spectra of the TiNT/RVC obtained by anodic electrophoretic deposition non-calcined and calcined at  $450\text{ }^{\circ}\text{C}$ .

After calcination the anatase phase gives rise to Raman bands at  $151$ ,  $185\text{ cm}^{-1}$ ,  $390\text{ cm}^{-1}$ ,  $450\text{ cm}^{-1}$  and  $629\text{ cm}^{-1}$  indicating that the heat treatment converted the substrate from titanate to anatase phase as reported in the literature [43-46]. Figure 5.5 also shows peaks

at  $278\text{ cm}^{-1}$  and  $447\text{ cm}^{-1}$  for non-calcined coating which disappeared after calcination indicating a phase transformation of the titanate to the anatase phase.

### 5.3.2 Photocatalytic oxidation of methylene blue

Figure 5.6 shows the normalized concentration of methylene blue dye after 20 min of photocatalytic oxidation with RVC, RVC/TiNT and calcined RVC/TiNT. The initial concentration of methylene blue dye was  $1.29 \times 10^{-6}\text{ mol dm}^{-3}$ . The electrophoretically deposited TiNT coating on the RVC substrate improves the oxidation of MB dye by about 20 % after 20 min of UV radiation treatment in comparison to pre-treated RVC alone. Similar experiments performed by Lin *et al.* for decolourisation of methylene blue for open-ended TiNT films under UV irradiation resulted in 100 % color removal in addition to water splitting [47].

In the case of calcined TiNT/RVC, the percentage of dye discolouration was about 91 % in 20 min (Figure.5.6). This is due to the synergetic photocatalytic effect similar to the results reported in the literature for graphene/TiO<sub>2</sub> (P25) under UV light irradiation for oxidation of methylene blue dye [48]. The synergetic effect produce charge separation which reduce the expected re-combination of holes and electrons thereby producing active photo induced charge separation which enhances the number of holes taking part in the active photo oxidation process [49]. In another example the discolouration and mineralization of Blue V dye, TiO<sub>2</sub> based photo-catalyst deposited with gold metal particles a mineralization of 67 % and discolouration of 93 % was reported [50].

The time dependent profiles of the normalised concentration  $c/c_0$  for the photocatalytic oxidation of the dye using RVC, RVC/TiNT and RVC/TiNT (calcined) are shown as a semi logarithmic plot in Figure 5.7.

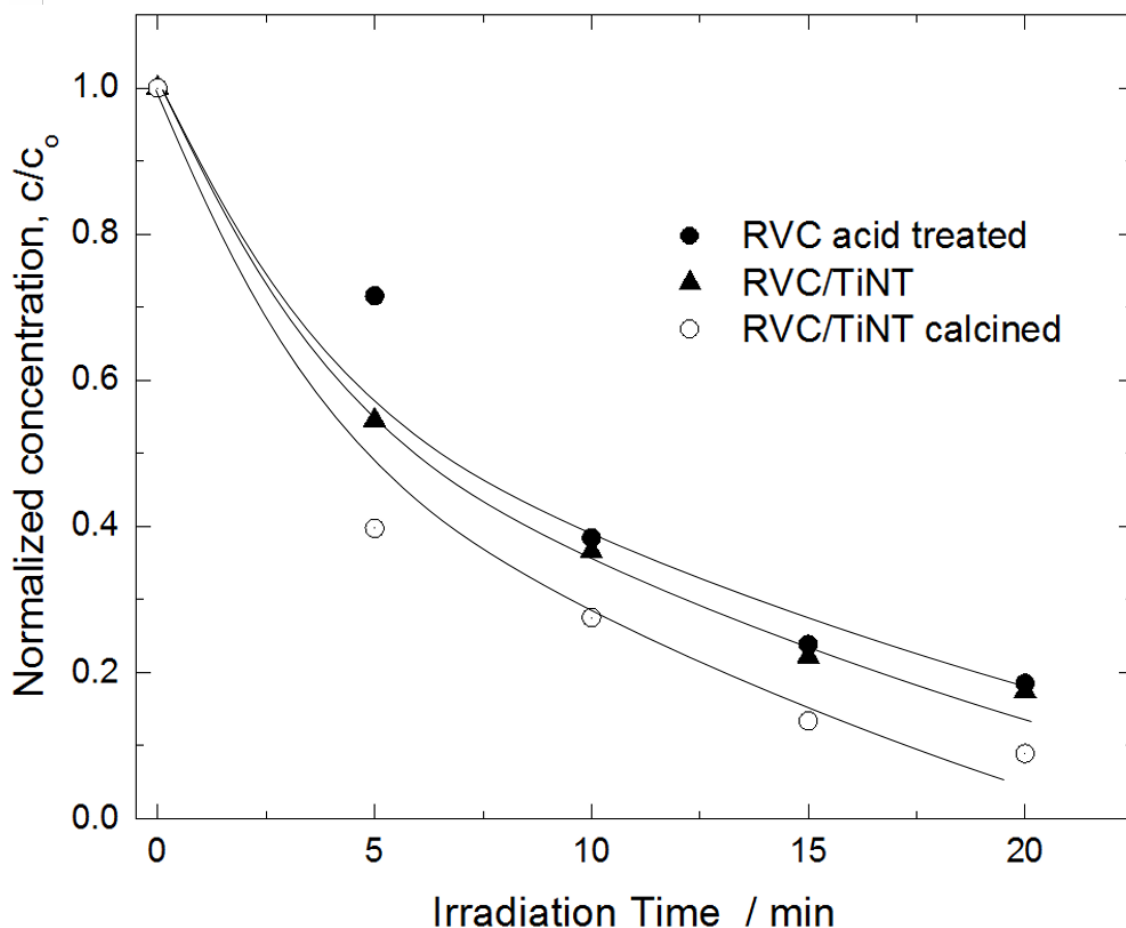


Figure 5.6 Photocatalytic oxidation of  $1.29 \times 10^{-6} \text{ mol dm}^{-3}$  methylene blue dye and  $0.5 \text{ mol dm}^{-3} \text{ Na}_2\text{SO}_4$  illuminated by UV radiation by using (●) RVC acid treated, (▲) TiNT/RVC and (○) TiNT/RVC calcined (Experimental conditions: UV lamp intensity =  $1.5 \text{ mW cm}^{-2}$ ,  $T = 25 \text{ }^\circ\text{C}$ ).

The linear data for the oxidation on different electrodes suggests a pseudo- first order reaction kinetics for the oxidation of methylene blue dye according to the equation 2.20 in section 2.9. The comparison of the pseudo rate constant  $k$  presented in Table 5.1 shows



that values are  $-0.0894 \text{ min}^{-1}$ ,  $-0.0879 \text{ min}^{-1}$ ,  $-0.1185 \text{ min}^{-1}$ , for the RVC, TiNT/RVC and calcined TiNT/RVC, respectively.

These values are found to be higher (95%) than the values reported for open ended TiNT and closed ended TiNT with constant rate values of  $0.0035 \text{ min}^{-1}$  and  $0.0046 \text{ min}^{-1}$  respectively [47]. These results also compare favourably with study regarding the photocatalytic oxidation using  $\text{TiO}_2$ /Carbon felt substrate which reported oxidation rate values of  $0.044 \text{ min}^{-1}$  for volatile organic compounds [51]. The faster rate of discolouration is due to the better support provided by the RVC to TiNT.

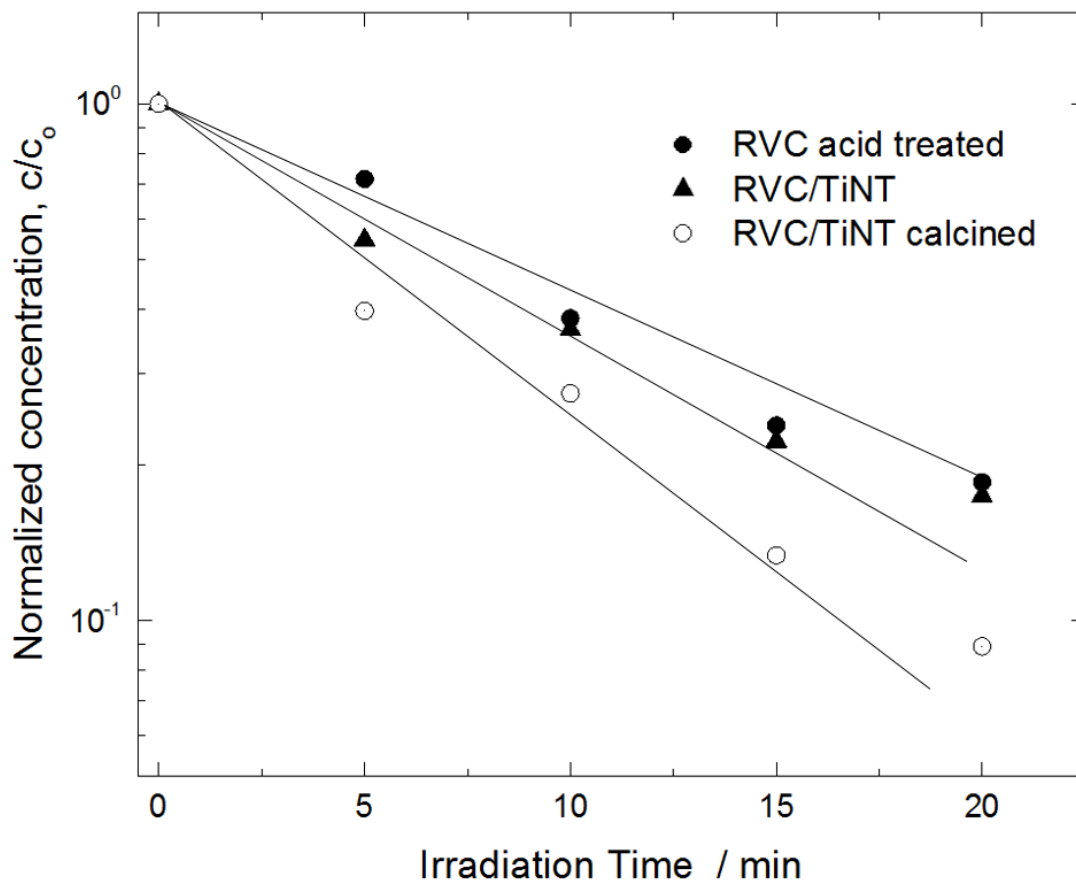


Figure 5.7 Photocatalytic pseudo oxidation kinetics of  $1.29 \times 10^{-6} \text{ mol dm}^{-3}$  methylene blue dye and  $0.5 \text{ mol dm}^{-3} \text{ Na}_2\text{SO}_4$  methylene blue dye illuminated by UV radiation by using ●) RVC acid treated, ▲) TiNT/RVC and ○) TiNT/RVC calcined (Experimental conditions: UV lamp intensity =  $1.5 \text{ mW cm}^{-2}$ ,  $T = 25 \text{ }^\circ\text{C}$ ).

The calcination of nanotubes increases the rate of photocatalytic activity by around 26 % in comparison to the non-calcined TiNT/RVC as seen in Figure 5.7. This increase can be observed from the values of the pseudo rate constant  $k$ . The annealing converted TiNT to the anatase phase which improved the photocatalytic activity. In case of TiNT/RVC, the methylene blue discolouration was 82 % and found lower as compared with calcined substrate which was 91% in 20 min. This is due to the absence of anatase phase in the

photocatalyst (TiNT) on the substrate; the TiNT photocatalyst loading over the surface of RVC was  $0.103 \text{ mg cm}^{-2}$ . The difference in the photocatalytic activity of both substrates i.e. TiNT/RVC calcined and TiNT/RVC non-calcined ascribed due to the combination of electron hole pairs, which scatter the incident UV irradiation at an intensity of  $10 \text{ mW cm}^{-2}$  and allow less number of holes to participate in the photocatalysis [47]. The crystal structure of TiNT without calcination is less photocatalytic in comparison with calcined samples, as shown from the photocatalysis results.

<b>Substrate</b>	<b>Optimum conditions</b>	<b><math>-k / \text{min}^{-1}</math></b>	<b>Reference</b>
RVC	pH = 3, 25 °C, UV intensity $1.5 \text{ mW cm}^{-2}$	0.0894	In this study
TiNT/RVC	pH = 3, 25 °C, UV intensity $1.5 \text{ mW cm}^{-2}$	0.0879	In this study
TiNT/RVC (Calcined)	pH = 3, 25 °C, UV intensity $1.5 \text{ mW cm}^{-2}$	0.1185	In this study
TiNT/FTO	UV intensity 10 $\text{mW cm}^{-2}$	0.0035	[47]

Substrate	Optimum conditions	$-k / \text{min}^{-1}$	Reference
TiO <sub>2</sub> / CF	300W mercury lamp, pH = 3 to 9	0.044	[51]
TiNT / O <sub>2</sub>	UV intensity 12 mW cm <sup>-2</sup>	0.0040	[52]

Table 5.1 Comparison of pseudo rate constants for photocatalytic oxidation of methylene blue dye by RVC, TiNT/RVC and calcined TiNT/RVC and other related values from selected literature.

#### 5.4 Conclusions

This work demonstrates the deposition of TiNT coatings over RVC substrates by anodic electrophoresis. After the acid treatment the RVC substrate showed more active functional groups over its surface. These functional groups assisted the deposition of TiNT and improved homogeneity. Raman studies revealed that upon calcination of TiNT/RVC coating up to 450 °C the anatase phase was formed. These TiNT/RVC composites have been used to study the oxidation kinetics of methylene blue solution. The calcined TiNT/RVC substrate showed a pseudo first order decontamination kinetics and 91 % of photocatalytic discolouration of the dye was achieved, which arises due to the anatase phase of TiNT enhanced by the calcination process. The rate of decolourisation due to anatase phase was 32.5 % greater than the RVC alone in 20 min. Thermal resistance of RVC is also improved by TiNT coating deposition. Therefore, these electrodes could potentially benefit the motive of environmental remediation of

wastewater by employing low cost efficient electrodes like RVC in combination with TiNT as an advanced coating material.

## 5.5 References

1. D. Seckler, U. Amarasinghe, D. Molden, R. De Silva, R. Barker, World water demand and supply, 1990 to 2025: Scenarios and issues, International Irrigation Management Institute (IIMI) IIMI Research Report , Colombo, Sri Lanka, 19, (1998) <http://www.dx.doi.org/10.3910/2009.019> Accessed: 07 May 2017.
2. V.V. Ranade, V. M. Bhandari, Industrial wastewater treatment, recycling and reuse, first ed., Butterworth-Heinemann / Elsevier Science. (2014).
3. M.M.D. Jiménez, M.P.E. González, V. H. Montoya, Performance of mango seed adsorbents in the adsorption of anthraquinone and azo acid dyes in single and binary aqueous solutions, *Bioresour. Technol.* 100 (2009) 6199-6206.
4. S. Song, J. Fan, Z. He, L. Zhan, Z. Liu, J. Chen, X. Xu, Electrochemical oxidation of azo dye C.I. Reactive Red 195 by anodic oxidation on Ti/SnO<sub>2</sub>-Sb/PbO<sub>2</sub> electrodes, *Electrochim. Acta.* 55 (2010) 3606-3613.
5. Y. Satyawali, M. Balakrishnan, Treatment of distillery effluent in a membrane bioreactor (MBR) equipped with mesh filter, *Sep. Purif. Technol.* 63 (2008) 278-286.
6. J. Wu, M.A. Eiteman, S.E. Law, Evaluation of membrane filtration and ozonation processes for treatment of reactive-dye wastewater, *J. Environ. Eng.* 124 (1998) 272-277.

7. E. Brillas, C.A.M. Huitle, Decontamination of wastewaters containing synthetic organic dyes by electrochemical methods. An updated review, *Appl. Catal., B.* 166–167 (2015) 603-643.
8. M.A. Rodrigo, N. Oturan., M.A. Oturan., Electrochemically assisted oxidation of pesticides in soils and water: a review, *Chem. Rev.* 114 (2014) 8720-8745.
9. E. Brillas, I. Sirés, Electrochemical removal of pharmaceuticals from water streams: Reactivity elucidation by mass spectrometry, *TrAC, Trends Anal. Chem.* 70 (2015) 112-121.
10. K. Singh, S. Arora, Removal of synthetic textile dyes from wastewaters: a critical review on present treatment technologies, *Crit Rev Environ Sci Technol.* 41 (2011) 807-878.
11. Vasconcelos VM, Ponce-de-León C, Nava JL, Lanza MR Electrochemical oxidation of RB-5 dye by anodic oxidation, electro-Fenton and by combining anodic oxidation–electro-Fenton in a filter-press flow cell. *J Electroanal Chem* 765 (2016) 179-187.
12. S. Figueroa, L. Vázquez, A. A. Gallegos, Decolourizing textile wastewater with Fenton's reagent electrogenerated with a solar photovoltaic cell, *Water Res.* 43 (2009) 283-294.
13. F.M. Mohammed, E.P.L. Roberts, A. Hill, A.K. Campen, N.W. Brown, Continuous water treatment by adsorption and electrochemical regeneration. *Water Res.* 45 (2011) 3065-3074.
14. Y.Y. Lau, Y.S. Wong, T.T Teng, N. Morad, M. Rafatullah, S.A. Ong, Coagulation-flocculation of azo dye acid orange 7 with green refined laterite soil, *Chem. Eng. J.* 246 ( 2014) 383-390.

15. J.M.P.Hernández, Y.M.Vong, F.J.Rodríguez,T.W. Chapman, M.I.Maldonado, L.A.Godínez, In situ electrochemical and photo-electrochemical generation of the fenton reagent: A potentially important new water treatment technology, *Water Res.* 40 (2006) 1754-1762.
16. C. Miranda, H. Mansilla, J. Yáñez, S. Obregón, G. Colón, Improved photocatalytic activity of g-C<sub>3</sub>N<sub>4</sub>/TiO<sub>2</sub> composites prepared by a simple impregnation method, *J. Photochem. Photobiol. A.* 25 (2013) 16-21.
17. C. Tang, V. Chen, The photocatalytic oxidation of reactive black 5 using TiO<sub>2</sub>/UV in an annular photoreactor, *Water Res.* 38 (2004) 2775-2781.
18. A.Vincenzo, V. Loddo, M. J. López-Muñoz, C. Márquez-Alvarez, G. Palmisano, L. Palmisano, S. Yurdakal. Home-prepared anatase, rutile, and brookite TiO<sub>2</sub> for selective photocatalytic oxidation of 4-methoxybenzyl alcohol in water: reactivity and ATR-FTIR study, *Photochemical & Photobiological Sciences*, 8 (2009) 663-669.
19. Y.B. Xie, X.Z. Li, Interactive oxidation of photoelectrocatalysis and electro-Fenton for azo dye oxidation using TiO<sub>2</sub>-Ti mesh and reticulated vitreous carbon electrodes, *Mater Chem. Phys.* 95 (2006) 39-50.
20. J.M. Macák, H. Tsuchiya, A. Ghicov, P. Schmuki, Dye-sensitized anodic TiO<sub>2</sub> nanotubes, *Electrochem Commun.* 7(2005) 1133-1137.
21. X. Quan, X. Ruan, H. Zhao, Photoelectrocatalytic oxidation of pentachlorophenol in aqueous solution using a TiO<sub>2</sub> nanotube film electrode, *Environ Pollut.* 147 (2007) 409-414.

22. N. Wang, X. Li, Y. Wang, X. Quan, G. Chen, Evaluation of bias potential enhanced photocatalytic oxidation of 4-chlorophenol with TiO<sub>2</sub> nanotube fabricated by anodic oxidation method, *Chem. Eng. J.* 147 (2009)30-35.
23. J. Bandy., Q. Zhang, G. Cao, Electrophoretic deposition of titanium oxide nanoparticle films for dye-sensitized solar cell applications, *Mater Sci Appl.* 2 (2011) 1427-143.
24. K. Pirkanniemi, M. Sillanpää, Heterogeneous water phase catalysis as an environmental application: a review, *Chemosphere.* 48 (2002) 1047-1060.
25. M.B. Muneer, D. Qamar, M. Tariq, M.A. Faisal, Photocatalysed reaction of few selected organic systems in presence of titanium dioxide. *Appl. Catal., A*, 289 (2005) 224-230.
26. R.K. Ma, T. Sasaki, M. Osada, Y. Bando, Structural features of titanate nanotubes/nanobelts revealed by raman, x-ray absorption fine structure and electron diffraction characterizations, *J. Phys. Chem. B* 109 (2005) 6210-6214.
27. P. Herrasti, A.N. Kulak, D.V. Bavykin, C. Ponce de León, J.Zekonyte, F.C. Walsh, Electrodeposition of polypyrrole–titanate nanotube composites coatings and their corrosion resistance, *Electrochim. Acta.* 56 (2011)1323-1328.
28. R. Savitha, R. Raghunathan, R. Chetty, Rutile nanotubes by electrochemical anodization, *RSC Adv.* 6 (2016) 74510-74514.
29. J. Friedrich, C. Ponce de León, G. Reade, F.C. Walsh, Reticulated vitreous carbon as an electrode material, *J. Electroanal. Chem.* 561 (2004) 203-217.
30. G. Ramírez, F.J. Recio, P. Herrasti, C. Ponce de León, I. Sirés, Effect of RVC porosity on the performance of PbO<sub>2</sub> composite coatings with titanate nanotubes



- for the electrochemical oxidation of azo dyes, *Electrochim. Acta.* 204 (2016) 9-17.
31. A.B. Velichenko, R. Amadelli, V.A. Knysh, T.V. Luk'yanenko, F.I. Danilov, Kinetics of lead dioxide electrodeposition from nitrate solutions containing colloidal TiO<sub>2</sub>, *J. Electroanal. Chem.* 632 (2009) 192-196.
32. G. Zhang, F. Yang, M. Gao, X. Fang, L. Liu, Electro-Fenton oxidation of azo dye using polypyrrole/anthraquinonedisulphonate composite film modified graphite cathode in acidic aqueous solutions, *Electrochim. Acta.* 53(2008) 5155-5161.
33. C. Ponce de León, D. Pletcher, Removal of formaldehyde from aqueous solutions via oxygen reduction using a reticulated vitreous carbon cathode cell, *J. Appl. Electrochem.* 25 (1995) 307-314.
34. F.R.Valadez, C.O. Éxiga, J.G. Ibanez, A.A.Ordaz, S.G.Granados, Electroreduction of Cr (VI) to Cr (III) on reticulated vitreous carbon electrodes in a parallel-plate reactor with recirculation, *Environ Sci. Technol.* 39 (2005) 1875-1879.
35. G.W. Reade, A.H. Nahle, P. Bond, J.M. Friedrich, F.C. Walsh, Removal of cupric ions from acidic sulfate solution using reticulated vitreous carbon rotating cylinder electrodes, *J. Chem. Technol. Biotechnol.* 79 (2004) 935-945.
36. M.M. Saleh, M.H. El-Ankily, M.S. El-Deab, B. El-Anadouli, Electrocatalytic activity of metal-loaded reticulated vitreous carbon electrodes for hydrogen evolution from flowing alkaline solutions, *Bull. Chem. Soc. Jpn.* 79 (2006) 1711-1718.

37. M. Hossein, M.M. Momeni, Preparation and characterisation of TiO<sub>2</sub> nanotubular arrays for electro-oxidation of organic compounds: effect of immobilization of the noble metal particles, *Int. J. Mod. Phys.* 5 (2012) 41–48.
38. D.V. Bavykin, J.M. Friedrich, A.A. Lapkin, F.C. Walsh, Stability of aqueous suspensions of titanate nanotubes, *Chem. Mater.* 18 (2006) 1124-1129.
39. M.J. Frisch, G.W. Trucks, H.B. Schlegel, G.E. Scuseria, M.A. Robb, J.R. Cheeseman, G. Scalmani, V. Barone, B. Mennucci, G.A. Petersson, H. Nakatsuji, Gaussian 09, p. 6492. Gaussian, Inc., Wallingford (2009).
40. G. Mathieu, A. Louvet, N. Keller, V. Keller. Layer-by-layer deposited titanate-based nanotubes for solar photocatalytic removal of chemical warfare agents from textiles, *Angewandte Chemie Int. Edition.* 48 (2009)161-164.
41. O. Kenji, G. Asakura, Y. Tokudome, A. Nakahira, M. Takahashi. Macroporous titanate nanotube/TiO<sub>2</sub> monolith for fast and large-capacity cation exchange, *Chem. Mater.* 27 (2015) 1885-1891.
42. A.R. Czerwiński, Z. Obrębowski, Sz. Siwek, H. Paleska, I. Chotkowski, M. Łukaszewski, RVC as new carbon material for batteries. *J. Appl. Electrochem.* 39 (2009) 559-567.
43. S. Xiaojun, J. Zhang, B. Tian, Facile tailoring of titanate nanostructures at low alkaline concentration by a solvothermal route, *J. Mater. Sci.* 47 (2012) 3855-3866.
44. A. Kukovecz, K. Krisztián, K. János, K. Zoltán, Atomic scale characterization and surface chemistry of metal modified titanate nanotubes and nanowires, *Surf Sci Rep.* 71 (2016) 473-546.

45. S. Li, D. Yihui, G. Meirong, Photocatalytic activity of different morphologies TiO<sub>2</sub> nanofibers, *Appl Surf Sci.* 258 (2012) 8015-8018.
46. S.J. Kim, Y.U. Yun, H.J. Oh, S.H. Hong, C.A. Roberts, K. Routray, I.E. Wachs, Characterization of Hydrothermally Prepared Titanate Nanotube Powders by Ambient and In Situ Raman Spectroscopy, *J. Phys. Chem Lett.* 1 (2010) 130-135.
47. C.J. Lin, Y. Zhang, L. Wang, Y. Zhang, D. Wang, M. Yang, C. Li, Fabrication of open-ended high aspect-ratio anodic TiO<sub>2</sub> nanotube films for photocatalytic and photoelectrocatalytic applications, *Chem. Commun.* 45 (2008) 6031-6033.
48. H. Zhang, X. Lv, Y. Li, Y. Wang, J. Li, P25-graphene composite as a high performance photocatalyst, *ACS Nano.* 4 (2010) 380-386.
49. Y. Wang, R. Shi, J. Lin, Y. Zhu, Significant photocatalytic enhancement in methylene blue oxidation of TiO<sub>2</sub> photocatalysts via graphene-like carbon in situ hybridization, *Appl. Catal. B.* 100 (2010) 179-183.
50. V. Vaiano, G. Iervolino, D. Sannino, J.J. Murcia, M.C. Hidalgo, P. Ciambelli, J.A. Navío, Photocatalytic removal of patent blue V dye on Au-TiO<sub>2</sub> and Pt-TiO<sub>2</sub> catalysts, *Appl. Catal. B.* 188 (2016) 134-146.
51. Y. Shen, W. Wang, K. Xiao, Synthesis of three-dimensional carbon felt supported TiO<sub>2</sub> monoliths for photocatalytic oxidation of methyl orange, *J. Environ. Chem. Eng.* 4 (2016) 1259-1266.
52. S. Weon, C. Wonyong, TiO<sub>2</sub> Nanotubes with Open Channels as Deactivation-resistant Photocatalyst for the Oxidation of Volatile Organic Compounds, *Environ. Sci. Technol.* 50 (2016) 2556-2563.



## Chapter 6: **Grass inspired anodised ZnO-TiO<sub>2</sub> core-shell decorated by PbO<sub>2</sub> for the oxidation of reactive black-5 dye**

In this chapter, zinc oxide structures are deployed for important applications in photocatalytic waste water treatment. The operational conditions to produce ZnO nanowires by electrochemical anodisation over Zn metal plate were determined. The surface of the anodised nanowires were dip-coated with TiO<sub>2</sub> in order to produce a core-shell coating of ZnO-TiO<sub>2</sub>. PbO<sub>2</sub> was subsequently electrodeposited over the coating producing hybrid core (ZnO-TiO<sub>2</sub>)-shell (PbO<sub>2</sub>) coating. The structural and morphological characteristics of this hybrid coating were examined by field emission scanning electron microscopy (FESEM) and Raman spectroscopy which provided information on the chemical composition. The electrochemical and photocatalytic behaviour of the coatings were tested for the removal of RB-5 dye. The electrochemical oxidation involved the formation of free radicals over the hybrid core (ZnO-TiO<sub>2</sub>)-shell (PbO<sub>2</sub>) surface and assisted in the decomposition of RB-5 dye. The photocatalytic characteristics of the coating were improved by calcination at 400 °C for 60 min in air, creating the photocatalytically active anatase TiO<sub>2</sub> and wurtzite ZnO phases. The removal mechanism was driven by the synergetic photocatalytic effect imparted by the photo-induced holes and the free electron acceptors produced under UV light illumination.

### **6.1 Introduction**

ZnO has been shown to offer a flexible coating having significant applications in many scientific areas including photocatalysis [1], piezoelectrics [2], photovoltaics [3], gas chemical sensing [4] and water splitting [5]. Its useful characteristics that include versatile electron mobility and its band gap of 3.37 eV permits absorption in the zone of UV

irradiation [6]. One of the most attractive characteristics is its structural morphology which can range from micron to nanometre features, after anodizing Zn-based materials.

Nanostructures obtained from ZnO can be classified as Zn nanowires. However, these nanowires can be generated on different substrates by adopting techniques such as atomic layer deposition [7], chemical vapour deposition [8], hydrothermal growth [9] and sol gel deposition [10]. Ordered growth of nanowires produced by these techniques encounters a lower growth rate, which increases reaction time to obtain a required length of the nanowires. Another issue is the requirement of high temperatures ( $> 900^{\circ}\text{C}$ ) [7] which requires expensive setups and limits the choice of substrate to one that can withstand such high temperatures.

Electrodeposition resolved these potential problems at room temperature and has been employed extensively to grow ZnO nanowires [11, 12]. Another technique employed by Hu. *et al.* for ZnO nanowires over Zn foil was anodising [13]. Nanodots, nanoflowers, nanostripes and nanowires have all been synthesised by using solutions with basic electrolytes, e.g. NaOH or acidic solutions containing hydrofluoric acid [14, 15, 16, 17, 18].

ZnO nanoarrays can be improved by controlled synthesis of ZnO-TiO<sub>2</sub> core-shell structures, which can enhance the photocatalytic properties of the composite [19]. Nanowires are contributing to synthesize advanced materials with improved photocatalytic and electrocatalytic characteristics that yield robust and unusual substitute that contribute towards water splitting [5] and photoelectrochemical removal of organic materials [20].

The efficiency of PbO<sub>2</sub> in anodic oxidation process has been verified by many authors [21, 22, 23]. Recent studies have also evidenced the synthesis of more efficient electrode

materials such as  $\text{PbO}_2$  or titanium dioxide nanotubes produced with different materials that contribute to the improvement for the decolourisation of Reactive Blue 194 [21], Acid Black 194 [22] and Reactive Red 195 [23] dyes with enhanced current efficiencies. Some Studies have reported that  $\text{PbO}_2$  coatings can be preserved from corrosion by applying anodic potential for its potential application, while at cathodic potential the dissolution of coatings may occur [24].

More durable  $\text{PbO}_2$  coatings are required for advanced economic treatments systems to highlight the commercial significance of  $\text{PbO}_2$  electrode for environmental oxidation of organic compounds. Having this in mind, the goal of this study is to synthesize Zn nanowires by using Zn metal (99.99 %) in neutral bicarbonate solutions over Zn plates and further produce ZnO- $\text{TiO}_2$  core-shell was prepared by dip coating which can serve as a support for electrodeposited  $\text{PbO}_2$ , forming a hybrid ZnO- $\text{TiO}_2$  core-shell  $\text{PbO}_2$ . These core shell formed fascinating nanoflower-like nanostructures that can be used for electrochemical and photocatalytic oxidation of RB-5 dye. .

## **6.2 Experimental Details**

Reagent grade lead nitrate, sodium bicarbonate, sodium sulphate, ethanol (98 %) and acetone obtained from Fischer scientific and titanium (IV) butoxide and reactive black-5 (RB-5) dye were purchased from Sigma Aldrich, while Boric acid was purchased from Riedel-de Haen and all reagents were used as received.

### **6.2.1 Synthesis of Zn nanoforest, grass-like nanowires by anodising**

Zinc plates samples were pre-treated in an ultrasonic bath using acetone for 5 min to separate of any accumulated dirt and grease. After the pre-treatment the samples were

polished with sand paper (2000 grit) and washed with ethyl alcohol and ultrapure water to detach any remaining dust. Anodizing experiments were performed in an undivided 100 cm<sup>3</sup> glass cell. The polished Zn plates of 2 cm × 3 cm × 0.20 cm dimensions were employed as anodes and linked to a power supply via a stainless steel alligator clip. A graphite plate of dimensions 1.5 cm × 6 cm × 1.2 cm was employed as cathode with an interelectrode gap ≈ 1 cm. The solution was magnetically stirred with a 0.06 cm diameter, 0.25 cm long PTFE laminated, cylindrical stirrer (Fischer Scientific) at 200 rev min<sup>-1</sup> to ensure constant concentration of the electrolyte and good mass transport to the Zn plate. The Zn plates were anodised at various concentrations of NaHCO<sub>3</sub>, from 6.8 × 10<sup>-3</sup> mol dm<sup>-3</sup> to 100 × 10<sup>-3</sup> mol dm<sup>-3</sup>. A potential gradient of 5-10 V cm<sup>-1</sup> was provided by imposed a cell potential difference of 5-10 V for 10 min at 25 °C by using 300 W Aim-TTi model EX752M power supply. After the anodization the plates were rinsed thoroughly with deionised water and finally dried with nitrogen for 5 min.

### **6.2.2 Preparation of ZnO-TiO<sub>2</sub> core-shell nanorods structures by dip coating**

The film of Zn nanowires on the Zn plate obtained as mentioned in the previous section were coated with a layer of TiO<sub>2</sub> to synthesize the ZnO-TiO<sub>2</sub> core-shell nanorods structures. A dip coating process was employed for deposition and titanium (IV) butoxide was used as a precursor for the preparation ZnO-TiO<sub>2</sub> core-shell nanorods. 300 μL titanium (IV) butoxide into 10 cm<sup>3</sup> of ethanol were stirred until a clear solution was achieved [25]. The films of Zn nanowires were immersed in this solution for 10 s followed by drying the Zn nanowires were dried and rinsed with D.I water. The films were calcined at 400 °C to obtain ZnO-TiO<sub>2</sub> core-shell nanorods, the samples were left to cool down overnight and washed again with D.I water and dried by stream of nitrogen gas. In order



to obtain a uniform coating, a 2 stage deposition was performed with subsequent calcination. Finally the obtained samples were washed with D.I water.

### 6.2.3 Heat treatment

After dip coating, the Zn nanowires samples were calcined at 400 °C for 60 min in air. Annealing yield wurtzite phase of ZnO and anatase phase of TiO<sub>2</sub> without affecting the mechanical characteristics of the substrate at such a higher temperature, whereas the presence of the TiO<sub>2</sub> prevented the oxidation of the coating. The ZnO-TiO<sub>2</sub> core-shell nanorod substrate was obtained after heat treatment and showed a more uniform core-shell coating.

### 6.2.4 Anodic electrodeposition

The electrodeposition of Pb(II) on the ZnO-TiO<sub>2</sub> core-shell nanorods substrate was performed in a bath containing 0.1 mol dm<sup>-3</sup> boric acid (to deposit  $\alpha$ -PbO<sub>2</sub>) with 0.01 mol dm<sup>-3</sup> Pb(NO<sub>3</sub>)<sub>2</sub> under galvanostatic conditions at a current density of 5 mA cm<sup>-2</sup> for 30 min to synthesize hybrid ZnO-TiO<sub>2</sub> core-shell PbO<sub>2</sub> coatings. The ZnO-TiO<sub>2</sub> core-shell nanorod substrate, with dimensions 2 cm × 3 cm × 0.20 cm, was used as an anode. A Cu wire was connected using a Zn plated stainless steel alligator clip, to a direct current power supply. A graphite plate with dimensions 1.5 cm × 6 cm × 1.2 cm was employed as a cathode with an interelectrode gap of 1 cm. The electrolyte was magnetically stirred with a 0.06 cm diameter, 0.25 cm long PTFE-coated, cylindrical steel bar at 700 rev min<sup>-1</sup> to ensure constant concentration of the electrolyte.

### 6.2.5 Characterization of coated substrate

The samples obtained after anodization, dip coating and electrodeposition were characterized by field emission scanning electron microscope (FESEM), using a JEOL

6500F at an accelerating voltage of 20 kV to characterise its surface morphology. Raman spectra were obtained using a confocal microscope (Renishaw, RM 2000) fitted with a light source of 632.8 nm wavelength to evaluate the presence of different phases for ZnO-TiO<sub>2</sub> core-shell nanorods and hybrid ZnO-TiO<sub>2</sub> core-shell PbO<sub>2</sub> coatings. The exposure time was 30 seconds with a 10 % intensity of laser radiation.

### 6.2.6 Electrochemical Experiments

The electrochemical studies were conducted by using computer aided PGSTAT302 N potentiostat/galvanostat from Autolab (EcoChemie, Netherlands) by means of Nova 1.11 software. The coatings including ZnO-TiO<sub>2</sub> core-shell nanorods and hybrid ZnO-TiO<sub>2</sub> core-shell PbO<sub>2</sub> coatings mentioned in the previous section were thoroughly washed by using D.I water and cleaned. A solution of 100 cm<sup>3</sup> of  $2 \times 10^{-5}$  mol dm<sup>-3</sup> of RB-5 dye in 0.6 mol dm<sup>-3</sup> of sodium sulphate (background electrolyte) was electrolyzed at 1.0 V vs. [Hg/HgO] NaOH (sat.), pH 3 by addition of H<sub>2</sub>SO<sub>4</sub> and 25 °C. The pH of the electrolyte was very stable during the stirring throughout the electrochemical experiments. Hg/HgO and Pt mesh were employed as a reference and a counter electrode, respectively.

### 6.2.7 Photocatalytic Experiments

The photocatalytic experiments were performed by evaluating the oxidation of  $2 \times 10^{-5}$  mol dm<sup>-3</sup> of RB-5 dye contained in 10 cm<sup>3</sup> of 0.6 mol dm<sup>-3</sup> of sodium sulphate solution at pH 3 under UV irradiation. The 300 W Ceralux model 300 BUV 10 F xenon UV lamp with intensity of 1.5mWcm<sup>-2</sup>. The two catalysts which were produced as ZnO-TiO<sub>2</sub> core-shell nanorods and hybrid ZnO-TiO<sub>2</sub> core-shell PbO<sub>2</sub> coatings were added to the solution. Prior to the photocatalytic experiments, the solution was kept in the dark for 90 min to achieve maximum adsorption of RB-5 dye by both coatings and no significant change in the concentration of the dye was observed after the adsorption studies. The UV irradiation

was provided at 5 min intervals to each RB-5 dye sample at pH 3 containing ZnO-TiO<sub>2</sub> core-shell nanorods and hybrid ZnO-TiO<sub>2</sub> core-shell PbO<sub>2</sub> coatings. The absorbance of the RB-5 in an electrolyte was measured in a Hitachi U3010 UV-vis spectrophotometer at a wavelength of 597 nm. A linear calibration curve fulfilling the Beer-Lambert law was used to determine the concentration of RB-5 from the solutions after oxidation.

### **6.2.8 Ultrasonic stability for coatings**

The stability of the ZnO-TiO<sub>2</sub> core-shell nanorods and hybrid ZnO-TiO<sub>2</sub> core-shell PbO<sub>2</sub> coatings were estimated by sonication in an ultrasonic bath equipped with a transducer, which vibrates perpendicularly to the bottom of the container. The calcined coating was sonicated for 2 min in 0.5 mol dm<sup>-3</sup> acetone.

## **6.3 Results and discussion**

### **6.3.1 Surface characterization of Zn nano forest grass like nanowires**

Figure 6.1a) shows an SEM image of distinctive anodised zinc metal plate of 2 cm × 3 cm × 0.20 cm dimensions. The anodising was conducted in a bicarbonate solution at a cell voltage of 5 V for 10 min. The foil was rinsed with DI water and dried with nitrogen for 10 min. The figure shows that the zinc metal plate was blanketed with a white oxide layer. Further characterization of the samples was carried out to study the morphology of the anodised surface. The cross-sectional view of anodized Zn plate showed in Figure 6.1b). Zn based nanowires (NWs) exhibited forest grass-like structure emerged from the base of surface, as shown in Figure 6.1c).

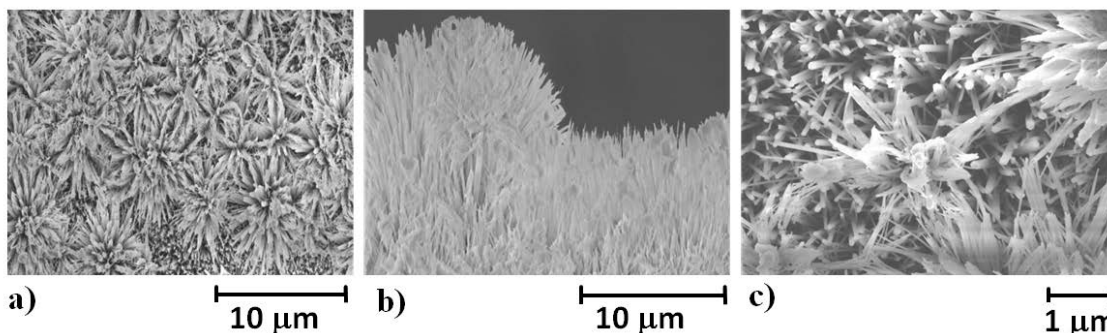


Figure 6.1 FESEM (a) surface morphology (b) cross-sectional view of anodised Zn plate complete film layer over zinc surface with forest grass like structure (c) more magnified image of (a), in an electrolyte containing  $30 \times 10^{-3} \text{ mol dm}^{-3} \text{ NaHCO}_3$  at 5 V for 10 min.

Higher magnification images of the anodized Zn plate displayed that the film is comprised of NWs as shown in Figure 6.2 a), having a diameter in the range 70 to 100 nm as seen in Figure 6.2 b). All NWs had a thin needle like structure as shown in Figure 6.2c).

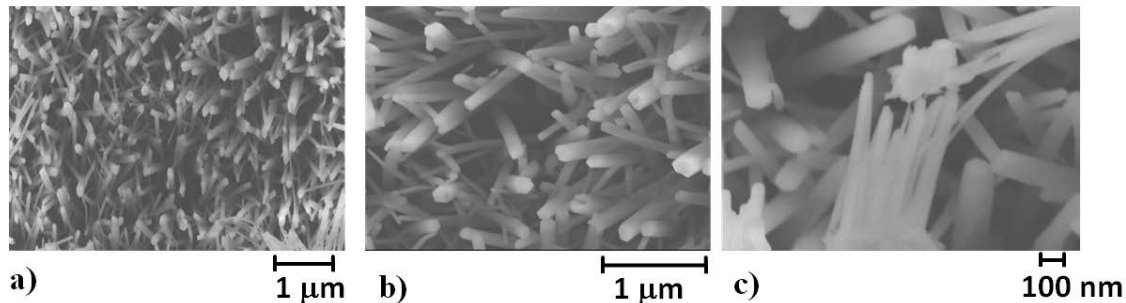
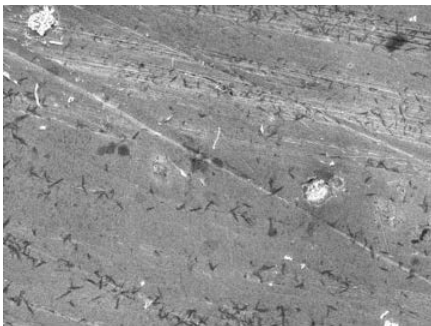
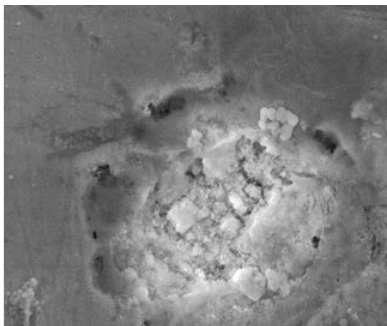
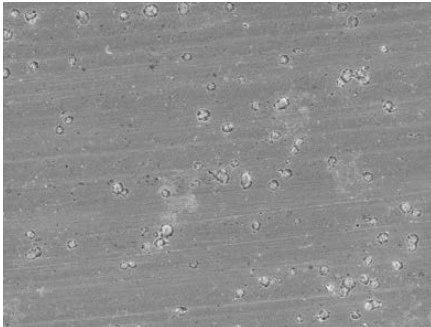
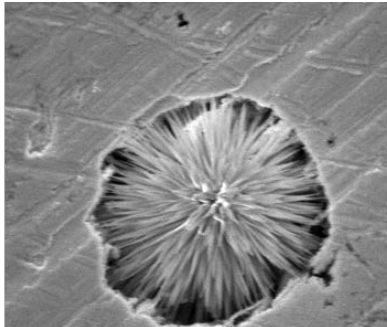
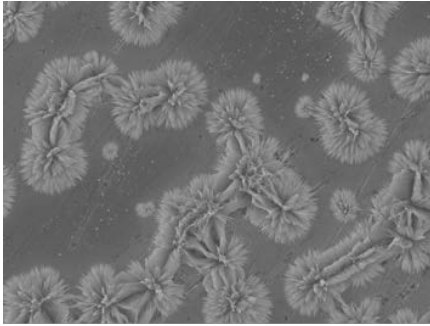
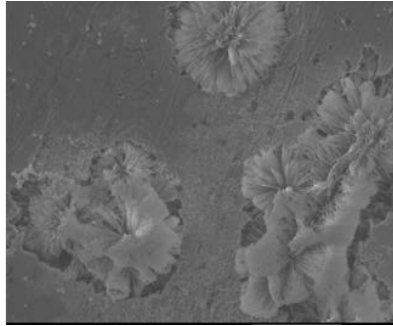
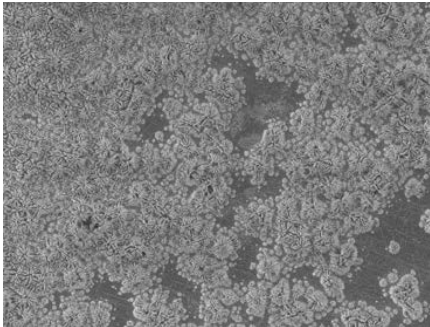
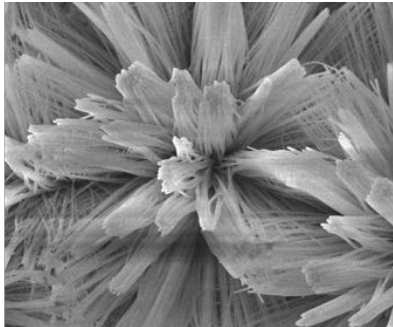
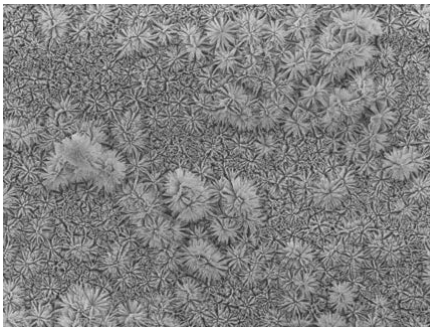
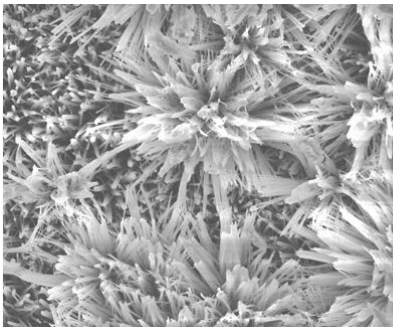
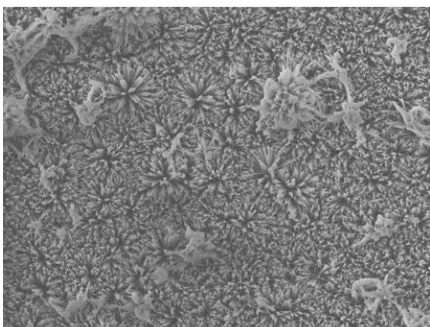



Figure 6.2 FESEM (a) magnified surface morphology of anodized Zn plate (b) the evolution of a layered pattern with regular hexagonal wires complete film layer over zinc surface with forest grass like structure (c) surface morphologies and cross-sections demonstrating the primary development of scattered nanowires in an electrolyte containing  $30 \times 10^{-3} \text{ mol dm}^{-3} \text{ NaHCO}_3$  at 5 V for 10 min.

Zn is a reactive metal and the anodising conditions depend on the applied voltage and the type and concentration of the solution which can modify the anodising, via chemical and electrochemical etching causing, dissolution of the zinc substrate. In order to find the optimum conditions, various potential difference were applied together with varying concentrations of the electrolyte.

SEM analysis was used to understand the generation and formation of the Zn NWs, on samples anodized at 5 V and 10 V. The results are shown in Table.6.1 (Images 1-7).

Concentration of NaHCO <sub>3</sub> / × 10 <sup>-3</sup> mol dm <sup>-3</sup>	Volts / V	FESEM image	
6.8	10		
		Image 1 a)	10 μm <sup>b)</sup> 1 μm
6.8	5		
		Image 2 a)	10 μm <sup>b)</sup> 1 μm

Concentration of $\text{NaHCO}_3$ $/ \times 10^{-3} \text{ mol dm}^{-3}$	Volts / V	FESEM image	
13.6	10	 Image 3 a)	 b)
13.6	5	 Image 4 a)	 b)
30	5	 Image 5 a)	 b)
50	5	 Image 6 a)	 b)

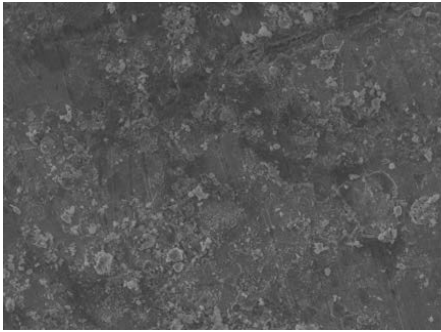

Concentration of NaHCO <sub>3</sub> / $\times 10^{-3}$ mol dm <sup>-3</sup>	Volts / V	FESEM image	
100	5		

Table 6.1 Morphological evolution of anodized Zn plate at different conditions for finding the optimum conditions for Zn forest grass like nanowires Image 1 a) 10 V and  $6.8 \times 10^{-3}$  mol dm<sup>-3</sup>, 2 a) 5 V and  $6.8 \times 10^{-3}$  mol dm<sup>-3</sup>, Image 3 a) 10 V and  $13.6 \times 10^{-3}$  mol dm<sup>-3</sup>, Image 4 a) 5 V and  $13.6 \times 10^{-3}$  mol dm<sup>-3</sup>, Image 5 a) 5 V and  $30 \times 10^{-3}$  mol dm<sup>-3</sup> Image, 6 a) 5 V and  $50 \times 10^{-3}$  mol dm<sup>-3</sup>, Image 7a) 5 V and  $100 \times 10^{-3}$  mol dm<sup>-3</sup> where images 1-7 b) are FESEM morphologies of the image represented in images 1-7 a) at higher magnification.

In the anodising experiments at 10 V in  $6.8 \times 10^{-3}$  mol dm<sup>-3</sup> NaHCO<sub>3</sub> (Image 1 a table 6.1) carried out for 10 min, inconsistent marks were seen due to the etching of the anode. The magnified image of the mark can be seen in image 1 b of table 6.1. By changing the cell voltage to 5 V under the above conditions, several pits were seen on the zinc plate as shown in image 2a and b of table 6.1. When anodisation was carried out at 10 V in  $13.6 \times 10^{-3}$  mol dm<sup>-3</sup> NaHCO<sub>3</sub>, needle-like structures emerged from the pits with defined roots (image 3 a and b, Table 6.1). The nanoforest of grass-like structures appeared at this point after anodising. After this stage the experiments were further performed to seek the optimum conditions to obtain a uniform grass nanoforest. Anodising was conducted at 5 V in  $13.6 \times 10^{-3}$  mol dm<sup>-3</sup> NaHCO<sub>3</sub> and the anodising time was restricted to 5 min, which

form more discrete sites creating nanoforest grass but this is still non-uniform as seen in image 4 a and b of Table 6.1. By changing the concentration to  $30 \times 10^{-3} \text{ mol dm}^{-3}$  and at above conditions, the nano grass turn longer and expanded uniformly over the whole surface. It was judged from the image 5 b Table 6.1 that the nanograss fibres were about  $5 \mu\text{m}$ . However, at  $50 \times 10^{-3} \text{ mol dm}^{-3}$  concentration of  $\text{NaHCO}_3$ , the structure grown radially outwards from the base of Zn foil resembling forest grass, as revealed in image 6 b of Table 6.1. The length of the NW arrays was up to  $100 \mu\text{m}$  with diameter varying from 30 to 70 nm. The uniform and consistent films grown by anodization at 5 V shown in image 5 and 6 at concentration of  $\text{NaHCO}_3$   $30 \times 10^{-3} \text{ mol dm}^{-3}$  and  $50 \times 10^{-3} \text{ mol dm}^{-3}$  respectively. The pits appeared due to physical and chemical instabilities of the electrolyte and fluctuations of the Zn metal surface, due to local changes in the concentration of the solution. For example, at a concentration of  $100 \times 10^{-3} \text{ mol dm}^{-3}$   $\text{NaHCO}_3$ , the Zn plate was dissolved during the anodising (see image 7 of Table 6.1).

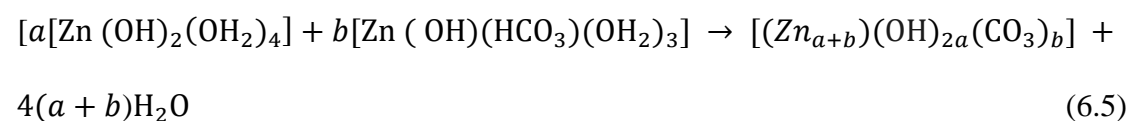
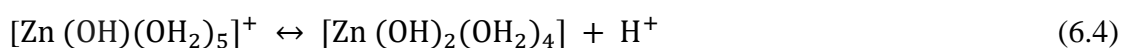
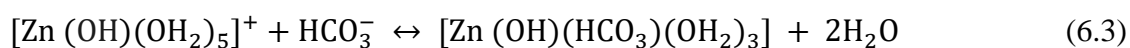
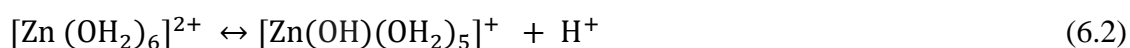
### 6.3.2 Mechanism of nanowire growth

We now inspect the electrochemical activity implicated during anodization of Zn plate. In order to rationalize the mechanism of unique instant formation of Zn NWs arrays, it is essential to determine the chemical composition of Zn NWs arrays and establish a possible growth mechanism. The chemistry of Zn anodising depends on factors such as electrode potential (potential of the Zn surface) and concentration of the electrolyte. The formation of zinc hydroxyl carbonate in the aqueous solution has been mentioned by Bitenc *et al* [26]. Stable hydrated ions, such as  $[\text{Zn}(\text{OH}_2)_6]^{2+}$  and  $[\text{Zn}(\text{OH})(\text{OH}_2)_5]^+$  can be formed in aqueous solutions. These ions may be converted into  $[\text{Zn}(\text{OH})_2(\text{OH}_2)_4]$  by olation (which is the synthesis of metal ion hydroxide complexes by connecting metal ion



with hydroxyl groups as a bridge). In the case of bicarbonate solution, two water molecules can be eliminated or substituted to form a  $[\text{Zn}(\text{OH})(\text{HCO}_3)(\text{OH}_2)_3]$  complex. The above anodising mechanism may be initiated by the following electrochemical reactions [27].

#### At the anode



#### At the cathode



The hydrogen evolution (reduction of  $\text{H}^+$  ions) at negative electrode as depicted in reaction (6.6), speeds up reaction (6.2) and ultimately improved the complex formation by condensation via olation mechanism as shown in reaction (6.3). The condensation of the complex may be effected by the diffusion of metal oxides during anodising. In this case, due to the stirring of the electrolyte, anodising is uniform and NWs eventually grow without any mass transport. The bicarbonate ions in the electrolyte will further speed up reaction (6.3), by substitution of water molecules [27].

### 6.3.3 Effect of cell potential difference on film growth

Effect of changing the applied potential difference between 1-5 V in  $30 \times 10^{-3} \text{ mol dm}^{-3}$  of  $\text{NaHCO}_3$  for a 10 min anodising was meaningful. Under these conditions, resulting samples generates considerable impact on nanowire growth rates. In the case of anodization experiments at 5 V uniform nanowire films were grown, whereas when the volts were changed to 1 V no nanowires were observed as shown in Figure 6.3.

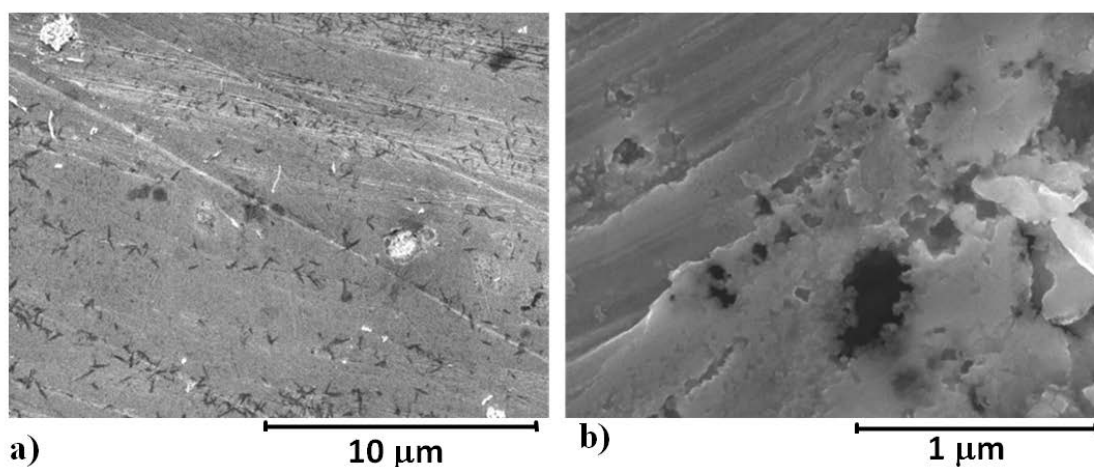


Figure 6.3 FESEM Images of a) Anodization of Zn plate at 1V and  $30 \times 10^{-3} \text{ mol dm}^{-3}$  b) magnified image of a).

However, extreme flaking and peeling of the treated surface was obtained at 10 V with the same conditions as mentioned above (see Figure 6.4). The main justification for the flaking and peeling of the film is the effect of higher potential difference, which ultimately break the coating due to the oxygen evolution reaction at the anode surface. At higher potential difference (40 V), peeling was also seen by Hu *et al.* during anodization in  $\text{KHCO}_3$  solution [13]. This was caused by oxygen evolution underneath the film, which in turn releases entrapped gas bubbles from the surface, produced cracking of the film.

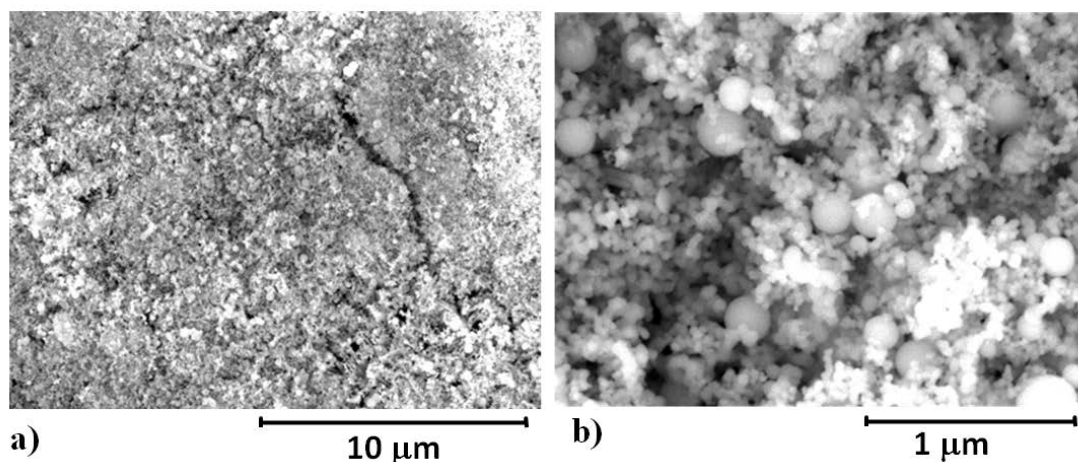


Figure 6.4 FESEM Images of a) Anodising of Zn plate at 10 V b) magnified image of a).

It is important to mention that the film rupturing via oxygen evolution in these experiments was observed at much lower voltage (10 V) in comparison to higher voltage (40 V) applied by Hu *et al* [13]. For uniform nanowire films it is strongly recommended to apply a cell voltage of 5V in a suitable concentration of electrolyte ( $30\text{-}50 \times 10^{-3} \text{ mol dm}^{-3} \text{ NaHCO}_3$ ).

#### 6.3.4 Effect of $\text{NaHCO}_3$ concentration on evolution of nanowires

In order to analyse the influence of bicarbonate concentration on forest grass like nanowire evolution by anodisation, the cell voltage, temperature and anodising time were set to 5 V, 25 °C and 10 min, respectively and varying  $\text{NaHCO}_3$  concentration from  $6.8 \times 10^{-3} \text{ mol dm}^{-3}$  to  $100 \times 10^{-3} \text{ mol dm}^{-3}$ . SEM images of the anodised specimen showed that the  $\text{NaHCO}_3$  concentration had a particular outcome on the rate of nanowire evolution (Table 6.1). At concentration of  $100 \times 10^{-3} \text{ mol dm}^{-3} \text{ NaHCO}_3$ , the Zn plate was dissolved during the anodization with no evidence of nanowires. At a concentration of  $50 \times 10^{-3}$

mol dm<sup>-3</sup> (table 6.1 Image 6 a) and b)) and  $30 \times 10^{-3}$  mol dm<sup>-3</sup> NaHCO<sub>3</sub>, uniform NW films were observed with no cracks. At a lower concentration  $13.6 \times 10^{-3}$  mol dm<sup>-3</sup>, some spots of nanowires were observed with some oxide layers. However, at  $6.8 \times 10^{-3}$  mol dm<sup>-3</sup> NaHCO<sub>3</sub>, some pits of nanowires can be observed due to slight dissolution of Zn metal during anodising. The stages of change in electrolyte concentration can be seen in the table 6.1. This expresses that controlling the concentration of the NaHCO<sub>3</sub> electrolyte, enhances the growth of NWs without damaging the integrity of the film. In conclusion from the above observations, the concentration of the electrolyte used during experiments is also an influencing factor for the growth of ZnO nanowires during anodization process.

### 6.3.5 ZnO/ TiO<sub>2</sub> core-shell surface characterization

The ZnO-TiO<sub>2</sub> core-shell were successfully synthesized via a dip coating method by with a TiO<sub>2</sub> film over the Zn NWs. The FESEM images show uniform deposition, as seen in Figure 6.5a), and at higher resolution in Figure 6.5b) indicates consistent morphology of the developed TiO<sub>2</sub> coating over the ZnO nanowires.

The inset indicates high resolution image, which exhibits clear and smooth interior morphology of the TiO<sub>2</sub> shell layer, deposited over the ZnO nanorods core after two cycles of dip coating and subsequent calcination at 400 °C.

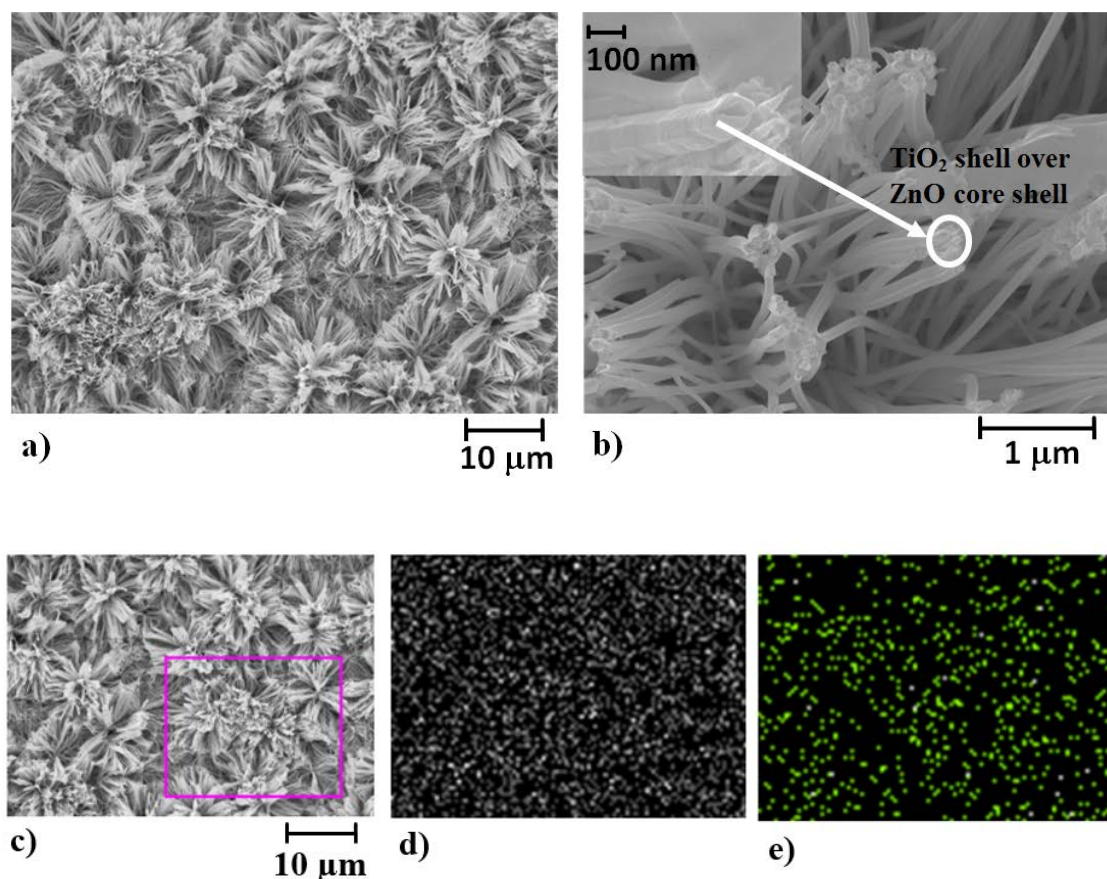


Figure 6.5 FESEM Images of a) dip coating and calcination (400 °C) of anodized zinc plate at optimum conditions (5 V and  $30 \times 10^{-3} \text{ mol dm}^{-3} \text{ NaHCO}_3$  at 10 min anodising time) (b) magnified image of a) with inset showing up the ZnO/ TiO<sub>2</sub> core-shell, c) EDX elemental analysis of ZnO/ TiO<sub>2</sub> core-shell coating d) Zn elemental analysis e) Ti elemental analysis.

### 6.3.6 PbO<sub>2</sub> multi core shell over the ZnO-TiO<sub>2</sub> core shell characterization

The images of the structural characteristics of the hybrid core ZnO-TiO<sub>2</sub> core-shell PbO<sub>2</sub> coatings, analysed by FESEM, are shown in Figure 6.6 (a-b). During the following electrodeposition of PbO<sub>2</sub>, the Pb<sup>2+</sup> ions in the boric acid solution transformed into solid lead dioxide [28]. Considerable variation exist between Figure 6.6a) and Figure 6.5a) as ZnO-TiO<sub>2</sub> core-shell (fig 6.5 a) now covered with PbO<sub>2</sub> (fig 6.5 a) coating, which suggest

the deposition of agglomerates of  $\text{PbO}_2$ , developing hybrid  $\text{ZnO-TiO}_2$  core-shell  $\text{PbO}_2$  coating.

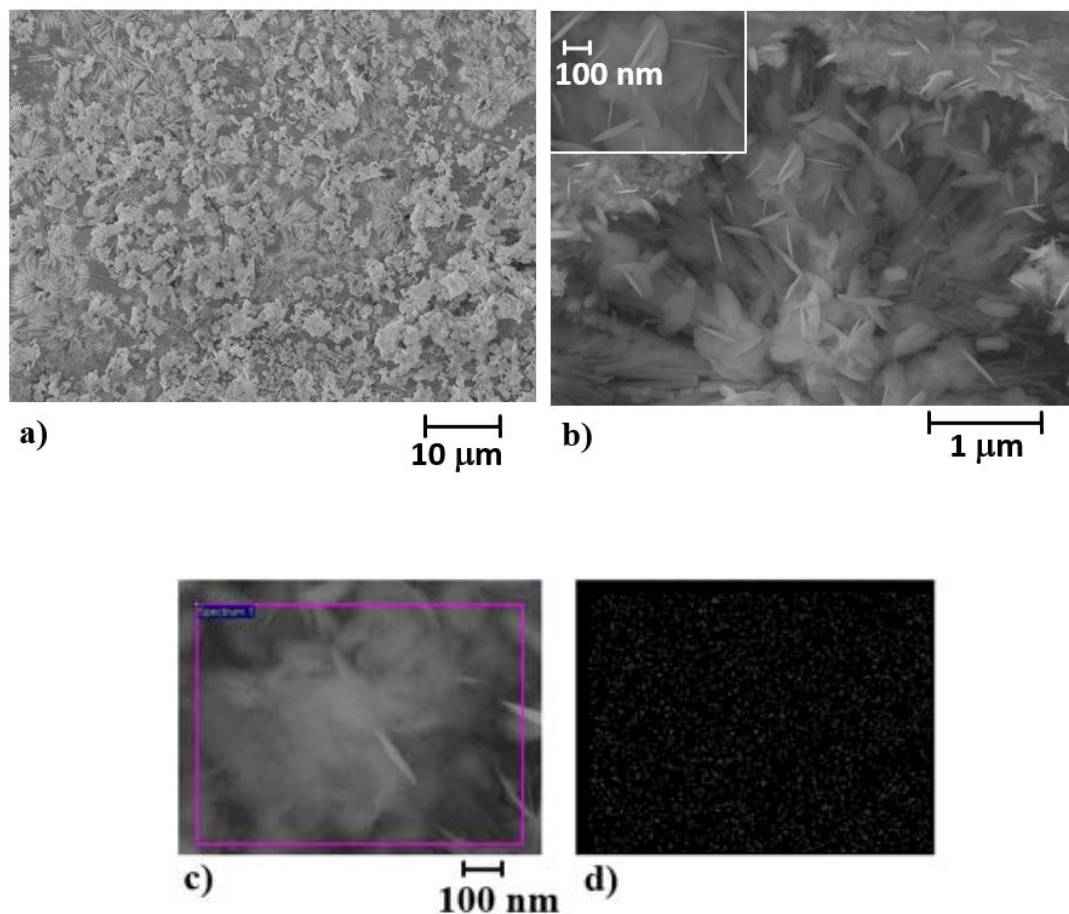


Figure 6.6 FESEM images of a) electrodeposition of  $\text{PbO}_2$  using  $\text{ZnO/TiO}_2$  core-shell in a bath containing  $80 \text{ cm}^3$  of  $0.1 \text{ mol dm}^{-3}$  boric acid with  $0.01 \text{ mol dm}^{-3}$   $\text{Pb}(\text{NO}_3)_2$  at a current density of  $5 \text{ mA cm}^{-2}$  under galvanostatic conditions for 30 min, b) magnified image of a) with inset showing up the hybrid core (ZnO-TiO<sub>2</sub>)-shell ( $\text{PbO}_2$ ), c) coating hybrid core (ZnO-TiO<sub>2</sub>)-shell ( $\text{PbO}_2$ ) at 30000 magnification (d) lead elemental analysis.

On increasing the magnification of the same image of the confined region,  $\text{PbO}_2$  particles were deposited over the  $\text{ZnO-TiO}_2$  core-shell as shown in Figure 6.6 b). The elemental analysis of the coating was determined by EDX from the micrograph shown in Figure 6.6

c-e). It confirmed that the coating contained lead, carbon and oxygen elements. The  $\text{PbO}_2$  particles were tightly attached over the core shell forming a multicore shell by electrodeposition. Each nanoforest grass-like  $\text{ZnO-TiO}_2$  core-shell covered with  $\text{PbO}_2$  expected to be an electrochemically active by nature and can be used to decolourize Reactive Black-5 dye.

The structural characteristics related to the formation of anatase phase of  $\text{TiO}_2$  and the wurtzite phase of  $\text{ZnO}$  were seen by Raman spectroscopy in Figure 6.7. No peaks were observed for the non-calcined substrate after anodization of Zn plate and dip coating with titanium (IV) butoxide as seen in Figure 6.7 a) due to the absence of phases in the substrate.

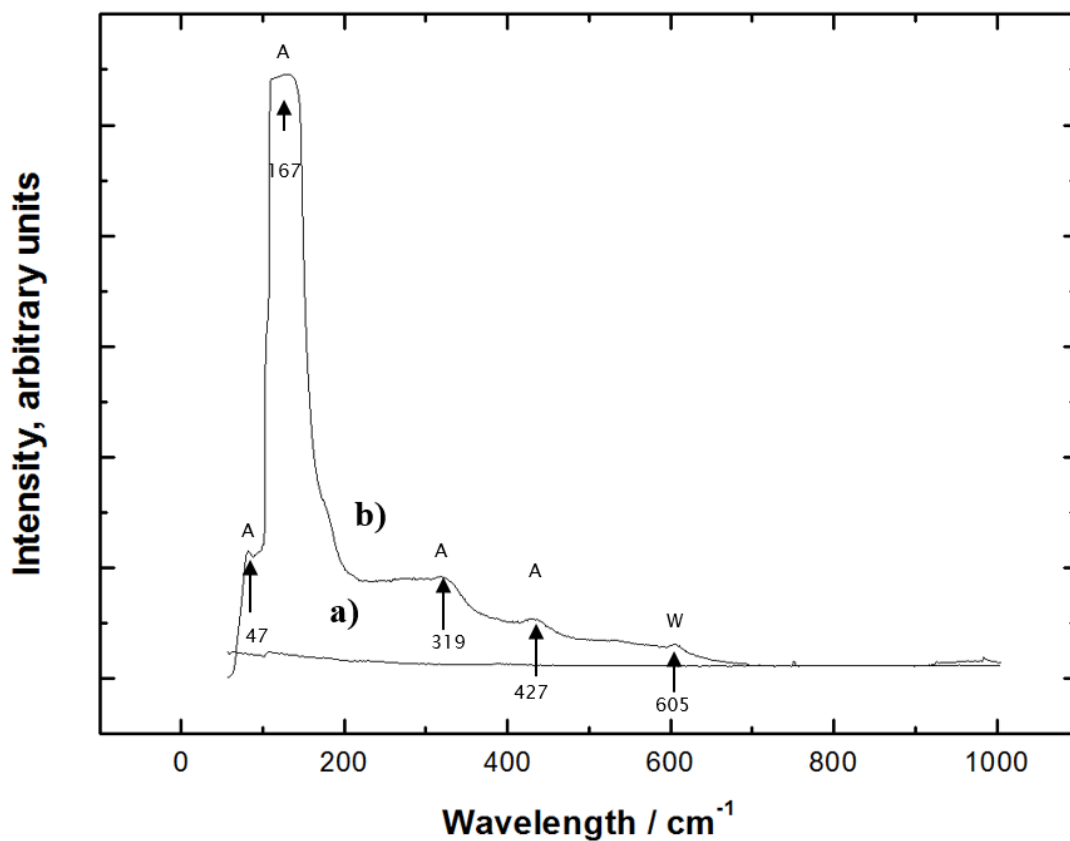


Figure 6.7 Raman spectra of a) non calcined substrate after anodization of Zn plate and dip coating with titanium (IV) butoxide ( $\text{ZnO-TiO}_2$  core-shell coating) and b) calcined  $\text{ZnO-TiO}_2$  core-shell coating calcined at  $400^\circ\text{C}$ .

The distinct peaks seen at  $47\text{ cm}^{-1}$ ,  $167\text{ cm}^{-1}$ ,  $319\text{ cm}^{-1}$ ,  $427\text{ cm}^{-1}$  corresponds to anatase phase (A) of  $\text{TiO}_2$  and peak at  $605\text{ cm}^{-1}$  relates to the wurtzite phase (W) of  $\text{ZnO}$  as seen in Figure 6.7 b), indicating that heat treatment converted the substrate to the anatase and wurtzite phases in a calcined  $\text{ZnO-TiO}_2$  core-shell coating at  $400^\circ\text{C}$ .



### 6.3.7 Electrochemical measurements on the coatings

The oxygen evolution reaction (OER) is the result of intermediate reactions in which the hydroxyl radicals are produced. The first step is the water discharge which produce  $\bullet\text{OH}$  radical as shown in Eq. (2.1) reported in section 2.2. The subsequent reactions depend upon the interaction of the  $\bullet\text{OH}$  radical and the electrode surface. Two classes of the electrode material have been generally reported in the literature: “active” and “non-active” electrodes [29]. Active electrodes have a strong relationship with the hydroxyl radical and the oxygen evolution reaction takes place after the formation of relevant oxides during the electrochemical process [30]. In the case of non-active electrodes, the hydroxyl radicals are weakly adsorbed over the substrate and instead they tend to initiate the oxidation of the electroactive species leading to carbon dioxide production. For example, Pt is said to be an active anode as it has strong interaction with hydroxyl radical and tends to attract hydroxyl radicals. While adsorption enthalpies in case of  $\text{PbO}_2$  are lower towards hydroxyl radicals and hence  $\text{PbO}_2$  weakly attracts the  $\bullet\text{OH}$  radicals on its surface. The polarization curves of  $\text{ZnO-TiO}_2$  core-shell coating, hybrid  $\text{ZnO-TiO}_2$  core-shell  $\text{PbO}_2$  coating obtained in  $0.05 \text{ mol dm}^{-3} \text{ H}_2\text{SO}_4$  at a potential sweep rate of  $5 \text{ mV s}^{-1}$  are shown in figure 6.8.

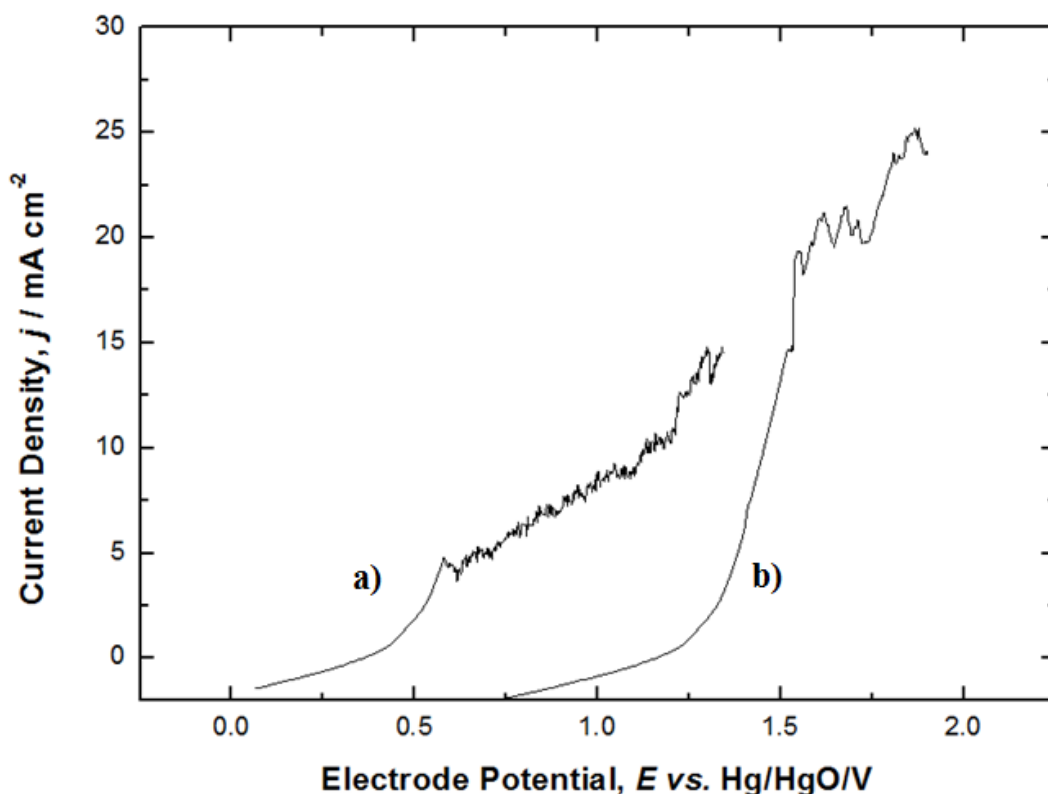


Figure 6.8 Polarization curves by using coatings a) ZnO-TiO<sub>2</sub> core-shell coating as anode in an electrolyte containing 0.05 mol dm<sup>-3</sup> H<sub>2</sub>SO<sub>4</sub>. b) hybrid core (ZnO-TiO<sub>2</sub>)-shell (PbO<sub>2</sub>) coating as an anode after calcination at 400°C in an electrolyte containing 0.05 mol dm<sup>-3</sup> H<sub>2</sub>SO<sub>4</sub>, Experimental conditions: Potential sweep rate 5 mV s<sup>-1</sup>, temperature: 25 °C.

The onset of the evolution of oxygen on each coating exhibit different potential which relies on the electrocatalytic substrate. Oxygen evolution starts from around 0.25 V vs. Hg/HgO (NaOH sat.) for ZnO-TiO<sub>2</sub> core-shell coating (curve a) and at 0.75 V vs. Hg/HgO for hybrid ZnO-TiO<sub>2</sub> core-shell PbO<sub>2</sub> coating. Oxygen evolution reaction kept increasing in both coatings and for ZnO-TiO<sub>2</sub> electrode, the current slightly increased (> 5 mA cm<sup>-2</sup>) followed by massive O<sub>2</sub> evolution reaching up to 15 mA cm<sup>-2</sup>. This lower potential makes ZnO-TiO<sub>2</sub> core-shell coating to be a good electrocatalyst for the oxygen evolution reaction, while hybrid ZnO-TiO<sub>2</sub> core-shell PbO<sub>2</sub> coating has high massive

oxygen evolution only after 1.2 V *vs.* Hg/ HgO (curve 2) [30] and consequently is a poor electrocatalyst for the OER [30]. The potential of OER was evident at more positive potentials when a hybrid ZnO-TiO<sub>2</sub> core-shell PbO<sub>2</sub> coating was utilized. In this case the massive oxygen evolution seems to occur at 1.3 V *vs.* Hg/ HgO (NaOH sat.) and rising to 1.7 V *vs.* Hg/ HgO (NaOH sat.) (curve b), reaching almost 25 mA cm<sup>-2</sup> (Figure 6.8) which evidenced oxygen evolution at higher potential, this behaviour shows that oxygen evolution seemed unfavourable for hybrid ZnO-TiO<sub>2</sub> core-shell PbO<sub>2</sub> coating and the electrode tends to possess electrocatalytic nature for electrochemical removal of organic species in solution which is due to smaller adsorption of oxidizing species •OH radicals over the anode surface [31]. In this context, an organic compound (RB-5 dye) was opted as a model organic pollutant in order to verify the oxidising properties of the anodes.

### 6.3.8 Electrochemical discolouration of RB-5 dye

Anodic oxidation studies were conducted in order to evaluate discolouration of model pollutant in waste water by using ZnO-TiO<sub>2</sub> core-shell and hybrid ZnO-TiO<sub>2</sub> core-shell PbO<sub>2</sub> coatings as anodes by applying constant potential of 1.0 V *vs.* Hg/HgO (NaOH sat.). 100 cm<sup>3</sup> of electrolyte comprised of 20 mg dm<sup>-3</sup> of RB-5 dye and 0.6 mol dm<sup>-3</sup> of Na<sub>2</sub>SO<sub>4</sub> at pH 3 (adjusted by using H<sub>2</sub>SO<sub>4</sub>) was employed for the electrolysis experiments with ZnO-TiO<sub>2</sub> core-shell coating or hybrid ZnO-TiO<sub>2</sub> core-shell PbO<sub>2</sub> coating, as working as working electrodes while platinum and Hg/HgO (NaOH sat.) were the counter and reference electrodes, respectively. During the anodic oxidation studies of the waste water, samples of 2cm<sup>3</sup> were extracted every 15 min during the electrolysis. The samples were assessed by UV-vis spectra in the range of visible light ( $\lambda_{\text{max}} = 597 \text{ nm}$ ) of RB-5 dye. The intensity of the visible light band dropped continuously, until total discolouration of the

solution was obtained after 120 min as shown in Figure 6.9. The absorbance values decreased at a reasonable rate, indicating that dye oxidation involve formation of simple organics [31]. The oxidation of RB -5 dye involves removal of the chromophore (azo) group (-N=N-) which imparts the colour to RB-5 dye. The displacement of chromophore group (-N=N-) of complex RB-5 dye can result in the generation of aromatic and aliphatic intermediates, which ultimately might degrade to into basic inorganic CO<sub>2</sub> molecules or low molecular weight compounds. The normalised concentration against time during the anodic oxidation electrolysis experiments of the RB-5 dye using ZnO nanoflowers, ZnO-TiO<sub>2</sub> core-shell coating and hybrid ZnO-TiO<sub>2</sub> core-shell PbO<sub>2</sub> coatings as an anode electrodes is shown in Figure 6.9.

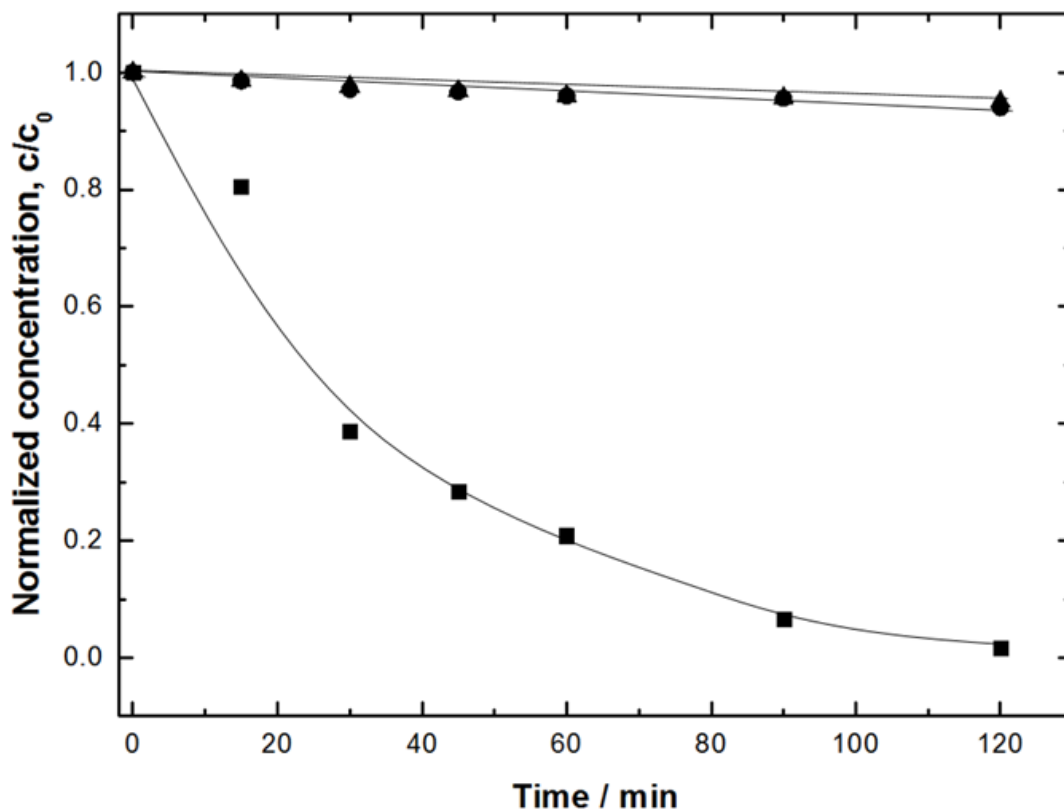


Figure 6.9 Electrochemical oxidation of  $20 \text{ mg dm}^{-3}$  RB-5 dye and  $0.6 \text{ mol dm}^{-3}$   $\text{Na}_2\text{SO}_4$  (Experimental conditions: applied potential =  $1.0 \text{ V vs. Hg/HgO}$  pH = 3.0,  $T = 25 \text{ }^\circ\text{C}$ ) by using (▲) ZnO nanoflower coating, (●) ZnO-TiO<sub>2</sub> core-shell coating and (■) hybrid core (ZnO-TiO<sub>2</sub>)-shell (PbO<sub>2</sub>) coating.

Assuming that the oxidation rate follows a first order constants kinetics, the pseudo-first order reaction kinetics constant, which quantifies the rate of dye oxidation were calculated via equation 2.20. A comparison of  $k$  values is given in Table 6.2.

Substrate	$-k / \text{min}^{-1}$	% Decolourisation	Time / min	Reference
ZnO-TiO <sub>2</sub> core-shell coating	0.0005	6	120	This study
ZnO nanoflower coating	0.0004	4.96	120	This study

Substrate	$-k / \text{min}^{-1}$	% Decolourisation	Time / min	Reference
Hybrid core (ZnO-TiO <sub>2</sub> )-shell (PbO <sub>2</sub> ) coating	0.034	98	120	This study
ZnO-TiO <sub>2</sub> core-shell coating	0.1476	98.77	25	Photochemical rate in this study
ZnO nanoflower coating	0.0872	93.37	25	Photochemical rate in this study
Hybrid core (ZnO-TiO <sub>2</sub> )-shell (PbO <sub>2</sub> ) coating	0.0159	35	25	Photochemical rate in this study

Table 6.2 Comparison of pseudo rate constants for oxidation of RB-5 dye by using ZnO nanoflower coating ZnO-TiO<sub>2</sub> core-shell coating and hybrid core (ZnO-TiO<sub>2</sub>)-shell (PbO<sub>2</sub>) coating by electrochemical and photocatalytic treatment.

The mechanism of dye oxidation can be explained via the interaction with hybrid ZnO-TiO<sub>2</sub> core-shell PbO<sub>2</sub> coating anode, the •OH free radical is produced by water discharge. This mediated •OH free radical transformed into dioxygen species as indicated by equation 3.7 or it can directly attack the azo dye towards complete oxidation eliminating chromophore group of RB-5 dye in reaction 3.8. However, for ZnO-TiO<sub>2</sub> core-shell coating the generation of •OH free radical may be classified as unfavourable due to oxygen evolution reaction found to be more significant at reduced potential (0.6 V vs. Hg/HgO), which might be inefficient for the decolouration of organic dye. The exponential oxidation curves showed in Figure 6.9 for anodic oxidation collating the two electrodes, i.e. ZnO-TiO<sub>2</sub> core-shell coating and hybrid ZnO-TiO<sub>2</sub> core-shell PbO<sub>2</sub> anodes

demonstrated that hybrid ZnO-TiO<sub>2</sub> core-shell PbO<sub>2</sub> coating exhibits about 98 % of decolouration.

The pseudo rate constant,  $k$  equals to 0.034 min<sup>-1</sup> was calculated from the linear pseudo first order oxidation curves (shown in Figure 6.10) at a constant potential of 1 V vs. Hg/HgO to a hybrid ZnO-TiO<sub>2</sub> core-shell PbO<sub>2</sub> coating as a working electrode (anode).

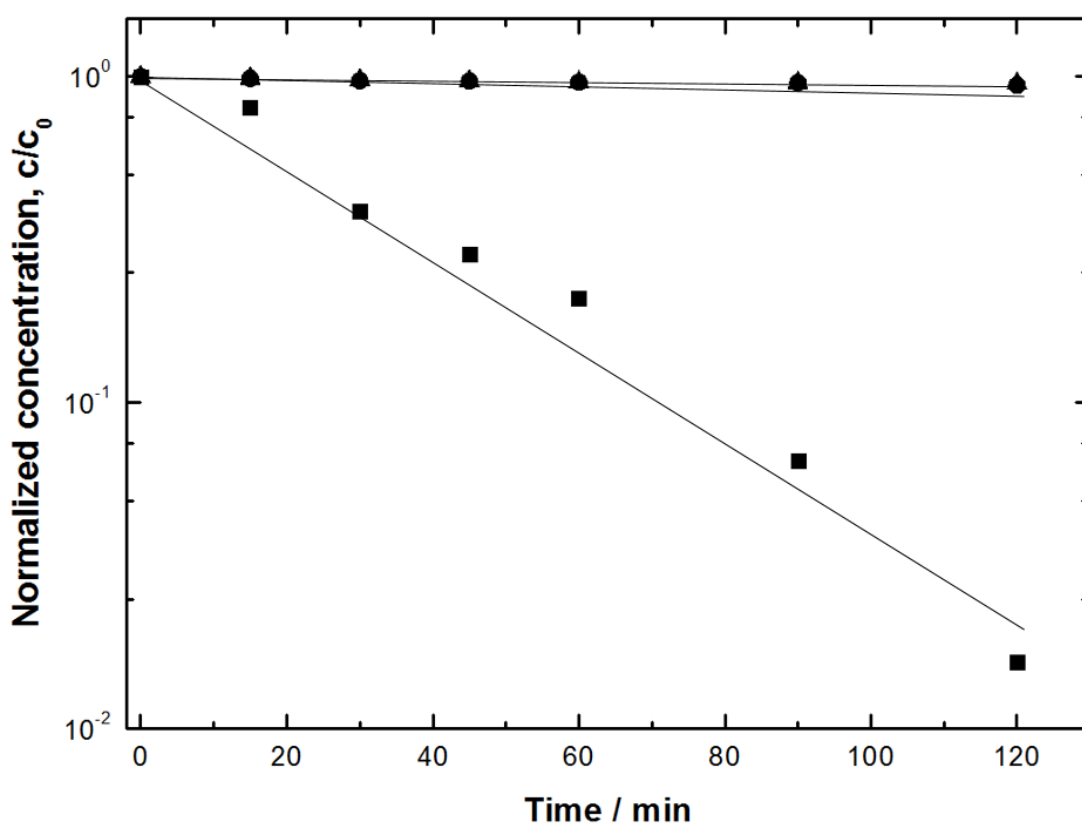


Figure 6.10 Electrochemical oxidation kinetics of RB-5 dye of 20 mg dm<sup>-3</sup> RB-5 dye and 0.6 mol dm<sup>-3</sup> Na<sub>2</sub>SO<sub>4</sub> (Experimental conditions: applied potential = 1.0 V vs. Hg/HgO pH = 3.0, T = 25 °C) by using ▲) ZnO nanoflower coating, ●) ZnO-TiO<sub>2</sub> core-shell coating and ■) hybrid core (ZnO-TiO<sub>2</sub>)-shell (PbO<sub>2</sub>) coating.

### 6.3.9 Photocatalytic discolouration of RB-5 dye

The Raman spectroscopy studies revealed the presence of anatase phase for TiO<sub>2</sub> and wurtzite ZnO phase in figure 6.7. The active nature of anatase and wurtzite ZnO phase was tested through photocatalytic studies of ZnO-TiO<sub>2</sub> core-shell nanorods and ZnO nanoflowers coatings ZnO-TiO<sub>2</sub> core-shell PbO<sub>2</sub> coatings for the discolouration of solution containing RB-5 dye as pollutant in Na<sub>2</sub>SO<sub>4</sub> at pH 3. The photocatalytic behaviour of the coatings relates to the features such as protonation of anatase TiO<sub>2</sub> under acidic conditions [32], the origination of holes and electrons over the anatase TiO<sub>2</sub> under illuminated UV-irradiation [33, 34]. The anatase TiO<sub>2</sub> acts as a positively charged specie under acidic pH as indicated by equation (6.7), in turn it tends to attract the negatively charged RB 5 dye, following oxidation of RB 5 dye [35].



Under UV-light illumination, there is the formation of electrons in the conduction band and holes (h<sup>+</sup>) in the valance band of the anatase TiO<sub>2</sub> and the wurtzite ZnO phase [36] as seen in equation (6.8).The electron produced interacts with dioxygen molecule to generate active oxidizing radicals (shown in equation 6.9) [35].







The overall performance of the anatase  $\text{TiO}_2$  and the wurtzite  $\text{ZnO}$  phase depends upon the created holes and radicals which play a decisive role in the photocatalytic performance and oxidation of RB-5 dye as indicated by equations (6.10), (6.11), (6.12) producing  $\cdot\text{OH}$  radicals which ultimately decompose the dye as shown in reaction (6.13). However, for hybrid  $\text{ZnO-TiO}_2$  core-shell  $\text{PbO}_2$  coating,  $\text{PbO}_2$  dominate and absorb the UV light at the top surface of conduction band of  $\text{TiO}_2$  and  $\text{ZnO}$ . UV light may excite the hole pair of valance band related to the anatase  $\text{TiO}_2$  and nanoparticle states of wurtzite  $\text{ZnO}$  phase for  $\text{ZnO-TiO}_2$  core-shell nanorods and  $\text{ZnO}$  coatings. The formation of the hole pair relates to the oxidation of dye with  $\text{ZnO-TiO}_2$  core-shell nanorods and  $\text{ZnO}$  nanorod coatings upon photoexcitation. The photocatalytic oxidation is represented in Figure 6.11, the time dependent concentration of reactive black-5 dye after 25 min of photocatalytic oxidation by  $\text{ZnO}$  nanorod coatings,  $\text{ZnO-TiO}_2$  core-shell nanorods and hybrid  $\text{ZnO-TiO}_2$  core-shell  $\text{PbO}_2$  coatings are shown.

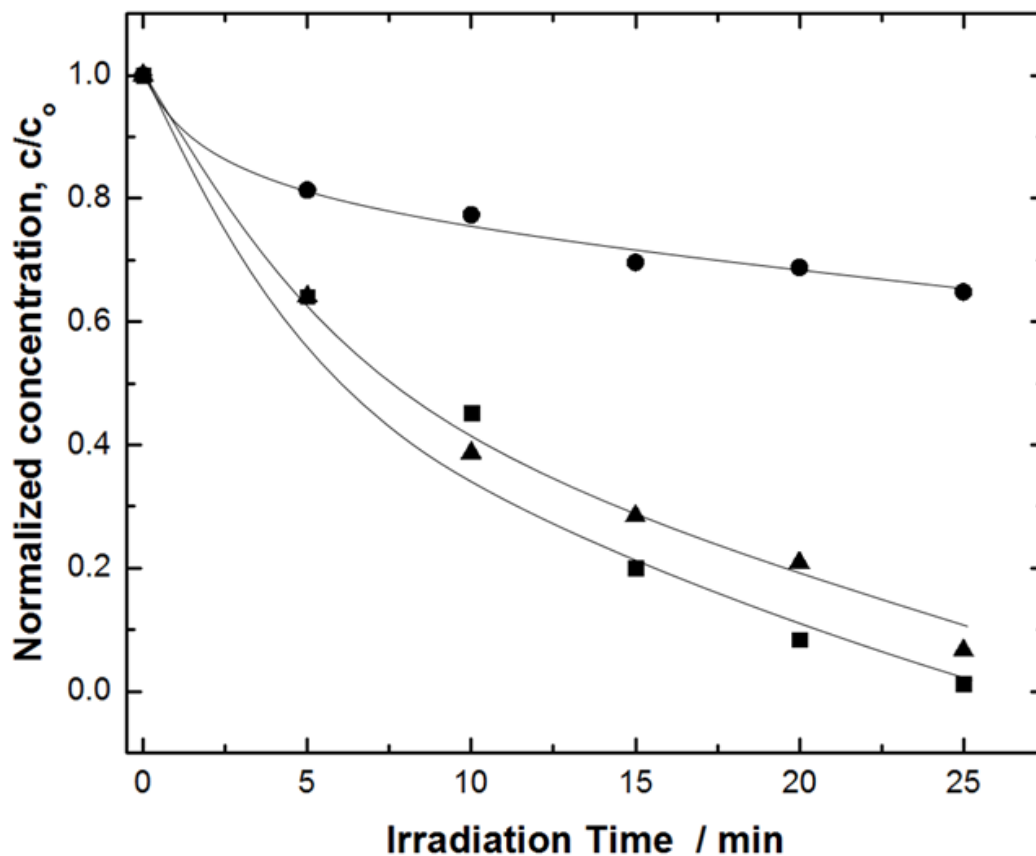


Figure 6.11 Photocatalytic oxidation of  $20 \text{ mg dm}^{-3}$  RB-5 dye and  $0.6 \text{ mol dm}^{-3}$   $\text{Na}_2\text{SO}_4$  (Experimental conditions: UV lamp intensity =  $1.5 \text{ mW cm}^{-2}$ , pH = 3.0, T =  $25 \text{ }^\circ\text{C}$ ) in  $0.6 \text{ mol dm}^{-3}$  of sodium sulphate by using (●) hybrid core (ZnO-TiO<sub>2</sub> core-shell coating)-shell (PbO<sub>2</sub>) coating, (▲) ZnO nanorods coating, and (■) ZnO-TiO<sub>2</sub> core-shell coating.

The logarithmic of the normalised concentration decay  $c/c_0$ , data in Figure 6.12 for the removal of RB-5 dye by using ZnO-TiO<sub>2</sub> core-shell nanorods and ZnO nanoflowers coatings indicates that the reaction follows a pseudo-first order reaction kinetics for the oxidation of reactive black-5 dye. The photocatalytic reaction kinetics for the oxidation of dyes were calculated by employing pseudo first order reaction as indicated by equation (2.20).

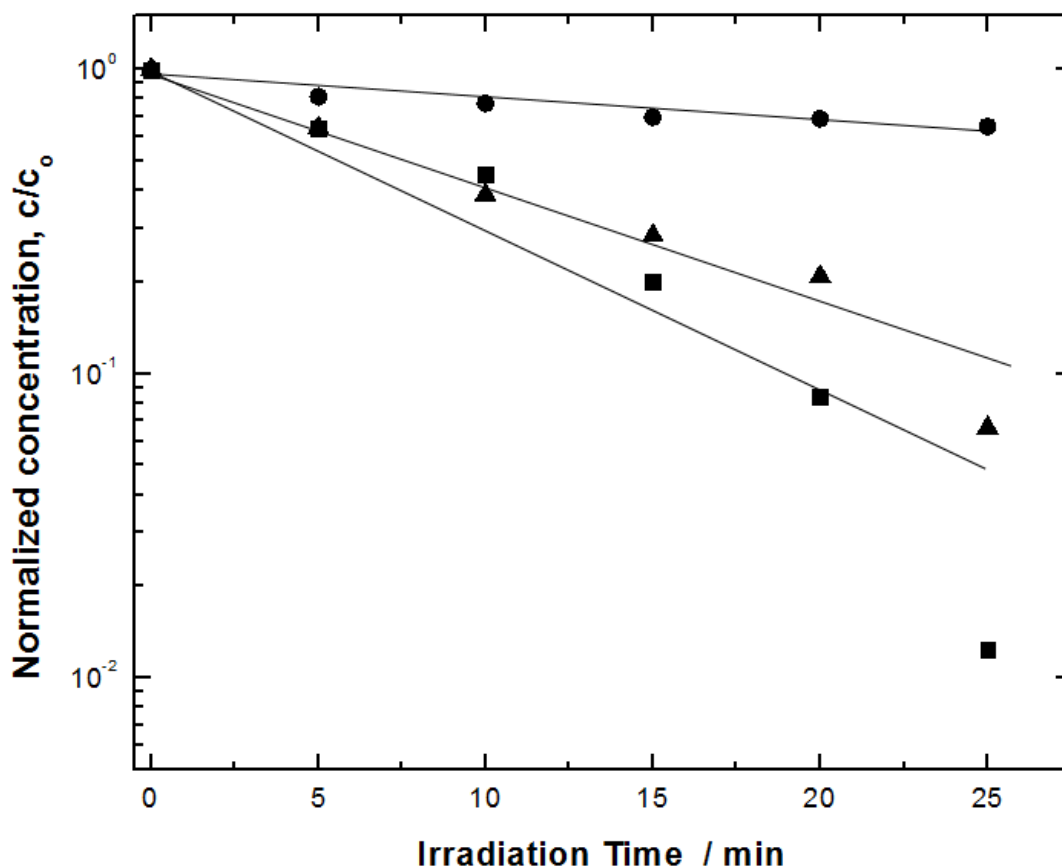


Figure 6.12 Photocatalytic oxidation kinetics of  $20 \text{ mg dm}^{-3}$  RB-5 dye and  $0.6 \text{ mol dm}^{-3}$   $\text{Na}_2\text{SO}_4$  (Experimental conditions: UV lamp intensity =  $20 \text{ mW cm}^{-2}$ , pH = 3.0, T =  $25 \text{ }^\circ\text{C}$ ) in  $0.6 \text{ mol dm}^{-3}$  of sodium sulphate by using ●) hybrid core (ZnO-TiO<sub>2</sub> core-shell coating)-shell (PbO<sub>2</sub>) coating, ▲) ZnO nanoflower coating and ■) ZnO-TiO<sub>2</sub> core-shell coating.

The comparison of pseudo rate constant ( $k$ ) for photochemical colour removal ( $-0.1476 \text{ min}^{-1}$ ) with electrochemical removal ( $-0.034 \text{ min}^{-1}$ ) shows that photocatalytic activity increased by 77 %. The annealing activates anatase (TiO<sub>2</sub>) and wurtzite ZnO which improved the photocatalytic activity when irradiated to UV light. In case of ZnO-TiO<sub>2</sub> core-shell nanorods, the reactive black-5 was removed in 25 min.

## 6.4 Conclusion

The results show that it is possible to growth of Zn nanowires over Zn plate surface via effective anodization method in an electrolyte containing bicarbonate salt. The best conditions for Zn nanowire growth have been identified by changing the parameters of cell voltage and concentration of the electrolyte. Furthermore, ZnO-TiO<sub>2</sub> core-shell nanorods produced by dip coating technique and employed the coating as a photocatalyst for the environmental oxidation of organic dye. Electrodeposition of PbO<sub>2</sub> created a hybrid ZnO-TiO<sub>2</sub> core-shell PbO<sub>2</sub> coating and used that for electrochemical oxidation of the dye. Electrochemical oxidation and photocatalytic colour removal of RB-5 dye found to be favourable by using hybrid ZnO-TiO<sub>2</sub> core-shell PbO<sub>2</sub> coating ZnO-TiO<sub>2</sub> core-shell nanorod coating, respectively. This study will open an important area to the researchers in developing metal oxide shell (PbO<sub>2</sub>) over anodized ZnO-TiO<sub>2</sub> core-shell over an inexpensive zinc substrate, for applications in wastewater treatment.

## 6.5 References

- [1] O. Mekasuwandumrong, P. Pawinrat, P. Praserttham, J. Panpranot, Effects of synthesis conditions and annealing post-treatment on the photocatalytic activities of ZnO nanoparticles in the oxidation of methylene blue dye, *Chem. Eng. J.* 164 (2010) 77-84.
- [2] B. Kumar, S.W. Kim, Energy harvesting based on semiconducting piezoelectric ZnO nanostructures, *Nano Energy.* 1 (2012) 342-355.
- [3] Q. Zhang, C.S. Dandeneau, X. Zhou, G. Cao, ZnO nanostructures for dye-sensitized solar cells, *Adv. Mater.* 21 (2009) 4087-4108.

- [4] A. Wei, L. Pan, W. Huang, Recent progress in the ZnO nanostructure-based sensors, *Mater. Sci. Eng. B*, 176 (2011) 1409-1421.
- [5] J.S. Souza, W.M. Carvalho, F.L. Souza, C. Ponce-de-Leon, D.V. Bavykin, W.A. Alves, Multihierarchical electrodes based on titanate nanotubes and zinc oxide nanorods for photo-electrochemical water splitting, *J. Mater. Chem. A*, 4 (2016) 944-952.
- [6] D.C. Look, D.C. Reynolds, J.R. Sizelove, R.L. Jones, C.W. Litton, G. Cantwell, W. C. Harsch, Electrical properties of bulk ZnO, *Solid State Commun.* 105 (1998) 399-401.
- [7] K. Subannajui, F. Güder, J. Danhof, A. Menzel, Y. Yang L. Kirste C. Wang, V. Cimalla, U. Schwarz, M. Zacharias, An advanced fabrication method of highly ordered ZnO nanowire arrays on silicon substrates by atomic layer deposition, *Nanotechnology*. 23 (2012) 235607-235614.
- [8] E. Galoppini, J. Rochford, H. Chen, G. Saraf, Y. Lu A. Hagfeldt, G. Boschloo, Fast electron transport in metal organic vapor deposition grown dye-sensitized ZnO nanorod solar cells, *J. Phys. Chem. B*, 110 (2006) 16159-61.
- [9] L.E Greene, M. Law, J. Goldberger, F. Kim, J.C. Johnson, Y. Zhang, R.J. Saykally, P. Yang, Low-temperature wafer-scale production of ZnO nanowire arrays, *Chem. Int. Ed.* 42 (2003) 3031-4.
- [10] S.E. Ahn, J.S. Lee, H. Kim, S. Kim, B.H. Kang, K.H. Kim, G.T. Kim, Photoresponse of sol-gel-synthesized ZnO nanorods, *Appl. Phys. Lett.* 84 (2004) 5022-5024.

- [11] H. Zeng, J. Cui, B. Cao, U. Gibson, Y. Bando, D. Golberg, Electrochemical deposition of ZnO nanowire arrays: organization, doping, and properties, *Sci. Adv. Mater.* 2 (2010) 336–358.
- [12] M. Skompska, K. Zarebska, Electrodeposition of ZnO nanorod arrays on transparent conducting substrates—a review, *Electrochim. Acta*, 127 (2014) 467–488.
- [13] Z. Hu, Q. Chen, Z. Li, Y. Yu L.M. Peng, Large-scale and rapid synthesis of ultralong ZnO nanowire films via anodization, *J. Phys. Chem. C*, 114 (2010) 881–889.
- [14] S.J. Kim, J. Choi, Self-assembled arrays of ZnO stripes by anodization, *Electrochem. Commun.* 10 (2008) 175–179.
- [15] Z. Hu, Q. Chen, Z. Li, Y. Yu, L.M. Peng, Large-scale and rapid synthesis of ultralong ZnO nanowire films via anodization *J. Phys. Chem. C*, 114 (2010) 881–889.
- [16] S. He, M. Zheng, L. Yao, X. Yuan, M. Li, L. Ma, W. Shen, Preparation and properties of ZnO nanostructures by electrochemical anodization method, *Appl. Surf. Sci.* 256 (2010) 2557–2562.
- [17] J.L. Zhao, X.X. Wang, J.J. Liu, Y.C. Meng, X.W. Xu, C.C. Tang, Controllable growth of zinc oxide nanosheets and sunflower structures by anodization method *Mater. Chem. Phys.* 126 (2011) 555–559.
- [18] A. Ramirez-Canon, D. O. Miles, P. J. Cameron and D. Mattia, Zinc oxide nanostructured films produced via anodization: a rational design approach, *RSC Adv.* 3 (2013) 25323–25330.
- [19] M. Kwiatkowski, R. Chassagnon, O. Heintz, N. Geoffroy, M. Skompska, I. Bezverkhyy, Improvement of photoelectrochemical and photoelectrochemical activity of

- ZnO / TiO<sub>2</sub> /core shell system through additional calcination: Insight into the mechanism, *Appl.Catal.B:Environ.* 204 (2017) 200-208.
- [20] M. Cerro-Lopez, Y. Meas-Vong, M.A. Méndez-Rojas, C.A. Martínez-Huitle, M.A. Quiroz, Formation and growth of PbO<sub>2</sub> inside TiO<sub>2</sub> nanotubes for environmental applications, *Appl. Catal. B: Environ.* 144 (2014) 174–181.
- [21] H. An, H. Cui, W. Zhang, J. Zhai, Y. Qian, X. Xie, Q. Li, Fabrication and electrochemical treatment application of a microstructured TiO<sub>2</sub>-NTs/Sb–SnO<sub>2</sub>/PbO<sub>2</sub> anode in the oxidation of C.I. Reactive Blue 194 (RB194), *Chem. Eng. J.* 209 (2012) 86–93.
- [22] Z. He, C. Huang, Q. Wang, Z. Jiang, J. Chen, S. Song, Preparation of a praseodymium modified Ti/SnO<sub>2</sub>-Sb/PbO<sub>2</sub> electrode and its application in the anodic oxidation of the azo dye acid black 194, *Int. J. Electrochem. Sci.* 6 (2011) 4341–4354.
- [23] S. Song, J. Fan, Z. He, L. Zhan, Z. Liu, J. Chen, X. Xu, Electrochemical oxidation of azo dye C.I. Reactive Red 195 by anodic oxidation on Ti/SnO<sub>2</sub>–Sb/PbO<sub>2</sub> electrodes, *Electrochim. Acta* 55 (2010) 3606–3613.
- [24] X. Li, D. Pletcher, F.C. Walsh, Electrodeposited lead dioxide coatings. *Chem. Soc. Rev.* 40 (2011) 3879.
- [25] J. Yao C.M. Lin, S.S Yin, P. Ruffin, C. Brantley, E. Edwards, High open-circuit voltage dye-sensitized solar cells based on a nanocomposite photoelectrode, *J. Photonics Energy.* 5 (2015) 053088-053098.

- [26] M. Bitenc, P. Podbrscek, P. Dubcek, S. Bernstorff, G. Drazic, B. Orel, Z.C Orel, The growth mechanism of zinc oxide and hydrozincite: a study using electron microscopies and in situ SAXS, *Cryst. Eng. Comm.* 14 (2012) 3080-3088.
- [27] D.O. Miles, P.J. Cameron, D. Mattia, Hierarchical 3D ZnO nanowire structures via fast anodization of zinc. *Journal of Materials Chemistry A*, 3 (2015) 17569-17577.
- [28] J. Lee, H. Varela, S. Uhm, Y. Tak, Electrodeposition of PbO<sub>2</sub> onto Au and Ti substrates, *Electrochem. Commun.* 2 (2000) 646-652.
- [29] B. Marselli, J. Garcia-Gomez, P.A. Michaud, M.A. Rodrigo, C. Cominellis, Electrogeneration of hydroxyl radicals on boron-doped diamond electrodes. *J. Electrochem. Soc.* 150 (2003) 79–83.
- [30] C.A. Martínez-Huitle, S. Ferro, Electrochemical oxidation of organic pollutants for the wastewater treatment: direct and indirect processes, *Chem.Soc. Rev.* 35 (2006) 1324–1340.
- [31] M. Panizza, G. Cerisola, Electrocatalytic materials for the electrochemical oxidation of synthetic dyes. *Appl. Catal. B: Environ.* 75 (2007) 95–101.
- [32] N.M. Mahmoodia, M. Arami, N.Y. Limaee, N.S. Tabrizi, Decolourisation and aromatic ring oxidation kinetics of direct red 80 by UV oxidation in the presence of hydrogen peroxide utilizing TiO<sub>2</sub> as a photocatalyst, *Chem. Eng. J.* 112 (2005) 191-196.
- [33] Y. Jiang, W.N. Wang, P. Biswas, J.D. Fortner, Facile aerosol synthesis and characterization of ternary crumpled graphene - TiO<sub>2</sub> - magnetite nanocomposites



for advanced water treatment, *ACS Appl. Mater. Interfaces* 6 (2014) 11766-11774.

- [34] I. Ilisz, Z. Laszlo, A. Dombi, Investigation of the photodecomposition of phenol in near-UV-irradiated aqueous TiO<sub>2</sub> suspensions. I: effect of charge-trapping species on the oxidation kinetics, *Appl. Catal. A*. 180 (1999) 25-33.
- [35] Y. Shen, W. Wang, K. Xiao, Synthesis of three-dimensional carbon felt supported TiO<sub>2</sub> monoliths for photocatalytic oxidation of methyl orange, *J. Env. Chem. Eng.* 4 (2016) 1259-1266.
- [36] O. Mekasuwandumrong, P. Pawinrat, P. Prasertdam, J. Panpranot, Effects of synthesis conditions and annealing post-treatment on the photocatalytic activities of ZnO nanoparticles in the oxidation of methylene blue dye, *Chem. Eng. J.* 164 (2010) 77-84



## Chapter 7:

### **Conclusion and Suggestions for Future Work**

#### **7.1 Conclusions**

The work presented in this thesis highlighted the effect of incorporation of titanate nanostructures, namely titanate nanosheets, titanate nanotubes over cheap substrate like titanium felt and RVC, with metal oxides deposited over these surfaces. After reviewing the performance of these novel and low cost coatings it has become clear that new electrode materials can improve the performance and decrease the cost of anodic oxidation process for the oxidation of organic compounds by using this advanced oxidation process (AOP).

In the first part of this thesis, titanium nanotubes were synthesized over titanium felt substrate by anodization method. Further,  $\text{PbO}_2$  was successfully inserted in nanotubes by layer immersion techniques. Anodic oxidation has been evaluated as a powerful technology for the oxidation of toxic and perverse organic pollutant such as RB-5 dye. The oxidation of this RB-5 dye through the hydroxyl radical produced over the non-active  $\text{PbO}_2$  over nanotubes on Ti felt anode substrate, after annealing coating was employed for photocatalytic oxidation and found capable of oxidation and colour removal. Instead, the carbon based substrate, such as RVC has demonstrated strengths for use in the anodic oxidation process by coating it with  $\text{PbO}_2$  and titanate nanosheets by electrophoretic deposition and applied the coating for electrochemical and photochemical water treatment. Further, TiNTs were deposited over RVC by electrophoretic deposition and found effective at 91% colour removal for photochemical decolourisation of methylene blue dye. The electrodes presented are novel and low cost to invest in the technology.

The important conclusions from the research presented in this thesis are:

- ❖ Chapter 3, the Ti based substrate was anodized in an electrolyte containing MSA (up to  $1 \text{ mol dm}^{-3}$ ) with ammonium fluoride (1.0 wt. %) to produce titanate nanotubes at an applied cell potential of 15 V (graphite as cathode) for small nanotubes (wall thickness = 10 nm) and 20 V for large nanotubes (wall thickness = 20 nm) are discussed.
- ❖ The  $\text{PbO}_2$  has been deposited inside the nanotubes by immersion of anodized Ti felt in a solution containing  $\text{Pb}(\text{NO}_3)_2$  and structure directing agent (PVP) at immersion time = 15 min, 6 h and 12 h and further oxidized by ammonium persulphate. The  $\text{PbO}_2$  growth acquire a shape from lemon to cauliflower like structure depending upon the immersion time.
- ❖ The application of these coatings showed that Ti felt/  $\text{TiO}_2$  nanotubes / $\text{PbO}_2$  exhibits the electrochemical dye discolouration of about 99 % in 60 min at more positive potential (1.5 V vs. Hg/HgO).
- ❖ The samples produced by 15 min immersion time of Ti felt/  $\text{TiO}_2$  nanotubes / $\text{PbO}_2$  and after calcination, found effective for the photochemical oxidation of the RB-5 dye (97 %) oxidation as indicated in chapter 3.
- ❖ The RVC, a high porosity carbon based substrate after acid treatment showed active functional groups appeared over its surface as shown in chapter 3.
- ❖ Electrophoretic deposition experiment revealed the formation of stable  $\text{PbO}_2$  and Titanate nanosheets (TiNS) coating over the RVC substrate.
- ❖ Using calcined TiNS/ $\text{PbO}_2$ /RVC electrodes, the pseudo first order oxidation reaction of RB-5 dye has been accomplished at pH 3.

- ❖ Raman results indicated the transformation of titanate phase of TiNS/PbO<sub>2</sub>/RVC to the anatase structure after calcination at 450 °C.
- ❖ Photocatalytic studies revealed the complete first order decolourisation of RB-5 dye under acidic conditions in 20 min as indicated in chapter 3.
- ❖ In chapter 5, RVC substrates coated with TiNT coatings by using anodic electrophoretic deposition were prepared and photocatalytic activity of these electrodes are discussed.
- ❖ Raman studies revealed that upon calcination of TiNT/RVC coating the formation of anatase phase was observed up to 450 °C.
- ❖ The calcined TiNT/RVC substrate showed higher pseudo first order decontamination kinetics for the photocatalytic oxidation of the dye with 91 % dye degraded in 20 min as reported in chapter 5.
- ❖ In chapter 6, ZnO<sub>2</sub> nanoflowers have been prepared on a Zn plate substrate by employing anodization technique in bicarbonates solutions.
- ❖ The best conditions for Zn nanowire growth have been identified by changing the parameters of cell voltage and concentration of the electrolyte and it was revealed that the best conditions for anodization Zn nanowire synthesis were obtained at an applied cell voltage of 5 V in an electrolyte containing  $30 \times 10^{-3} \text{ mol dm}^{-3} \text{ NaHCO}_3$  for an electrochemical reaction time of 10 min.
- ❖ ZnO-TiO<sub>2</sub> core-shell nanorods produced by dip coating technique and employed the coating as a photocatalyst for the environmental oxidation (98.8%) of organic dye.
- ❖ Electrodeposition of PbO<sub>2</sub> created a hybrid ZnO-TiO<sub>2</sub> core-shell PbO<sub>2</sub> coating and used that for electrochemical oxidation of the dye.
- ❖ Raman studies showed the presence of anatase phase and wurtzite phases over the hybrid ZnO-TiO<sub>2</sub> core-shell PbO<sub>2</sub> coating.

- ❖ Electrochemical oxidation by using hybrid core (ZnO-TiO<sub>2</sub>)-shell (PbO<sub>2</sub>) coating and photocatalytic oxidation by using ZnO-TiO<sub>2</sub> core-shell coating and ZnO nanoflower coating of RB-5 dye was about 98.8 % and 98 % and 93 % respectively.

The aims and objectives which were: 1) anodising titanium felt to grow arrays of titanium dioxide nanotubes decorated with PbO<sub>2</sub>: characterisation and application, 2) preparation of PbO<sub>2</sub>/TiO<sub>2</sub> nanosheets at an RVC substrate by anodic electrophoretic deposition for electrochemical waste water treatment, 3) deposition of titanate nanotubes at an RVC substrate by anodic electrophoretic deposition with for photocatalytic oxidation of organic material in waste water, 4) development of ZnO<sub>2</sub> nanowire arrays on Zn metal substrate by using electrochemical anodization, formation of a ZnO-TiO<sub>2</sub> core-shell decorated by PbO<sub>2</sub> on a Zn metal substrate for removal of RB-5 dye from aqueous solution. All these aims have been accomplished by the development and characterization of innovative coatings and further application of those coatings for effective electrochemical and photochemical removal of RB-5 and MB dye.

Anodic oxidation is an important and efficient technique for the oxidation of organics in electrochemical advanced waste water treatment. This has the potential for industrial use and should be disseminate as one of the preferable technologies, when facing issues with toxic, refractory, non-biodegradable pollutant in waste water. The demand is to develop low cost and reliable electrodes to decrease the cost of the process. Improved methods need to be investigated aimed at rendering a full understanding of the mechanism and the generation of by-products and the derived outcome. In this way the electrochemical water treatment method is still just on the edge of outreach for necessary level of perfection.

It can be concluded from the above points, the use of 3D Ti-felt and carbon foam materials found to be effective for the anodic waste water treatment. The reason might be their

improved surface area, durability, low ohmic losses and conductivity in aqueous solutions [1]. These materials are found to be low cost than the expensive rare earth materials like platinum, ruthenium, gold or boron doped diamond (BDD) electrodes. The price of titanium is £20 per pound [1] whereas carbon foam is £15 per pound [3], considerable lower than the rare earth rare earth metals and BDD.

## 7.2 References

- [1] Bekaert transformation and coating technologies (2019)  
<https://www.bekaert.com/en/products/basic-materials/filtration/sintered-metal-fiber-filtration-media>. Accessed on 07 May 2019.
- [2] The MetalMiner North American Titanium Price Index (2019)  
<https://agmetalmminer.com/metal-prices/titanium/>. Accessed: 07 May 2019
- [3] Ali baba global trading services (2019)  
<https://www.alibaba.com/showroom/carbon-foam.html>. Accessed: 07 May 2019

## 7.3 Future Work

### 7.3.1 DSA electrodes over Ti felt substrate for anodic oxidation of Azo dyes

Preliminary experiments have been performed by using IL and Pechni methods over Ti felt substrate for dimensional stable electrodes (DSA electrodes. Uniform DSA electrodes over Ti felt substrate has been achieved. The same substrate will be utilized for anodic oxidation in order to acquire experience with its operation and monitoring for electro-oxidation of organic matter residue. The cell will use a DSA electrodes over Ti felt

substrate as an anode and Platinum metal as cathode. The analysis will comprise of following important aspects:

- ❖ Characterization of DSA electrodes by FESEM and XRD.
- ❖ Evaluation of flow through cell, percentage of removal kinetics of organics.
- ❖ Total organic carbon (TOC) and colour removal evaluation of the textile dyes before and after the electrochemical anodic oxidation.

### **7.3.2 Evaluation of new electrode materials**

Subsequent experiments will focus on testing different novel coatings electrode materials prepared by the electrophoretic deposition method.

- ❖ Electrochemical preparation of TiNS and PbO<sub>2</sub> coated over the C felt substrate.
- ❖ Modification of C felt by the addition of surfactants (Tetrabutylammonium hydroxide) followed by EPD.
- ❖ Characterization of the C felt using SEM.
- ❖ Possible evaluation of TiNS / PbO<sub>2</sub> / C felt in electrochemical flow cell.
- ❖ Photocatalytic activity of TiNS / PbO<sub>2</sub> / C felt for the discolouration of RB-5 dye.
- ❖ Stability test at different current densities and potentials.

### **7.3.3 Planned Publications**

Proposed and published publications from this research project are shown in the table 7.1



Table 7.1 **List of planned publications.**

Suggested title	Target journal	Style	Scope	Contents	Status
1. Oxidation of RB-5 dye at an RVC substrate coated with $\beta$ -PbO <sub>2</sub> / Ti-dioxide nanosheets prepared by anodic electrophoretic deposition	Journal of solid state Electrochemistry	Experimental work	Anodic Electrophoretic deposition of PbO <sub>2</sub> and TiNS over RVC substrate and subsequent application for electrochemical and Photocatalytic oxidation	RVC as a substrate for EPD, EPD with TiNS solute and TBAOH as surfactant and ethanol as solvent, SEM and Raman analysis of 2 D uniform layers of RVC (100 ppi) coated with PbO <sub>2</sub> TiNS, RB-5 dye electrochemical and photocatalytic oxidation with annealed TiNS/PbO <sub>2</sub> /RVC (100ppi).	Published
2. Photocatalytic oxidation of dye solution with Ti-nanotubes over RVC based substrate prepared by Anodic Electrophoretic Deposition	Applied Catalysis B: Environmental	Experimental work	Anodic Electrophoretic deposition of TiNT over RVC substrate and subsequent application for Photocatalytic oxidation	RVC as a substrate for EPD, EPD with TiNT solute and TBAOH as surfactant and ethanol as solvent, SEM and Raman analysis of 2 D uniform layers of RVC (100ppi) coated with TiNT, best methylene blue photocatalytic oxidation with annealed TiNT/RVC (100 ppi),	Draft Dec, 2018

---

removal efficiency.

---

3. Anodising of titanium felt to grow titanium dioxide nanotube arrays decorated with PbO <sub>2</sub> : Characterization and Application	Surface and Coatings and Technology	Experimental Research Article	Research article about anodising Ti felt with nanotubes and PbO <sub>2</sub> , electrochemical waste water treatment and their evaluation	Ti felt as substrate, anodization of Ti felt, coated with PbO <sub>2</sub> , characterization of substrate with nanotubes and PbO <sub>2</sub> , Raman studies, electrochemical treatment using the coating for RB-5 coating waste water, photochemical treatment	Draft: Dec, 2018
---	-------------------------------------	-------------------------------	---	---	------------------

---

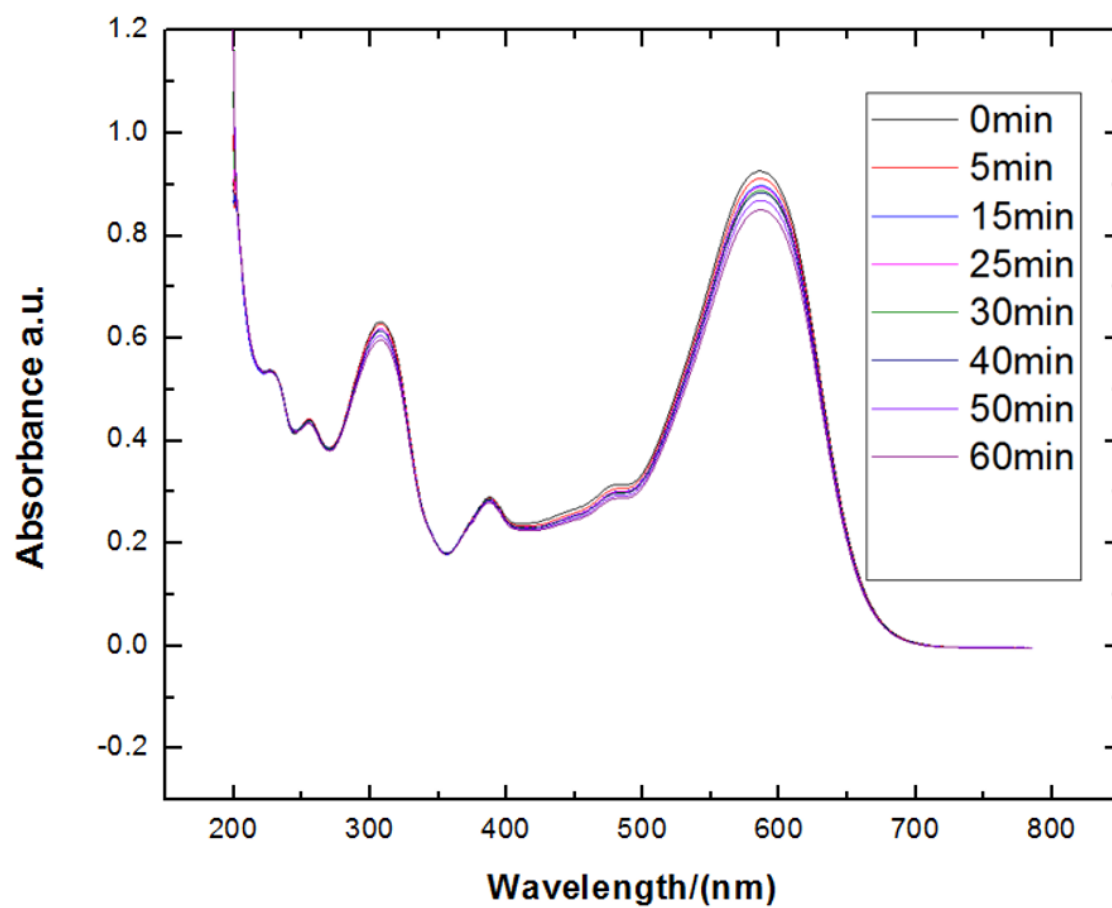
**Appendix**

Figure A 1 UV-vis spectra for the oxidation of RB-5 dye by using Ti-felt as an anode.

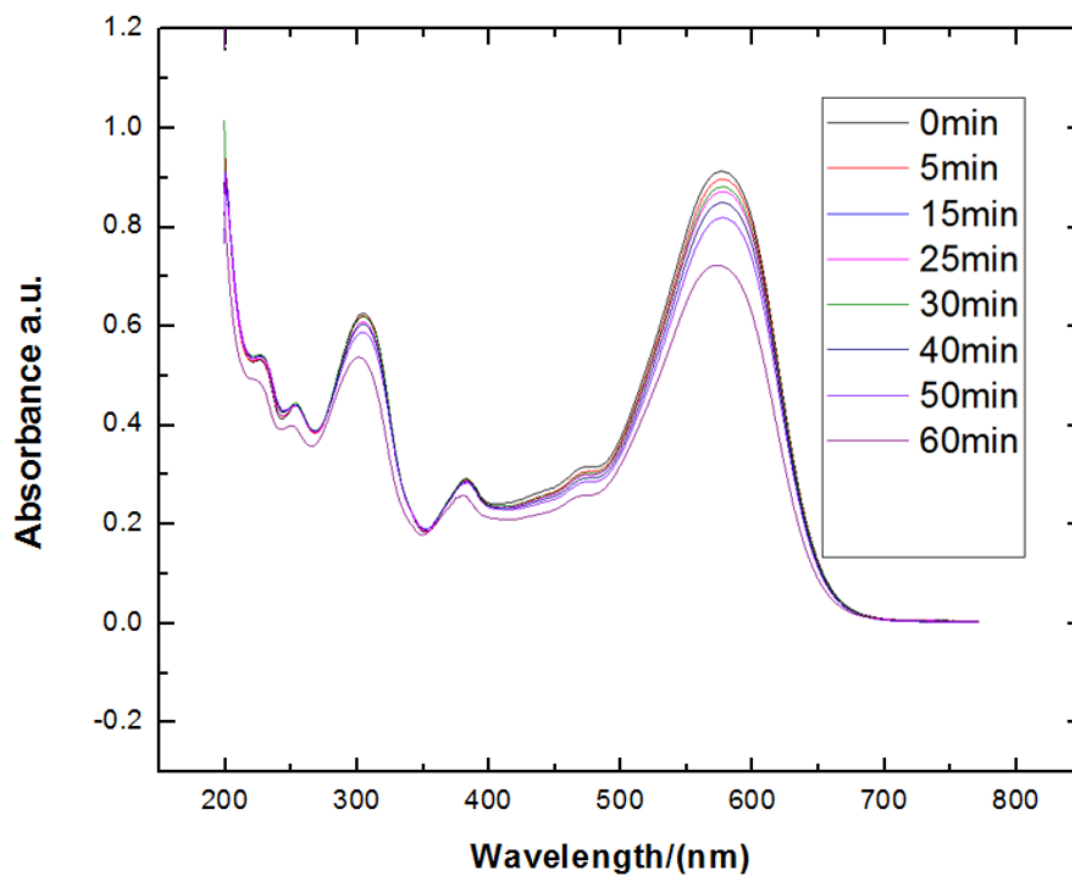


Figure A 2 UV-vis spectra for the oxidation of RB-5 dye by using Ti-felt/nanotube as an anode.

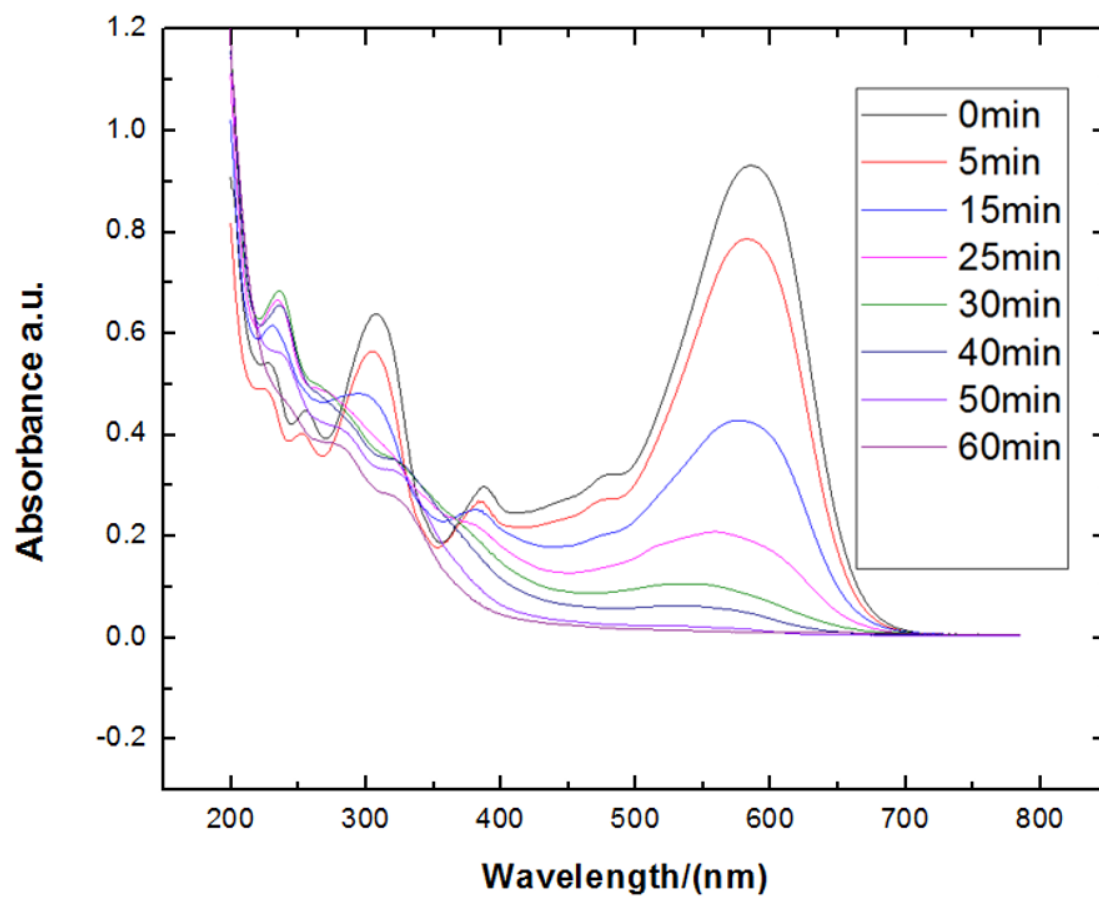


Figure A 3 UV-vis spectra for the oxidation of RB-5 dye by using Ti-felt/nanotube/PbO<sub>2</sub> as an anode.

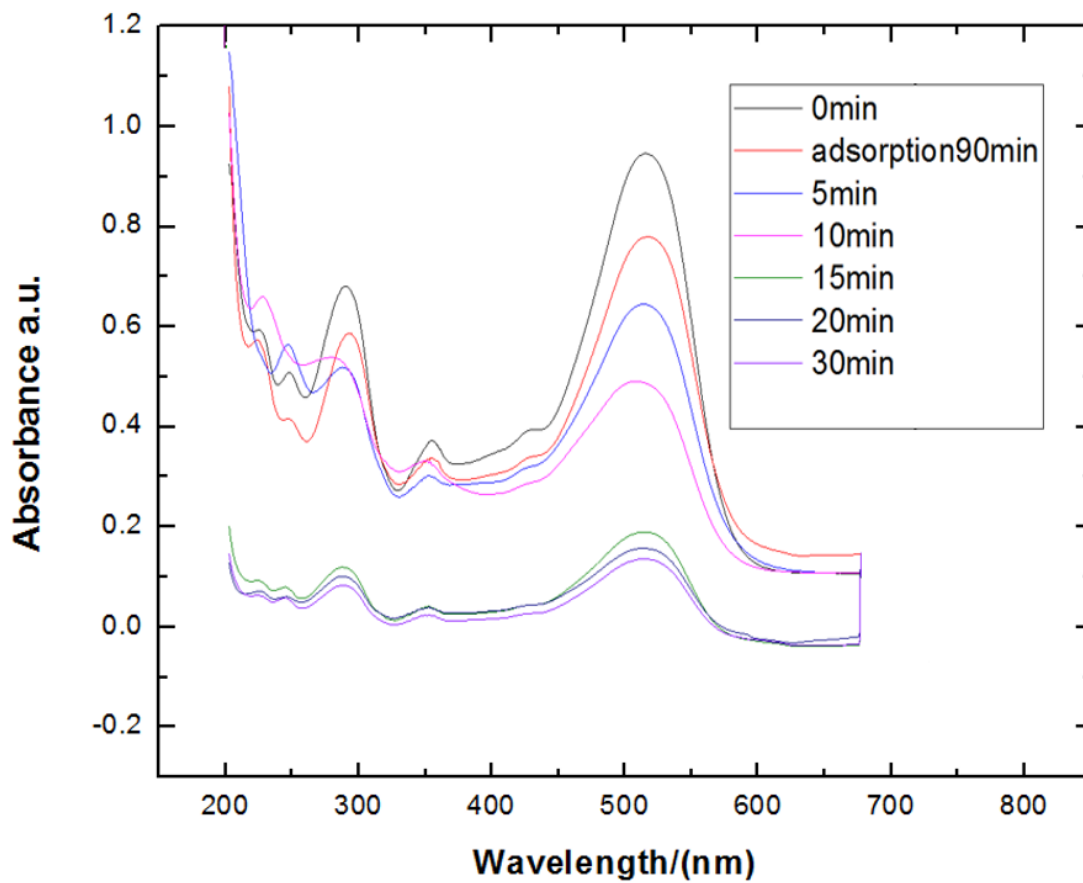


Figure A 4 UV-vis spectra for the oxidation of RB-5 dye by using calcined Ti-felt /nanotubes/PbO<sub>2</sub> as a photocatalyst.

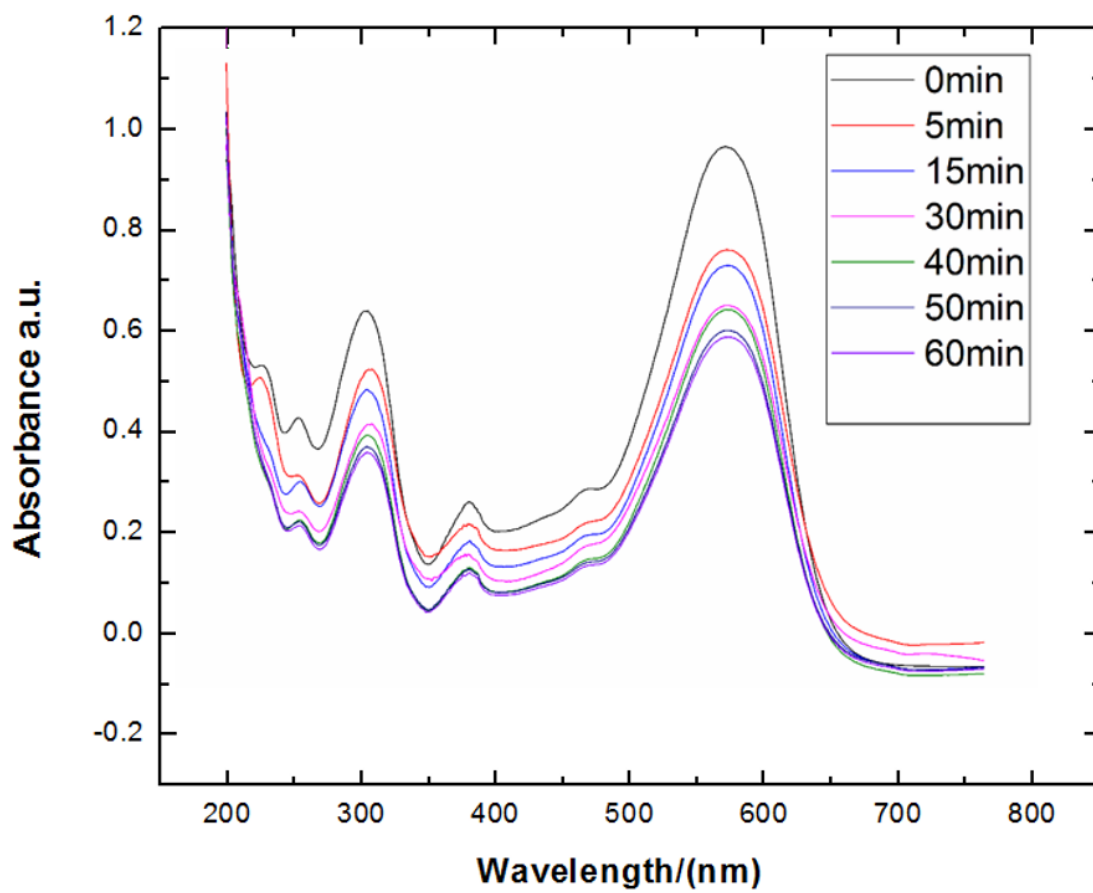


Figure A 5 UV-vis spectra for the oxidation of RB-5 dye by using RVC as a anode.



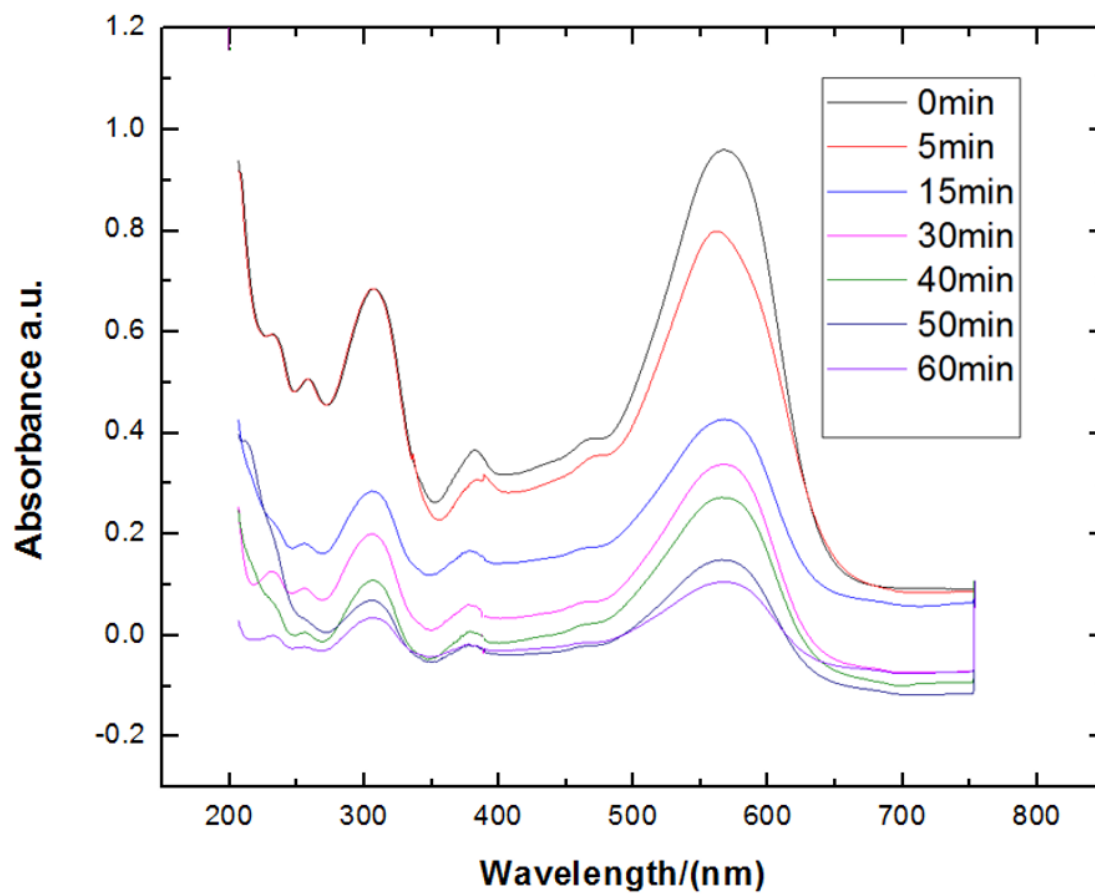


Figure A 6 UV-vis spectra for the oxidation of RB-5 dye by using RVC/PbO<sub>2</sub> as an anode.

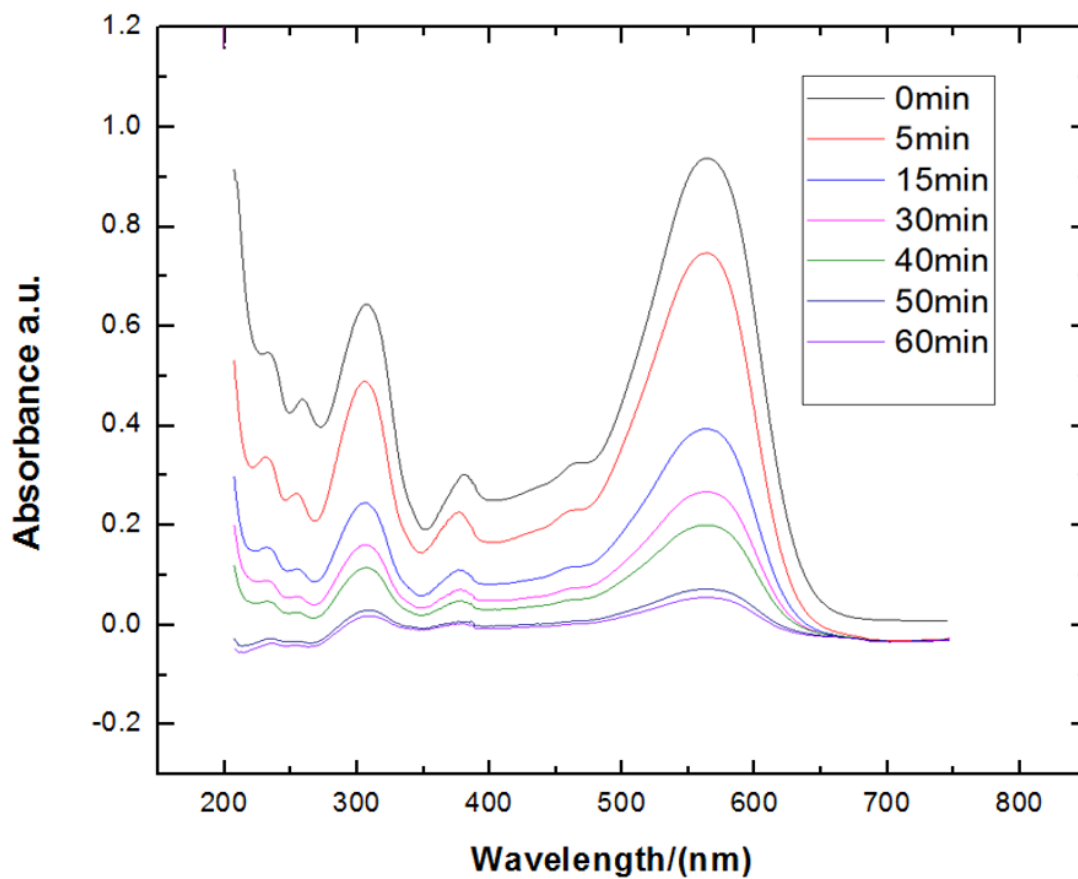


Figure A 7 UV-vis spectra for the oxidation of RB-5 dye by using RVC/PbO<sub>2</sub>/TiNS as an anode.

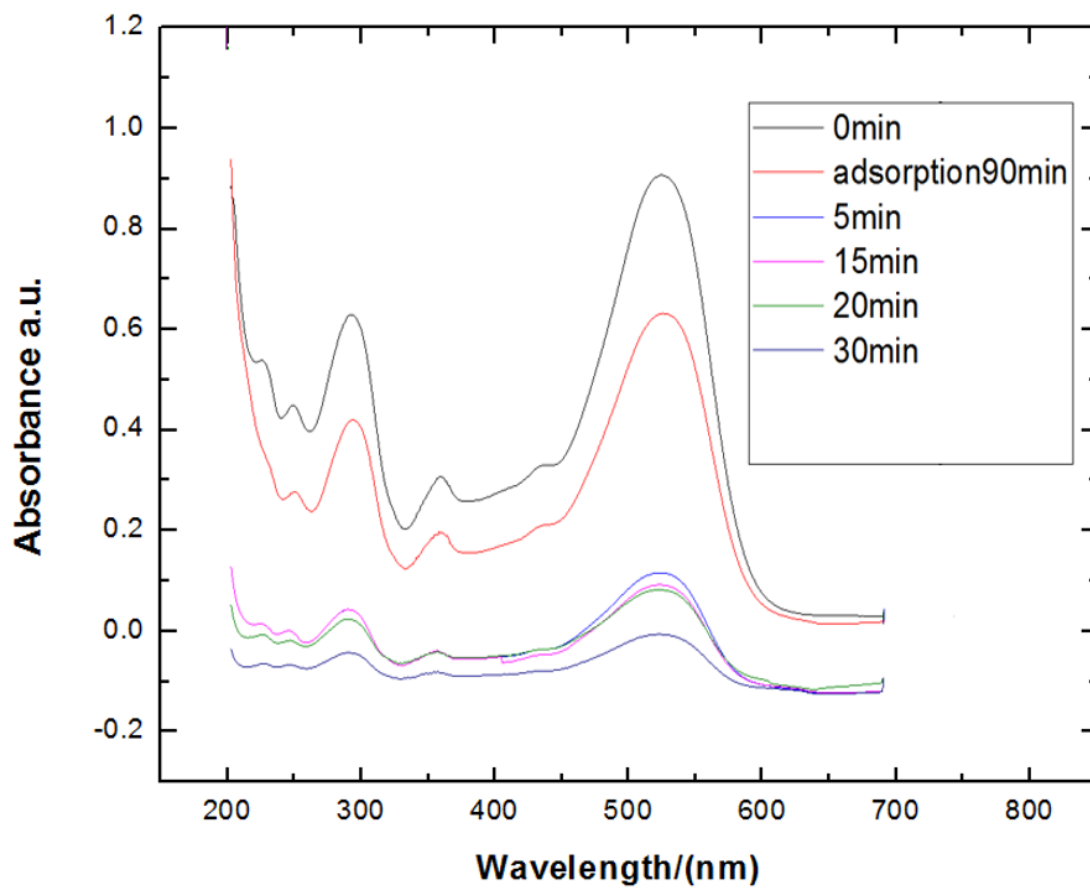


Figure A 8. UV-vis spectra for the oxidation of RB-5 dye by using calcined RVC/PbO<sub>2</sub>/TiNS as a photocatalyst.

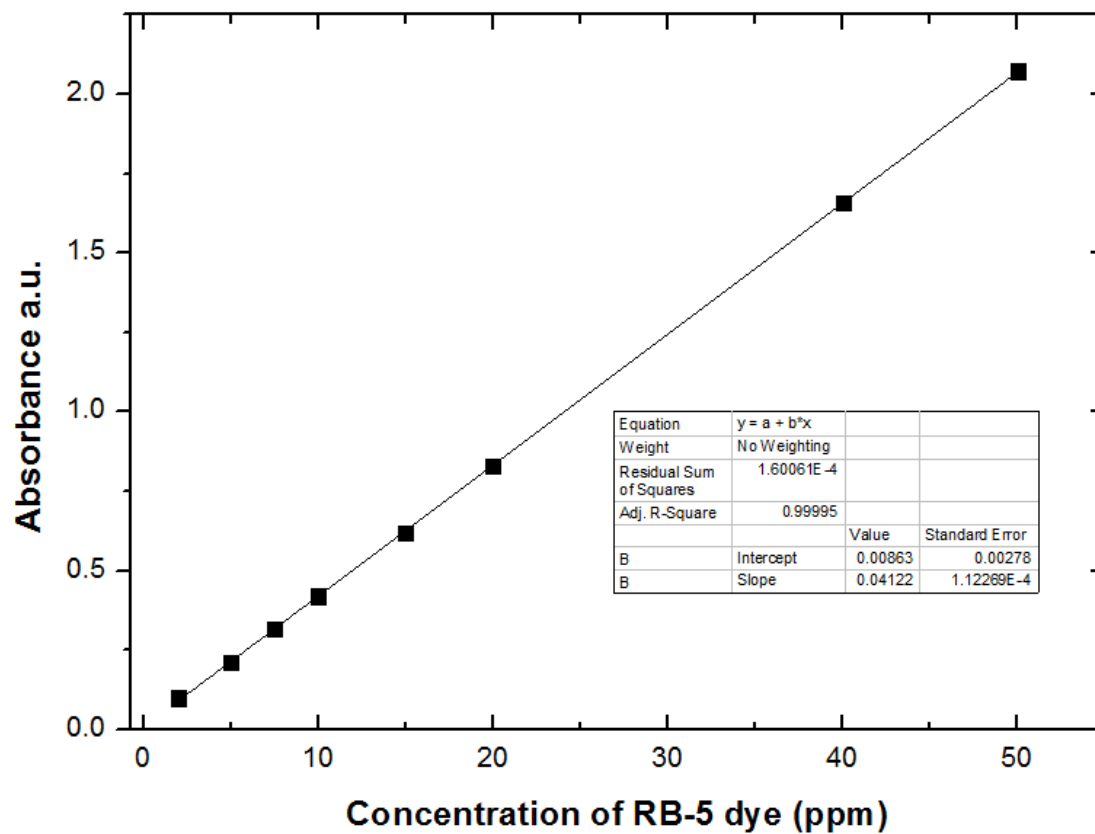


Figure A 9. Calibration curve for the RB-5 dye.

**SPRINGER NATURE LICENSE  
TERMS AND CONDITIONS**

May 15, 2019

This Agreement between University of Southampton ("You") and Springer Nature ("Springer Nature") consists of your license details and the terms and conditions provided by Springer Nature and Copyright Clearance Center.

License Number	4478841372616
License date	Nov 30, 2018
Licensed Content Publisher	Springer Nature
Licensed Content Publication	Journal of Solid State Electrochemistry
Licensed Content Title	Decolourisation of reactive black-5 at an RVC substrate decorated with PbO <sub>2</sub> /TiO <sub>2</sub> nanosheets prepared by anodic electrodeposition
Licensed Content Author	S. Z. J. Zaidi, C. Harito, F. C. Walsh, C. Ponce de León
Licensed Content Date	Jun 1, 2018
Licensed Content Volume	22
Licensed Content Issue	9
Type of Use	Thesis/Dissertation
Requestor type	academic/university or research institute
Format	print and electronic
Portion	full article/chapter
Will you be translating?	no
Circulation/distribution	> 50,000
Author of this Springer Nature content	yes
Title	Decolourisation of reactive black-5 at an RVC substrate decorated with PbO <sub>2</sub> /TiO <sub>2</sub> nanosheets prepared by anodic electrodeposition
Institution name	University of Southampton
Expected presentation date	Jan 2019
Requestor Location	University of Southampton Building 25 room 2021 Highfield Southampton  Southampton, SO17 1BJ United Kingdom Attn: University of Southampton
Billing Type	Invoice
Billing Address	University of Southampton Building 25 room 2021 Highfield Southampton  Southampton, United Kingdom SO17 1BJ Attn: University of Southampton



67<sup>th</sup> Annual Meeting  
of the International Society of Electrochemistry

21-26 August, 2016, The Hague, The Netherlands

CERTIFICATE

This is to certify that **Syed Zohaib Javaid Zaidi** has participated  
in the 67<sup>th</sup> Annual Meeting of the International Society of Electrochemistry held from  
21-26 August, 2016 in The Hague, The Netherlands.

A handwritten signature in blue ink, appearing to read 'MK', is positioned above the name of the signatory.

Dr. Marc Koper  
*Co-Chair, Organizing Committee*  
*Annual ISE Meeting 2016*



## Journées d'Electrochimie

26 - 29 Juin 2017  
Bordeaux - France

---

### Attestation de participation

En tant qu'organisateur des Journées d'Électrochimie 2017, qui ont lieu à Bordeaux du 26 au 29 juin 2017, nous attestons de la participation de **Syed Zohaib Javaid ZAIDI** à cette conférence.

Fait à Talence, le 26 juin 2017

Stéphane ARBAULT

Neso SOJIC



ELECTROCHEMICAL MICRO & NANO SYSTEM TECHNOLOGIES

## Certificate of Attendance

*This is to certify that*

***Syed Zohaib Javaid Zaidi***

*attended the International Conference EMNT2018*

*- ELECTROCHEMICAL MICRO & NANO SYSTEM TECHNOLOGIES -*

*held in Milan (Italy); 28<sup>th</sup> August – 1<sup>st</sup> September 2018.*

*He performed the following oral presentation:*

*“Roses inspired novel coatings prepared by anodic electrophoretic deposition of Ti-nanosheets over Carbon based substrate: Characterization and Application”*



Conference Local Committee

A handwritten signature in black ink, which appears to read 'Luca Magagnin'.

Prof. Luca Magagnin  
Conference Chairman